LA-8994-PR
Progress Report

UC-28
Issued: September 1981

Progress at LAMPF

January—June 1981

Clinton P. Anderson Meson Physics Facility

Editor

John C. Allred

Scientific Editorial Board

Olin B. van Dyck
Richard L. Hutson
M. Stanley Livingston
Mario E. Schillaci

Production Staff

Kit Ruminer
Beverly H. Talley

Los Alamos National Laboratory
Los Alamos, New Mexico 87545

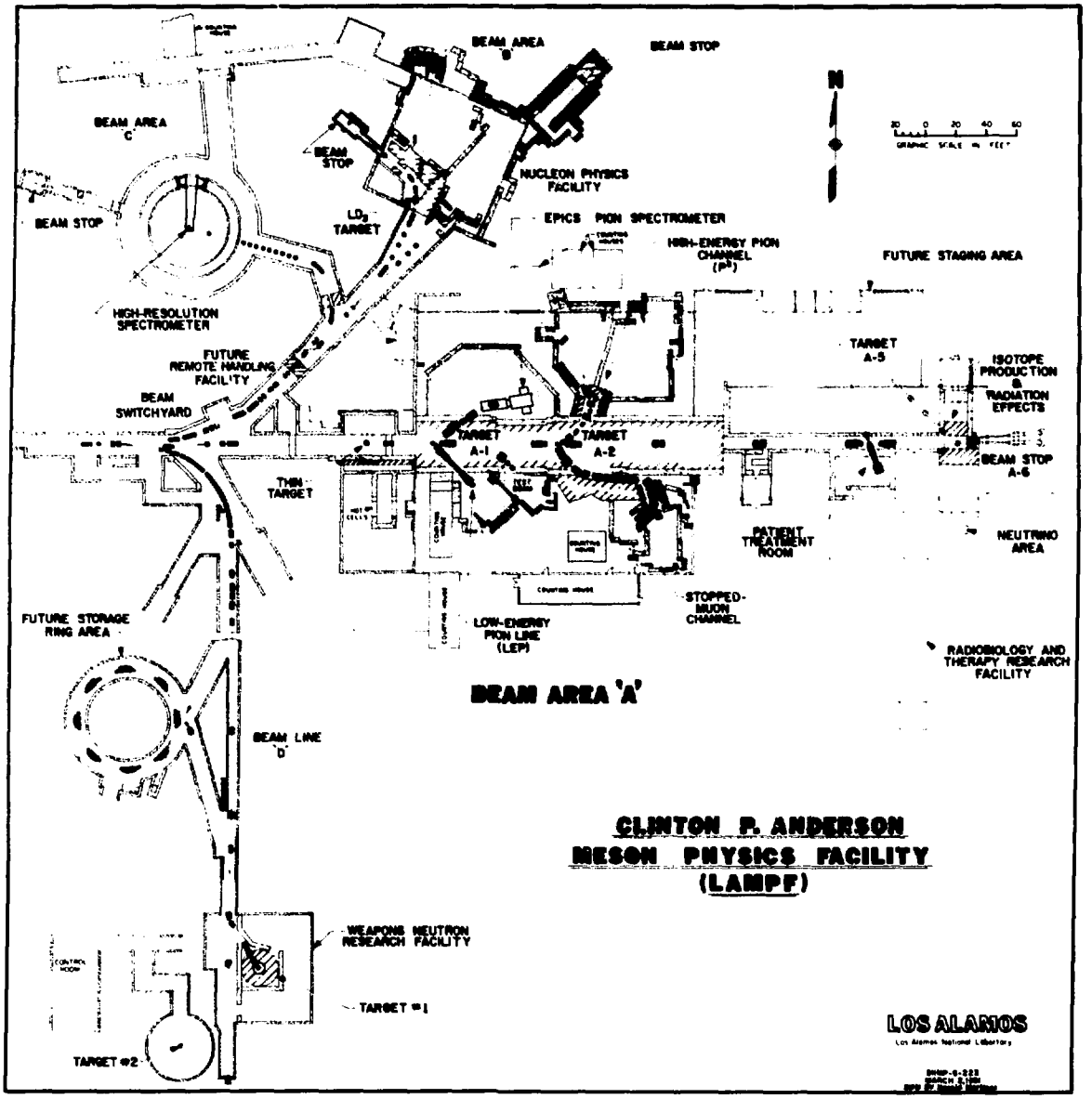
BEAM AREA B
BEAM STOP
BEAM AREA C
BEAM STOP
BEAM STOP
LD_2 TARGET
NUCLEON PHYSICS FACILITY
EPICS PION SPECTROMETER
HIGH-ENERGY PION CHANNEL (π^3)
FUTURE STAGING AREA
HIGH-RESOLUTION SPECTROMETER
FUTURE REMOTE HANDLING FACILITY
BEAM SWITCHYARD
TARGET A-5
ISOTOPE PRODUCTION & RADIATION EFFECTS
TARGET A-1
TARGET A-2
BEAM STOP A-6
THIN TARGET
PATIENT TREATMENT ROOM
NEUTRINO AREA
STOPPED-MUON CHANNEL
LOW-ENERGY PION LINE (LEP)
RADIOBIOLOGY AND THERAPY RESEARCH FACILITY
FUTURE STORAGE RING AREA
BEAM AREA 'A'
BEAM LINE 'D'
CLINTON P. ANDERSON
MESON PHYSICS FACILITY
(LAMPF)
WEAPONS NEUTRON RESEARCH FACILITY
TARGET #1
TARGET #2
LOS ALAMOS
Los Alamos National Laboratory

CONTENTS

EXPERIMENTAL AREAS

Primary beam lines in experimental areas:

Line A – Main Beam Line for Pion and Muon Channels
Line B – Neutron and Proton Beams and Nuclear Chemistry Facility
Line C – High-Resolution Proton Spectrometer
Line D – Weapons Neutron Research Facility

Experimental beam lines:

Area A:

BSA – Beam Stop A
EPICS – Energetic Pion Channel and Spectrometer
LEP – Low-Energy Pion Channel
P^3 – High-Energy Pion Channel
SMC – Stopped Muon Channel
TTA – Thin Target Area

Area B (AB or Nucleon Physics Facility):

BR – Neutrons and Protons
EPB – External Proton Beam
LB-NC – Line B — Nuclear Chemistry

Area C:

CCH – Area C Control and Counting House
HRS – High-Resolution Proton Spectrometer

Area A-East:

Biomedical Pion Channel
TA-5 – Target A-5
ISORAD – Isotope Production and Radiation Effects Facility
Neutrino Area

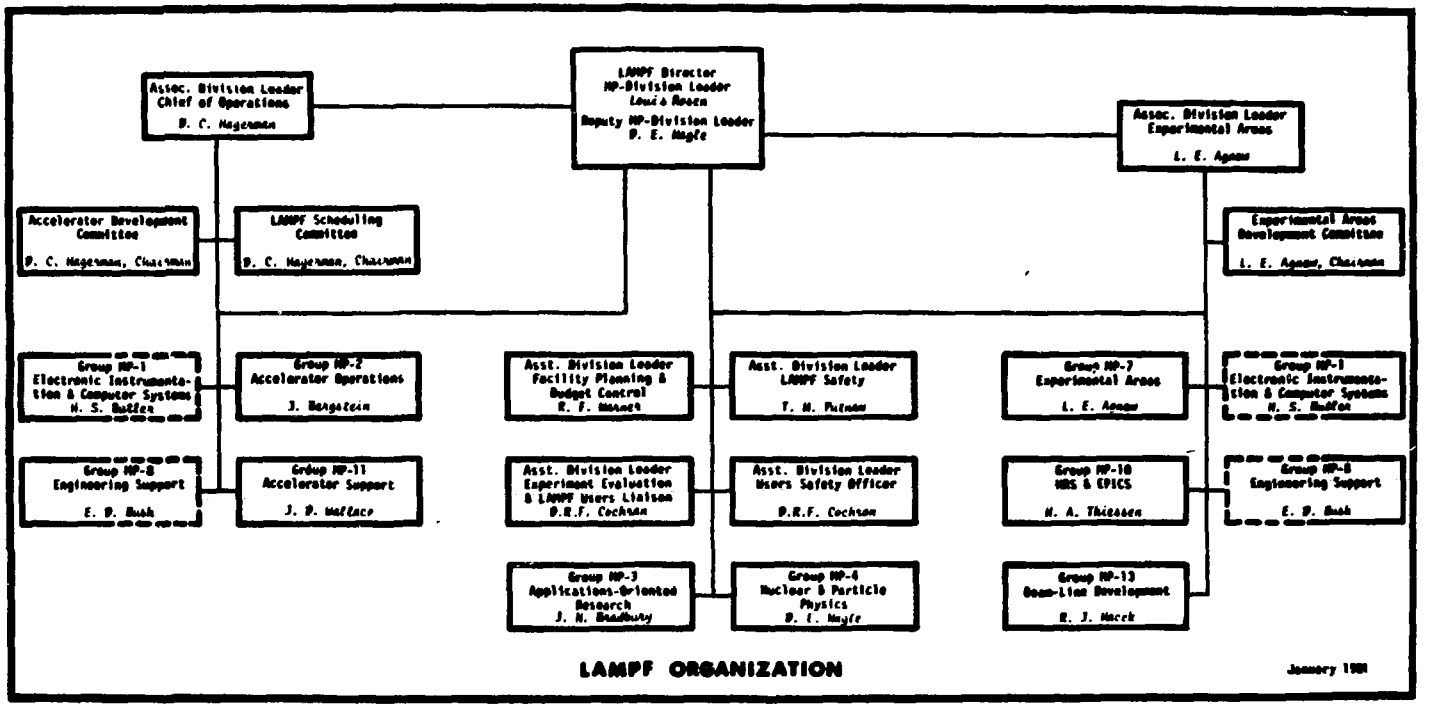
Assoc. Division Leader
Chief of Operations
P. C. Hagemann
LAMPF Director
MP-Division Leader
Louis Rosen
Deputy MP-Division Leader
P. E. Nagle
Assoc. Division Leader
Experimental Areas
L. E. Agnew
Accelerator Development Committee
P. C. Hagemann, Chairman
LAMPF Scheduling Committee
P. C. Hagemann, Chairman
Experimental Areas Development Committee
L. E. Agnew, Chairman
Group MP-1
Electronic Instrumentation & Computer Systems
W. S. Hutton
Group MP-2
Accelerator Operations
J. Bergstein
Asst. Division Leader
Facility Planning & Budget Control
R. F. Hibbard
Asst. Division Leader
LAMPF Safety
T. H. Putnam
Group MP-7
Experimental Areas
L. E. Agnew
Group MP-1
Electronic Instrumentation & Computer Systems
W. S. Hutton
Group MP-8
Engineering Support
E. D. Bush
Group MP-11
Accelerator Support
J. D. Wallace
Asst. Division Leader
Experiment Evaluation & LAMPF Users Liaison
D.R.F. Cochran
Asst. Division Leader
Users Safety Officer
D.R.F. Cochran
Group MP-10
MRS & EPICS
H. A. Thiessen
Group MP-8
Engineering Support
E. D. Bush
Group MP-3
Applications-Oriented Research
J. N. Bradbury
Group MP-4
Nuclear & Particle Physics
P. E. Nagle
Group MP-13
Beam-Line Development
R. J. Macek
LAMPF ORGANIZATION
January 1981

From the Washington Scene:

FY 81 activities at LAMPF have taxed personnel and equipment to their limits, even though we reduced operations to 23 weeks of production. However, I am delighted to report that relief appears to be in sight.

Our sponsors in DOE were successful in obtaining budget increases for FY 82 that offset much of what was lost to inflation during FY 81, and this will help mightily to maintain the momentum of experimental programs. The House and Senate supported these increases. In addition, the House Armed Services Committee and House Committee on Appropriations have seen fit to include an additional $3M for increased operation of LAMPF to correct a severe disparity between LAMPF capabilities and projected operating schedules. This sum supplements nuclear physics moneys, which still comprise 90% of our budget.

I cherish this initiative not only because it will permit a very substantial increase in physics output from LAMPF, but also because it reflects the concern of the Congress for the viability of LAMPF and the programs to which it is dedicated. It also is recognition of the fact that we have, through the years, kept faith with the DOE and Congress by honoring our commitments and fulfilling their expectations. All of this is, of course, a tribute to the creativeness, competence, and diligence of all the people at LAMPF. I look forward to even greater achievements in the future.

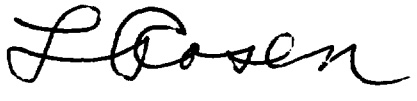

Louis Rosen
Director, LAMPF

PROGRESS AT LAMPF

JANUARY — JUNE 1981

Clinton P. Anderson Meson Physics Facility

ABSTRACT

Progress at LAMPF is the semiannual progress report of the MP Division of the Los Alamos National Laboratory. The report includes brief reports on research done at LAMPF by researchers from other institutions and Los Alamos divisions.

I. RESEARCH

Nuclear and Particle Physics

Free np Analyzing Power Measurements at Medium Energies
(Exp. 65, AB)

(Los Alamos, Texas A&M Univ., Univ. of Texas)
Spokesman: J. E. Simmons (Los Alamos)

A major objective of our nucleon-nucleon work at LAMPF has been the determination of the scattering amplitudes at energies in the range 500-800 MeV. As part of this effort, we have now completed accurate free np analyzing power measurements[1] as functions of energy and angle. In addition to their intrinsic value from the point of view of determining the $I = 0$ phase parameters, such measurements have the practical value of being useful for measurement of the polarization of neutron beams.

The neutron beam for this experiment was obtained from the reaction $p + {}^{9}Be \rightarrow n$ at 0° with 800-MeV protons. The neutrons produced at 0° were collimated and scattered from a polarized proton target. Simultaneous measurements of the scattering angle and momentum of the recoiling proton and the direction of the scattered neutron enabled unambiguous selection of the elastic np events. The incident neutron energy ranged from 300-800 MeV. This spread of the incident neutron beam energy together with our experimental method permitted the measurement of free np analyzing power at different energies simultaneously. The angular range covered in this experiment was $60° \leq \theta_{c.m.} \leq 160°$. Analyzing power data thus obtained were binned into 10 bins with respect to the incident neutron beam energy, with 50-MeV bin width.

The angular distributions of the analyzing power are shown in Fig. 1 for two bins at 475 and 775 MeV. Figure 2 shows the energy dependence of A(110° c.m.) for our data, previous experiments, and a recent phase-shift fit of Arndt and VerWest.[2] These data show a very interesting behavior, which is not yet understood, by exhibiting a marked minimum near 600 MeV.

REFERENCES

1. C. R. Newsom, Thesis, University of Texas (1980).

2. R. A. Arndt and B. J. VerWest, Proc. Fifth Int. Symp. on Polarization Phenomena in Nuclear Physics, Santa Fe, New Mexico (1980).

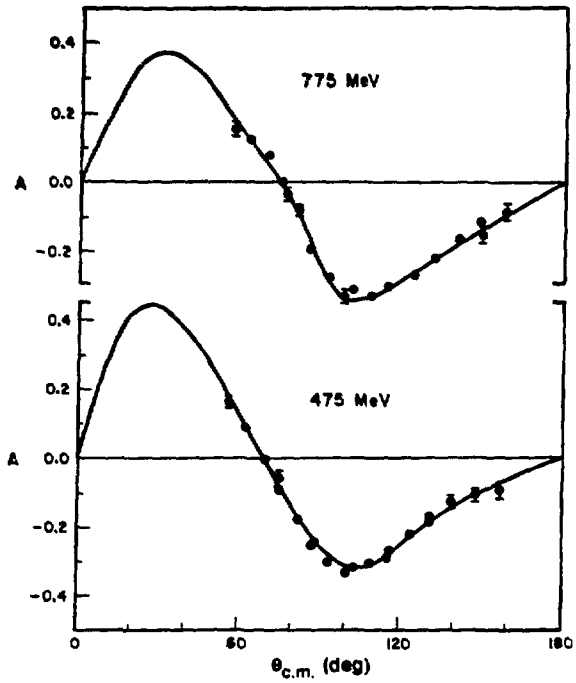

Fig. 1.
Comparison of a phase-shift parameterization by Arndt and VerWest (Ref. 2) with the experimental results of Exp. 65 at 475 and 775 MeV.

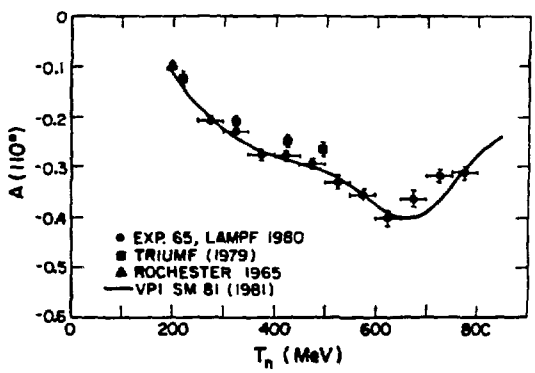

Fig. 2.
Experimental results from Exp. 65 for the np analyzing power at 110° c.m., A(110°), vs incident neutron energy and comparison to some other data. Also shown is the 1981 energy-dependent phase-shift fit of Arndt and VerWest (Ref. 2).

Spin-Correlation Parameter A_{NN} for Free np Scattering at Medium Energies (Exp. 66, AB)

(Los Alamos, Texas A&M Univ., Univ. of Texas)
Spokesman: J. E. Simmons (Los Alamos)

Spin Correlation A_{NN} for Free np Scattering

The spin-correlation parameter A_{NN} has been measured for free np scattering for incident neutron kinetic energies 390-665 MeV over an angular range 70-165° c.m. This is the first such np A_{NN} measurement[*,1] above 50 MeV. The measurement relates to the spin dependence of the isoscalar part of the nuclear force and was performed by scattering a polarized neutron beam from a polarized proton target. Further description of the neutron beam[**,1] is given below. The scattering cross section contains a spin-correlation term $(\langle\sigma_1\rangle \cdot \hat{n})(\langle\sigma_2\rangle \cdot \hat{n})\, A_{NN}(\theta)$, in which the dot products represent beam and target polarization components normal to the plane of scattering. The quantity A_{NN} may be obtained from suitable combinations of scattered intensities with parallel and antiparallel polarization vectors. The detection of recoil proton momentum together with neutron angle and rf timing allowed unambiguous selection of elastic events.

Figure 1 shows the np A_{NN} data as a function of center-of-mass angle at 390, 465, 565, and 665 MeV in energy bins of 100-MeV nominal width. At back angles the parameter goes strongly negative in the charge-exchange region. Also shown are phase-shift predictions of Arndt and VerWest[2] made a year ago. At 665 MeV, these data together with other np data from our group and elsewhere have significantly improved knowledge of isoscalar NN scattering amplitudes.

The Polarized Neutron Beam

Polarized neutrons were produced by quasi-free pn scattering of the incident unpolarized proton beam from a liquid deuterium target. A beam of polarized neutrons was formed at 20° by a steel collimator. Two 2-m-long precession magnets were used to change the direction of neutron polarization from up to down. Knowledge of the np analyzing power from Exp. 65 was used to measure the beam polarization. The energy spectrum of the

*,**T. S. Bhatia et al. have discussed the np A_{NN} measurements (p. 123) and neutron beam (p. 871) in Ref. 1.

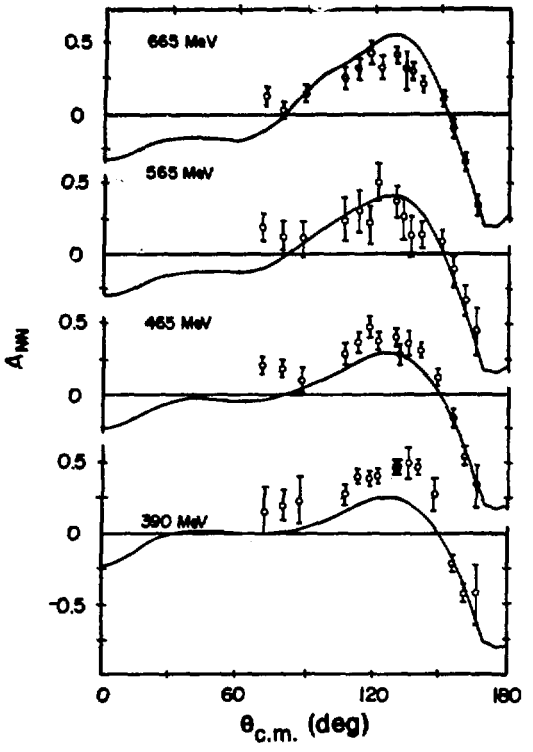

Fig. 1.
Data from Exp. 66 showing the angular distribution of the spin-correlation parameter A_{NN} in free np scattering. The curves are energy-dependent phase-shift predictions of Arndt and Ver West (Ref. 2).

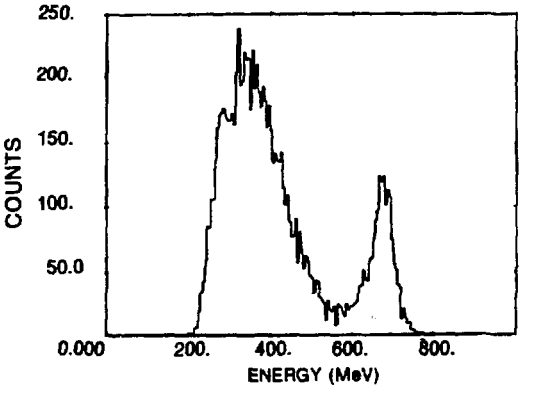

Fig. 2.
Energy spectrum from $p + d \rightarrow n$ at 20° lab, as measured in Exp. 66. Note that the lower cutoff is instrumental.

neutron beam is shown in Fig. 2; the polarization is shown in Fig. 3. The neutron polarization is near 0.2, almost independent of energy. This was expected at the quasi-free scattering peak; however, the significant polarization at lower neutron energies was a surprise.

Zero-Crossing Angle in the np Analyzing Power and its Relation to Charge Symmetry Invariance

A strong test of charge symmetry breaking in NN scattering at medium energy is represented by the equality $A(\vec{n}p,\theta) = A(n\vec{p},\theta)$, where the left- and right-hand sides of the equality represent the np analyzing powers as measured with a polarized neutron beam and with a polarized proton target, respectively. Such a measurement is not easy because of the difficulty of measuring the absolute values of the polarizations. An alternative is to compare the shapes of the two analyzing powers through the respective zero-crossing angles θ_0, which are independent of precise knowledge of the polarizations.

From the np scattering studies of Exp. 66 we have obtained the angular distributions for the analyzing powers for $\vec{n}p$ and $n\vec{p}$ elastic processes by averaging over the target and beam polarizations, respectively. These angular distributions then lead to a knowledge of $\theta_0(\vec{n}p)$ and $\theta_0(n\vec{p})$. The zero-crossing angles thus obtained for three energy bins, 425, 565, and 665 MeV, are shown in Fig. 4. Also shown in this figure is the predicted energy dependence of the zero-crossing angle for np analyzing

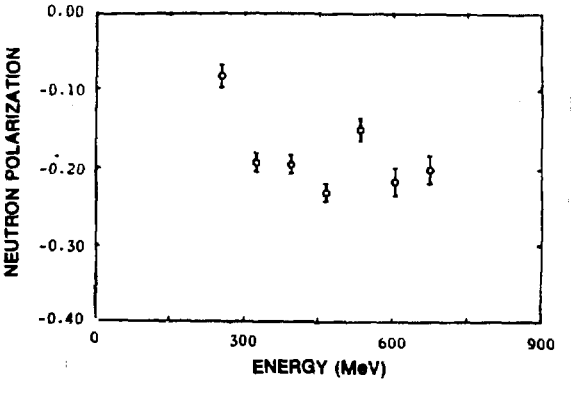

Fig. 3.
Neutron polarization as a function of energy from the process $p + d \rightarrow n$ at 20° lab.

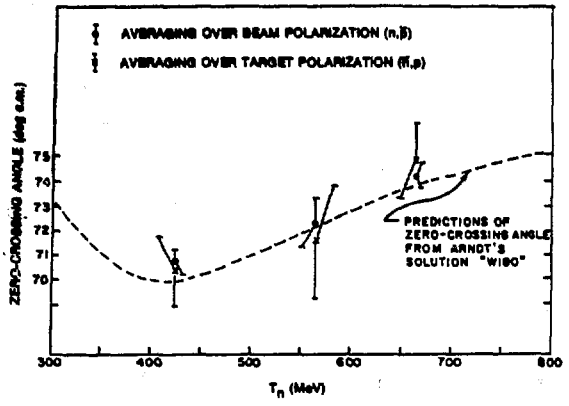

Fig. 4.
Zero-crossing angles θ_0, for np analyzing powers obtained using polarized proton target and polarized beam, vs incident neutron energy. Also shown are predictions for θ_0 from the phase-shift solution W180 of Arndt et al. (Ref. 2). Charge symmetry requires equality of the two types of zero-crossing angles.

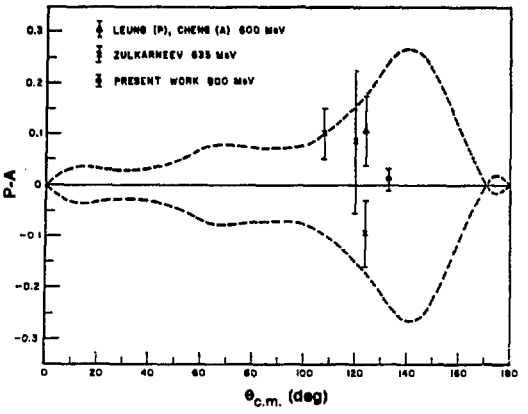

Fig. 5.
Comparison of the difference between polarization and analyzing power P-A in pn scattering at energies between 600 and 800 MeV. The dashed curve represents theoretical calculations of Bryan et al. (Ref. 5) at 600 MeV.

power based on the energy-dependent phase-shift solution W180 of Arndt and VerWest.[2] The measured $\theta_0(\vec{n}p)$ values agree well with those for $\theta_0(n\vec{p})$ for each of the three energy bins reported and the measured values are generally in agreement with the phase-shift prediction. In this first report of the zero-crossing test we see no evidence for charge symmetry breaking in np scattering.

Polarization-Analyzing (P-A) Power for np Scattering: Check of Time-Reversal Invariance

Based on Sudarshan's theory of strong, weak, and electromagnetic interactions[3] in which C and T invariance are broken in the strong interaction, Bryan and Gersten[4] have developed a T-asymmetric one-boson-exchange nucleon-nucleon potential model where T asymmetry becomes pronounced only at intermediate and higher energies. Calculations based on the Bryan-Gersten model show that the effects for np scattering may be large, with a maximum near 140° c.m. at LAMPF energies.

It is known that if the polarization, P, equals the analyzing power, A, the interaction must be invariant under time reversal. This is the so-called P-A test.

For np scattering at medium energy two tests have been reported: Bryan[5] compared the np P data of Leung et al. with the pn A data of Cheng et al. at 600 MeV; Zulkarneev et al.[6] have also published a P-A comparison for pn scattering near 635 MeV. We have measured the polarization of neutrons from 800-MeV quasi-free pn scattering at 133° c.m. with the result P = −0.20 ± 0.018. From Exp. 65 (Ref. 7), the analyzing power for 800-MeV free np elastic scattering at 133° was −0.211 ± 0.009. We have assumed charge symmetry. This leads to P-A = 0.01 ± 0.02. The theoretical predictions of Bryan et al.[5] at 600 MeV are shown in Fig. 5 together with our measurements and the other experiments noted above. It is clear from this figure that the predicted value of P-A at 133° c.m. differs considerably from zero and thus disagrees with our experimental result.

REFERENCES

1. T. S. Bhatia et al., Proc. Fifth Int. Symp. on Polarization Phenomena in Nuclear Physics, Santa Fe, New Mexico (1980), pp. 123 and 871.

2. R. A. Arndt and B. J. VerWest, Proc. Fifth Int. Symp. on Polarization Phenomena in Nuclear Physics, Santa Fe, New Mexico (1980), p. 179.

3. E. C. G. Sudarshan, Proc. R. Soc. A305, 319 (1968).

4. R. Bryan and A. Gersten, Phys. Rev. Lett. 26, 1000 (1971); also, R. Bryan, A. Gersten, and J. Binstock, to be published in Ann. Phys.

5. R. Bryan, Phys. Rev. C12, 1968 (1975).

6. R. Zulkarneev et al., Phys. Lett. 61B, 164 (1976).

7. C. R. Newsom, Thesis, University of Texas (1980).

The Measurement of K_{NN}, K_{LL} in pd → nX and p ^{9}Be → nX at 800 MeV (Exp. 360, AB)

(Los Alamos, Univ. of Texas, Texas A&M Univ.)

Spokesmen: P. J. Riley (Univ. of Texas) and J. E. Simmons (Los Alamos)

Using the LAMPF 800-MeV polarized proton beam incident on liquid deuterium and beryllium targets, we have measured the outgoing neutron polarization at 0° to obtain the polarization transfer parameters K_{NN} and K_{LL}. Such measurements in (p,n) reactions are of interest to determine the feasibility of producing polarized neutron beams, and in addition the transfer parameters measured on deuterium provide information concerning the basic np interaction. The measurements indicate that neutron polarization near 0.5 can be produced at 0° at an intensity that is usable for some cases now and that will increase with future ion source improvements.

The results[1] for the K_{NN} and K_{LL} measurements for the process $p + d \rightarrow n + X$ are shown in Fig. 1.

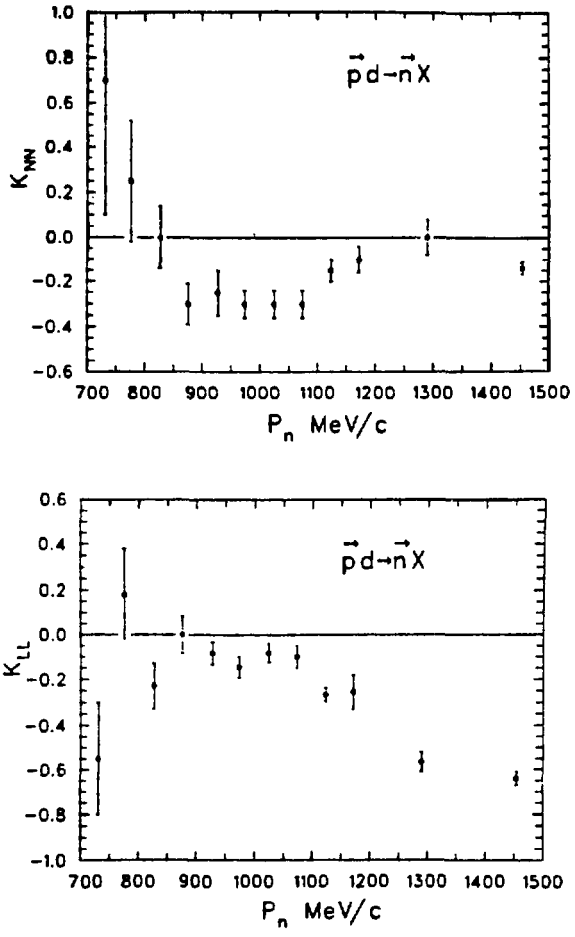

Fig. 1.
K_{NN} and K_{LL} for $p + d \rightarrow n + X$ at 800 MeV and 0°. The sign convention is such that a negative value of K_{LL} implies that the spin of the outgoing neutron is antiparallel to that of the incident proton.

REFERENCE

1. P. J. Riley et al., to be published in Phys. Lett.

The One- and Two-Electron Thresholds in the Photodetachment of H^- Ions (Exp. 449, EPB)

(Univ. of New Mexico, Los Alamos)

Spokesmen: H. C. Bryant (Univ. of New Mexico) and J. B. Donahue (Los Alamos)

Our measurements of the resonance structure of the H^- ion observed in the reaction $\gamma + H^- \rightarrow e^- + H^0$ have been presented in a series of progress reports and articles[1-3] starting in 1977. Here we report measurements of the energy dependence of the cross section in two threshold regions, the first near 0.75 eV where the detachment of single electrons begins, and the second near 14.35 eV where the ejection of two electrons by a single photon, $\gamma + H^- \rightarrow e^- + e^- + H^+$, becomes possible.

The relativistic Doppler-shift method[1] of creating a finely tunable beam of 0.5- to 20-eV photons as well as strong motion-induced electric fields has been described often enough to permit its omission here. In previous experiments the detached electrons, all of which are projected in the forward direction in the laboratory, were detected. To observe the two-electron detachment cross

section in the presence of the 100-times-larger single-detachment process,[4] it was necessary to redesign the apparatus to detect protons. At the same time, the equipment was made capable of detecting H^0's. This capability has certain advantages when there are strong magnetic fields in the interaction region. Figure 1 represents the new experimental arrangement. The downstream H^0 and H^+ "spectrometer" occupies the interior of a 20-cm-diam beam pipe; the few-gauss analyzing field is induced by a pair of single-turn coils 6 *m* long, carrying 100-200 A and deployed along the same pipe.

We learned to use the weak, long field after we found that stronger fields produce a troublesome background by the two-step process,

$$\gamma + H^- \rightarrow H^{0*} + e^-$$

followed by

$$H^{0*} + (\vec{v} \times \vec{B}) \rightarrow p^+ + e^- \quad .$$

The second reaction describes the stripping of excited neutral atoms by the motion-induced electric field in the spectrometer. For a given field strength there is a minimum principal quantum-number state in which the atom may occur, above which stripping becomes very probable. For example, at a field of 22 G atoms in states above n = 14 are stripped. We have taken advantage of this circumstance by adjusting the field to detect protons stripped from atoms left in selected excited states after the initial single-electron detachment. Quite unexpected Feshbach resonances were discovered near n = 6 by this method.[5] Without selection, that is, by detecting the H^0 or e^-, the continuum processes in this energy region overwhelm any hint of structure beyond n = 3. For future reference Fig. 1 also depicts a new photon beam transport that simultaneously introduces the first, second, and fourth harmonics of the yttrium-aluminum-garnet (YAG) laser light into the scattering chamber. Only the fourth harmonic enters through the rotating mirror system that varies the angle of intersection with the H^- beam. This equipment was used in the latest experiments to establish the absolute calibration of the relationship between the intersection angle and energy by finding the angle at which detachment from the n = 2 state of neutral hydrogen occurred. This procedure will become a permanent part of our experiments. The three-harmonic system will be used to study the properties of hydrogen atoms in very strong (>10-MV/cm) electric fields.

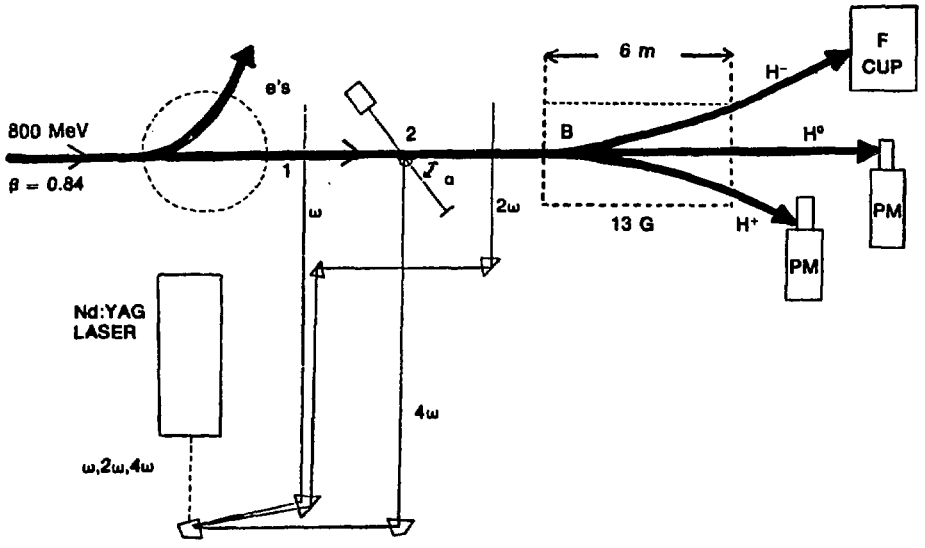

Fig. 1.
Schematic diagram of the apparatus.

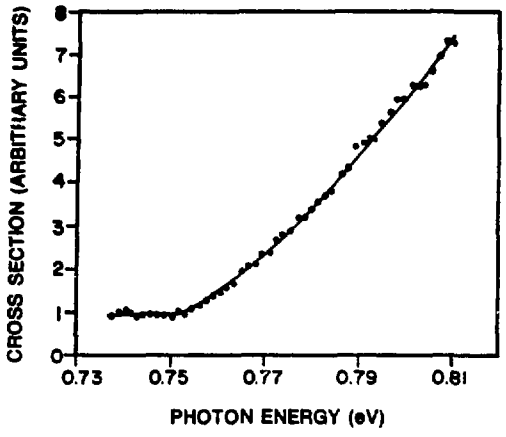

Fig. 2.
Photodetachment cross section near threshold. The curve is the result of the fit discussed in the text.

Our observations near the one-electron detachment threshold are shown in Fig. 2 (Ref. 6). Precise calculation of the binding energy of the H^- ion is a lengthy but straightforward computational task. The result from a calculation in 1962 by Pekeris,[7] using determinants up to the order of n = 444, is −0.754215(2) eV. Our data do not yet challenge this precision. We find −0.753 ± 0.005 eV, which is nevertheless the best measurement to date. Most of the error is systematic, originating from imperfect knowledge of the zero of the angle between the beams and of the velocity of the H^- ion. Considerable improvements are possible.

Of greater interest is the form of the threshold law. On very general grounds Wigner[8] predicted that near threshold the cross section for the ejection of a bound particle should vary as $k^{(2\ell+1)}$, where k is the momentum and ℓ is the orbital angular momentum of the particle. The question is, Over what energy region near threshold does this rule prevail? For photon absorption by the 1s ground state of H^-, ℓ equals 1; hence, the cross section should vary as $(E - E_{Th})^{3/2}$. A fit of the data to $\sigma(E) = A(E - E_{Th})^n + C$ yields $n \simeq 3/2$, only if the region of energy considered is limited to ~0.025 eV above threshold.[9,10] (Our energy resolution in this region is ~0.001 eV.) If the energy range is expanded, even to as little as 0.060 eV above threshold, n is 1.28. In this reaction the Wigner rule prevails only up to ~3% from threshold.

Even at its peak the double-detachment cross section is expected to be about two orders of magnitude smaller than the single-detachment cross section at the same energy. Theoretical analysis of the mechanism by which a single photon contrives to eject both electrons is not at all straightforward. It is difficult to describe the dynamics of three charged particles. Several proposals for the form of the threshold law have been advanced, including one that predicts an oscillatory function of energy above threshold.[11] When the energy available to the two electrons is just enough for both to escape, ~14.35 eV, it is far more likely that one of them will get away with most of the energy, leaving the other bound as an excited state of H^0, than it is that both will depart with only a little energy each. Moreover, because the photon absorption operator is a one-body operator, the photon's energy is initially given to only one of the electrons. The correlation of the two electrons is a crucial factor in the double-detachment process.

Wannier[12] studied the problem classically, essentially by classifying the possible orbits accessible to the two electrons as a function of energy, ignoring how the energy was given to the system. His conclusions were later confirmed quantum mechanically.[13] A power law $\sigma(E) \propto (E - E_{Th})^n$ organizes the predictions. If the energy were shared randomly between the two electrons, that is, if they were completely uncorrelated, n = 1. If the electrons are allowed to screen each other, n depends on the charge of the nucleus they orbit; in our case, Z = 1, for which n = 1.127. Our measurements so far yield n = 1.03 ± 0.15 in a restricted region near the threshold (Fig. 3). The statistics are not good enough to suggest a

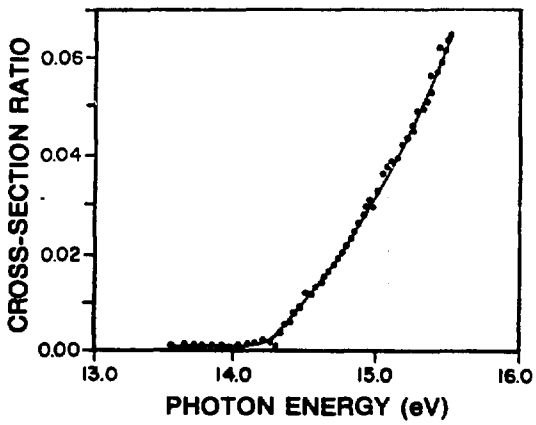

Fig. 3.
Proton counting rate near the double-photodetachment threshold. The curve is the result of the fit discussed in the text.

conclusion about possible oscillations. Much better data have recently been acquired and are being analyzed.

These studies of threshold laws, like the studies of resonances we have pursued previously, illustrate once again the importance of the H^- system as a simple "laboratory" in which to work out an understanding of multiparticle dynamics.

REFERENCES

1. H. C. Bryant, B. D. Dieterle, J. Donahue, H. Sharifian, H. Tootoonchi, D. M. Wolfe, P. A. M. Gram, and M. A. Yates-Williams, Phys. Rev. Lett. 38, 228 (1977).

2. P. A. M. Gram, J. C. Pratt, M. A. Yates-Williams, H. C. Bryant, J. Donahue, H. Sharifian, and H. Tootoonchi, Phys. Rev. Lett. 40, 107 (1978).

3. M. E. Hamm, R. W. Hamm, J. Donahue, P. A. M. Gram, D. A. Clark, H. C. Bryant, C. A. Frost, and W. W. Smith, Phys. Rev. Lett. 43, 1715 (1979).

4. J. T. Broad and W. P. Reinhardt, Phys. Rev. A14, 2159 (1976).

5. D. A. Clark, H. C. Bryant, K. B. Butterfield, C. A. Frost, J. B. Donahue, P. A. M. Gram, M. E. Hamm, R. W. Hamm, and W. W. Smith, "Observation of Structure in the H^- Photodetachment Cross Section Below n = 6," Bull. Am. Phys. Soc. 25, 1137 (1980).

6. C. A. Frost, "Measurements of the Threshold Behavior for One- and Two-Electron Photodetachment from the H^- Ion," Ph.D. dissertation, University of New Mexico (December 1980).

7. C. L. Pekeris, Phys. Rev. 126, 1470 (1962).

8. E. Wigner, Phys Rev. 73, 1002 (1948).

9. J. B. Donahue, P. A. M. Gram, M. E. Hamm, R. W. Hamm, H. C. Bryant, K. B. Butterfield, D. A. Clark, C. A. Frost, and W. W. Smith, "Photodetachment of Relativistic Ions," IEEE Trans. Nucl. Sci. NS-28, 1203 (April 1981).

10. H. C. Bryant, K. B. Butterfield, D. A. Clark, C. A. Frost, J. B. Donahue, P. A. M. Gram, M. E. Hamm, R. W. Hamm, and W. W. Smith, in *Atomic Physics VII*, Eds., D. Kleppner and F. M. Pipkin, Proc. 7th Int. Conf. on Atomic Physics, Boston, Massachusetts (Plenum, New York, 1981).

11. A. Temkin, J. Phys. B: Atom. Molec. Phys. 7, L450 (1974).

12. G. H. Wannier, Phys. Rev. 90, 817 (1953).

13. A. R. P. Rau, Phys. Rev. A4, 207 (1971).

H^- Field Detachment
(Exp. 530, EPB)
(Los Alamos, Univ. of New Mexico)
Spokesman: A. J. Jason (Los Alamos)

The stripping rate for H^- in an electric field has been measured over five orders of magnitude with sufficient precision to specify its functional dependence. Also, a field-stripping experiment on the polarized 800-MeV H^- beam showed that polarization transfer for such a process is close to 100%. The H^- field-ionization rates are of interest to several areas of current research, such as surface structure studies, and are essential for ion beam transport design and neutral beam preparation.

The experiment was performed in the EPB area at LAMPF using a magnet with a maximum field of 1.8 T. Within the magnet, H^- ions traveling at 0.84 c see a maximum electric field, $F = \gamma\beta cB$, of 840 MV/m plus a magnetic field, $B' = \gamma B$, of 3.3 T. Here, $\beta\gamma = P/m_0c = 1.56$ and $\gamma = E/m_0c^2 = 1.85$, where P, E, and m_0 are the ion momentum, total energy, and rest mass, respectively.

Figure 1 is a schematic diagram of the experimental apparatus. It consists of a special stripper magnet "Gypsy" and a multiwire proportional drift chamber (MWPC) located 6 m downstream from Gypsy. The stripper magnet field increases linearly along the beam line for 20 cm, then remains constant at its maximum value for 4 cm of path, and finally falls to nearly zero in 1 cm (the "hard edge" of the magnet). Gypsy was installed with the linear edge upstream for continuous field measurements at intermediate intensities and with its

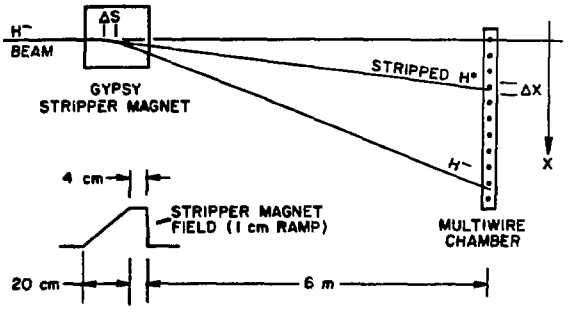

Fig. 1.
Schematic representation of experimental apparatus. The stripper magnet is oriented linear edge upstream; its field is shown in the lower figure (see text for details).

hard edge upstream for discrete field value measurements at very low and very high fields. With the linear edge upstream, the stripping length is measured as a continuous function for all field intensities in that portion of the magnet.

The H^- ions enter Gypsy from the left (Fig. 1) and follow a curved path until stripping occurs. Thereafter, they follow a straight-line path to the MWPC, where they are detected as a function of lateral position X. The fraction of ions stripped in the interval ΔS at S is given by the stripping length λ,

$$\frac{\Delta N}{N(S)} = \frac{\Delta S}{\lambda} \quad .$$

The counts ΔN appear in the position spectrum at X(S) in an interval $\Delta X = (dX/dS)\Delta S$, so the measured spectrum $\Delta N(X)$ is related to the stripping length λ through the equation

$$\frac{\Delta N}{N(X)} = \frac{dS}{dX}\frac{\Delta X}{\lambda} \quad ,$$

where N(X) is the cumulative distribution from large deflections down to X.

The mapping of S(X), which this equation shows is required to derive the stripping length from the spectrum, was accomplished in two ways. First, the deflection X is given by the field integral up to the stripping point S; an accurate field map allowed reconstruction of S from X. Second, a thin (60-$\mu g/cm^2$) plastic foil with precise position readout could be moved through the field region to produce a foil-stripped peak of H^0 with both X and S measured.

A distribution on the MWPC taken while Gypsy was oriented linear edge upstream is shown in Fig. 2. The peak field value of 1.0 T is low enough that many H^- ions survive transit through the entire magnet.

Figure 3 is a plot of H^- lifetime vs electric field F in the ion rest frame. The top- and right-hand axes are

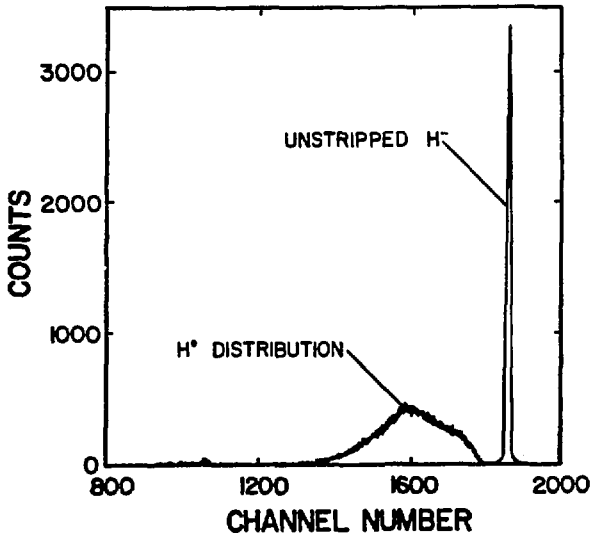

Fig. 2.

A distribution observed at the multiwire detector for 800-MeV H^- ions passing through magnet Gypsy. Gypsy was energized to a peak field of 1.0 T and oriented linear edge upstream. The sharp peak on the right is due to surviving H^- ions while the broad peak represents the angular distribution of stripped ions. The MWPC calibration is ~4 channels/mm.

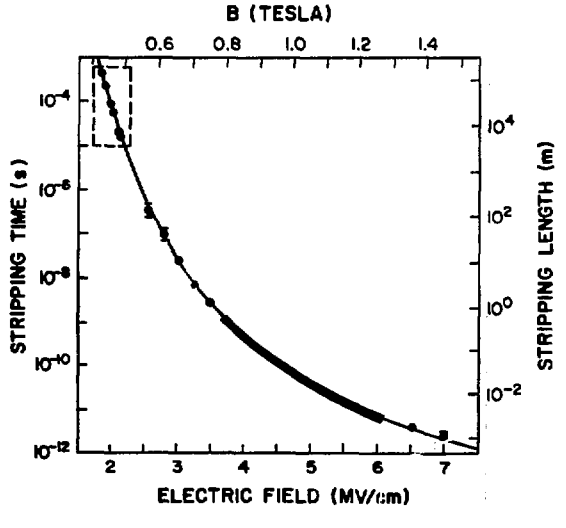

Fig. 3.

The H^- lifetime vs rest-frame electric field. The points enclosed by the dashed line are data from an earlier experiment (Ref. 1). The dark band is the result of the measurement of stripping length as a continuous function in the field ramp region, and the lighter line passing through all points is a fit of the data to Eq. (1). Stripping length vs magnetic field are given by the right-hand and top axes for an 800-MeV beam.

labeled with magnetic field and stripping length, respectively, for an 800-MeV beam. The ion lifetime τ is related to λ by

$$\lambda = \gamma\beta c\tau \quad .$$

Points enclosed by the dashed line are the data of Stinson et al.[1] and are included to indicate the wide range over which the lifetime has been experimentally observed and to demonstrate the match between the two data sets. The results of this experiment taken with Gypsy oriented linear edge upstream are shown by the heavy line with vertical thickness equal to the outside limits of experimental error; the remaining points are discrete data taken with Gypsy oriented hard edge upstream. The curve represents a fit to the equation,

$$\tau = \frac{A_1}{F}\exp(A_2/F) \quad , \qquad (1)$$

with constants determined as

$$A_1 = 2.47(\pm 0.09) \times 10^{-6} \text{ V} \cdot \text{s/m}$$

and

$$A_2 = 4.494(\pm 0.010) \times 10^9 \text{ V/m} \quad ,$$

where the uncertainties are statistical fitting errors obtained by least-squares analysis using the experimental uncertainties in the discrete data points. The constants A_1 and A_2 are highly correlated in the fitting process; their covariance gives a correlation coefficient of -0.90. The experimental results of Stinson et al.[1] are included in the calculation constants A_1 and A_2. Without these additional data the constants change slightly but are within the stated uncertainties.

Equation (1) was derived in a recent calculation by Scherk,[2] in which the H^- detachment lifetime was related to the atomic structure. His results are

$$A_1 = 2.66 \times 10^{-6} \text{ V} \cdot \text{s/m}$$

and

$$A_2 = 4.47 \times 10^9 \text{ V/m} \quad ,$$

which are in good agreement with our experimental results. Agreement of the preexponential factors is the more significant of the two because it confirms a theoretical calculation based on the details of atomic structure, whereas the exponential factor is largely determined by the asymptotic behavior of the ionic potential.[3]

REFERENCES

1. G. M. Stinson, W. C. Olson, W. J. McDonald, P. Ford, D. Axen, and E. W. Blackmore, Nucl. Instrum. Methods 74, 333 (1969).

2. L. Scherk, Can. J. Phys. 57, 558 (1979).

3. Andrew J. Jason, Daniel W. Hudgings, Olin B. van Dyck, William Folkner, and David A. Clark, submitted to Phys. Rev. Lett., April 1981.

Measurement of Parity Violation in the p-Nucleon Total Cross Sections at 800 MeV (Exp. 634, EPB)

(Univ. of Illinois, Los Alamos)

Spokesmen: R. Carlini and R. Talaga (Los Alamos) and V. Yuan (Univ. of Illinois)

We have essentially completed the initial phase of Exp. 634, which consisted of the development of low-noise ion chambers. As discussed in our proposal, low-noise chambers are essential to the attainment of a statistical precision of 1 part in 10^7 in a parity measurement.

The ion chamber design, which achieved the desired low-noise characteristics, is a parallel plate arrangement in which the beam direction is parallel to the plates, thereby eliminating spallation fragments from beam interactions with the collection plates. Figure 1 shows a plot of the ion chamber noise/counting statistics vs hydrogen gas pressure for a two-chamber arrangement with no scattering target. In the first case (solid points), thin foils were placed 11 cm upstream of the active collection region in the chambers. This was done to deliberately produce spallation fragments as the beam passes through the foils. The solid points show our experimental results and the solid curve indicates a theoretical prediction derived from spallation cross sections. As the pressure is increased the spallation products

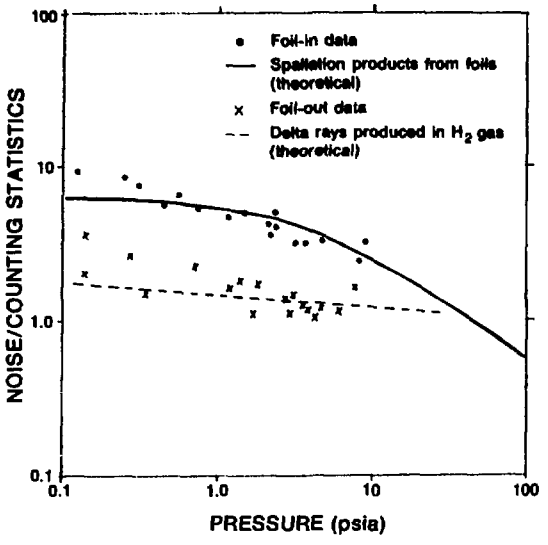

Fig. 1.
Ion chamber noise/counting statistics vs hydrogen-gas pressure for a two-chamber arrangement with no scattering target.

begin to disappear on account of selective absorption. The second case (crosses) shows data taken with no foils. In this arrangement the nearest sources of spallation fragments are the chamber windows 60 cm from the collection region. The resulting plot is consistent with a model for delta-ray production (dashed line) within the gas. We are confident that this ion chamber design will allow us to achieve a statistical precision of 1 part in 10^7 on the parity measurement.

This experiment has running time scheduled for July and November 1981. The July run will be a shakedown run for the experimental apparatus as a whole, and we are anticipating that the November run will be the first production run to acquire data.

D_{NN}, D_{SS}, D_{LS} for pp → pp at 647 MeV (Exp. 194, EPB)

(Los Alamos, Univ. of Texas, Univ. of California at Los Angeles, Rice Univ., Case Western Reserve Univ.)
Spokesman: M. W. McNaughton (Los Alamos)

Preliminary results are shown in Fig. 1 for pp elastic spin transfer parameters at 647 MeV. Note that because $D(\theta) = K(\pi - \theta)$, the data, which are plotted as three parameters, give information on six parameters in total.

The techniques are the same as for our recent 800-MeV data[1] and are described in a recent thesis[2] and an internal report.[3]

The data resolve some ambiguities in the single-energy phase-shift solutions (see Fig. 1),* but are in fair agreement with the energy-dependent solution (Arndt SM 81 in the figure).

REFERENCES

1. M. W. McNaughton et al., Proc. 1980 Santa Fe Conf. (AIP Publication #69), Santa Fe, New Mexico (1981), p. 149; and Los Alamos Scientific Laboratory report LA-8456-PR (1980), p. 19.

2. R. D. Ransome, Ph.D. thesis, University of Texas (1981).

*Data in the figure are from Ref. 4 and private communication.

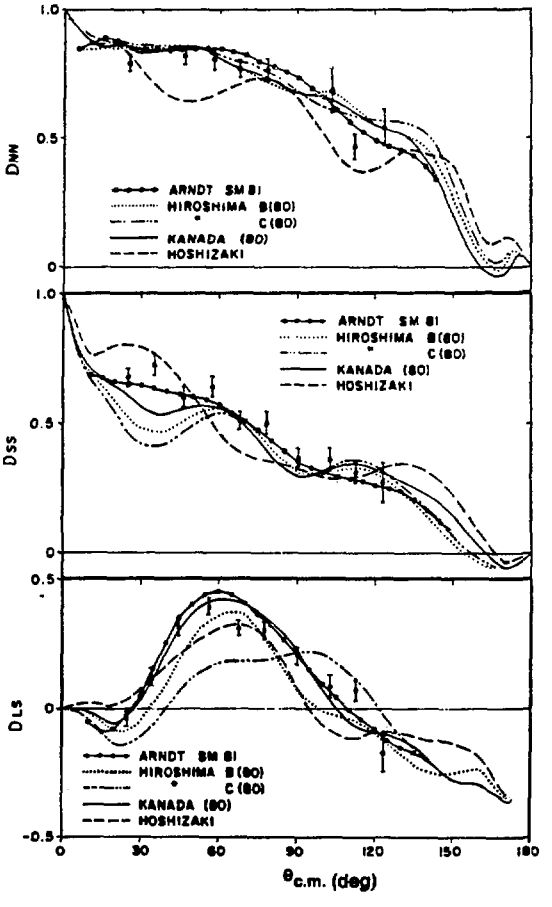

Fig. 1.
D_{NN}, D_{SS}, D_{LS} for pp → pp at 647 MeV.

3. M. W. McNaughton, Los Alamos Scientific Laboratory internal report MP-13/MWM/X80-01 (1980).

4. N. Hoshizaki, Progr. Theor. Phys. 60, 1796 (1978), and Progr. Theor. Phys. 61, 129 (1979).

Search for Pure Neutron/Proton Transitions in ^{14}C (Exp. 539, EPICS)

(Univ. of Minnesota, Los Alamos, Univ. of North Carolina, Oak Ridge, New Mexico State Univ.)

Investigation of the Strong Cancellations of Neutron/Proton Transition Amplitudes in ^{14}C (Exp. 622, EPICS)

(Univ. of Minnesota, Los Alamos, New Mexico State Univ., Univ. of Texas at Austin)

Spokesmen: H. W. Baer (Los Alamos) and D. B. Holtkamp (Univ. of Minnesota)

This investigation of inelastic π^+ and π^- scattering on ^{14}C using EPICS has produced some unique results. Recently,[1] we reported the first observation of ratios $R = \sigma(\pi^+)/\sigma(\pi^-)$ for inelastic scattering on nuclei, which were significantly larger than the free nucleon value of 9. The most striking case is that of the second 2^+ state in ^{14}C at 8.32 MeV. Figure 1 shows the inelastic spectra for π^+ and π^- scattering at an angle of 42°, which is near the peak of the $L = 2$ angular distribution for 2^+ states. The figure also shows the complete absence of the 2_2^+ state in π^- scattering. The measured lower limit for the ratio of cross sections is $R > 27$, a large value that we believe is produced by a nearly complete cancellation of the proton and neutron transition amplitudes in the π^- scattering. The neutron transition amplitude corresponds to recoupling $(sd)_0^2$ to $(sd)^2$ by the π^- neutron interaction; the proton transition amplitude corresponds to recoupling the two proton holes $(p^{-2})_0$ to $(p^{-2})_2$ by the π^- proton interaction. These amplitudes interfere destructively to bring about the vanishing π^- cross section. If the eight neutrons of ^{14}C were a closed shell, as is often assumed, this cancellation would not be present. Thus, the absence of a peak for the 2_2^+ state in π^- scattering is a measure of the degree of neutron shell breaking in the ^{14}C ground state. The direct manifestation of such cancellation phenomena in a simple comparison of the measured π^+ and π^- spectra demonstrates the value of pion scattering for elucidating the structure of nuclear states.

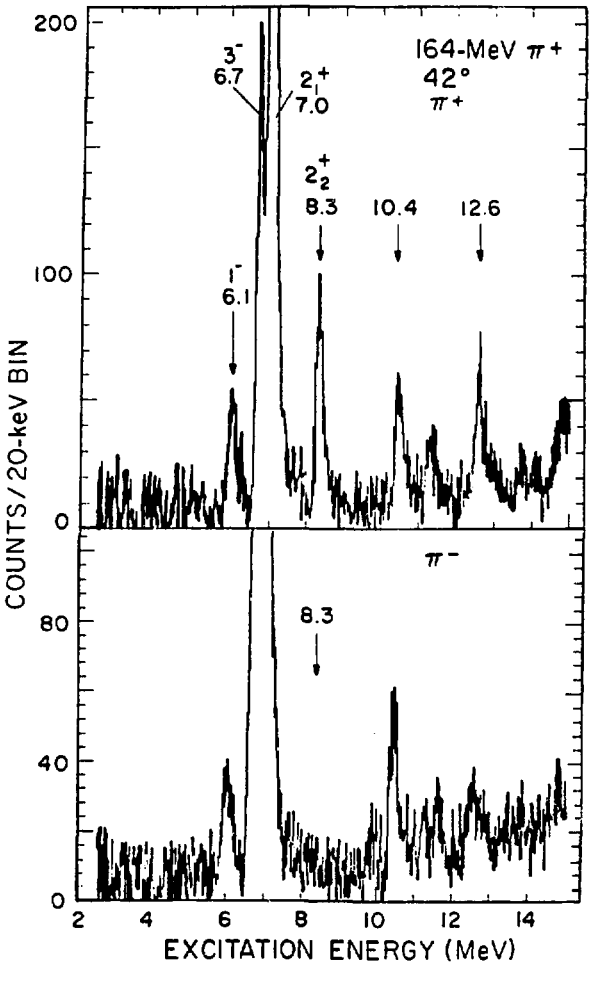

Fig. 1.
The spectra of π^+ and π^- scattering on ^{14}C showing the absence of the second 2^+ state in π^- scattering.

REFERENCE

1. D. B. Holtkamp, S. J. Seestrom-Morris, S. Chakravarti, D. Dehnhard, H. W. Baer, C. L. Morris, S. J. Greene, and C. J. Harvey, submitted to Phys. Rev. Lett., April 1981.

Pion Double Charge Exchange (Exps. 310/448, EPICS)

(Univ. of Texas at Austin, New Mexico State Univ., Los Alamos)

Spokesmen: C. L. Morris (Los Alamos) and G. R. Burleson (New Mexico State Univ.)

The systematics of pion double-charge-exchange (DCX) reactions are starting to emerge. The (π^+,π^-) reactions exciting discrete double-analog and nonanalog transitions are the subject of intense study at EPICS. It has long been hoped[1] that these reactions could be used to probe nucleon correlations inside the nucleus.

The EPICS spectrometer was modified by this collaboration, as shown schematically in Fig. 1, to enable (π^+,π^-) experimentation at near-forward angles. The DCX data acquired here show systematic trends as functions of target isospin and mass and of incident pion kinetic energy.

Excitation functions for two T = 0,1 isotopic pairs, ^{16,18}O and ^{24,26}Mg, have been measured across the (3,3) resonance, as shown in Figs. 2 and 3. The transitions to the double-isobaric analog state (DIAS) of the T = 1 nuclei are practically identical in shape, differing only by a scale factor. The nonanalog ground-state (g.s.) transitions from the T = 0 nuclei also exhibit similar structures, although the resemblance is not as strong as for the DIAS.

Angular distributions at 292-MeV incident pion energy were measured for the DIAS from ^{18}O and ^{26}Mg.

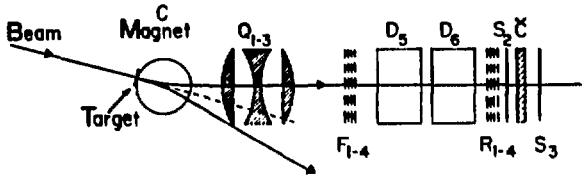

Fig. 1.
Schematic plan view of the small-angle DCX setup at EPICS.

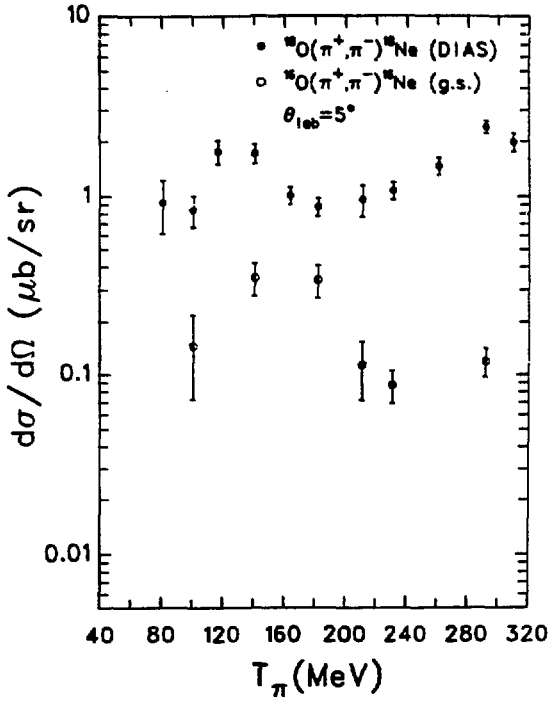

Fig. 2.
Excitation functions for the g.s. transitions in the reactions $^{16,18}O(\pi^+,\pi^-)^{16,18}Ne$.

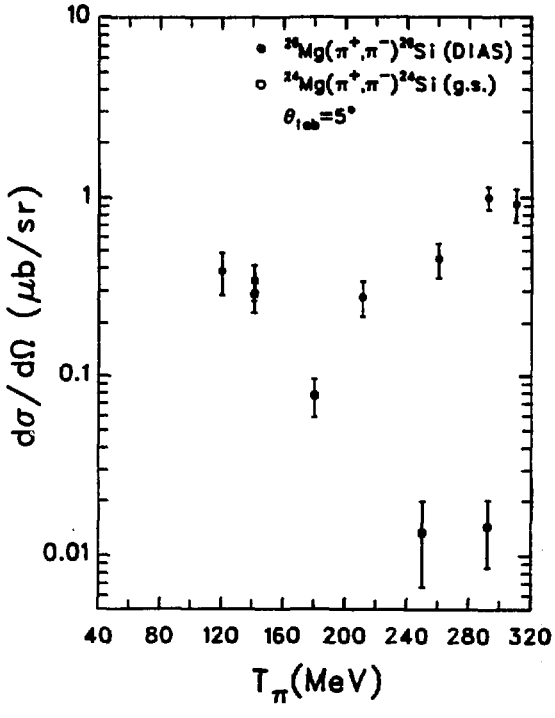

Fig. 3.
Excitation functions for the g.s. transitions in the reactions $^{24,26}Mg(\pi^+,\pi^-)^{24,26}Si$.

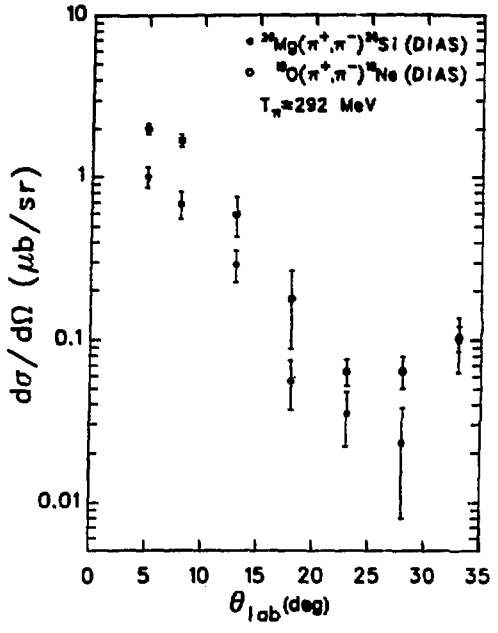

Fig. 4.
DIAS angular distributions at 292 MeV from DCX on ^{18}O and ^{26}Mg.

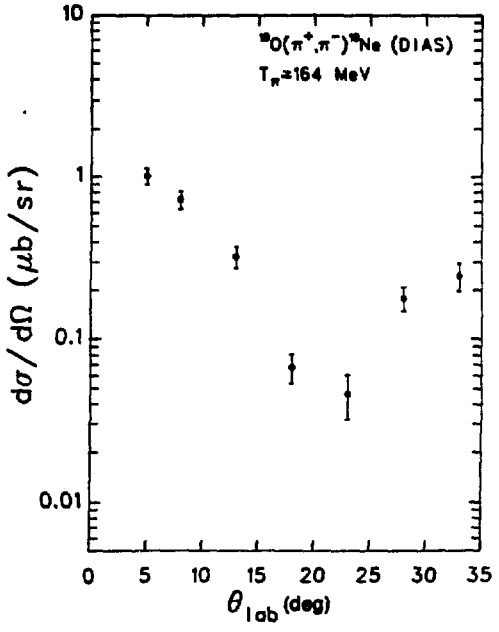

Fig. 5.
DIAS angular distribution at 164 MeV from DCX on ^{18}O.

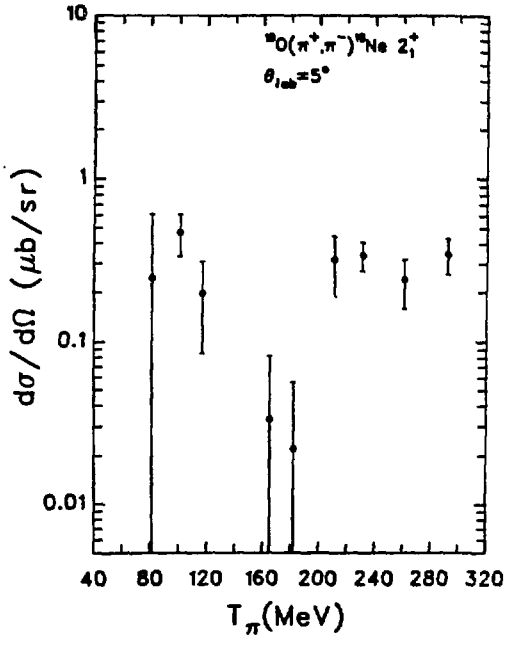

Fig. 6.
Excitation function for the 2_1^+, 1.89-MeV state from DCX on ^{18}O.

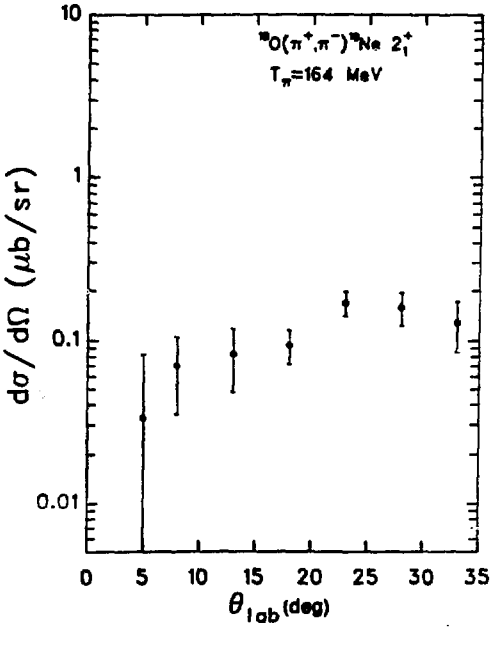

Fig. 7.
The 2_1^+ state angular distribution at 164 MeV from DCX on ^{18}O.

Figure 4 shows these distributions, which are remarkably similar in shape through the forward region and which seem to differ mostly by only a scale factor. The positions of the first minimum are consistent with the diffractive scattering of a strongly absorbed probe from these nuclei, with strong-absorption radii consistent with radii determined from electron scattering. This characterization does not hold at 164 MeV. As shown in Fig. 5, the ^{18}O, 164-MeV angular distribution has a first minimum near 21°, which in a strong-absorption diffractive model would place the 0.1 nuclear density point at a radius of 5.7 F, in disagreement with the electron-scattering value of ~3.6 F.

The 2_1^+ first-excited state in the reaction $^{18}O(\pi^+,\pi^-)^{18}Ne$ was observed. Figures 6 and 7 are the excitation function and angular distribution, respectively, for this state. The angular distribution is similar to simple $\ell = 2$ transition shapes.

The cross section as a function of nucleon number A has been determined, with some qualification, over a limited range; Fig. 8 shows 5° cross sections as a function of A. Notice, in this limited mass range, that the data may be grouped into three families, as shown in the figure. The solid line is a calculation from the semiclassical theory of Mikkel Johnson[2] that has been normalized to the ^{18}O point. This supports the $A^{-10/3}$ dependence predicted for the DIAS in that simple theory. Since $N - Z = 2$ for our targets, it is possible there is some $N - Z$ dependence not seen here but which might be observed in DCX on elements of isotopic chains such as ^{42,44,48}Ca or ^{116,118,120}Sn. Figure 9 shows an $A^{-10/3}$ fit to three DIAS points at 292 MeV. The scaling mentioned for the excitation functions and angular distributions are consistent with this $A^{-10/3}$ scaling.

Efforts to understand these data have proceeded mainly through analysis of the ^{18}O data. A phenomenological parameterization in terms of a second-order optical potential, as described by M. B. Johnson and E. R. Siciliano,[2] is being developed. A qualitative picture,[3] which is consistent with the ^{16,18}O excitation functions and the ^{18}O angular distributions, has been proposed. Two amplitudes are proposed for the transition to the DIAS: (1) a double isobaric analog transition (DIAT) amplitude connecting the initial (parent) state with the DIAS through the intermediate isobaric analog state (IAS), and (2) a non-DIAT amplitude connecting initial and final states through non-IAS intermediate states.

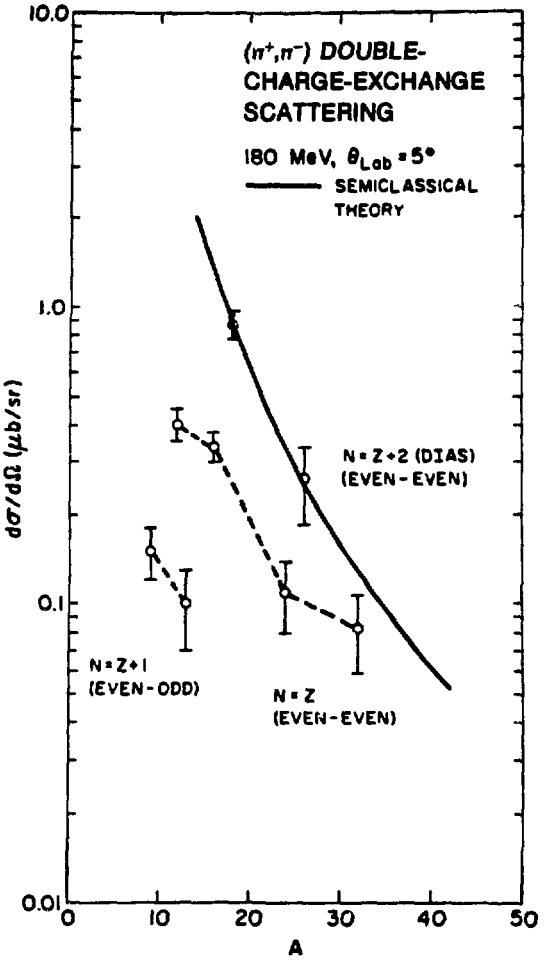

Fig. 8.
Cross sections at 5° and 180 MeV for DCX on various nuclei, as a function of nucleon number A.

The present state of the extant data and theory suggests that more experimental work is needed to pin down and/or separate reaction mechanism and nuclear structure effects in DCX and to form the basis for additional LAMPF proposals.

REFERENCES

1. T. E. O. Ericson, in "Proc. of the 1963 Int. Conf. on High-Energy Physics and Nuclear Structure," CERN report 63-28 (1963); and G. A. Miller and J. E. Spencer, Los Alamos Scientific Laboratory report LA-5948-MS (1975).

2. M. B. Johnson, in "Proc. of the LAMPF Workshop on Pion Single Charge Exchange," Los Alamos Scientific Laboratory report LA-7892-C, 342 (1979); and M. B. Johnson and E. R. Siciliano, to be published.

3. S. J. Greene, D. B. Holtkamp, W. B. Cottingame, C. F. Moore, G. R. Burleson, C. L. Morris, H. A. Thiessen, and H. T. Fortune, to be published.

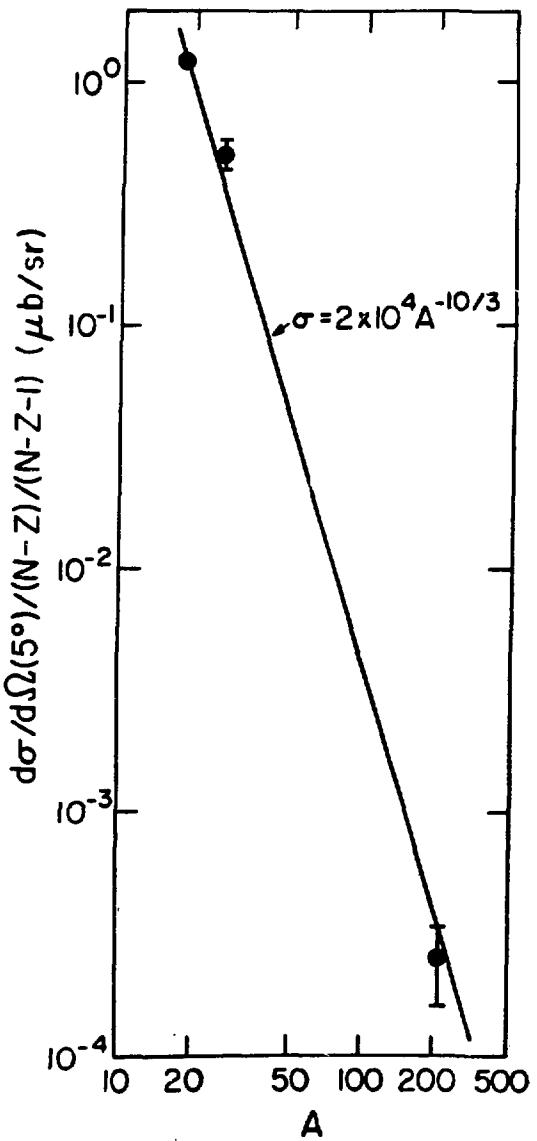

Fig. 9.
Cross sections at 5° and 292 MeV for DCX on various nuclei, as a function of nucleon number A.

Investigation of the Structure of ^{16}O with Pion Inelastic Scattering
(Exp. 570, EPICS)

(Univ. of Minnesota, Univ. of Pennsylvania, Los Alamos, New Mexico State Univ.)
Spokesmen: D. Holtkamp (Univ. of Minnesota) and H. T. Fortune (Univ. of Pennsylvania)

This experiment ran successfully in April 1981 (Cycle 29) and was the first to use the new cooled-gas target system, which performed above all expectations. Angular distributions were measured between 18 and 90° for both elastic and inelastic scattering.

One of the aims of the experiment was to investigate the amount of isospin mixing in the 2^- and 3^- levels near 13-MeV excitation. Figure 1 compares π^+ and π^- spectra at a laboratory scattering angle of 30°. The inhibition of the cross section for the 12.53-MeV 2^-, $T = 0$ state in the π^- spectrum relative to that in the π^+ data indicates appreciable isospin mixing. Quantitative results for this mixing must await further analysis.

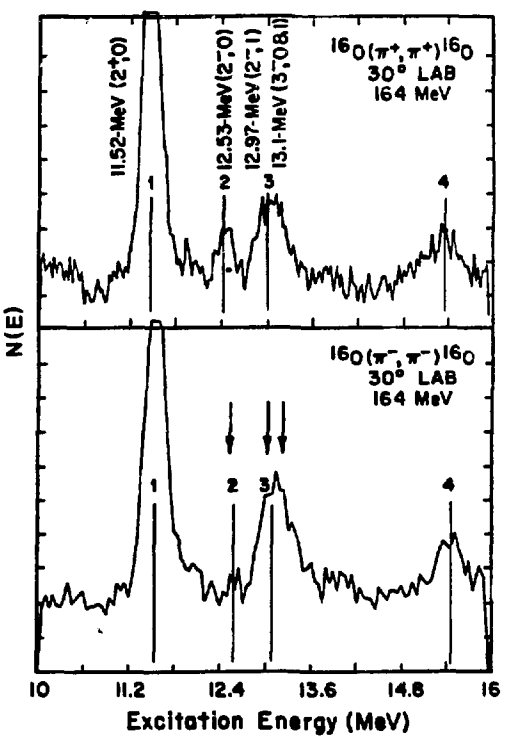

Fig. 1.
Spectra for π^+ and π^- scattering on ^{16}O at an incident energy of 164 MeV.

Elastic and Inelastic Scattering of 547-MeV Polarized Protons from ^{13}C (Exp. 580, EPICS)

(Univ. of Minnesota, Los Alamos)

Spokesmen: S. J. Seestrom-Morris (Los Alamos) and D. Dehnhard (Univ. of Minnesota)

In October 1980, Exp. 580 ran for approximately one-half of the time allotted by the Program Advisory Committee (PAC). During this time cross sections and analyzing powers were measured for 547-MeV proton scattering to states in ^{13}C up to 15-MeV excitation energy from $\theta_L = 6.5$ to 34.5°. Figure 1 shows a typical missing-mass histogram. The energy resolution (FWHM) is about 120 keV. All data tapes have been replayed and angular distributions (with preliminary normalization) have been extracted. Figure 2 shows the angular distribution and Fig. 3 the analyzing power for elastic scattering. The solid curve in Fig. 2 is the optical-model fit obtained with the fitting code RELOM. So far we have not been able to obtain satisfactory fits to the cross section and analyzing power simultaneously and the analysis is continuing.

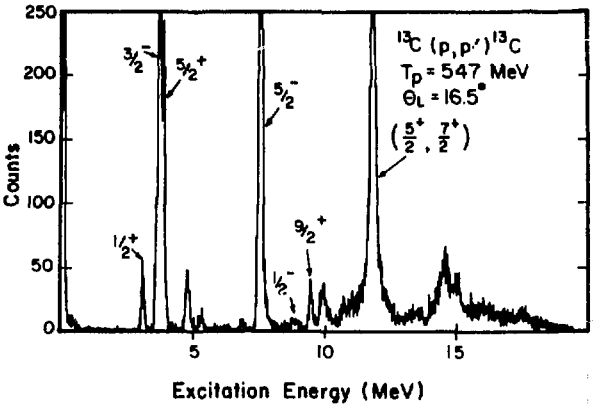

Fig. 1.
Missing-mass histogram for scattering of 547-MeV protons on ^{13}C.

The optical potential, which fits the elastic differential cross sections reasonably well, has been used to generate distorted waves in a microscopic calculation for several

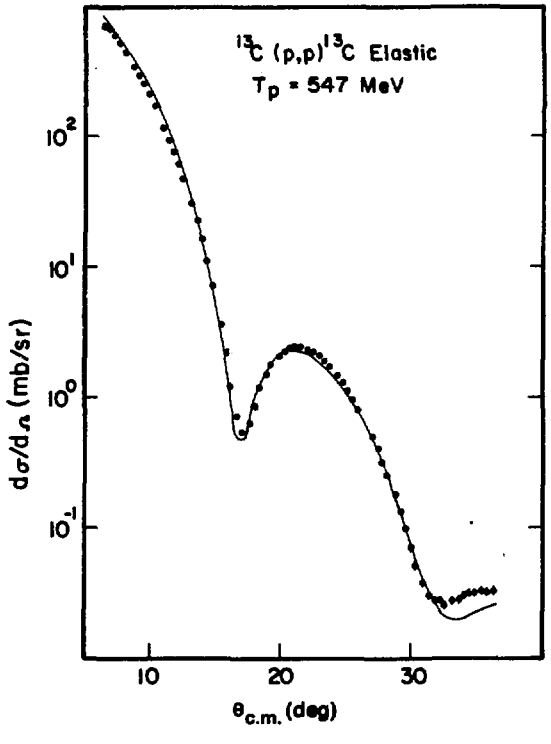

Fig. 2.
Angular distribution for elastic scattering.

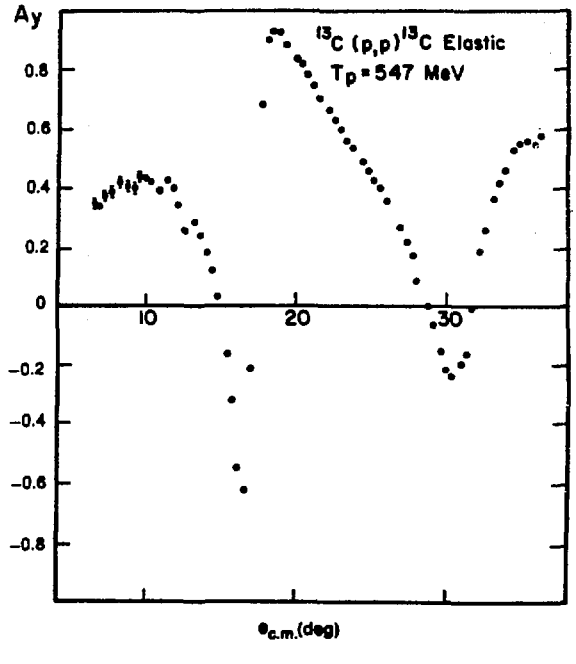

Fig. 3.
Analyzing power for elastic scattering.

inelastic transitions using the code DWBA-70 and the effective nucleon-nucleon interaction of Love and Franey.[1] Calculations were done for the $(\frac{1}{2})^+$ (3.09-MeV) and $(\frac{9}{2})^+$ (9.50-MeV) states. The data for the transition to the $(\frac{9}{2})^+$ state, along with the calculation, are shown in Fig. 4.

For the $(\frac{9}{2})^+$ state the calculations reproduce the shape of the data quite well, but they are larger than the data by a factor of $\simeq 2$ at the maximum of the angular distribution. This effect was also seen in a comparison of microscopic calculations* with the 800-MeV (p,p′) data of Blanpied.** The distorted wave impulse approximation (DWIA) cross sections for pion inelastic scattering to this state are also larger than the data,[2] but by a smaller amount.

In contrast to the reasonable agreement between the data and microscopic calculations for the 9.50-MeV state for both (p,p′) and (π,π′), we find large differences between theory and experiment for the $(\frac{1}{2})^+$ state This discrepancy exists for proton scattering at the energy of this experiment and at 800 MeV as well as for π^+ scattering at 162 MeV. The consistent disagreement for all probes indicates that the problem lies in the wave function rather than the reaction mechanism.

*M. A. Franey, private communication.

**G. S. Blanpied, private communication.

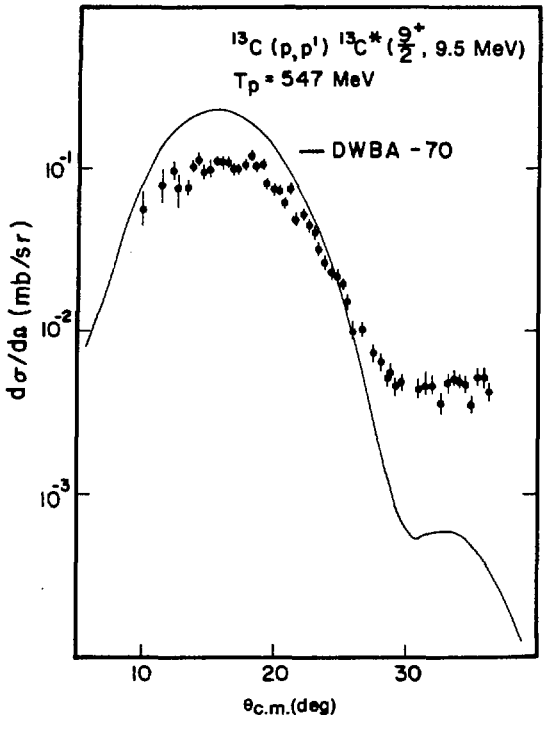

Fig. 4.
Angular distribution to the $(\frac{9}{2})^+$ state in ^{13}C. The solid curve is a microscopic calculation using DWBA-70.

REFERENCES

1. W. G. Love and M. A. Franey, to be published in Phys. Rev. C.

2. S. J. Seestrom-Morris, to be published in Phys. Rev. C.; and Ph.D. thesis, University of Minnesota (1981).

Subthreshold Kaon Production (Exp. 651, EPICS)

(Los Alamos, Univ. of Texas at Austin)
Spokesman: C. L. Morris (Los Alamos)

We have used EPICS to search for subthreshold kaon production with 800-MeV protons. The experiment was run with ~100 nA of 40-ns chopped H^- beam stripped into Area A. We attempted to identify the 236-MeV/c muons arising from decays of kaons stopped in the A-1 production target by their time delay with respect to prompt muons arising from pion decays. Muons were identified by (1) differentially absorbing incident pions before the spectrometer, (2) measuring time of flight (TOF) through the spectrometer, (3) using a threshold Cerenkov counter to eliminate electrons in the spectrometer focal plane, and (4) selecting momentum of the degraded muon beam.

The results of one 4-h run are shown in Fig. 1. We measured no delayed muons while counting $\sim 1.5 \times 10^6$ prompt muons. When the branching ratio and an estimate of the stopping probability are included, we reach an upper limit for the angle-averaged differential cross section for kaon production of $d\sigma/d\Omega \approx 10$ pb/sr.

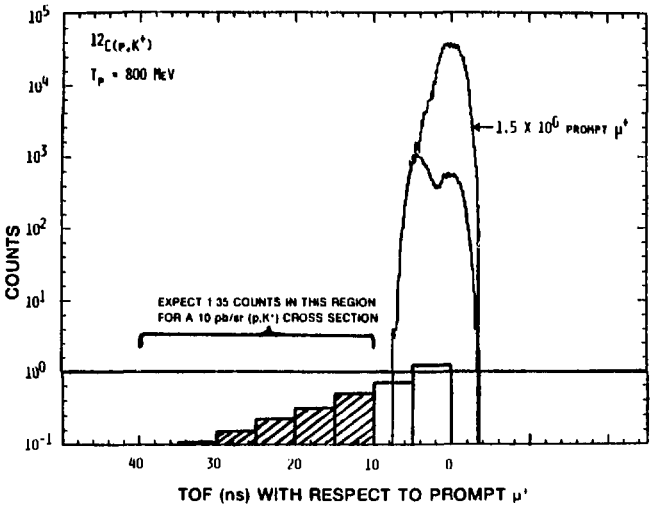

Fig. 1.
Muon time spectrum with respect to the accelerator rf. The expected time distribution for muons arising from kaon decays is shown by the solid line.

Large-Angle $\vec{p}$ + ^{208}Pb Elastic Scattering at 800 MeV (Exp. 355, HRS)

(Univ. of Texas at Austin, Los Alamos, Univ. of California at Los Angeles, Rutgers Univ., Univ. of South Carolina)
Spokesman: G. W. Hoffmann (Univ. of Texas)

The availability of high-quality 800-MeV $\vec{p}$ + nucleus elastic differential cross section and analyzing power data has made possible a number of detailed, systematic studies of the adequacy of microscopic descriptions of intermediate-energy proton-nucleus scattering. Although the results obtained so far are encouraging, calculations using no adjustable parameters have yet to be successful.

One of the difficulties encountered in previous work was the inability to compute, from first principles, analyzing powers that were in quantitative agreement with experiment, even at the very forward angles. Speculation on the reasons for this difficulty centered on the possible lack of accurate knowledge of key amplitudes needed for the calculations; it was argued that the needed amplitudes could not be determined from nucleon-nucleon data because a complete set of such data did not exist at relevant energies.

Thus, most of the reported analyses of the 800-MeV $\vec{p}$ + nucleus elastic $A_y(\theta)$ data used an empirical amplitude for the isospin-averaged spin-dependent part of the nucleon-nucleon interaction. This Gaussian amplitude was adjusted, from nucleus to nucleus, to obtain a best fit to the analyzing power data. Nonetheless, even with the additional degree of flexibility provided, the analyzing powers computed with the empirical Gaussian amplitudes were not in good quantitative agreement with experiment. An examination of the fits to data for target nuclei ranging from ^{12}C to ^{208}Pb reveals significant systematic differences between computed and experimental values. These discrepancies, which exist at both small and large angles, are disturbing and form part of the motivation for Exp. 355. To provide more and better quality data for the investigation of the 800-MeV $\vec{p}$ + ^{208}Pb elastic analyzing power, data were remeasured with improved statistical accuracy and extended to center-of-mass scattering angles >32°.

The new data were presented in the last progress report. We have performed a considerable amount of additional theoretical work to explore the sensitivity of the predicted analyzing powers to the various ingredients of the theory.

We find that when the electromagnetic one-photon-exchange contribution to the proton-proton spin-orbit amplitude, as well as the target-nucleon correlation contributions to the second-order optical potential, are properly taken into account, a better description of the

data results from impulse approximation predictions that use nucleon-nucleon amplitudes obtained from phase-shift analysis of nucleon-nucleon data. Figure 1 compares the data with the "best" theoretical result (solid curve) to date. The effect of the electromagnetic spin-orbit contribution on the analyzing power prediction is seen by comparing the solid and dashed curves. The differences between the two curves are surprising. Including the electromagnetic contribution shifts the angular positions of the maxima and minima in the predicted analyzing power into alignment with the data at all forward angles where previous calculations have failed. The data for angles <8° are now qualitatively reproduced by the parameter-free prediction. There is still not enough structure predicted between 8 and 20°, but at least the diffractive pattern is now in alignment with the data. The leveling off of the analyzing power envelope at a value of 0.65 for angles >20° is correctly predicted by the best microscopic calculation.

We have also investigated the sensitivity of the predicted analyzing power to N-N amplitude uncertainties and to second-order correlation contributions and have found these sensitivities to be significant. These uncertainties could possibly account for the remaining discrepancy between the best microscopic prediction and the data.

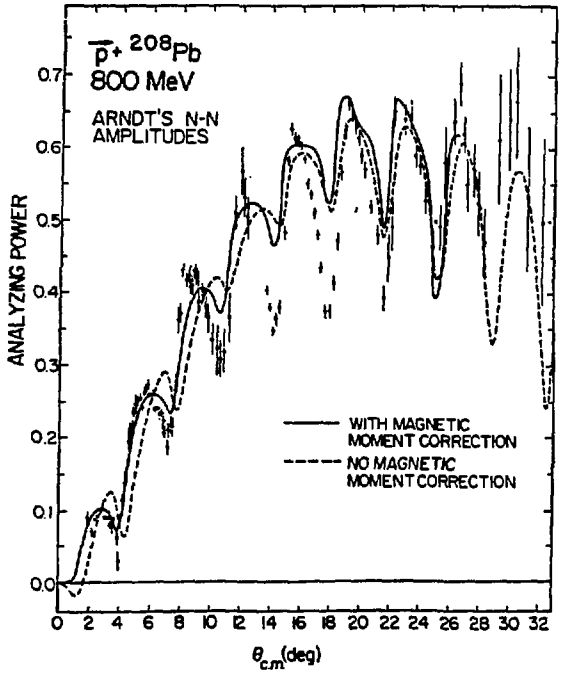

Fig. 1.
The analyzing power data for 800-MeV $\vec{p}$ + ^{208}Pb elastic scattering are compared to Kerman-McManus-Thaler predictions obtained using nucleon-nucleon amplitudes from phase-shift analysis of nucleon-nucleon data. The effect of the one-photon-exchange contribution to the electromagnetic spin-orbit amplitude is seen by comparing the solid and dashed curves.

Excitation of Simple States in 800-MeV Inclusive Scattering (Exp. 356, HRS)

(Univ. of Georgia, Rutgers Univ., Univ. of California at Los Angeles, Los Alamos, Oregon State Univ., Univ. of Texas at Austin)
Spokesmen: C. Glashausser (Rutgers Univ.) and F. T. Baker and A. Scott (Univ. of Georgia)

The ^{90,92}Zr($\vec{p}$,p') Reactions

Angular distributions of differential cross sections and analyzing powers have been measured for elastic and inelastic scattering of 800-MeV protons from ^{90}Zr and ^{92}Zr. The data, acquired in 0.3° steps for the angular range 2-20°, were obtained using the HRS. Excited states for which data have been obtained are the 2^+ (2.18-MeV), 5^-, 3^-, 4^+, 2^+ (3.31-MeV), 6^+, and 8^+ states for ^{90}Zr and the 2^+ (0.93-MeV), 4^+, 2^+ (1.83-MeV), 3^-, and 5^- states for ^{92}Zr. The data for elastic scattering were well fitted using an optical potential previously determined[1] for 800-MeV proton elastic scattering from ^{90}Zr; the fits for ^{92}Zr are shown in Fig. 1. Data for inelastic scattering to collective 3^- and 5^- states are virtually identical for the two nuclei. Collective-model distorted wave Born approximation (DWBA) analyses provide excellent fits to these data and, particularly from the fits to the analyzing power data, strongly indicate the need for deforming the spin-orbit potential. An example of this is shown in Fig. 2 where the dashed curves are with no spin-orbit deformation and the solid curves include a full Thomas deformation with the same deformation parameter as for the central potential. Significant differences have been observed for excitation of the less collective first 2^+ and 4^+ states. The data for the 4^+ states are compared to collective-model DWBA predictions in Figs. 3 and 4. Although microscopic model analyses of these data have not yet been completed, a

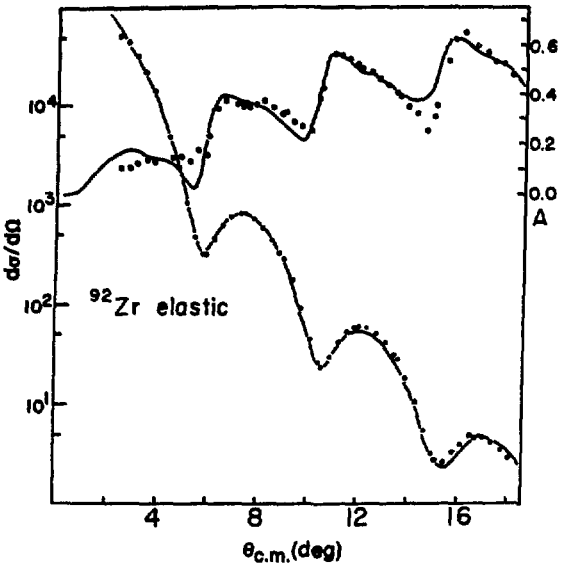

Fig. 1.
Optical-model fits for ^{92}Zr elastic scattering.

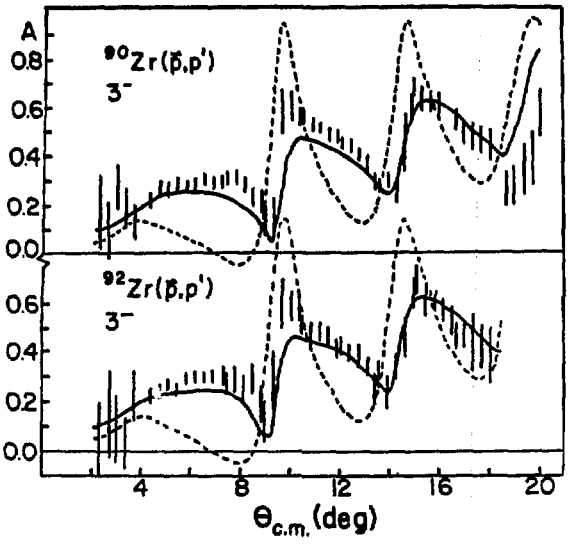

Fig. 2.
Analyzing power fits, where the dashed curves are with no spin-orbit deformation and the solid curves include a spin-orbit deformation.

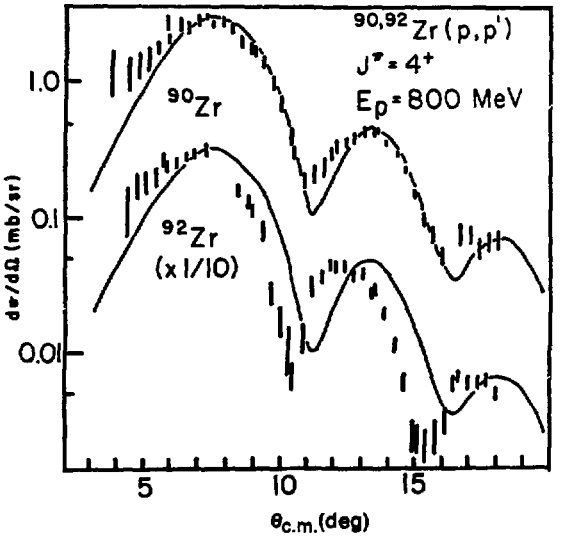

Fig. 3.
Collective-model DWBA predictions for the cross sections to 4^+ states.

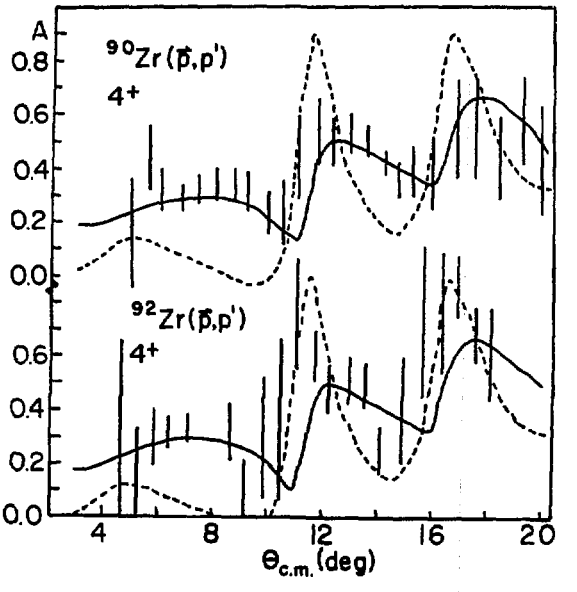

Fig. 4.
Collective-model DWBA predictions for the analyzing power to 4^+ states.

possible origin of these differences would be the differences in the microscopic structure of these states; it is generally assumed that the dominant configurations of these $J = 2,4$ states are $(\pi g_{9/2})^2$ for ^{90}Zr and $(\nu d_{5/2})^2$ for ^{92}Zr. We therefore expect that microscopic model impulse approximation analyses of these data will yield interesting results concerning the sensitivity of intermediate-energy proton scattering to the microscopic nature of the states excited.

The $^{18}O(\vec{p},p')^{18}O$ Reaction

The inelastic scattering of 800-MeV polarized protons from ^{18}O has been measured in the same experiment. Angular distributions of $d\sigma/d\Omega$ and A_y were obtained for strong states up to about 8 MeV of excitation over the angular range 5-19° (c.m.). The $d\sigma/d\Omega$ and A_y data for the 1.98-MeV 2^+ state are shifted in angle relative to distorted wave impulse approximation (DWIA) predictions; the shift is similar to that observed for ^{92}Zr. This shift is larger for the 3.92-MeV 2^+ state. The data for the 1^- state at 4.45 MeV are in complete disagreement with this calculation; in fact, they are similar to the data for the 5.09-MeV 3^- state. This indicates a failure also of simple semiclassical models that predict the shape of the inelastic cross section from the shape of the elastic cross section.[1] A microscopic analysis of these results will be attempted. Preliminary coupled-channels calculations based on the rotational model for the 0^+, 2^+ (1.98-MeV), and 4^+ (7.12-MeV) states yield reasonable agreement with both $d\sigma/d\Omega$ and A_y provided β_4 is large. This is the first observation of significant channel-coupling effects in A_y at intermediate energy. We also expect to extract from these data relative neutron radii for ^{18}O and ^{16}O as well as the ratio of neutron to proton transition matrix elements for the 2_1^+ to 0_1^+ transition.

REFERENCE

1. R. D. Amado et al., Phys. Rev. C22, 2094 (1980).

$\vec{p}$ + Nucleus Elastic Scattering at 500 MeV (Exps. 425/433, HRS)

(Univ. of Texas at Austin, Northwestern Univ.)
Spokesmen: G. W. Hoffmann (Univ. of Texas) and K. K. Seth (Northwestern Univ.)

In this experiment we obtained high-quality elastic-scattering differential cross section and analyzing power data for 500-MeV $\vec{p}$ + ^{1}H, ^{12}C, ^{40,48}Ca, ^{90}Zr, and ^{208}Pb over the laboratory angular range 5-30°. The HRS was moved in 1.5° steps and sufficient elastic data were obtained to get 1% statistical uncertainty for 0.2° angular binning at most angles. The beam energy (496.5 ± 0.2 MeV) and absolute scattering angle (~0.03°) were determined by looking at the kinematic limit of the $p + p \rightarrow d + \pi$ reaction in conjunction with a high-precision crossover technique involving the 4.4-MeV state of ^{12}C and p + p elastic scattering.

This experiment was done to provide data at an energy where the nucleon-nucleon (N-N) amplitudes are supposedly known and the use of the impulse approximation is believed valid. Thus, it is hoped that analysis of these data will not be hampered by uncertainties in the key amplitudes needed by the theory so that a rigorous test of theory can be made.

Shown in Fig. 1(a)-(d) are preliminary versions of the data, along with Kerman-McManus-Thaler (KMT) predictions, obtained using the 500-MeV amplitudes recently obtained by Arndt and VerWest.[1] As seen from these figures, the theoretical curves do not reproduce much of the data, especially at small momentum transfers. A similar, but not as serious, problem exists at 800 MeV for the analyzing power when phase-shift amplitudes are used. Although no extensive theoretical analysis has yet been made at 500 MeV, it is clear that serious problems exist.

Another very disturbing problem is that the neutron-proton rms radius differences (Δr_{np}) obtained from the preliminary 500-MeV analysis are about 0.1 F smaller than the corresponding values obtained at 800 MeV, again using phase-shift amplitudes. Thus, an energy dependence is seen for Δr_{np} when using KMT and nucleon-nucleon amplitudes obtained from a consistent (global) phase-shift analysis of N-N data. The results at 500 and 800 MeV suggest that our use of the impulse approximation must be reevaluated.

REFERENCE

1. R. A. Arndt and B. VerWest, "N-N Scattering Analyses Below 850 MeV: A Status Report," U.S. Department of Energy report DOE-ER-05223-29 (August 1980).

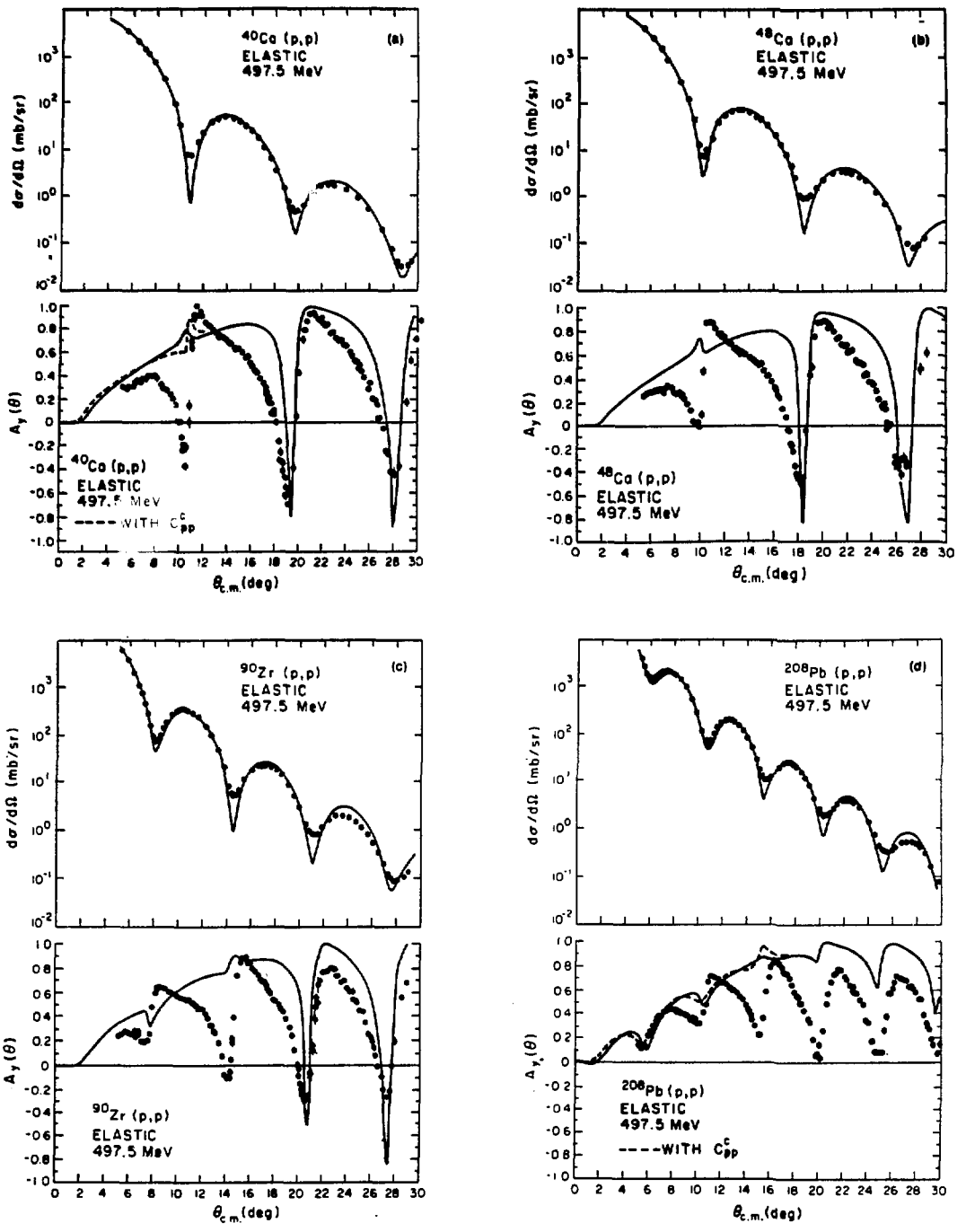

Fig. 1(a)-(d).

Elastic differential cross section and analyzing power data for 800-MeV (a) $\vec{p}$ + ^{40}Ca, (b) $\vec{p}$ + ^{48}Ca, (c) $\vec{p}$ + ^{90}Zr, and (d) $\vec{p}$ + ^{208}Pb are compared to KMT results obtained using the impulse approximation and nucleon-nucleon amplitudes determined from phase-shift analysis of nucleon-nucleon data (Ref. 1).

Measurement of Spin-Flip Probabilities in Proton Inelastic Scattering at 800 MeV and Search for Collective Spin-Flip Modes, Preliminary Survey (Exp. 411, HRS)

(Los Alamos, Univ. of Minnesota, Rutgers Univ.)
Spokesmen: N. M. Hintz (Univ. of Minnesota) and J. M. Moss (Los Alamos)

Experiment 411 received most of its allotted time in two runs, at 400 MeV during Cycle 28 and 500 MeV during Cycle 29. The 500-MeV run was used to measure the spin-flip probability (SFP) for unnatural parity states in ^{16}O; these data have not yet been analyzed. The 400-MeV run was used to measure the SFP for states in ^{12}C between 7- and 22-MeV excitation energy. A limited amount of data was also taken on ^{208}Pb at 400 MeV.

Replay of the 400-MeV data is complete and analysis in terms of the distorted wave impulse approximation (DWIA) is under way. Figure 1 shows the SFP for the 15.11-MeV 1^+ state of ^{12}C along with a DWIA calculation using the Franey-Love interaction in conjunction with the Cohen-Kurath wave functions. Qualitatively, the calculation is in agreement with experiment. As is expected for unnatural parity states the SFP is large at all angles. At larger momentum transfer there is obviously some divergence between theory and experiment. The possible reasons for this are currently under investigation.

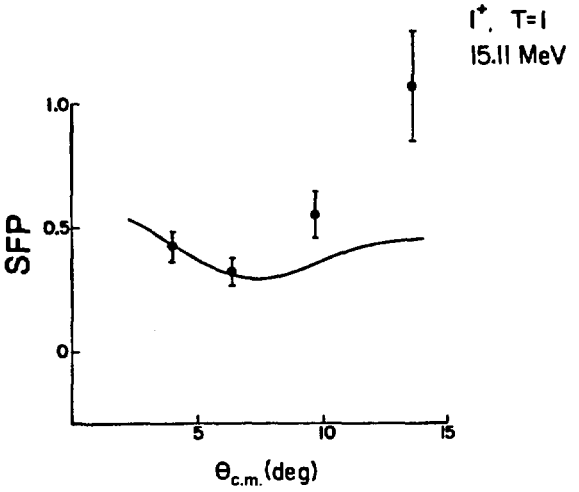

Fig. 1.
The SFP for the $^{12}C(p,p')^{12}C$ reaction at $E_p = 400$ MeV, exciting the 15.11-MeV 1^+ state.

Other states of interest, whose SFPs have been obtained at 900 MeV, include 1^+, T = 0, 12.71 MeV; 2^+, T = 1, 16.11 MeV; and the multiples of 2^- and 4^- states between 18 and 19.5 MeV. Thus, the data from this experiment, when fully analyzed, should give a good overview of the physics explored by the SFP at intermediate energies.

The $^{12}C(\vec{p},p')^{12}C$ Reaction at 400, 600, and 700 MeV (Exp. 432, HRS)

(Rutgers Univ., Los Alamos, Saclay, Univ. of Minnesota, Univ. of California at Los Angeles, Univ. of Georgia, Univ. of Pittsburgh)
Spokesmen: C. Glashausser (Rutgers Univ.) and J. Moss (Los Alamos)

Differential cross sections and analyzing powers for the $^{12}C(\vec{p},p')^{12}C$ reaction have been measured for incident proton energies of 400, 600, and 700 MeV. Results were obtained for states up to about 21 MeV in excitation over the momentum transfer range from 0.3 to about 2.1 F^{-1}. Of primary interest are the data for the 12.71-MeV, 1^+, T = 0 and the 15.11-MeV, 1^+, T = 1 states; these test the spin-dependent terms in the effective N-N interaction. An enhanced tensor term in the T = 1 channel might be evidence for pion precursors.

Our preliminary cross sections at the three energies reveal almost no energy dependence in shape or absolute cross section between 400 and 800 MeV for either state. In agreement with previous results,[1] no evidence for significant precursor effects is observed. Analyzing powers at these energies are also similar, but different for the two states. Preliminary data at 400 MeV are shown in Fig. 1, together with distorted wave impulse approximation (DWIA) predictions, which use a free N-N interaction based on a fit to N-N phase shifts. The similarity between the 400- and 800-MeV data also is reasonably well explained by the DWIA despite the fact that the contributions of individual terms in the N-N interaction change significantly with energy. The energy independence noted for these states is in sharp contrast to the strong energy dependence observed for natural parity states. It seems to preclude strong two-step contributions to the 1^+ excitations.

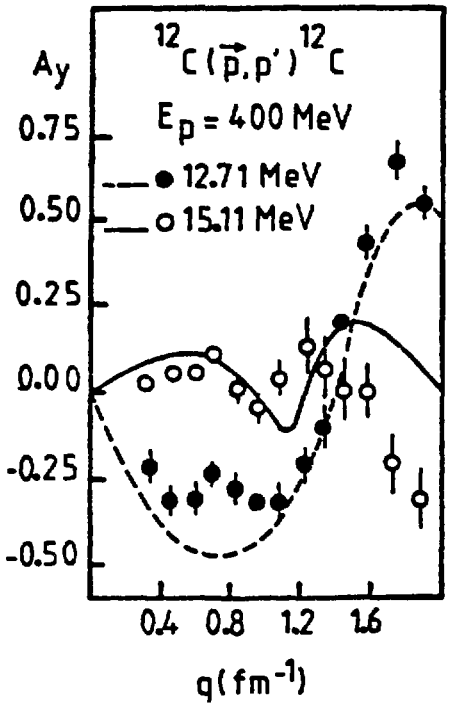

Fig. 1.
Preliminary data at 400 MeV together with DWIA predictions.

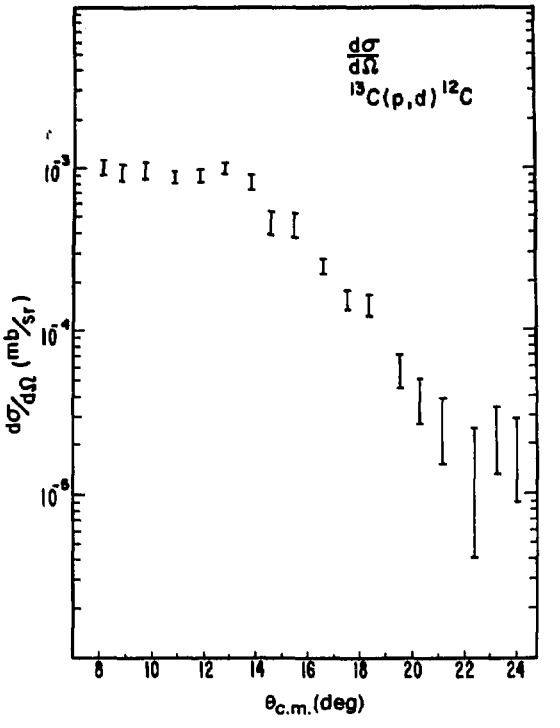

Fig. 1.
Cross section to the ground state for the $^{13}C(p,d)^{12}C$ reaction at an incident proton energy of 530 MeV.

REFERENCE

1. J. R. Comfort and W. G. Love, Phys. Rev. Lett. **44**, 1656 (1980); M. Haji-Sacid et al., Phys. Rev. Lett. **45**, 880 (1980); and J.-L. Escudie et al., to be published.

The (p,d) Reaction on ^{7}Li, ^{12}C, ^{13}C, and ^{28}Si (Exp. 438, HRS)

(Univ. of California at Los Angeles, Univ. of Minnesota)
Spokesman: C. A. Whitten, Jr. (Univ. of California at Los Angeles)

We have measured scattering cross section and analyzing power in the (p,d) reaction for the ground state and excited states in ^{7}Li (530 MeV), ^{12}C (500 MeV), ^{13}C (530 MeV), and ^{28}Si (450 MeV). The experiment covered a range of laboratory angles from 6-22°. The analyzing power measurements indicate a great deal of structure, in contrast to the nearly featureless cross sections. Exact finite-range distorted wave Born approximation calculations, which include contributions from the deuteron D state, are currently under way. Figures 1 and 2 show

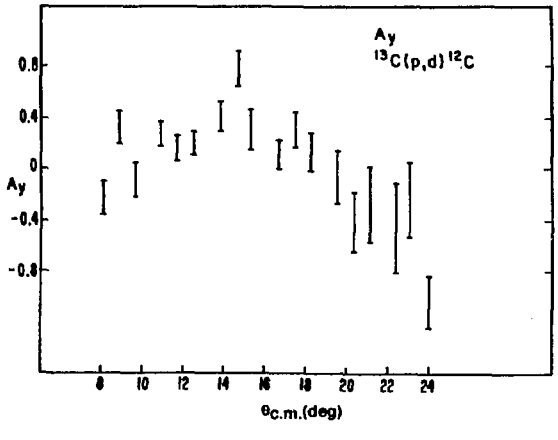

Fig. 2.
Analyzing power for the ground-state transition in the $^{13}C(p,d)^{12}C$ reaction.

the scattering cross section and analyzing power for the ground-state transition of $^{13}C(p,d)^{12}C$.

Giant Resonances with 800-MeV Protons (Exp. 473, HRS)

(Los Alamos, Massachusetts Institute of Technology, Univ. of Minnesota)

Spokesmen: J. M. Moss and T. A. Carey (Los Alamos) and G. S. Adams (Massachusetts Institute of Technology)

Experiment 473 received its allotment of time, with polarized beam during Cycle 28 and with unpolarized beam during Cycle 29. The primary objectives of these experiments were to search for giant resonances with $\ell > 3$ and to map out the A dependence of the newly discovered high-energy octupole giant resonance (HEOR).

Spectra of high statistical accuracy obtained for ^{116}Sn over a broad angular range and over a smaller angular range for ^{208}Pb show no evidence of any $\ell = 5$ strength in the region of the HEOR. This is in apparent disagreement with 480-MeV alpha-scattering data from Saclay.[1] Furthermore, we can find no evidence for the excitation of a $\Delta T = 0$ giant dipole resonance reported last year by a group at Julich[2] using 780-MeV alpha scattering. At present the reasons for these apparently conflicting results are not known.

The survey of the systematics of the HEOR included the new targets ^{53}Ni, ^{144}Sm, ^{148}Sm, and ^{152}Sm. Figure 1 shows the current energy systematics from our data and recent ^{3}He scattering data from Osaka.[3]

One of the main objectives of the survey run was to determine the effect of permanent deformation on the structure of the HEOR. The data on the samarium isotopes, which span the onset of deformation, definitely show a broadening for deformed ^{103}Sm. The analysis is not yet complete enough to make more quantitative statements.

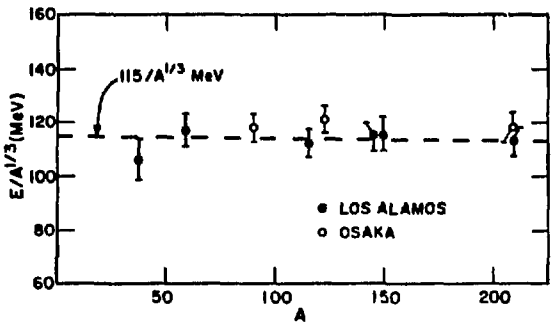

Fig. 1.
Energy systematics of the high-energy octupole giant resonance.

Search for the (p,p′) Process Leading to π-Atomic States (Exp. 556, HRS)

(Massachusetts Institute of Technology, Los Alamos, Univ. of Texas, Univ. of California at Los Angeles)

Spokesman: W. Bertozzi (Massachusetts Institute of Technology)

At HRS we observed proton scattering from ^{17}O and aluminum in an attempt to detect the direct production of pions into bound atomic states. At 750-MeV incident proton energy we detected scattered protons at 12 and 4°. We also examined the region of 140-MeV energy loss for evidence of the scattering peak that would reveal the production of this bound final state.

Preliminary analysis of 12° data indicates the cross section for the analog transition $^{17}O(p,p')\pi^- \otimes {}^{17}F$ leading to an atomic pion is <0.5 μb/sr with 95% confidence. This estimate is about one-half the value obtained by using a simple single-particle calculation that includes the effects of pion absorption and repulsion.[1]

A more sensitive analysis of these data will lower this upper limit and may reveal the effect. Analysis of aluminum will follow the completion of the oxygen analysis.

REFERENCES

1. B. Bonin et al., postdeadline abstract at the Int. Conf. on Nuclear Physics, Berkeley, California, August 24-30, 1980.

2. H. P. Marsh et al., Phys. Rev. Lett. 45, 337 (1980).

3. Y. Yagamata et al., Phys. Rev. C23, 937 (1981).

1. "Upper Limit on Direct Production of Pions into Atomic States via Proton-Nucleus Scattering at 800 MeV," Bull. Am. Phys. Soc. 26, 606 (1981).

Measurement of the Angular Distribution of Tensor Polarization in Pion-Deuteron Elastic Scattering (Exp. 483, LEP)

(Argonne, Los Alamos, Indiana Univ., Univ. of Illinois)
Spokesman: R. J. Holt (Argonne)

We have measured an angular distribution of the recoil deuteron tensor polarization* t_{20} in π^+-d elastic scattering.[1] A schematic diagram of the experimental arrangement is shown in Fig. 1. In this experiment a 142-MeV π^+ beam with an intensity of 2×10^8 π^+/s and a 2% full-width momentum spread was obtained from the LEP channel and directed onto a CD_2 target. Deuterons emitted from the target were focused into a polarimeter by a quadrupole doublet, and scattered pions were detected by a plastic scintillator array. Measurements were taken at recoil deuteron laboratory angles of 17.5, 28.9, and 40.9°, corresponding to pion-scattering angles in the center-of-mass frame of 144.8, 121.9, and 97.8°, respectively. The basic features of the polarimeter are similar to those described in Ref. 2, where the ^{3}He(d,p)^{4}He reaction was used as the analyzer for the tensor polarization t_{20}. The polarimeter used in the present work, however, was designed to operate at deuteron energies as low as 27 MeV, substantially lower than the polarimeter described in Ref. 2. The efficiency ε, defined as the ratio of the number of detected ^{3}He(d,p)^{4}He events to the number of incident deuterons, is the quantity obtained from the polarimeter. The efficiency for a polarized beam depends on the efficiency ε_0 for an unpolarized beam, the polarimeter analyzing power T_{20}, and the deuteron polarization t_{20}, according to the relation

$$\varepsilon = \varepsilon_0(1 + T_{20}t_{20}) \quad .$$

The quantities ε_0 and T_{20} were measured in a separate experiment using the polarized deuteron beam at the Berkeley 88-in. cyclotron. Results from Exp. 483 are shown in Fig. 2, along with the measurement at $\theta_d = 0°$ from Ref. 3 and the most recent theoretical predictions.[4-6]

All the predictions shown in Fig. 2 are relativistic three-body calculations, which include the effects of the true pion-absorption channel except for the dashed curve

*The polarization moment t_{20} describes the population of the m = 0 spin substate of the deuteron beam. The polarization is defined according to the Madison Convention as given in Ref. 1.

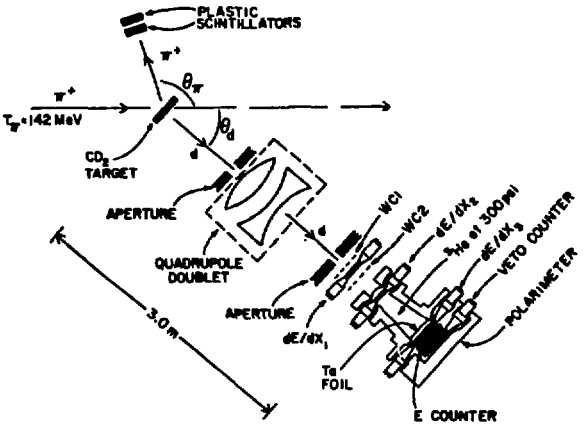

Fig. 1.
Schematic diagram of the experimental arrangement at LAMPF.

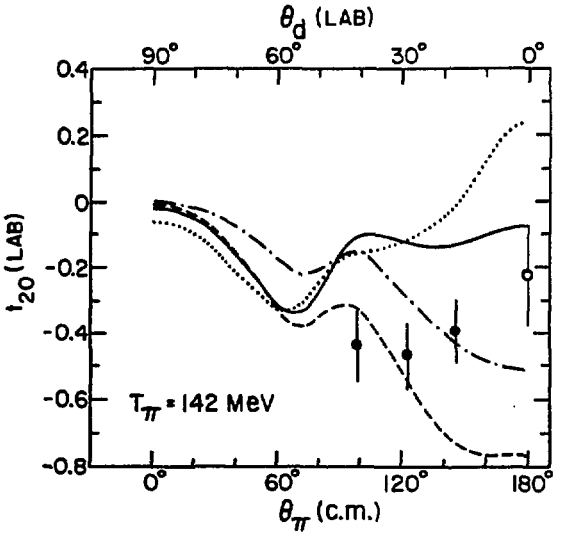

Fig. 2.
Angular distribution of t_{20} at T_π = 142 MeV. The open-circle data point is from Ref. 3 and the solid circles are from the present experiment. The dashed curve represents a calculation from Ref. 4, which does not include pion absorption. The dotted, solid, and dashed-dot curves represent calculations from Refs. 4, 5, and 6, respectively, which include absorption.

where absorption is not included. The major difference between the calculations is the manner in which absorption is treated. Absorption is described in a somewhat microscopic manner in Refs. 4 and 5 in that the results depend explicitly on the πNN, $\pi N\Delta$, ρNN, and $\rho N\Delta$ coupling constants. Fayard et al.[5] also include the P_{11} nonpole amplitude in the πN part of the interaction. It is the P_{11} πN or ρN amplitude that dominates the absorption process. In a more phenomenological approach, Betz and Lee[6] obtain an effective interaction potential to describe the $NN \rightarrow N\Delta$ transition. As we might expect, these three theories, which treat the effects of absorption differently, give rise to three very different predictions of t_{20} near $\theta_\pi = 180°$, where absorption has the largest effect.

One remarkable feature of the calculations is that near $\theta_\pi = 90°$ the three predictions are in agreement. This agreement is predicted, however, by the single-scattering impulse approximation, which indicates that near $\theta_\pi = 90°$, sensitivity of t_{20} to both the πN amplitude and the deuteron wave function is greatly diminished. In all three calculations the effect, near 90°, of including the absorption channel is to increase t_{20}, which worsens the disagreement with the datum at $\theta_\pi = 98°$. Thus, it is expected that whereas improving the description of the absorption channel may bring the empirical and theoretical values into better agreement at large angles, it will not yield the measured value of t_{20} at 98°.

We note that all three of these calculations have omitted the effects of a possible dibaryon resonance. Phase-shift analyses[7] of NN scattering data have indicated that these resonances have large inelasticities. In the energy region $T_\pi \sim 140$ MeV it has been suggested that a $^1D_2$ dibaryon resonance may be excited in πd scattering. Kubodera et al.[8] have estimated the effect that the reported[9] dibaryon resonances would have on the πd scattering amplitudes. They found that these resonances, because of large values of spin and orbital angular momenta ($^{2S+1}L_J = {}^1D_2, {}^3F_3, {}^1G_4$), can produce oscillations in the angular dependence of the polarization observables. Moreover, Bolger et al.[10] have measured the angular dependence of the vector polarization at T_π = 142 and 256 MeV. At 256 MeV oscillations were found and were consistent with the existence of a $^3F_3$ dibaryon resonance, whereas at 142 MeV no oscillations were found. These vector polarization data indicate that either the $^1D_2$ dibaryon resonance does not exist or that the resonance occurs predominantly in the $\ell = 1$ partial wave. To test the notion that the discrepancy between the measured values and predicted values of t_{20} at 98° might be due to the $^1D_2$ dibaryon resonance, a calculation was performed in the same manner as that of Kubodera et al.[8] A parameter, which is discussed in detail (as ε) in Ref. 8, represents the relative amount of coupling to $\ell = j + 1$ and $\ell = j - 1$, where j is the total angular momentum in πd scattering. If this parameter is assigned the value of –0.5, then the inclusion of the $^1D_2$ dibaryon resonance not only gives good agreement with the observed vector analyzing power but also produces more negative values of t_{20}. In this example, t_{20} changes by 0.1 if the $^1D_2$ resonance is included. Although this simple calculation does not remove the present discrepancy, the indication is that the inclusion of a dibaryon resonance into a more sophisticated calculation, which includes the absorption channel, should lead to better agreement with the present experiment. Presently, it is not known what other physical phenomena would have the same effect.

Clearly, further theoretical development will be necessary to account for the present results. If, indeed, the dibaryon resonances are responsible for the discrepancy, then a knowledge of the energy dependence of t_{20} would be useful to further define the effect.

This research was performed under the auspices of the United States Department of Energy and the National Science Foundation.

REFERENCES

1. *Polarization Phenomena in Nuclear Reactions*, Eds., H. H. Barschall and W. Haeberli (University of Wisconsin Press, Madison, Wisconsin, 1971), p. XXV.

2. E. J. Stephenson, R. J. Holt, J. R. Specht, J. D. Moses, R. L. Burman, G. D. Crocker, J. S. Frank, M. J. Leitch, and R. M. Laszewski, Nucl. Instrum. Methods 178, 345 (1980).

3. R. J. Holt, J. R. Specht, E. J. Stephenson, B. Zeidman, R. L. Burman, J. S. Frank, M. J. Leitch, J. D. Moses, M. A. Yates, R. M. Laszewski, and R. P. Redwine, Phys. Rev. Lett. 43, 1229 (1979).

4. A. S. Rinat, E. Hammel, Y. Stark, and A. W. Thomas, Nucl. Phys. A329, 285 (1979).

5. C. Fayard, G. H. Lamot, and T. Mizutani, Phys. Rev. Lett. 45, 524 (1980).

6. M. Betz and T. S.-H. Lee, Phys. Rev. C23, 375 (1981).

7. N. Hoshizaki, Prog. Theor. Phys. 61, 129 (1979).

8. K. Kubodera, M. P. Locher, F. Myhrer, and A. W. Thomas, J. Phys. G: 6, 171 (1980).

9. I. P. Auer, A. Beretvas, E. Colton, H. Halpern, D. Hill, K. Nield, B. Sandler, H. Spinka, G. Theodosiou, D. Underwood, Y. Watanabe, and A. Yokosawa, Phys. Rev. Lett. 41, 1436 (1978).

10. J. Bolger, E. Boschitz, G. Pröbstle, G. R. Smith, S. Mango, F. Vogler, R. R. Johnson, and J. Arvieux, Phys. Rev. Lett. 46, 167 (1981).

Study of the $^{14}C(\pi^+,\pi^0)^{14}N$ Reaction (Exp. 523, LEP)

(Los Alamos, Univ. of North Carolina, Tel Aviv Univ., Univ. of Neuchâtel, Univ. of Colorado, Indiana Univ.)
Spokesmen: C. D. Goodman (Indiana Univ.) and H. W. Baer (Los Alamos)

Data were obtained at a beam energy of 164 MeV and at 0 and 20° settings of the π^0 spectrometer. We used the much improved ^{14}C targets (designed for use in EPICS experiments) consisting of thin-windowed cells into which the ^{14}C powder was pressed. No organic binder was used as in the previous target design; consequently, the measured π^0 spectra contain much less ^{12}C and ^{16}O contamination. Figure 1 shows one of the measured spectra having a resolution of ≃3.5 MeV (FWHM). Also shown for comparison is the $^{13}C(\pi^+,\pi^0)$ spectrum measured in the same data-taking sequence. From these data we have determined preliminary values of the 5° differential cross section for the $^{14}C(\pi^+,\pi^0)^{14}N$ isobaric analog state (IAS) reaction,

$$\sigma(^{14}C, 5°) = 2.7 \pm 0.5 \text{ mb/sr} \quad ,$$

and the $^{14}C/^{13}C$ ratio of the 5° IAS differential cross sections,

$$\sigma(^{14}C, 5°)/\sigma(^{13}C, 5°) = 1.54 \pm 0.23 \quad .$$

The latter value is quite close to the ratio $2(14/13)^{4/3} = 1.8$ expected from the eikonal model of Johnson.[1]

The $^{14}C(\pi^+,\pi^0)^{14}N$ IAS measurement with the π^0 spectrometer constitutes one part of a complete set of

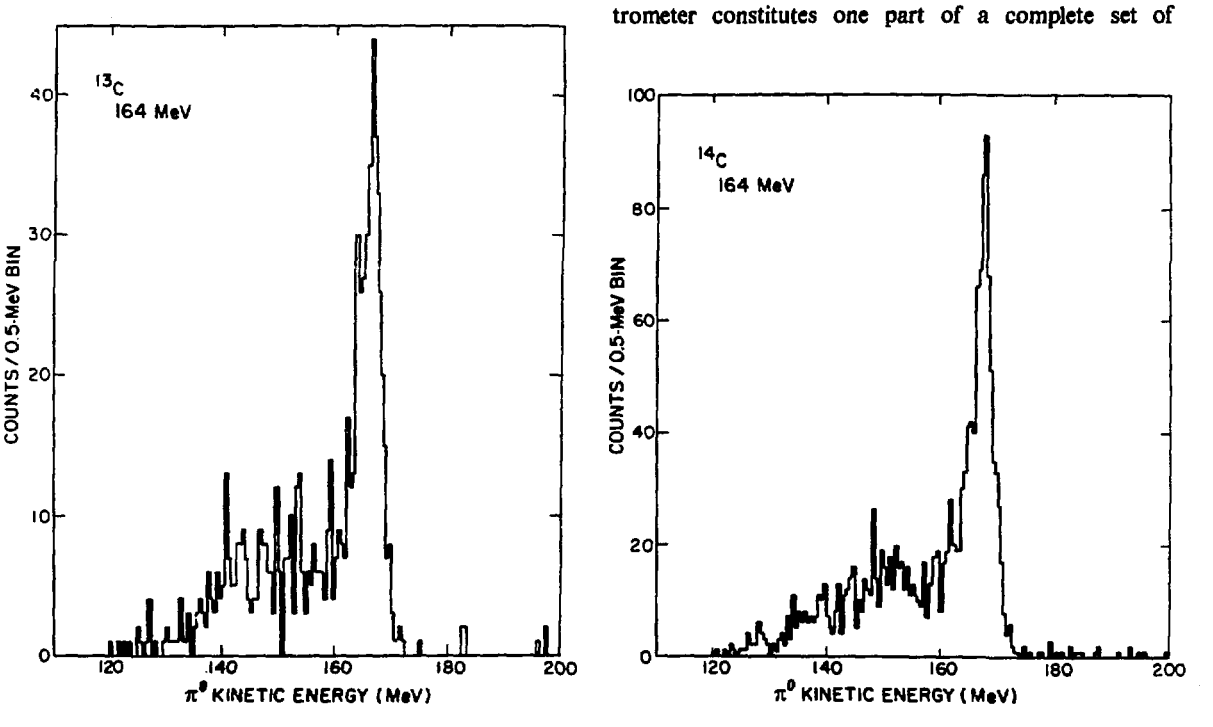

Fig. 1.
Spectra for the $^{13,14}C(\pi^+,\pi^0)$ reaction at 164 MeV measured in March 1981. The angular acceptance is 0-12°.

measurements at 164 MeV related through isospin invariance of π^+ and π^- elastic scattering, single-charge-exchange scattering to the analog state, and double-charge-exchange scattering to the double analog state. The elastic-scattering experiments are now complete and the double-charge-exchange experiment is an approved experiment for EPICS.

REFERENCE

1. M. Johnson, in Clinton P. Anderson Meson Physics Facility Workshop on Pion Single Charge Exchange, Los Alamos, New Mexico, 1979, Eds., H. Baer, J. D. Bowman, and M. Johnson (unpublished), p. 343; Los Alamos Scientific Laboratory report LA-7892-C (1979); and M. B. Johnson, Phys. Rev. C22, 192 (1980).

Measurement of the $^{15}N(\pi^+,\pi^0)^{15}O$ Isobaric Analog State Reaction (Exp. 401, LEP)

(Los Alamos, Case Western Reserve Univ., Tel Aviv Univ.)

Spokesmen: M. D. Cooper and J. D. Bowman (Los Alamos)

The data necessary for constructing angular distributions for $^{15}N(\pi^+,\pi^0)^{15}O$ isobaric analog states (IASs) have been acquired at 50 and 164 MeV, which are two contrasting regions of the pion-nucleus interaction. At 164 MeV the pion is strongly absorbed because of the presence of the 3-3 resonance, and the diffractive character of the interaction dominates the angular distribution. Preliminary analysis of the data, covering the angular region from 0-85°, shows at least one diffractive minimum. At 50 MeV the pion is weakly interacting and fewer partial waves can contribute to the cross section. Furthermore, the s- and p-wave pion-nuclear partial waves have a strong cancellation that produces a minimum in the 0° elementary cross section for charge exchange. Hence, the 50-MeV angular distribution is expected to have simpler structure but be harder to measure.

The observation of the IAS transition at 50 MeV was in question because of the difficulty we had in seeing the exploratory data runs in 1979. The IAS was observed at all angles between 0 and 150°, though it was a shoulder on the side of the continuum charge exchange at some angles. Figure 1 demonstrates clear observation of the IAS at 50 MeV and 40°. Other features of the spectrum are the small background from foils and air above the

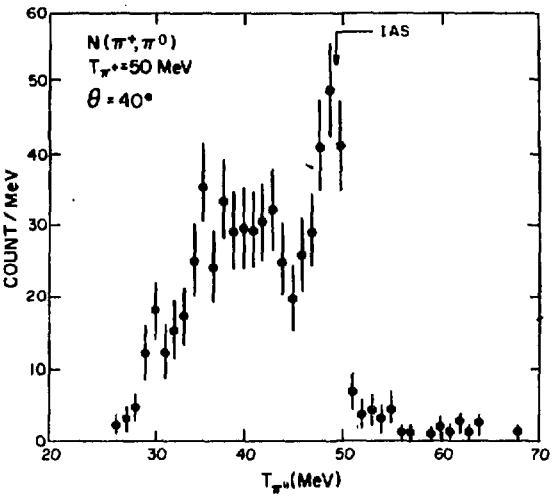

Fig. 1.
The $^{15}N(\pi^+,\pi^0)$ spectrum for 50-MeV π^+ and 40° π^0's. The IAS appears at the expected energy.

IAS, the continuum charge exchange below the IAS, and the falling spectrometer acceptance between 50 and 30 MeV. The IAS peak corresponds to a cross section of 16 ± 8 μb/sr, and the points in this angular distribution correspond to the smallest cross sections measured with the π^0 spectrometer. The details of the shape and a more precise normalization await further analysis. No published theoretical predictions for the IAS reaction at 50 MeV exist.

Study of Isovector Terms in π-Nucleus Interactions with (π^+,π^0) Reactions on $^{40,42,44,48}Ca$ and $^{112,118,124}Sn$ (Exp. 524, LEP)

(Los Alamos, Univ. of North Carolina, Tel Aviv Univ., Oak Ridge, Univ. of Neuchâtel)

Spokesmen: H. Baer, J. D. Bowman, and F. H. Cverna (Los Alamos)

The study of isobaric analog state (IAS) transitions has been completed at one energy, 180 MeV. The new $^{42,44}Ca$ data have increased the statistics on the IAS peaks by a factor of 10 and have clarified the problem of line broadening in the earlier low-statistics ^{42}Ca data. The spectra for all four isotopes measured at a 0° setting of the π^0 spectrometer are shown in Fig. 1. The IASs are clearly visible at the expected π^0 kinetic energy of 180

MeV, and the line widths for the three IASs are nearly equal. When the full data sample is analyzed, the relative error in the 0° IAS differential cross sections is expected to be about 10%. The largest contribution to the error is

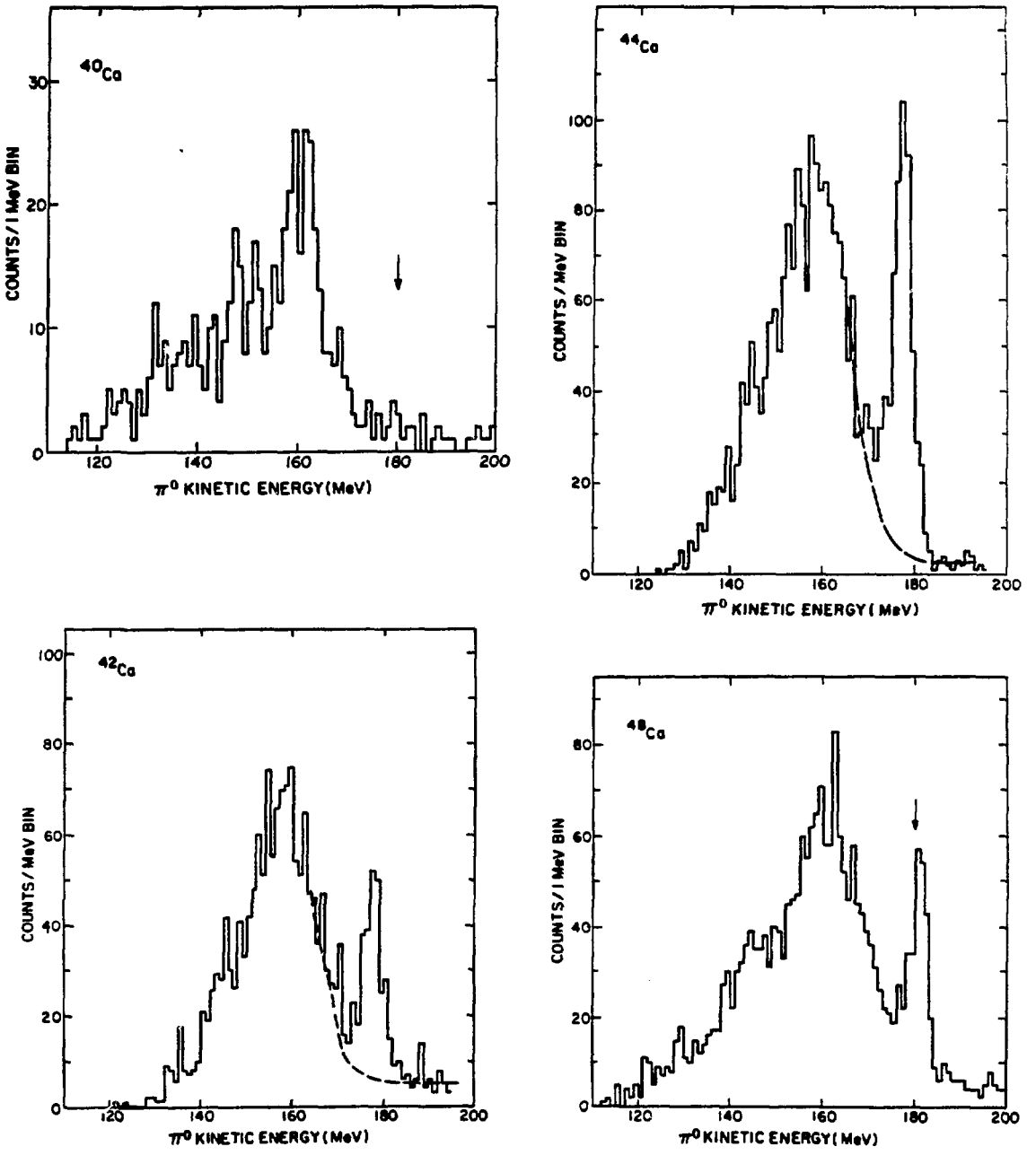

Fig. 1.
Spectra of the (π^+,π^0) reaction at 180 MeV on calcium isotopes. The angular acceptance is 0-14°. The arrows mark the expected position of the IASs.

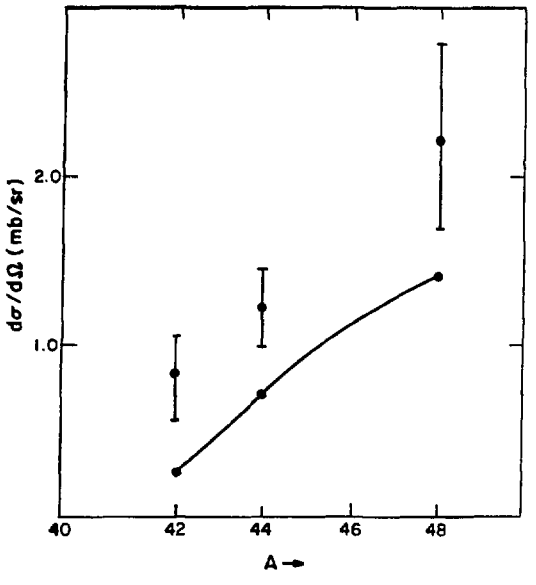

Fig. 2.
Preliminary values of the 0° IAS cross sections on calcium isotopes. The curve is the result of an eikonal model analysis of Germond and Johnson, which gave an excellent fit to the elastic π^+ and π^- data.*

in the estimation of the background shape underneath the IAS peaks.

Preliminary values of the 0° cross sections are shown in Fig. 2. The trend of increasing cross sections with increasing neutron number is reproduced quite well by the calculations of Germond and Johnson.* These calculations were performed in the first-order eikonal model using neutron and proton density distributions given by Negele's Hartree-Fock calculations.[1] The parameters of this model were adjusted to give excellent fits to π^+ and π^- elastic scattering at 180 MeV. However, the charge-exchange cross sections are low by a factor of ~2. This discrepancy is not unique to the eikonal model calculations, but also exists in comparisons with first-order optical-potential calculations performed by Siciliano.** Thus, the underestimation of single-charge-exchange cross sections by the various theoretical treatments continues to be a problem.

*This curve was supplied by Mikkel Johnson, Los Alamos National Laboratory Group MP-DO.

**Calculations are by E. Siciliano, Los Alamos National Laboratory Group MP-DO.

REFERENCE

1. J. W. Negele and D. Vautherin, Phys. Rev. C5, 1472 (1972), and Phys. Rev. C11, 1031 (1975).

Measurement of the $^3He(\pi^-,\pi^0)$ Reaction at T_π = 200 MeV (Exp. 284, LEP)

(Tel Aviv Univ., Los Alamos, Univ. of Virginia)
Spokesmen: M. D. Cooper and R. H. Heffner (Los Alamos)

Pion charge-exchange data on ^{3}He were acquired at $T_\pi = 200$ MeV using the LAMPF π^0 spectrometer and a liquid ^{3}He target. An angular distribution from 0-80° (laboratory) was taken in 3 days, with another 1-1/2 days devoted to background and target-thickness studies.

The data have been analyzed using the standard π^0 spectrometer computer programs. The normalization comes from a calibration of the solid angle by measurement of the $p(\pi^-,\pi^0)n$ reaction, whose cross section is known from phase shifts. The analog state cross section was separated from continuum charge exchange by fitting the excitation spectra with the sum of three components: a monoenergetic line shape, a continuum, and a flat background. The fit was found by maximizing the likelihood function

$$\mathcal{L} = \prod_i e^{-f_i} \frac{f_i^{k_i}}{k_i!} ,$$

where i is the channel number in the spectrum, k_i is the number of counts in channel i, and f_i is the predicted number of counts in channel i. The likelihood method was used to preserve the correspondence between the number of counts in the spectrum and the fit.

Figure 1 shows the excitation spectra as a function of angle. The decompositions of the spectra into components are plotted as solid lines and the arrows locate the energy of a π^0 from nucleon charge exchange. The spectra are corrected for spectrometer acceptance. Presently, there is no theory of the shape of the continuum.

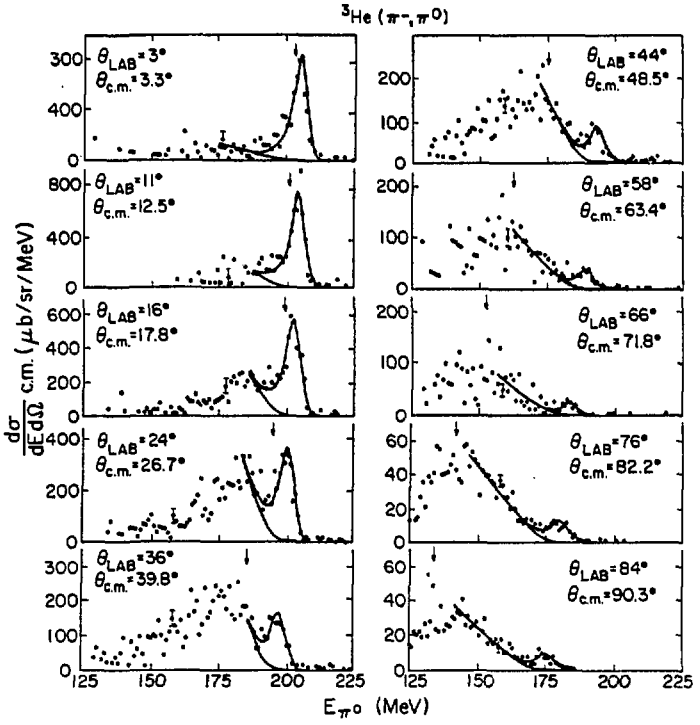

Fig. 1.

The double differential cross section for ^{3}He charge exchange is depicted vs energy and angle. A typical statistical error is shown in each panel. The fits to the analog state above the continuum background are shown by the solid curves. The arrow locates the energy appropriate for the free $p(\pi^-,\pi^0)n$ reaction.

The angular distribution for the analog state is shown in Fig. 2 along with the recoil data of Källne et al.[1] The cross section would have to have some rapid variations near 90° for the two experiments to be consistent. Together, the two experiments provide the first complete angular distribution for pion charge exchange on a nucleus. The curves are a Glauber calculation by Gerace et al.,[2] an optical-model calculation by Landau,[3] and a multiple-scattering calculation by Hess and Gibson.*[4] The Glauber calculation appears best, but fails badly in fits to elastic π^- data on ^{3}He. The authors claim that the choice of ^{3}He wave functions is the primary difference among the calculations. All three calculations miss the 0° cross section by 1.5 standard errors.

Figure 3 shows the angular distribution of the energy-integrated cross section for continuum charge exchange on ^{3}He. The solid curve is 1.03 times the free $p(\pi^-,\pi^0)n$ cross section in the ^{3}He center-of-mass system. Pauli blocking of the cross section is observed forward of 40° because no states of <6 MeV in excitation are available for charge exchange.

The short-dashed curve goes smoothly through the data; the long-dashed curve has the analog state added to the short-dashed one. The angular integral from 0-90° of the sum cross section is 1.10 ± 0.14 times that of nucleon charge exchange. This value for the effective number of nucleons involved agrees well with the energy and mass systematics of Ashery et al.[5]

The first angular distributions of pion charge exchange on ^{3}He have yielded an interesting comparison to theoretical calculations, an example of Pauli suppression of forward-angle scattering to the continuum, and a measure of the effective number of nucleons participating in charge exchange.

*B. F. Gibson, private communication (1979).

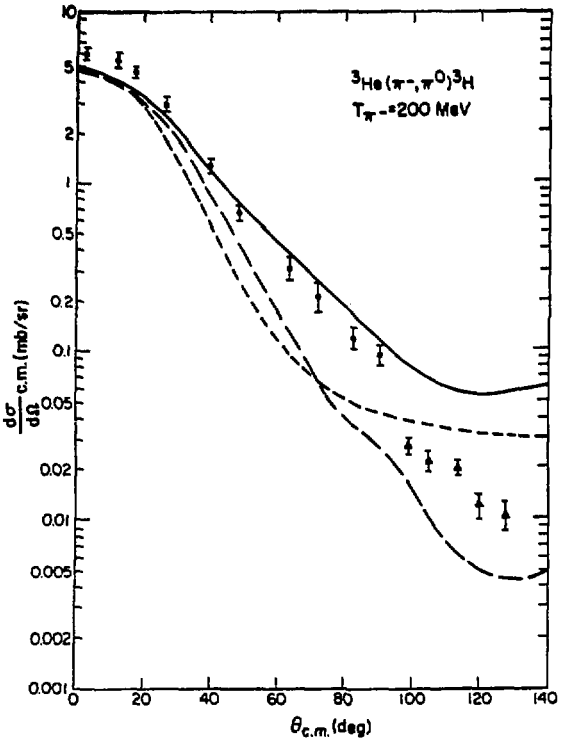

Fig. 2.
Angular distribution for $^3He(\pi^-,\pi^0)^3H$ from the present measurement (circles) and the tritium recoil experiment (triangles) of Källne et al. (Ref. 1). An absolute normalization uncertainty must be added in quadrature to the plotted standard deviations for both the present measurement (10%) and that of Källne et al. (15%). The curves are: solid line, Glauber calculations (Ref. 2); long-dashed line, optical-potential calculations (Ref. 3); and short-dashed line, multiple-scattering calculations (Ref. 4).

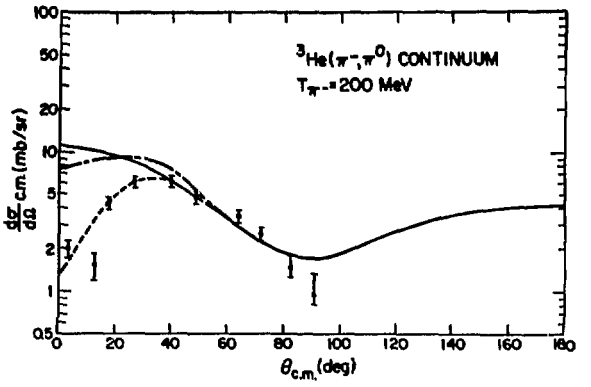

Fig. 3.
Angular distributions for continuum charge exchange from ^{3}He. The solid curve is 1.03 times the $p(\pi^-,\pi^0)n$ cross section in the ^{3}He center-of-mass system. The dashed curve goes smoothly through the data, and the dash-dot curve has the analog state cross section added to the dashed curve.

REFERENCES

1. J. Källne, H. A. Thiessen, C. L. Morris, S. L. Verbeck, M. J. Devereaux, G. R. Burleson, J. S. McCarthy, R. R. Whitney, J. R. Bolger, C. F. Moore, and C. A. Goulding, Phys. Rev. Lett. 42, 159 (1979).

2. W. J. Gerace, J. P. Mestre, J. F. Walker, and D. A. Sparrow, Phys. Rev. C22, 1197 (1980).

3. R. H. Landau, Phys. Rev. C15, 2127 (1977).

4. A. T. Hess and B. F. Gibson, Phys. Rev. C13, 749 (1976).

5. D. Ashery, I. Navon, G. Azuelos, H. K. Walter, H. J. Pfeiffer, and F. W. Schleputz, *Tel Aviv University preprint 836-80 (1980).*

Search for Collective Isovector States in the (π^-,π^0) Reaction on ^{90}Zr

(Exp. 412, LEP)

(Los Alamos, Case Western Reserve Univ., Tel Aviv Univ.)

Spokesmen: H. W. Baer, J. D. Bowman, and F. H. Cverna (Los Alamos)

Excitation of Isovector Transitions with Pion Single Charge Exchange on ^{12}C

(Exp. 525, LEP)

(Univ. of North Carolina, Los Alamos, Tel Aviv Univ., Univ. of Neuchâtel)

Spokesmen: N. S. P. King (Los Alamos) and M. Moinester (Tel Aviv Univ.)

Study of Isovector Giant Resonances with Pion Charge Exchange

(Exp. 607, LEP)

(Tel Aviv Univ., Los Alamos)

Spokesmen: J. Alster (Tel Aviv Univ.) and H. W. Baer and J. D. Bowman (Los Alamos)

Approximately 3 weeks of running time were devoted to the study of isovector resonances with the (π^-,π^0) reaction at 164 MeV. This reaction has the selection rule $\Delta T = 1$, thus providing a means of studying isovector excitations without the background of isoscalar excitations. Of primary interest are the giant resonances, because these are general features of nuclear collective motion and because much less is known about the isovector giant resonances than the isoscalar resonances. Our experiments concentrated on the forward-angle charge-exchange scattering (0-30°) to maximize the signal for transitions of multipolarity $\Delta L = 0$ and 1. Specifically, we were interested in the isovector monopole and dipole resonances. For this initial run we used targets from throughout the periodic table: ^2H, ^{12}C, ^{40}Ca, ^{90}Zr, ^{120}Sn, and ^{208}Pb. Each of these targets served a specific purpose in clarifying the nature of charge-exchange scattering to continuum states. For the $T = 0$ targets, ^2H, ^{12}C, and ^{40}Ca, it is useful to measure the charge-symmetric reaction (π^+,π^0) and to compare this to the (π^-,π^0) results for evidence of Coulomb force effects on the continuum. The lightest target, ^2H, was included to give some direct evidence on the extent of final-state interactions. Figure 1 shows a spectrum of the $\pi^+d \rightarrow \pi^0pp$ reaction measured with a CD_2 target at a mean scattering angle of 5°. Because we had ^{12}C data at the same spectrometer setting, we could perform a channel-by-channel subtraction of the ^{12}C in the CD_2 spectrum. The width of the π^0 peak corresponding to the π^0pp three-body final state is approximately 10 MeV (FWHM), and the resolution of the measurement is approximately 5 MeV. Thus, we have a rather dramatic peaking of the light particle spectrum (in a three-particle final state) toward the maximum kinetically allowed energy. To our knowledge this is the first measurement of the π^0 spectrum for this reaction. We expect it to be useful for the study of final-state interactions in charge-exchange scattering on nuclei and for the study of the πNN system.

The ^{12}C and ^{40}Ca targets were included in the study of the giant dipole resonance (GDR) in nuclei, where isospin splitting of the GDR does not broaden in resonance and where we can compare the (π^-,π^0) spectra with (π^+,π^0) spectra to get a better understanding of the continuum. We measured the $^{90}Zr(\pi^-,\pi^0)$ reaction to see

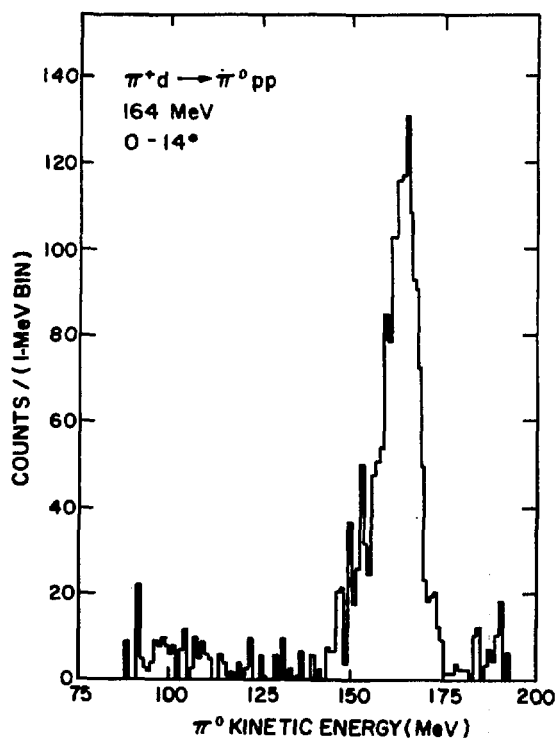

Fig. 1.

Spectrum of π^0's measured with a CD_2 target. The ^{12}C contribution was subtracted using a measured $^{12}C(\pi^+,\pi^0)$ spectrum taken during the same running period.

if the isospin splitting of the GDR could be observed and to look at the monopole state. The $^{120}Sn(\pi^-,\pi^0)$ and $^{208}Pb(\pi^-,\pi^0)$ reactions were measured primarily to search for the monopole resonance.

Because the run was just completed, we do not have a full analysis of the data. Nonetheless, we can give here some indication of the success of the run by presenting preliminary results on the $^{40}Ca(\pi^\pm,\pi^0)$ and $^{120}Sn(\pi^-,\pi^0)$ reactions at 164 MeV.

Search for the Isovector Monopole Resonance

In contrast to higher multipoles, in which the shape of the nucleus varies while maintaining constant interior density, monopole or breathing modes involve periodic compression and expansion of the proton and neutron densities in the interior coupled to oscillations in the distribution of nucleons on the surface. The neutron and proton motions are in phase for isoscalar oscillations and out of phase for isovector oscillations. Recently,[1] we have argued that the isovector monopole should be observable in the (π^-,π^0) reaction. Its characteristic features were predicted to be

- an excitation energy of $120/A^{1/3}$ MeV in the target nucleus, appropriately shifted for Coulomb displacement and mass differences in adjacent nuclei;
- a forward-peaked angular distribution of the form

$$\frac{d\sigma}{d\Omega}(\theta) = \frac{d\sigma}{d\Omega}(0)\, J_0^2(qR) \quad ;$$

and

- a 0° cross section of ~500 μb/sr.

We have searched for such a feature in the (π^-,π^0) charge-exchange reaction at 165 MeV for ^{40}Ca, ^{90}Zr, ^{120}Sn, and ^{208}Pb targets. Figure 2 shows the 3.6 and 10.8° spectra for ^{120}Sn, with the arrows indicating the predicted π^0 energy corresponding to excitation of the isovector monopole resonance. The excess counts in the forward spectrum amount to several hundred microbarns per steradian. The observed peak is consistent with the characteristics predicted for excitation of the isovector monopole resonance. Similar peaks appear in the ^{90}Zr and ^{208}Pb spectra but do not appear in the ^{40}Ca spectra where the excitation energy is large (~42 MeV). At present we are refining our analysis of the data as well as determining whether the interpretation of the observed peak as corresponding to the monopole remains unique.

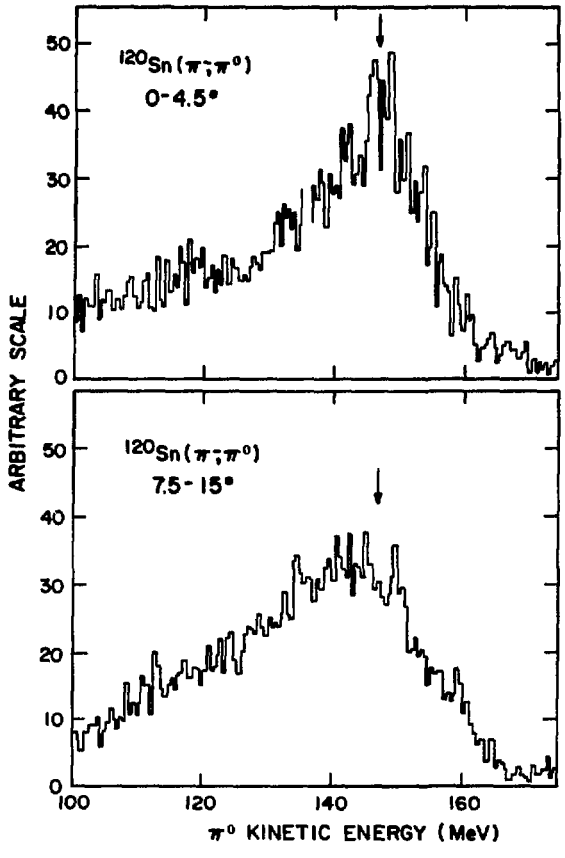

Fig. 2.
Measured spectra of the $^{120}Sn(\pi^-,\pi^0)$ reaction at 164 MeV. The arrow marks the position of a state in ^{120}In, whose analog in ^{120}Sn is at $170\,A^{-1/3}$ MeV.

Observation of Analogs of the GDR Resonance in Pion Single Charge Exchange on ^{40}Ca

The GDR corresponds to the fundamental frequency of absorption of electric dipole radiation by the nucleus. Its discovery and its systematic characterization over the past 30 years have come primarily through use of photon beams and the measurement of photoabsorption and photoneutron cross sections. Pion charge exchange may show new aspects of the GDR. First, in charge-exchange reactions the analogs of the GDR are observed, which

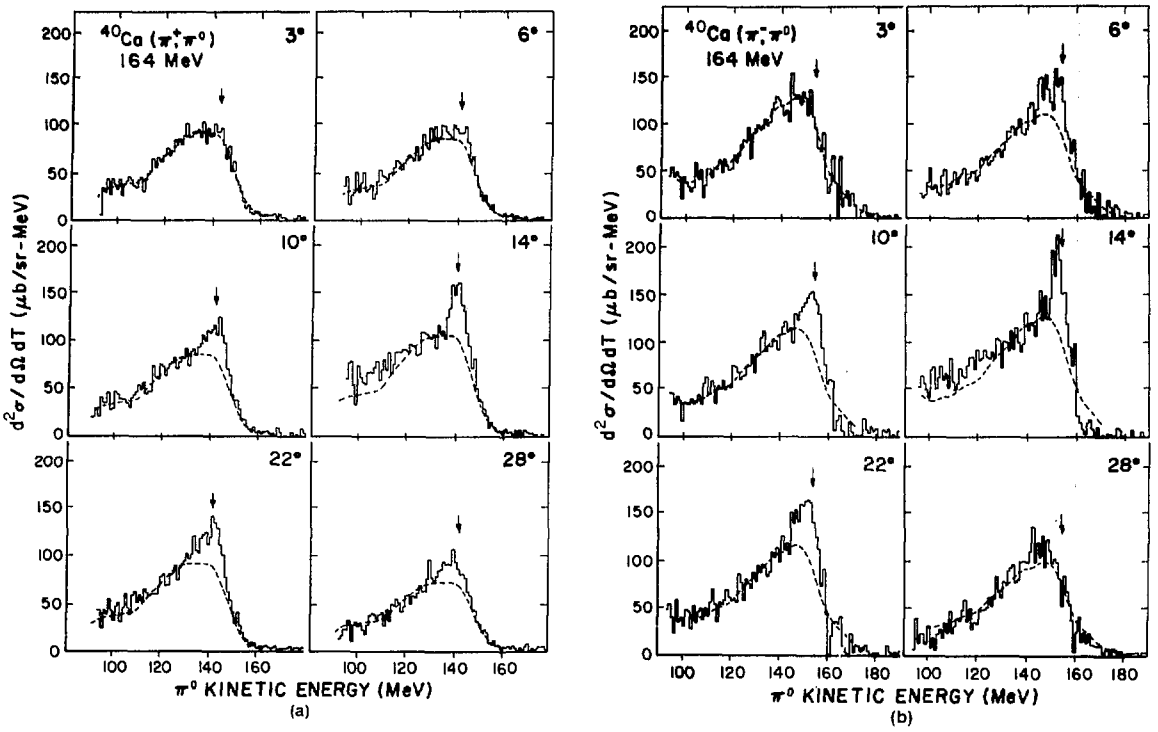

Fig. 3.
Spectra at six angles for the (a) $^{40}Ca(\pi^+,\pi^0)$ and (b) $^{40}Ca(\pi^-,\pi^0)$ reactions. The arrow marks the position of the GDR that occurs at 20-MeV excitation in ^{40}Ca.

occur at considerably different excitation energies than the target GDR. In ^{40}Ca the GDR is at 20-MeV excitation, whereas in the neighboring nuclei, ^{40}K and ^{40}Sc, the excitation energies of the analogs are both at 12 MeV. In view of the different decay branches for the GDR in the three nuclei, it is quite possible that the three widths will be different. The intrinsic widths (spreading widths) are expected to be nearly the same because the Coulomb force could shift the various components up uniformly in increasing Z. Thus, it is reasonable to expect that by measuring the widths of the GDR in the $M_T = \pm 1$ projections, and comparing these with the width of the GDR in ^{40}Ca measured by photonuclear reactions, a separate determination of intrinsic widths and decay widths may be achieved.

A second reason for studying the GDR with pion single charge exchange is to measure an angular distribution, which is not possible in photonuclear reactions. The GDR shows up in an absorption spectrum or in a $\sigma(\gamma,n)$ spectrum. Therefore, comparisons with theory have been limited largely to a comparison of the distribution of calculated E-1 matrix elements with the photoabsorption spectrum. The measurement of angular distributions is a new addition to the study of the GDR, which should be of considerable value in evaluating microscopic models.

A third area where pion single charge exchange holds great potential is in the study of isospin splitting of the GDR. For ^{40}Ca there is no isospin splitting, so the $^{40}Ca(\pi^\pm,\pi^0)$ reaction must be viewed as the calibration of future studies of isospin splitting in $T \neq 0$ targets. It is essential for these future studies of isospin splitting of the GDR, as well as for the study of isovector resonances of other multipolarities, that the $^{40}Ca(\pi^\pm,\pi^0)$ reaction show prominent excitation of the GDR. A large GDR signal is a demonstration of strong isovector coupling of the pion to collective excitations.

We measured both the $^{40}Ca(\pi^+,\pi^0)^{40}Sc$ and the $^{40}Ca(\pi^-,\pi^0)^{40}K$ reactions at 0 and 20° settings of the π^0 spectrometer. The π^0 scattering angle subtended with these settings is 0-35°. The data were binned into six histograms according to the measured π^0 scattering angle. The π^0 kinetic energy spectra corresponding to the six θ bins are shown in Fig. 3. The spectra have been

"acceptance" corrected and are presented in terms of the double differential cross sections $d^2\sigma/d\Omega dT$ in μb/sr·MeV. The expected π^0 energies for states in ^{40}Sc and ^{40}K that are analogs of a 20-MeV excitation in ^{40}Ca are 142.2 and 154.2 MeV, respectively, and are indicated with arrows in each panel. Examination of the spectra in order of increasing scattering angle shows a peak at the expected energy rising above the continuum as the scattering angle of 140 is approached. The sharpest delineation of the peak occurs at this angle in both the (π^+,π^0) and the (π^-,π^0) reactions. At larger angles the peak diminishes, and by 28° it is barely visible. This is the expected behavior for an L = 1 transition in pion scattering at 164 MeV. We can show[2] on very general grounds that a strongly absorbed projectile transferring one unit of angular momentum to the nucleus follows a $J_1^2(qk)$ slope in the angular distribution in the vicinity of the first diffraction maximum. Taking R = 4.80 F as the interaction radius for 164-MeV π's on ^{40}Ca, the first maximum of $J_1^2(qk)$ occurs at 15.4° for the (π^+,π^0) reaction and at 16.0° for the (π^-,π^0) reaction. These values are quite close to what is observed in Fig. 3. Therefore, both the energetic position of the peaks and the qualitative shape of the angular distribution support the identification of the observed peaks as the analogs of the GDR in ^{40}Ca.

To extract precise peak areas and centroids for the GDR peak it is necessary to understand the shape of the continuum. Fortunately, inspection of the spectra in Fig. 3 — in particular those at the smallest and largest angles — reveals that the structure of the continuum does not vary significantly over the angular region 0-30°. Therefore, a reasonable measure of the shape of this background for all angles is the 3° spectrum where the contribution of the GDR is expected to be at a minimum. This 3° spectrum was smoothed to reduce statistical fluctuations by a Gaussian smoothing algorithm. The dashed curves in each of the spectra represent this smoothed spectrum multiplied by a normalizing factor, which was chosen to give zero net counts over a 10-MeV region centered approximately 17 MeV below the GDR peak. Although this criterion is somewhat arbitrary, it was found that using other background subtraction criteria, such as changing the position or increasing the interval over which the normalization is done, changed the normalizing factor by about ±5% for the (π^+,π^0) data and ±7.5% for the (π^-,π^0) data.

The excess counts in a 12-MeV interval, centered on the expected position of the GDR, were used in the determination of the cross sections. A Gaussian fit was made to these counts to determine peak centroids and areas. For the three angles 10, 14, and 28° around the peak of the angular distribution, the peak centroid is constant to better than ±1 MeV. Preliminary values of the differential cross sections at 14° are 0.42 mb/sr for the ^{40}Ca$(\pi^+,\pi^0)^{40}$Sc GDR reaction, and 0.54 mb/sr for the ^{40}Ca$(\pi^-,\pi^0)^{40}$K giant monopole resonance reaction. The estimated error is 25%. We are in the process of refining our analyses and should have a full angular distribution and comparisons with theoretical calculations in the near future.

REFERENCES

1. J. D. Bowman, M. B. Johnson, and J. W. Negele, Los Alamos National Laboratory report LA-UR-81-751; submitted to Phys. Rev. Lett.

2. J. S. Blair, "Scattering of Strongly Absorbed Particles," in *Lectures in Theoretical Physics*, Eds., P. D. Kunz, D. A. Lind, and W. E. Brittin (University of Colorado Press, 1966), p. 343.

A Study of Neutrino-Electron Elastic Scattering at LAMPF

(Exp. 225, Neutrino-A)

(Univ. of California at Irvine, Los Alamos)

Spokesmen: R. Burman (Los Alamos) and H. Chen (Univ. of California at Irvine)

Introduction

The primary goal of Exp. 225 is a ν_e,e^- elastic-scattering measurement, and the LAMPF beam stop neutrino source continues to be unique for this study. However, during the past year there has been increased interest in neutrino physics and in searching for neutrino oscillations. We have submitted an addendum for Exp. 225 at LAMPF that addresses a $\bar{\nu}_\mu \rightarrow \bar{\nu}_e$ (appearance) and also a $\nu_e \rightarrow \nu_e$ (disappearance) measurement. Data for both oscillation measurements and ν_e,e^- elastic scattering are collected simultaneously at the present Exp. 225 location 9 m from the LAMPF beam stop. The oscillation measurements require an additional measurement 36 m from the beam stop, which would be done after the elastic-scattering data have been collected. The capabilities of the Exp. 225 detector will provide a benchmark for future oscillation experiments.

Instrumentation

The instrumentation design is completed and all components are either under construction or are being installed at the LAMPF neutrino area.

The electronics trailer has been installed and outfitted with the necessary electrical power, racks, and air conditioning, and the PDP-11/34 computer and the neon/helium gas-purification system have been installed in the trailer.

In the neutrino house the 13-cm iron shield (~150 tons) is in place, and a 2.5-cm-thick layer of lead now covers the inside of the iron shield on the north wall (toward the beam stop). A layer of multiwire proportional counters (MWPCs), used as cosmic-ray anticounters, is installed on the floor, and installation of MWPCs along the walls has begun, with 20 MWPCs in place that are being checked out. Conversion of the ~600 aluminum extrusions to MWPCs is progressing; at present about 200 MWPCs have been finished and are being installed.

The MWPC cosmic-ray antielectronics consists of three components, which are being assembled and tested: (1) an amplifier/discriminator for each MWPC, (2) prompt veto logic electronics, and (3) a data-recording/reduction system.

The neutrino detector stand and 10 flash chamber/scintillator layers (out of 40 total) of the central detector are in place, and another set of 10 has arrived in Los Alamos and is being installed. The remaining 20 modules are awaiting shipment from the University of California at Irvine. The high-voltage pulsed power supplies to drive these flash chambers have been designed and tested and are presently being manufactured.

The recent beam stop reconstruction will benefit Exp. 225 directly because a retractable water insert placed upstream from the beam stop is expected to increase the neutrino flux by ~40%.

Conclusion

The installation and testing of the Exp. 225 apparatus is under way and is expected to continue into this fall.

We feel that in addition to the physics contribution ($\nu_e e^-$ elastic scattering) Exp. 225 will influence greatly the design of future neutrino experiments at LAMPF.

Study of the Pion Absorption Mechanism through the (π,p), (π,2p), and (π,pn) Reactions (Exp. 562, P³)

(Argonne, California Institute of Technology, Northwestern Univ.)

Spokesmen: H. E. Jackson and J. P. Schiffer (Argonne)

As part of Exp. 562, we have taken ^{3}He, ^{4}He, C, Ni, and Ta (π,p) data at six angles for a pion kinetic energy of $T_\pi = 500$ MeV. The Large-Acceptance Spectrometer (LAS) was used to detect the protons. The spectrometer was originally designed for Exp. 390 to detect pions up to 500 MeV/c, but relatively minor modifications allowed detection of protons up to ~1400 MeV/c.

This work complements the results of Exp. 350, in which (π,p) cross sections were measured in the region of the Δ resonance.[1] The results of Exp. 350 imply that pion absorption proceeds through a relatively large number of nucleons. Without additional information off-resonance, however, it is difficult to disentangle unambiguously which features of the proton spectra originate from the pion absorption vertex and which from subsequent rescattering of the emerging protons. If the main features of the proton spectra in Exp. 350 are due to the absorption vertex, we expect qualitatively different results at $T_\pi = 500$ MeV, where the πN scattering cross section is roughly a factor of 10 smaller than at resonance. Analysis of the data is in progress.

In the second part of Exp. 562 we carried out a coincidence measurement of the He(π^+,2p) and (π^-,pn) reaction on ^{3}He and ^{4}He at 165 MeV. The ratio of the cross sections for these reactions is a sensitive test of the reaction mechanism. By using isospin Clebsch-Gordan coefficients for calculating this ratio and assuming Δ dominance of the process,[2] the result is $\sigma(\pi^-,pn)/\sigma(\pi^+,2p) = 0.13$ (for ^{3}He) and 0.08 (for ^{4}He). However, these results will be different if the reaction mechanism includes formation of a ΔN intermediate state with a well-defined angular momentum and parity before the ΔN → NN transition. In particular, if this intermediate state will have an even relative angular momentum ($L_{\Delta N} = 0,2$), absorption on a $T = 1$, $J = 0$ nucleon pair will be forbidden by angular momentum and parity conservation. This condition will lead to a strong suppression of the (π,pn) reaction in helium.

The measurements were done in the P³ channel by detecting protons with the LAS and the coincident

protons or neutrons with two 15- by 15- by 35-cm plastic scintillators. The scintillators were positioned so that one of them was at the angle where the direct (π,2N) nucleon-nucleon angular correlation is peaked and the second at the tail of this correlation. The experimental data allow for the separation of the direct (π,2N) absorption from the process where the pion energy is shared with more nucleons. Preliminary analysis of the data indicates that the direct (π,pn) reaction is strongly suppressed with respect to the predictions mentioned above.

This research was performed under the auspices of the United States Department of Energy and the National Science Foundation.

REFERENCES

1. R. D. McKeown et al., Phys. Rev. Lett. 44, 1033 (1980).

2. G. N. Ginocchio, Phys. Rev. C17, 195 (1978).

Elastic and Quasi-Free Scattering of $\pi^{\pm}$ from Helium Isotopes
(Exps. 154/513, P^3)

(Univ. of Virginia, Los Alamos)

Spokesmen: J. S. McCarthy and R. C. Minehart (Univ. of Virginia)

Experiments 154 and 513 were run in March 1981 using the University of Virginia liquid-helium target cryostat and the Large-Acceptance Spectrometer (LAS) in the P^3-East experimental area. The purpose of the experiment was to measure elastic and quasi-free scattering (QFS) cross sections for $\pi^{\pm}$ on ^{3}He and ^{4}He at energies above the 3-3 resonance. When the analysis of these data is completed, the cross sections can be combined with our earlier measurements at EPICS to provide a rather complete picture of these interactions from 100-500 MeV. In the energy region above the 3-3 πN resonance the ratio of the elementary cross sections, π^+p/π^+n, varies rapidly. We hope that by comparing π^+ and π^- QFS cross sections in ^{3}He and ^{4}He we can determine whether QFS is dominated by single-scattering processes and whether it reflects the elementary πN cross sections in a simple way.

The cryostat contained two target cells, one filled with ^{4}He and one with ^{3}He. Both were thermally coupled to a 1 K superfluid ^{4}He bath so that boiling was negligible.

When the beam parameters, which were selected to give a momentum spread of ~1% FWHM, were folded together with the resolution of the spectrometer, we were able to obtain an overall momentum resolution $\Delta p/p \sim 1.5\%$ FWHM. This resolution is more than adequate for the ^{4}He elastic data, but it limits our ^{3}He elastic data to forward angles where the cross section is relatively large compared to the inelastic cross sections.

Measurements were made at energies of 300, 350, 375, 400, and 500 MeV for π^+ mesons. At 500 MeV the π^+-^{4}He cross section was not measurable at 90° and beyond. At the other energies measurements were taken in 10° steps from 30-130°. At each step the spectrometer spanned an angular range of about 10°.

The π^- cross sections were measured at energies of 350, 450, and 475 MeV. Because the π^- incident beams were much less intense than the π^+ beams, a complete angle set was not possible at 400 and 475 MeV and measurements were confined to 60, 90, and 120°.

We are analyzing the data and hope that the elastic cross sections will be available by July 1981. The quasi-free data will require additional analysis to assess the relative importance of the (π,π'N) single-scattering processes. On-line reduction of a portion of the data indicated that the second minimum at 110° observed previously for the π-^{4}He elastic cross section at energies above the 3-3 resonance is still observed at 350 MeV. At 375 MeV the two minima seem to give way to a single broad and shallow minimum around 40°. Verification of these features observed in the on-line analysis must await the full off-line analysis presently under way.

Search for Fast Muonium in Vacuum
(Exp. 547, SMC)

(Yale Univ., Heidelberg Univ., College of William & Mary)

Spokesmen: V. W. Hughes (Yale Univ.) and P. D. Egan (Yale Univ./College of William & Mary)

Until now, muonium (μ^+e^-) has always been formed and observed when positive muons are stopped in material targets, for example, a heavy noble gas, so that experiments requiring collision-free μ^+e^- atoms have been impossible. There are a number of experiments that require muonium in a vacuum environment. In particular, muonium-antimuonium conversion, $\mu^+e^- \rightarrow \mu^-e^+$, which violates the additive law of lepton-number conversion, is extremely interesting in light of recent theories questioning the absolute nature of conservation laws. Also, spectroscopy of the excited muonium states, for example, a measurement of the Lamb shift in the

n = 2 state, is quite interesting in view of the purely leptonic nature of this system.

The principal goal of Exp. 547 is to show that muonium is produced when a low-energy μ^+ beam passes through a thin foil target. This technique is analogous to beam neutralization in proton beam foil spectroscopy. The muonium should have a velocity of $\sim\alpha c$ (hence the name "fast muonium") and therefore can be spatially separated from the charged portion of the beam by magnetic deflection. This technique should be sensitive to the detection of vacuum muonium production in the 0.1- to 30-keV energy range.

A diagram of the experimental apparatus is shown in Fig. 1. The LAMPF SMC is tuned for the "surface" μ^+ mode, providing 3×10^6 μ^+/s with a central kinetic energy of 4.0 MeV and a 5% energy spread (FWHM). The μ^+ are degraded in energy as they enter the experimental vacuum system so that their mean stopping range coincides with one of a selection of 7.5- or 5.0-cm-diam thin foil targets: gold (0.2 mg/cm^2), silver (0.2 mg/cm^2), copper (4 mg/cm^2), aluminum (0.2 mg/cm^2), carbon (3 mg/cm^2), or beryllium (5 mg/cm^2). The target thicknesses are considerably smaller than the stopping range width of the beam ($\sim$15 mg/cm^2 of CH_2). Only a small fraction of the dispersed beam emerges with energies below 30 keV, where the analogous proton beam foil data show a neutral beam fraction above 1%.

To separate the small neutral muonium fraction of the beam from the overwhelming charged background caused by μ^+, decay e^+, and beam contamination e^+, the target is followed by a 30-cm-long sweeping magnetic field of 5 kG, which has a bend radius of 20 cm for 4-MeV μ^+. Only neutrals can travel past the magnet to a Teflon beam stop, 160 cm from the foil target. The beam stop is viewed by a 25-cm-diam by 25-cm-thick NaI(Tℓ) detector whose output is gated by the scintillator coincidence telescope S1·S2. This detector is surrounded by scintillator anticoincidence counters A, and shielded by lead, concrete, and the magnet yoke. Thus, observation of the characteristic Michel energy spectrum from $\mu^+ \rightarrow e^+ \bar{\nu}_\mu \nu_e$ at the beam stop indicates the presence of a neutral system containing a muon, that is, muonium.

The apparatus is normally at a pressure of $< 5 \times 10^{-5}$ torr; however, helium gas can be introduced between the target and observation region. This serves to destroy muonium by ionizing collisions, $(\mu^+e^-) + He \rightarrow \mu^+ + e^- + He$, with the μ^+ being swept away by the magnet. Thus, by comparing detector spectra taken with

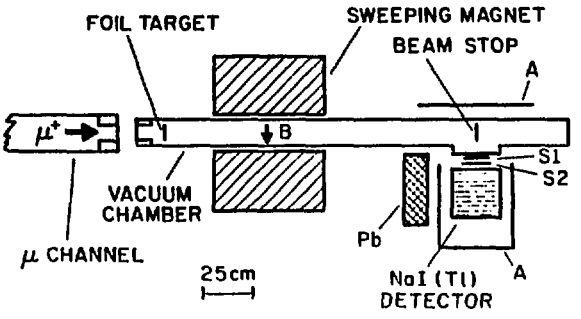

Fig. 1.
Schematic diagram of the experimental apparatus. S1, S2, and A are plastic scintillation counters. The beam passes through a 125-μ Mylar window at the end of the μ channel and a 50-μ titanium window as it enters the vacuum chamber.

vacuum and with a few torr of helium in the apparatus we can effectively separate the muonium signal from any residual backgrounds. An additional test of the cleanliness of the spectrum was made in the early stages of the experiment by installing an electromechanical shutter immediately after the foil target to chop the muonium flux. The shutter results showed that backgrounds in the energy region of interest were small, so the shutter was removed for subsequent runs to improve the experimental sensitivity.

An example of a typical NaI spectrum for a beryllium target is shown in Fig. 2. For the vacuum case, a distinct Michel spectrum with an end point energy of 53 MeV can be seen, while in contrast the data with helium show no evidence of muon decay. Noise at the low-energy end (E < 30 MeV) of the spectrum is due principally to bremsstrahlung from e^+ contamination, whereas that in the high-energy portion is due principally to cosmic rays. The shape of the Michel spectrum in our apparatus was measured by turning off the sweeping magnet and observing μ^+ in the beam stop.

The counting rates for Michel electrons in our detector, combined with the solid-angle efficiency and expected angular distribution, imply a muonium production rate at the foil target of $\sim$2-3 kHz, with very little dependence on target material. A measurement of the fast muonium transmission through helium, coupled with a knowledge of the hydrogen-helium ionization cross section, puts a rough upper limit of 20 keV on the muonium kinetic energy.

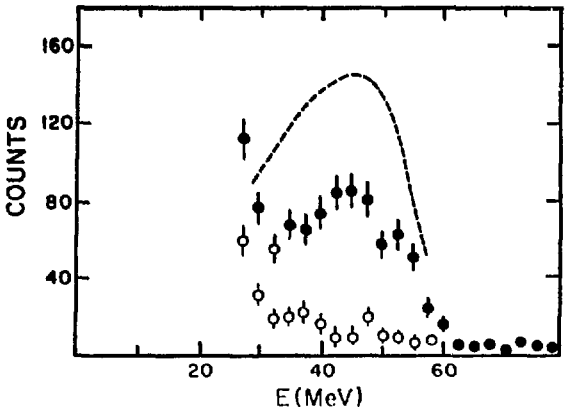

Fig. 2.
Measured NaI spectrum for a 25-μ beryllium foil target. Solid circles are with the apparatus evacuated; open circles are with 6-torr helium. For each case, 2.8 h of data are shown. The dotted line shows a μ^+ calibration spectrum with the sweeping field off.

We have therefore shown that a reasonable amount of fast muonium in vacuum can be attained using this technique. Future work will focus on improving the muonium rate by better beam transport and improved beam purity (electrostatic separator). Studies of the $\mu^+e^- \rightarrow \mu^-e^+$ experiment and of the muonium Lamb-shift measurement have begun.

Sensitive Search for $\mu^- \rightarrow e^-$ Conversion (Exp. 421, SMC)

(Yale Univ.)
Spokesmen: V. W. Hughes and P. A. Souder (Yale Univ.)

Beam time during the past cycle for this experiment was devoted to studying negative cloud muon beams. Data were obtained with production beam and with chopped development beam. With the production beam we developed a method for measuring relative intensities, which was ideal for optimizing the tunes, and with the chopped development beam we measured absolute rates, spot sizes, and contamination.

Figure 1 shows the apparatus used with the production beam. After muons were stopped in the target and identified by observing the high-energy portion of their Michel decay spectrum, we monitored beam electrons traversing the target by measuring the current in a photomultiplier viewing a scintillator downstream of the target. This technique worked well, featuring (1) easy identification of muons in a beam with 200 times as many electrons, and (2) high counting rates so that optimizing tunes progressed relatively quickly. Optimum tunes were obtained for 28.5, 30, and 35 MeV/c.

The tunes obtained in the first run were studied in more detail with the low-intensity chopped development beam. We used the standard Group MP-13 beam-tuning apparatus with an added 0.25-mm scintillator installed to provide the additional dE/dx information needed to distinguish muons from electrons. Indeed, correctly identifying muons, which are only 0.5% of the beam, was one of the main experimental difficulties. Using range and dE/dx information, however, we were able to obtain a hardware muon signal that was >90% efficient for muons and $<10^{-4}$ for electrons. These efficiencies were determined using information from pulse height and time-of-flight spectra. Because only the electrons are in time with the chopped beam, the time-of-flight test provided a very useful independent check of the purity of the muon signal.

Our final result is a 30-MeV/c beam tune with a rate of 2-kHz/μA proton current and a spot size 5 by 3 cm. This will be an excellent beam for the $\mu^- \rightarrow e^-$ conversion experiment.

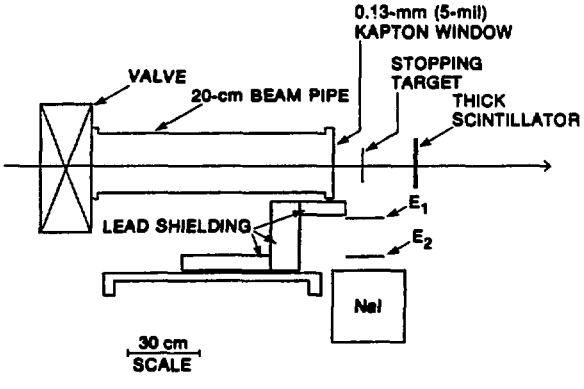

Fig. 1.
Apparatus for muon beam tuning with production beam. Decay electrons are identified by large pulses in the NaI crystal in coincidence with E_1 and E_2. Beam electrons are detected in the thick scintillator.

Strong-Interaction Shift in Pionic Hydrogen and Deuterium Atoms
(Exp. 491, SMC)

(California Institute of Technology, Univ. of Wyoming)
Spokesman: E. Bovet (California Institute of Technology)

The 2p-1s transition x rays in π^-H and π^-D atoms have been measured using a new reflection-type graphite spectrometer.

The experimental setup is shown in Fig. 1. Pionic atoms were produced in a pressurized gaseous H_2 (D_2) target, cooled to LN_2 temperature, and placed in the intense π^- beam of the East Leg of the SMC. After the low-energy transition x rays (~2.5 keV) passed through thin windows toward the curved graphite crystal located about 1.5 m from the target, the x rays were refracted by the crystal and focused along the focal circle at a position determined by the Bragg condition $\sin\theta = \lambda/2d$.

The detector was a position-sensitive gas proportional counter that enabled the simultaneous collection of all x rays over a large angular range. The entire region containing the target, crystal, and detector was filled with helium to reduce the x-ray absorption. Energy calibration of the spectrometer was performed using electronic x rays. The reflection-type point-focusing graphite crystal spectrometer for this experiment was developed at the California Institute of Technology.

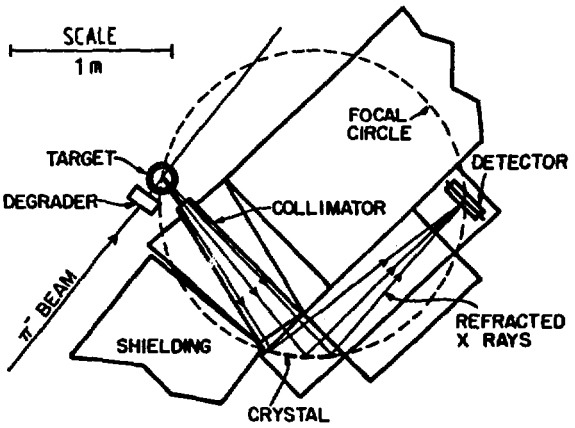

Fig. 1.
Experimental setup.

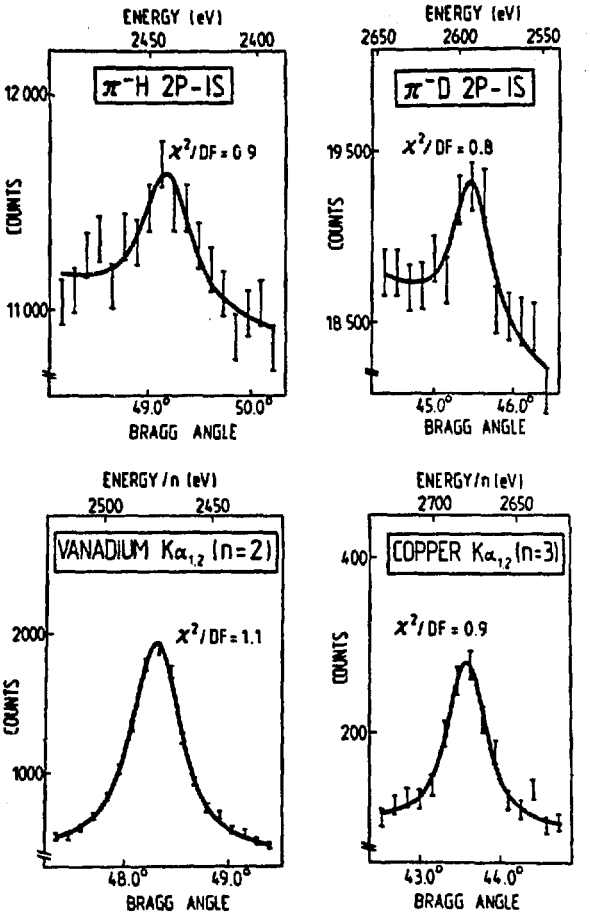

Fig. 2.
The observed 2p-1s transitions in π^-H and π^-D together with electronic x-ray calibration lines from vanadium and copper.

We performed this experiment with a π^- beam intensity of about 4×10^7 π^-/s, yielding an approximate stopping rate of 1.2×10^4 stopped π^-/s in the 3.6-mg/cm^2 gaseous target. The x-ray counting rate in our spectrometer was 0.5 counts/min. We identified the 2p-1s transition in both hydrogen and deuterium in spite of a very poor signal-to-noise ratio of about 1:20. The spectra are represented in Fig. 2 together with two calibration lines. A computer fit has been made for the π^-H and π^-D spectra using the line-shape parameters of the corresponding calibration lines. Preliminary results for the

TABLE I

OBSERVED 2p-1s TRANSITION ENERGIES IN π^-H AND π^-D
(ENERGIES IN ELECTRON VOLTS)

	π^-H	π^-D
E (2p-1s) (point nucleus)	2426.5	2594.3
Vacuum polarization	+3.2	+3.7
Finite-size effect	----	−0.4
Nuclear polarization	----	+0.5
TOTAL	2429.7	2598.1
Present experiment	2441.8 ± 2.9	2593.3 ± 2.3
Deduced strong-interaction shift	12.1 ± 2.9	−4.8 ± 2.3

2p-1s transition energies are given in Table I together with the deduced strong-interaction shifts.

Crystal Box Experiment (Exps. 400/445, SMC)

(Los Alamos, Stanford Univ., Univ. of Chicago)

Spokesmen: M. Duong-Van, C. M. Hoffman, J. D. Bowman, and H. S. Matis (Los Alamos)

This experiment is designed to search for the rare, lepton-flavor-violating decay modes $\mu^+ \rightarrow e^+e^+e^-$, $\mu^+ \rightarrow e^+\gamma$, and $\mu^+ \rightarrow e^+\gamma\gamma$ using a modularized sodium-iodide (NaI) detector, a cylindrical drift chamber, and plastic scintillation counters. The experiment and some aspects of the data-acquisition system have been described in the preceding two progress reports.

During a recent development run, several different beam tunes were tried to establish which is most suitable for the experiment. The nominal beam requirements are a uniform circular spot with a diameter of 10 cm, no large halo of either μ^+ or e^+, a flux variable from 4×10^5/s to 1×10^6/s (average), and a μ^+/e^+ ratio of no worse than 1:1. Although several beam tunes were capable of delivering an acceptable beam to the experiment, one of these tunes was clearly superior and will be adopted for future studies, which are needed to finalize some beam parameters.

During a test run in April, the NaI read-out scheme using an LSI-11/23 microprocessor and the "intelligent multiplexer" was exercised. Several hardware and software problems were uncovered. For example, several circuit errors in the Bi-Ra 1151 Data Access Port were identified and corrected. We now believe that the system works as intended and we are developing the final software.

Several problems at Harshaw Chemical Corporation have delayed the delivery of the NaI crystals. A hydration accident in their dry-room necessitated the repolishing and retesting of a large number of completed crystals. During the initial stacking of the crystals in the hermetic container, it was discovered that cumulative dimension errors required minor remachining of the container. Delivery of the crystals is now expected by July 1981.

Various electronic and mechanical parts have been fabricated, with more scheduled for construction this summer. All 550 photomultiplier tubes that will be used on the NaI and on the plastic scintillators have been tested. The drift chamber is scheduled for completion and checkout this summer, and test runs with one quadrant of the NaI and all plastic scintillators instrumented are also scheduled. Full instrumentation should be completed by the end of this year.

Materials Science

Muon Spin Rotation (μSR) Investigation of the Effects of Impurities on the Trapping and Diffusion of μ^+ Particles in bcc Metals
(Exp. 382, SMC)

(Los Alamos, Memphis State Univ., Bell Laboratories, College of William & Mary)

Spokesmen: R. H. Heffner and M. Leon (Los Alamos) and W. J. Kossler (College of William & Mary)

Introduction

Transverse-field muon spin rotation (μSR) has been employed to measure the mobility of positive muons in a variety of materials. When the muon is stationary, depolarization is caused by the surrounding nuclear magnetic moments; the depolarization rate is reduced by motional narrowing when the muon is moving. Often it has been found that the depolarization rate is a complicated function of temperature and that much of this structure is due to impurity defects in the target material, which can trap muons in certain temperature ranges. An example of this kind of behavior for impure niobium is sketched in Fig. 1. (See Ref. 1 for the actual transverse-field data.)

The conventional interpretation of the behavior shown in Fig. 1 is that the muon's mobility increases with temperature, and that at point ① all the muons are weakly bound to a high concentration trap; at point ② many escape from these traps by way of thermal excitation (hence motional narrowing); at point ③ the muons are beginning to find a lower concentration, deeper trap; at point ④ all muons are bound to these deeper traps; and at point ⑤ the muons are beginning to be activated out of the deeper traps.

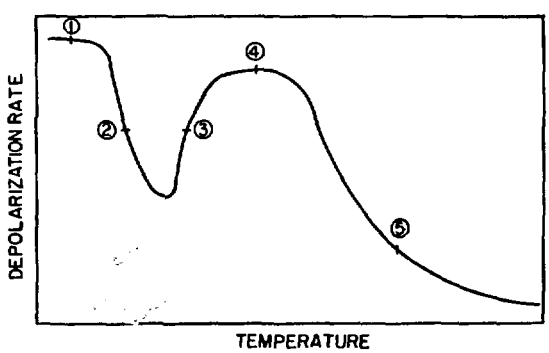

Fig. 1.
Schematic representation of the temperature dependence of the transverse-field depolarization rate obtained (Ref. 1) in a niobium sample containing impurities.

A drastically different interpretation has been offered for analogous behavior in bismuth.[2] There it is assumed that the muon mobility *increases* as the temperature decreases below point ④ [because of the onset of a coherent (quantum) diffusion mechanism], that the peak at point ④ is due to self-trapping in the host materiai, and that the peak at point ① is due to the muons finding traps because of their greatly increased mobility.

Whereas one cannot choose between these interpretations on the basis of transverse-field measurements, zero-field measurements can do so quite unambiguously, as pointed out by Petzinger.[3] This is because in zero field a muon that is static will have its polarization recover to one-third at long times, while a moving muon will have a polarization approaching zero at long times. Thus the difference between finding traps and escaping from traps becomes readily measurable.

Theory

If the trapping rate is ν and there is no release from traps, the polarization as a function of time is given quite generally (transverse, longitudinal, or zero external field) by

$$P(t) = e^{-\nu t} P_0(t) + \nu \int_0^t dt' \, e^{-\nu t'} P_1(t - t') P_0(t') \quad , \tag{1}$$

where $P_0(t)$ is the polarization in the free state and $P_1(t)$ that in the trapped state. If the hopping in the free state is *extremely* rapid, $P_0(t) = 1$. However, it will often be the case that the depolarization is *not* completely negligible in the free state; here we can approximate $P_0(t)$ by

$$P_0(t) = e^{-\lambda_0 t} \quad , \tag{2}$$

so that Eq. (1) becomes

$$P(t) = e^{-\bar{\nu} t} + \nu \int_0^t dt' \, e^{-\bar{\nu} t'} P_1(t - t') \quad ,$$

where (3)

$$\bar{\nu} \equiv \nu + \lambda_0 \quad .$$

For transverse field such that $\Delta/\omega_0 \ll 1$, where Δ is the second moment of the nucleus dipole field distribution and ω_0 is the Larmor precession frequency of the muon, we have

$$P_1(t) \cong e^{-\Delta^2 t^2/2} \quad , \tag{4a}$$

while for longitudinal (and zero) field

$$P_1(t) = 1 - 2\left(\frac{\Delta}{\omega_0}\right)^2 \left(1 - e^{-\Delta^2 t^2/2}\right) \cos(\omega_0 t) + 2\,\frac{\Delta^4}{\omega_0^3} \int_0^t d\tau e^{-\Delta^2\tau^2/2} \sin(\omega_0 \tau) \tag{4b}$$

Then for transverse fields Eq. (1) becomes

$$P(t) \cong e^{-\bar{\nu}t}\left[1 + \nu \int_0^t d\tau \exp(-\Delta^2\tau^2/2 + \bar{\nu}\tau)\right] \quad , \tag{5a}$$

while for longitudinal fields one has

$$P(t) = e^{-\bar{\nu}t}\left\{1 + \nu \int_0^t d\tau \left[\left[e^{\bar{\nu}\tau}\left\{1 - 2\left(\frac{\Delta}{\omega_0}\right)^2 \times \left[1 - \exp(-\Delta^2\tau^2/2)\cos(\omega_0\tau)\right]\right\} + \frac{2\Delta^4}{\bar{\nu}\omega_0^3}\left(e^{\bar{\nu}t} - e^{\bar{\nu}\tau}\right)\exp(-\Delta^2\tau^2/2)\sin(\omega_0\tau)\right]\right]\right\} . \tag{5b}$$

For zero field ($\omega_0 = 0$) and $\lambda_0 = 0$, Eq. (5b) reduces to Petzinger's Eq. (9) (Ref. 3).

For zero and longitudinal field, it is interesting to look at the $t > 0$ *extrema* of P(t). From Eq. (3)

$$P(T) = \frac{\nu}{\bar{\nu}} P_1(T) \quad ,$$

where (6a)

$$\frac{d}{dt} P(T) = 0 \quad .$$

This is the generalization of Petzinger's Eq. (10). We see that λ_0 can be determined directly from the ratio $P(T)/P_1(T)$. In particular, because $t = \infty$ is an extremum of P(t), we have

$$P(\infty) = \frac{\nu}{\bar{\nu}} P_1(\infty) \tag{6b}$$

for the asymptotic value of the polarization.

If the muon is escaping from traps rather than finding them, we have the situation already described by Kubo and Toyabe,[4] and discussed at length in the μSR context by Hayano et al.[5]

Discussion and Results

The polarization function P(t) is determined by measuring the time-differential μSR spectrum in the forward (F) and backward (B) directions with respect to the muon spin vector:[4]

$$\frac{dN^F}{dt} = N_0^F e^{-\lambda_\mu t}\left[1 + a^F P(t)\cos\theta\right] + b^F$$

for the forward ($\cos\theta = +1$) detector. One then has for the i^{th} time bin:

$$P(t_i) \approx \bar{a}\left(\frac{F_i - \alpha B_i}{{}_B F_i + {}_\alpha F_{B_i}}\right) ,$$

where $F_i = N_i^F - b^F$, etc. Here, the b's are the (constant) background parameters, $\alpha \equiv N_0^F/N_0^B$, and

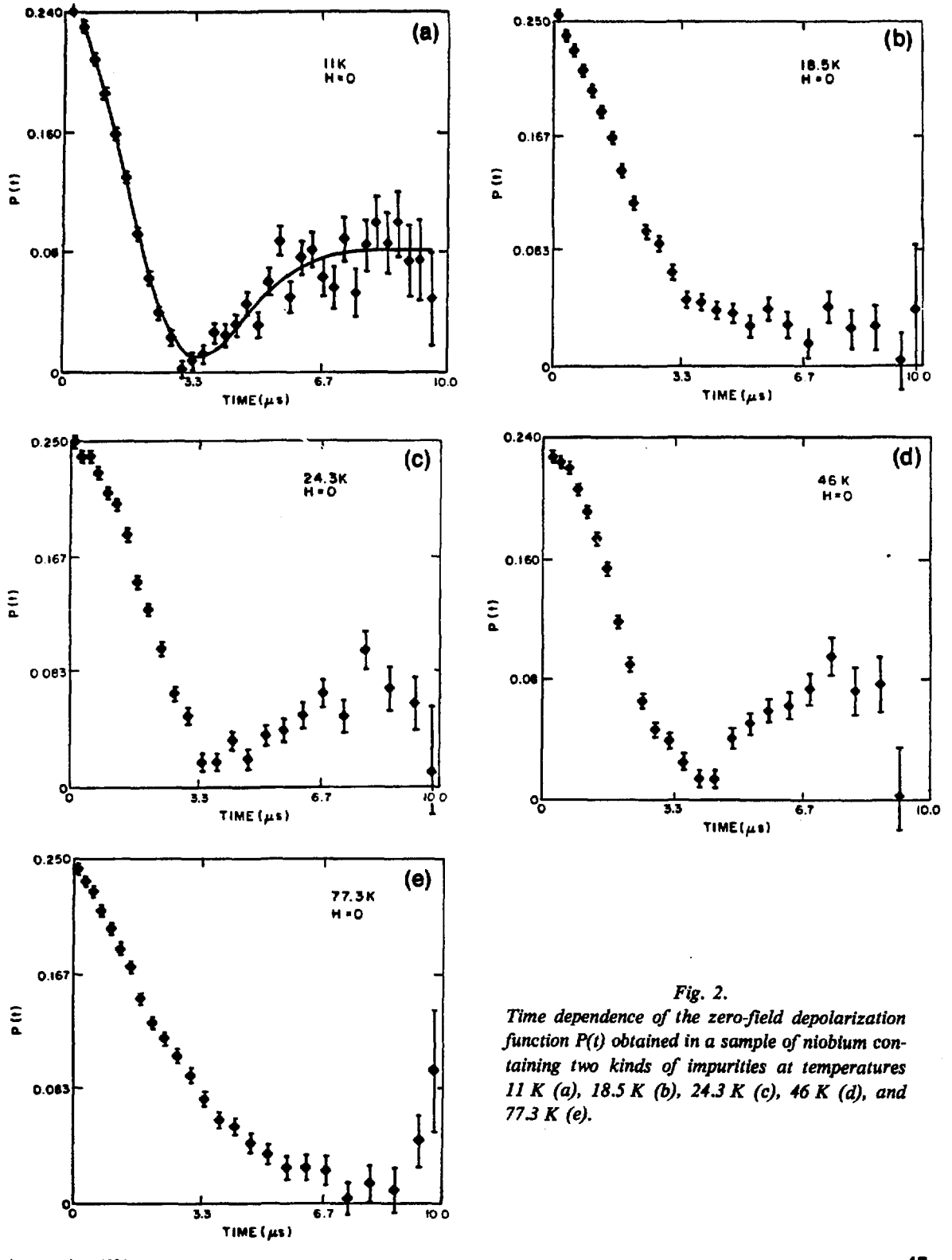

Fig. 2.
Time dependence of the zero-field depolarization function P(t) obtained in a sample of niobium containing two kinds of impurities at temperatures 11 K (a), 18.5 K (b), 24.3 K (c), 46 K (d), and 77.3 K (e).

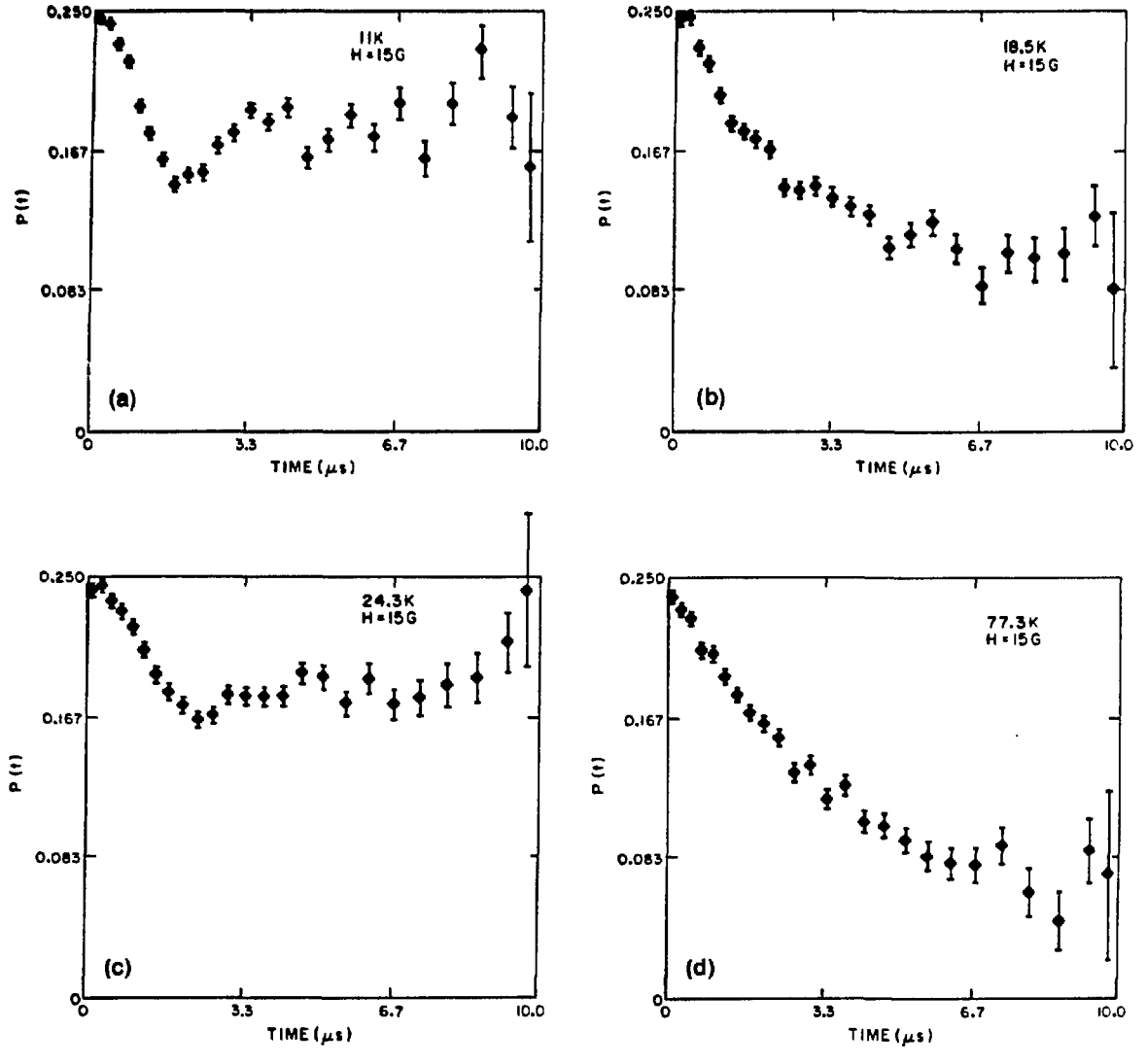

Fig. 3.
Time dependence of the depolarization function P(t) obtained in the same niobium sample as in Fig. 2 for a longitudinal applied field of 15 G at temperatures 11 K (a), 18.5 K (b), 24.3 K (c), and 77.3 K (d).

$$\bar{a} \equiv \frac{1}{2}(a^F + a^B)$$

is the average asymmetry.

The zero-field data for the temperatures 11, 18.5, 24.3, 46, and 77.3 K (corresponding to the five regions in Fig. 1) are shown in Fig. 2. The effect of applying a 15-G longitudinal field at four of the temperatures is shown in Fig. 3. The theoretical predictions [Eqs. (4) and (5)] are shown in Fig. 4, where the abscissa is σt. [Here, $\sigma = 0.50\ \mu s^{-1}$, as determined from a fit to the H = 0 curve in Fig. 2(a).]

The zero-field data (Fig. 2) show unambiguously that the muon mobility increases with temperature. At 11 K the muons are trapped, as displayed by the static P(t). At 18.5 K the data display motional narrowing rather than

a recovery of the polarization at long time; thus the muons are being released from traps rather than finding them. The opposite situation pertains at 24.3 K, namely, the muons are finding traps, and the recovery of the polarization at long times is apparent. At 46 K the data are again consistent with static behavior, while at 77.3 K motional narrowing caused by release from the second trap is evident. The agreement with the theoretical curves for both $H = 0$ and $H = 15$ G longitudinal fields is excellent. The hopping rate obtained from the transverse field measurements[1] was used in the theoretical calculations (1.4 μs^{-1}).

In Table I we compare the σ's measured in 100-G transverse[1] and in zero-applied fields at the plateau temperatures 11 and 46 K. [The transverse depolarization function is defined as $P(t) = \exp(-\sigma^2 t^2/2)$.] If the nuclear moments were free to precess around the external field, then, because the precession is rapid, the effective σ is reduced[4] and we would expect

$$\sigma_\perp = \sqrt{\frac{2}{5}}\ \sigma_0 \ .$$

Instead we see $\sigma_\perp \simeq \sigma_0$. This is because of the quadrupole moment of the niobium nuclei whose interaction with the muon's electric field gradient is much stronger than the Zeeman interaction for $H \ll 1$ kG. Thus the niobium nuclear moments precess rapidly around the radial electric field gradients surrounding the muon so that, in a polycrystalline sample, the same time average of the nuclear magnetic moments is seen in the parallel, perpendicular, or zero-field configurations. In fact, the niobium target used is a single crystal, but the anisotropy is known to be quite small in the low-field region. Thus $\sigma_\perp \simeq \sigma_0$. The relation $\sigma_0 = \sigma_{11}$ should hold independent of this approximate isotropy. Although we have not yet performed the fitting to the 15-G data, it is clear from the asymmetry plots that this relation holds very closely for our data.

TABLE I

MUON DEPOLARIZATION RATE OBTAINED IN A NIOBIUM SAMPLE AT 0- (σ_0) AND 100-G (σ) APPLIED FIELD

Temperature (K)	$H = 0$ $\sigma_0(\mu s^{-1})$	$H_\perp = 100$ G $\sigma(\mu s^{-1})$
11	0.501 ± 0.006	0.485 ± 0.011
46	0.432 ± 0.004	0.447 ± 0.014

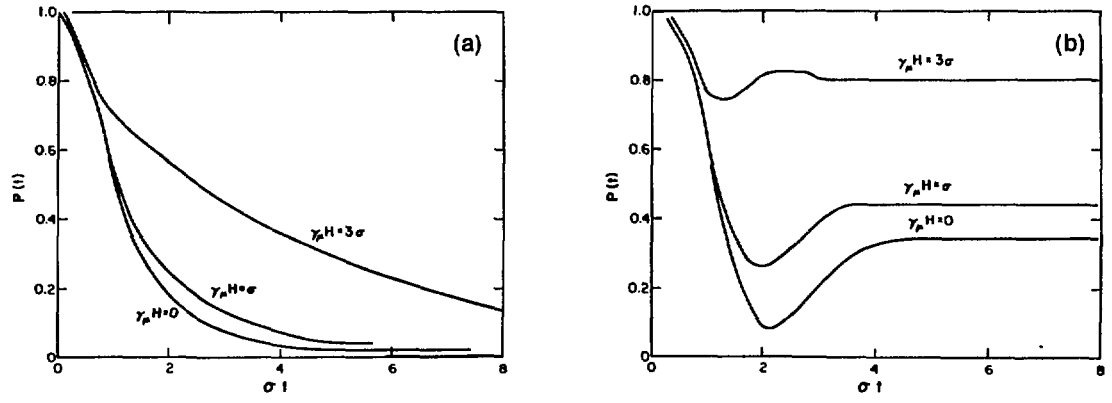

Fig. 4.
(a) Theoretical depolarization functions P(t) for muons in a stationary longitudinal field (H) of $H = 0$, $H = \sigma/\gamma_\mu$, and $H = 3\ \sigma/\gamma_\mu$. Here σ is the parameter characterizing the field inhomogeneity. (b) An equivalent set of theoretical curves for the case of time-varying fields produced by muon motion. The hopping rate used is 1.4 μs^{-1}.

REFERENCES

1. H. K. Birnbaum et al., Phys. Rev. B17, 4143 (1978); and Brown et al., Hyperfine Interactions 6, 233 (1979).

2. V. G. Grebinnik et al., Pis'ma Zh. Eksp. Teor. Fiz. 25, 322 (1977).

3. K. G. Petzinger, Hyperfine Interactions 8, 639 (1981).

4. R. Kubo and T. Toyabe, *Magnetic Resonance and Relaxation*, Ed., R. Blinc (North-Holland, Amsterdam, 1967), p. 810.

5. R. S. Hayano et al., Phys. Rev. 20B, 850 (1979).

Biomed

Visualization of Stopping Pion Distribution (Exp. 215, Biomed)

(Los Alamos, Univ. of California at San Francisco, Lawrence Berkeley Lab.)
Spokesmen: V. Perez-Mendez (Lawrence Berkeley Lab.) and J. N. Bradbury (Los Alamos)

Using high-energy gamma rays produced as a result of π^- capture, this experiment has demonstrated one-dimensional (Z) visualization with good spatial resolution employing typical fractionated treatment doses and dose rates. Important backgrounds have been identified and eliminated. One patient treatment has been observed with the system.

Figure 1 shows the apparatus, mounted on a rolling table, with the necessary large amount of shielding for reducing singles count rates in the detectors. In addition, the neutron-induced triggers are reduced by requiring triple scintillators separated by the aluminum absorber that sets the gamma-ray energy threshold. Figure 2 (top) gives the spatial resolution (1.2 cm FWHM) obtained from a thin Lucite sheet. Low background is evident in the two 7.5-cm air gaps. Figure 2 (bottom) shows the signal from a π^- beam in water. The peak width corresponds to the momentum spread of the beam. The plateau gamma rays from in-flight reactions present the biggest difficulty in the interpretation of the patient data. Additionally, the dynamic range shifter overlaps the peak regions with the plateau; however, we record the range shifter position with each event, thereby dividing the data into groups of beams that are not range shifted.

Future effort will include improving the present chamber or installing one designed for higher rates and performing more measurements on patients. We must then determine how the data can be used in routine treatment.

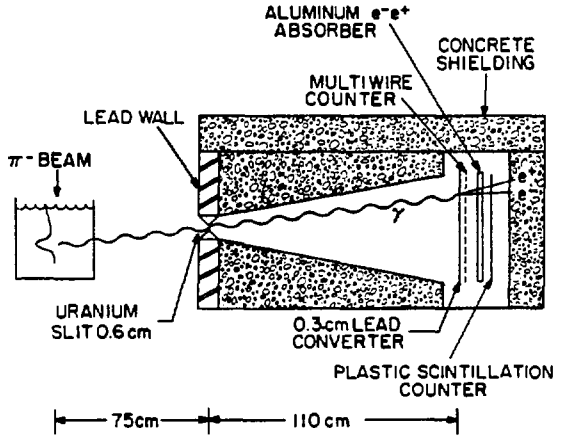

Fig. 1.
Side view of apparatus used for π^- visualization with high-energy gamma rays.

Treatment Planning Development (Biomed)

(Los Alamos)
P. A. Berardo and S. Zink (Los Alamos)

Following the installation of the EMI computerized tomography (CT) scanner, three different EMI software releases were incorporated into the treatment-planning programs. Principal changes among these releases pertained to the number of bits used for each pixel value, the ability to recover CT data from overlaid images, the methods of discriminating among regions-of-interest (ROI) overlays, and extraneous overlay data. These software releases were evaluated in terms of contractual commitments, Biomed requirements, and documentation. Several new treatment-planning capabilities were implemented as a result and are highlighted below.

Regions of Interest

The CT scanner consoles and software provide for up to six ROIs to be overlaid on a CT image. We have developed and implemented the automatic methods and algorithms to transcribe CT-scanner ROIs into vector contours for immediate use in existing treatment-planning programs. Using a track ball, physicians enter ROIs for target volumes and critical sites directly on CT images. Such ROIs have the resolution of the image, and the CT data can be displayed with optimum diagnostic contrast settings. With automatic surface detection (described below) and direct use of CT data for inhomogeneities, only the prescription ROI is required for treatment planning, but there is provision for five other critical-site ROIs per CT slice if desired.

Advantages to the physician include employment of the same equipment used for diagnosis, prescribing treatment from diagnostic-quality images, and the ability to prescribe concurrently with diagnosis. The advantages for treatment planning are automatic entry of contours, high-accuracy transcription of prescriptions, less

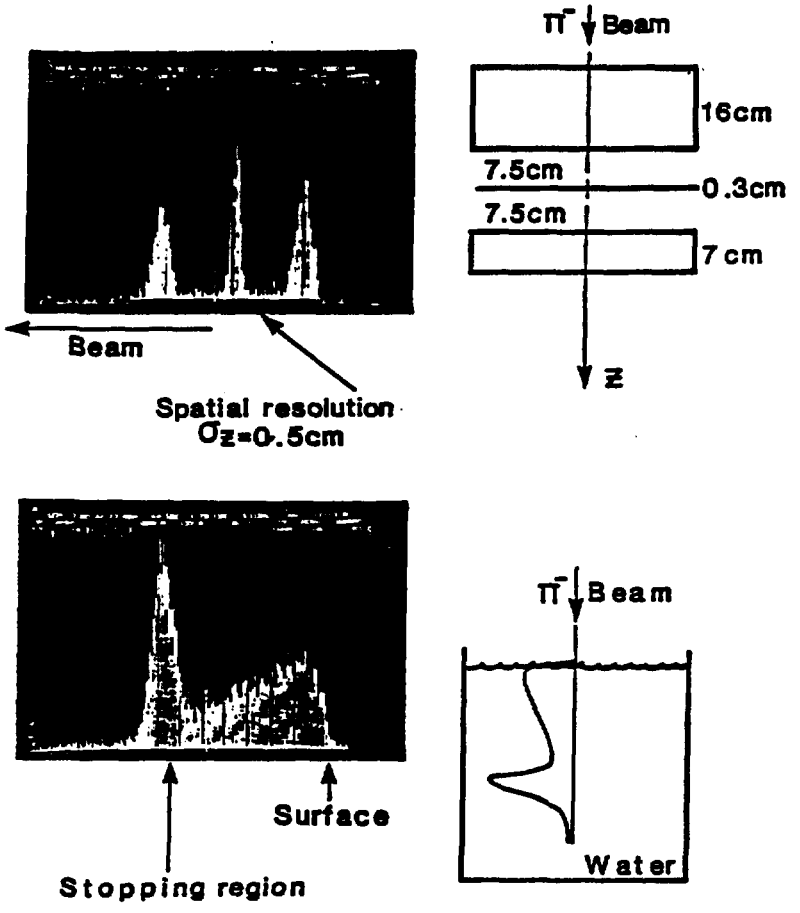

Fig. 2.
Upper plot demonstrates good spatial resolution using a split phantom with a 0.3-cm Lucite sheet as a narrow source of gamma rays. Lower plot is the full signal from a pion beam stopping in water. Pion interaction in flight produces the events in the plateau.

duplicated hardware, and greater use of existing programs.

ROIs are obtained by searching the ROI overlay bit-map, which is part of the CT image file, for the most exterior, contiguous pixels. The resulting pixels define one ROI. For single-ROI images, the locations of the ROI pixels are converted to x,y coordinates to define vector contours. Vector contours generally do not need the very high resolution obtained from contiguous-pixel ROIs. A vertex-reducing algorithm (described below) eliminates points too close together. For multiple-ROI images, the successive ROIs are obtained by subtracting the previous ROI from the current overlay bit-map and reapplying the exterior searching algorithm. Small leftover ROIs resulting from double-backs or "shaky-hand" input are neglected.

Contour Processing

The treatment-planning program PIPLAN does all its calculations in three dimensions. Contours, however, are entered on a series of parallel planes. Volumes are then effectively created by connecting the vertices of a contour on one plane with the corresponding contour vertices on an adjacent plane. It is critical to this procedure

that both contours have the same handedness, the same relative starting point, and essentially uniform spacing of vertices around the contours. These characteristics are automatically satisfied for ROIs transcribed from CT data tapes. Note that contrary to other surface generating methods the number of vertices need not be the same from plane to plane.

For manually entered contours, such as with the digitizing pen, these requirements are not obvious to the user. Handedness is automatically reversed if necessary. The relative starting points are monitored and the user alerted if substantial deviations occur. A new feature of PIPLAN is the automatic smoothing of contours to achieve smooth three-dimensional surfaces. A window is placed around each contour point as it is entered. Points too close together are rejected, and points are automatically embedded when input points are too far apart. A major use of this capability has been to change the number of contour vertices, after they have been entered, to maximize resolution without exceeding memory limitations. Ultimately, memory limitations do affect contour resolution because about 20 to 30 planes of contours must be accommodated in 6000 computer words.

We completed another major feature whereby intersecting contours on a given plane are resolved and automatically edited to remove ambiguous areas or densities. Because each plane is then unambiguous, volumes are, in principle, also unambiguous. This principle is violated only for nearly touching surfaces with too few defining vertices.

Integrated CT Radiography

We wrote a new computer code to reconstruct the same kind of image as digital x-ray radiography from integrated CT images. ROIs on the individual CT images are superimposed on the integrated CT radiography (ICTR) images, but without the distortion normally resulting from a point x-ray source. The processing is done on the Biomed computers, with an EMI CT tape as input. A new tape in EMI format is generated with reconstructed images for input to the CT scanner, where all the diagnostic imaging capabilities already exist.

In pion treatment planning, the target volume is given on the CT image and is used for designing boluses and collimators and for beam-tune selection. When planning is completed, x-ray simulation is used to confirm alignment of clinical appliances with the patient anatomy. At this stage ICTR with ROIs will play an important role in verifying the relative alignment of anatomical structure, appliances, and prescribed target volume.

Surface Detection From CT

If the patient surface is not entered as an ROI on the CT scanner, it can be detected automatically from the CT image at the same time that the image data and other ROIs are being transferred from the CT tape to the patient casefile. By using CT data directly in treatment planning, we need only the surface and target volume contours. By detecting the patient surface automatically, we find the required input and the preparation time are reduced by more than a factor of 2. Accuracy also increases.

After we average and smooth the image data, an applied threshold reduces the image to one of lands, lakes, and islands. Using an algorithm similar to that for ROI decoding, we establish shores. The merit of the procedure is that inland lakes and islands are neglected. The largest shore perimeter is then used as the surface ROI. The procedure to reduce the number of points in the ROI when transcribing to vector contours is the same as for physician-defined ROIs.

Dose Distributions on CT Console

A new display capability was developed whereby pion dose distributions are superimposed on the CT-scanner image and displayed on the cathode-ray tube (CRT) of the EMI-7070 CT scanner. The advantages of this display method are to be able to present the results of treatment planning to the radiotherapist in a most graphic way and to make full use of the scanner graphics software.

The data are transferred by magnetic tape from the PDP-11/(45,70) computer used for treatment planning to the scanner. Duplicating the complex EMI tape format is accomplished by simply replacing the image and ROI data in a copy of any EMI output tape. The limitation of this method is that only preconceived and saved images are available to the physician at the CT console.

Parameterization of seven of the nine tunes used in patient treatments was carried out and a representative sample of uncollimated range-shifted depth-dose curves and scans perpendicular to the beam were compared with dosimetry measurements. Examples are included in Fig. 1.

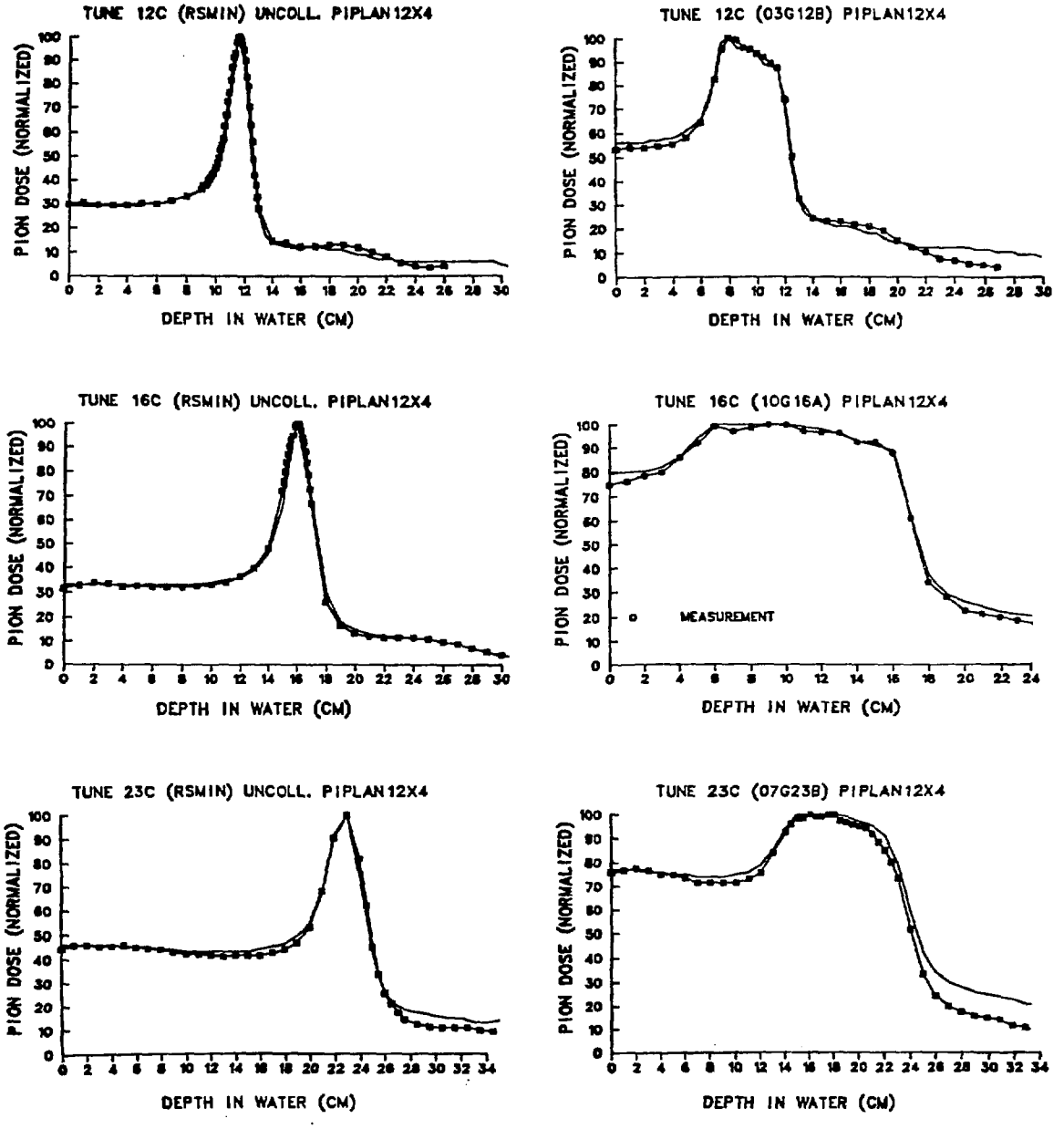

Fig. 1.
Pion dose vs depth in water for various beam tunes at the Biomedical facility.

Biomedical Instrumentation

(Los Alamos)

J. D. Doss

We continue to collaborate with the McGee Eye Institute (MEI) in improvement and testing of corneal modification instrumentation. Representatives from MEI visited Los Alamos in December 1980 for initial animal tests of the new system. As a result of these tests the equipment was modified in minor ways and transported to Oklahoma City for tests in the MEI facility. Results of these animal tests with the new bipolar probe and vacuum fluid drive indicate a higher level of damage to the inner wall of the cornea (endothelium) than was seen with the earlier monopolar probe. The damage appears to be related to the vacuum applied to hold the cornea to the new probe rather than to the different electrical/thermal properties of the bipolar probe. Because the precise mechanism of the damage to the endothelial cells is not yet understood, animal tests are currently under way, which should yield new information to assist us in any probe or fluid flow modifications that may be necessary to minimize this damage. Aside from the endothelial damage, the new probe has proven to be effective in heating stromal collagen and is far more convenient for the therapist and the patient than the earlier probe. The convenience is largely due to the combination of bipolar electrodes at the corneal surface and the vacuum developed at the probe tip. The bipolar electrode eliminates the need for a remote electrode on the rear of the patient's head. The vacuum tip eliminates the need for a relatively painful anesthetic injection for eye immobilization, and also provides a more accurate placement of the probe on the appropriate region of the diseased cornea. In addition to the instrumentation delivered to MEI in March 1981, two more systems are almost complete. One of these will be loaned to the University of New Mexico Medical School for the treatment of corneal disease. The second unit may be loaned temporarily to Fibrasonics, Inc., of Chicago, because this firm is planning to build their own version of the Los Alamos instrumentation. They already have their first order from ophthalmologists in California; retail cost of the first system is estimated to be approximately $15 000 to $20 000.

We are currently experimenting with techniques for casting the eye probe rather than using machining techniques. If this is successful, construction costs of the eye probe (which account for about 10% of the cost of a typical system) could be reduced substantially.

MP-Division Publications; Papers Submitted for Publication

C. Dalton, "A High-Voltage Pulse Monitor System for Neutrino-Electron Elastic Scattering," Los Alamos Scientific Laboratory report LA-8505-MS (August 1980).

D. E. Nagle, "Some Discrete Transforms and Their Continuous Analogs" (LA-UR-80-2367); to be published in *Supplementary Volume of Advances in Mathematics* (Academic Press, Inc., New York).

N. Lockyer, T. A. Romanowski, J. D. Bowman, C. M. Hoffman, R. E. Mischke, D. E. Nagle, J. M. Potter, R. L. Talaga, E. C. Swallow, D. M. Alde, D. R. Moffett, and J. Zyskind, "Parity Violation in Proton-Nucleus Scattering at 6 GeV/c," Int. Symp. on High-Energy Physics with Polarized Beams and Polarized Targets, Lausanne, Switzerland, September 25 - October 1, 1980 (LA-UR-80-2273); to be published in Phys. Rev. Lett.

H. W. Baer, R. D. Bolton, J. D. Bowman, M. D. Cooper, C. M. Hoffman, F. H. Cverna, N. S. P. King, J. Piffaretti, R. H. Heffner, J. Alster, A. Doron, S. Gilad, M. A. Moinester, P. R. Bevington, and E. Winkelmann, "Design, Construction, and Performance of a High-Resolution π^0 Spectrometer for Nuclear Physics Experiments," submitted to Nucl. Instrum. Methods.

H. D. Wohlfahrt, E. B. Shera, M. V. Hoehn, Y. Yamazaki, and R. M. Steffen, "Nuclear Charge Distributions in $1f_{7/2}$-Shell Nuclei from Muonic X-Ray Measurements" (LA-UR-80-1998); submitted to Phys. Rev. C.

R. E. Mischke, J. D. Bowman, C. M. Hoffman, D. E. Nagle, J. M. Potter, R. L. Talaga, N. Lockyer, T. A. Romanowski, E. C. Swallow, D. M. Alde, D. R. Moffett, and J. Zyskind, "Parity Violation in Proton-Nucleus Scattering at 6 GeV/c," Int. Symp. on High-Energy Physics with Polarized Beams and Polarized Targets, Lausanne, Switzerland, September 25 - October 1, 1980.

G. J. Krausse, C. G. Dalton, and J. Sarjeant, "Repetitive Mega-Ampere per Microsecond di/dt Pulsers for Driving Sub-Ohm Transmission Line Neutrino Particle Detectors," Pulse Power Symp., Orlando, Florida, June 1980.

P. Herczeg and C. M. Hoffman, "A Note on the Decays $\pi^0 \rightarrow \nu\nu'$," XX Int. Conf. on High-Energy Physics, Madison, Wisconsin, July 17-23, 1980 (LA-UR-80-1778); submitted to Phys. Lett. B.

P. A. M. Gram, C. A. Goulding, M. Hamm, M. A. Oothoudt, W. Swenson, K. Krane, A. Stetz, D. McDaniels, J. Faucett, B. Wood, H. S. Plendl, J. Norton, H. Funsten, and D. Joyce, "A Complete Coincidence Measurement of the $(\pi,\pi'p)$ Reaction in ^{12}C at 220 MeV," Int. Conf. on Nuclear Physics, Berkeley, California, August 24-30, 1980.

H. W. Baer, J. D. Bowman, M. D. Cooper, C. M. Hoffman, F. H. Cverna, M. B. Johnson, E. R. Siciliano, N. S. P. King, J. Piffaretti, J. Alster, A. Doron, S. Gilad, M. Moinester, P. R. Bevington, and E. Winkelmann, "Observation of Isobaric Analog States in Pion Single-Charge-Exchange Reactions," submitted to Phys. Rev. Lett.

F. Cverna, N. S. P. King, G. Hogan, H. W. Baer, R. E. Anderson, J. D. Bowman, M. D. Cooper, C. M. Hoffman, M. J. Leitch, C. D. Goodman, J. Alster, A. Doron, A. Erell, and M. Moinester, "Pion Single Charge Exchange on Carbon Isotopes," Int. Conf. on Nuclear Physics, Berkeley, California, August 24-30, 1980.

F. E. Obenshain, F. E. Bertrand, E. E. Gross, J. Wu, M. Blecher, K. Gotow, R. L. Burman, M. Hamm, M. J. Leitch, R. D. Edge, B. M. Preedom, M. Moinester, and R. P. Redwine, "Positive Pion-Nucleus Elastic Scattering at 20 MeV," Int. Conf. on Nuclear Physics, Berkeley, California, August 24-30, 1980.

C. M. Hoffman, "A Monochromatic K° Beam," Los Alamos Scientific Laboratory report LA-8444-MS (July 1980).

M. Duong-Van, "Grand Unification and Muon Decay," invited talk, to be published in Proc. XV Rencontre de Moriond Conf., Les Arcs, Savoie, France, 1980.

M. Duong-Van, "A LAMPF $\nu\mu$-Oscillation Experiment," invited talk, to be published in Proc. Telemark Neutrino Mass Workshop, University of Wisconsin, Madison, Wisconsin (1980).

C. Hoffman and M. Duong-Van, "The Search for Muon-Number Violation at LAMPF," Los Alamos Science 1, 62-67 (1980).

J. D. Doss and J. Albillar, "A Technique for Rapid Implantation of Multiple ^{125}I Seeds," Radiology 134, 258-259 (1980).

J. D. Doss and C. W. McCabe, "Portable Radio-Frequency Hyperthermia Instrumentation," Third Int. Symp: Cancer Therapy by Hyperthermia, Drugs, and Radiation, Fort Collins, Colorado, June 22, 1980.

J. D. Doss, R. L. Hutson, J. J. Rowsey, and R. Brown, "Method for Calculation of Corneal Profile and Power Distribution," Arch. Ophthalmol. (in press).

J. D. Doss, "Treating Cancer with Heat," New Mexico Academy of Sciences *Science Brief*, The New Mexico Independent 84 (August 15, 1980).

J. J. Rowsey and J. D. Doss, "Preliminary Report of Los Alamos Keratoplasty Techniques," Arch. Ophthalmol. (in press).

C. Tao, R. G. Hicks, H. L. Anderson, N. E. Booth, W. R. Francis, B. A. Gordon, W. W. Kinnison, T. B. W. Kirk, W. A. Loomis, H. S. Matis, L. W. Mo, L. C. Myrianthopoulos, F. M. Pipkin, J. Proudfoot, T. W. Quirk, A. L. Sessoms, W. D. Shambroom, A. Skuja, M. A. Staton, W. S. C. Williams, R. Wilson, and S. C. Wright, "Transverse Momentum and Angular Distributions of Hadrons in Muon-Proton Scattering and Tests of Quantum Chromodynamics," Phys. Rev. Lett. 44, 1726 (1980).

R. G. Hicks, H. L. Anderson, N. E. Booth, W. R. Francis, B. A. Gordon, W. W. Kinnison, T. B. W. Kirk, W. A. Loomis, H. S. Matis, L. W. Mo, L. C. Myrianthopoulos, F. M. Pipkin, J. Proudfoot, T. W. Quirk, A. L. Sessoms, W. D. Shambroom, A. Skuja, M. A. Staton, C. Tao, W. S. C. Williams, R. Wilson, and S. C. Wright, "Muoproduction of Neutral Strange Hadrons at 225 GeV," Phys. Rev. Lett. 45, 765 (1980).

H. S. Matis, "Search for Lepton Flavor Violating Decays at LAMPF," presented at the University of British Columbia, March 7, 1980.

R. L. Boudrie, J. F. Amann, G. C. Idzorek, S. J. Seestrom-Morris, D. B. Holtkamp, M. A. Franey, D. Dehnhard, and C. Goulding, "Scattering of 547-MeV Polarized Protons from ^{13}C," Am. Phys. Soc. Mtg., Baltimore, Maryland, April 20-23, 1981.

C. Harvey, H. W. Baer, C. L. Morris, D. B. Holtkamp, S. J. Seestrom-Morris, D. Dehnhard, and S. J. Greene, "A Study of the Neutron Density Distributions of $^{12,13,14}C$ from a Comparison of π^+ and π^- Elastic Scattering," Am. Phys. Soc. Mtg., Baltimore, Maryland, April 20-23, 1981.

D. B. Holtkamp, S. J. Seestrom-Morris, D. Dehnhard, H. W. Baer, C. L. Morris, S. J. Greene, and C. J. Harvey, "Strong Cancellations of Neutron and Proton Transition Amplitudes Observed in Pion Inelastic Scattering from ^{14}C," American Physical Society Mtg., Baltimore, Maryland, April 20-23, 1981.

C. F. Moore, W. B. Cottingame, S. J. Greene, C. J. Harvey, P. A. Seidl, S. J. Seestrom-Morris, D. B. Holtkamp, R. L. Boudrie, C. L. Morris, and J. Piffaretti, "Measurements of Pion Inelastic Scattering to States in the Giant Dipole Region of ^{12}C," IX Int. Conf. on High-Energy Physics and Nuclear Structure, Versailles, France, July 6-10, 1981.

C. L. Morris, R. L. Boudrie, J. Piffaretti, C. J. Harvey, C. F. Moore, P. A. Seidle, W. B. Cottingame, S. J. Greene, S. J. Seestrom-Morris, and D. B. Holtkamp, "Isospin Purity of the Giant Dipole Resonance in ^{12}C," Am. Phys. Soc. Mtg., Baltimore, Maryland, April 20-23, 1981.

B. Aas, E. Bleszynski, M. Bleszynski, M. Haji-Saeid, G. J. Igo, F. Irom, G. Pauletta, A. Rahbar, A. Wang, J. F. Amann, T. A. Carey, W. Cornelius, J. B. McClelland, M. Barlett, M. Gazzaly, C. Glashausser, and S. Nanda, "Spin-Rotation Measurement in $^{40}Ca(p,p)^{40}Ca$ Inelastic Scattering at 500 MeV," Am. Phys. Soc. Mtg., Baltimore, Maryland, April 20-23, 1981.

S. Seestrom-Morris, D. Dehnhard, D. B. Holtkamp, and C. L. Morris, "Identification of $\Delta S = 1$ Transitions in ^{13}C by Measurement of Pion Inelastic Excitation Functions," submitted to Phys. Rev. Lett.

S. J. Seestrom-Morris, D. Dehnhard, M. A. Franey, G. S. Kyle, C. L. Morris, R. L. Boudrie, J. Piffaretti, and H. A. Thiessen, "DWIA Analysis of Elastic and Inelastic Scattering of Pions from ^{13}C," Am. Phys. Soc. Mtg., Baltimore, Maryland, April 20-23, 1981.

R. L. Boudrie, C. L. Morris, J. Källne, R. C. Minehart, and R. R. Whitney, "The Nuclear $(\pi^{\pm},\pi^{\mp})$ Reactions to Continuum Final States," IX Int. Conf. on High-Energy Physics and Nuclear Structure, Versailles, France, July 6-10, 1981.

J. F. Amann, W. Cornelius, J. B. McClelland, and H. A. Thiessen, "A Polarimeter for Analyzing Nuclear States in p-Nucleus Reactions at Intermediate Energies," IX Int. Conf. on High-Energy Physics and Nuclear Structure, Versailles, France, July 6-10, 1981.

S. J. Greene, G. R. Burleson, W. B. Cottingame, H. T. Fortune, D. B. Holtkamp, C. F. Moore, and C. L. Morris, "Interference Effects in Pion Double Charge Exchange," Am. Phys. Soc. Mtg., Baltimore, Maryland, April 20-23, 1981; IX Int. Conf. on High-Energy Physics and Nuclear Structure, Versailles, France, July 6-10, 1981; and submitted to Phys. Rev. C.

K. G. Boyer, W. B. Cottingame, L. E. Smith, S. J. Greene, C. F. Moore, J. S. McCarthy, R. C. Minehart, J. F. Davis, G. R. Burleson, G. Blanpied, C. A. Goulding, H. A. Thiessen, and C. L. Morris, "Pion Inelastic Scattering to the Low-Lying States in $^{42,44,48}Ca$: A Determination of the Neutron and Proton Multipole Matrix Elements," submitted to Phys. Rev. C.

L. G. Atencio, J. F. Amann, R. L. Boudrie, and C. L. Morris, "Delay-Line Readout Drift Chambers," submitted to Nucl. Instrum. Methods.

J. F. Amann, J. B. McClelland, W. Cornelius, and H. A. Thiessen, "A Polarimeter for Analyzing Nuclear States in p-Nucleus Reactions between 300 and 800 MeV," Am. Phys. Society Mtg., Baltimore, Maryland, April 20-23, 1981.

W. G. Love and M. A. Franey, "An Effective Nucleon-Nucleon Interaction for Scattering at Intermediate Energies," submitted to Phys. Rev. C.

E. A. Hinds, W. D. Cornelius, and R. L. York, "Depolarization Effects in Optically Pumped Polarized Proton Sources," submitted to Nucl. Instrum. Methods.

R. D. Brown and C. F. Hansen, "A New Stringer for the LAMPF Radiation Effects Facility," 1981 Particle Accelerator Conf., Accelerator Engineering and Technology, Washington, DC, March 11-13, 1981.

R. D. Brown and D. L. Grisham, "Design and Operation, Water-Cooled Pyrolytic Graphite Targets at LAMPF," 1981 Particle Accelerator Conf., Accelerator Engineering and Technology, Washington, DC, March 11-13, 1981.

D. L. Grisham and J. E. Lambert, "Water-Cooled Beam-Line Components at LAMPF," 1981 Particle Accelerator Conf., Accelerator Engineering and Technology, Washington, DC, March 11-13, 1981.

D. L. Grisham, J. E. Lambert, T. S. Baldwin, and E. L. Ekberg, "Monitor 1981," 1981 Particle Accelerator Conf., Accelerator Engineering and Technology, Washington, DC, March 11-13, 1981.

D. L. Grisham and J. E. Lambert, "Why High-Capacity Manipulators and Lead-Glass Windows?" Am. Nucl. Soc. Ann. Mtg., Miami Beach, Florida, June 7-12, 1981.

J. K. Novak, F. J. Edeskuty, and J. R. Bartlit, "Cool-Down Flow-Rate Limits Imposed by Thermal Stresses in LNG Pipelines," Cryogenic Engineering Conf. and Int. Cryogenic Materials Conf. Board, San Diego, California, August 10-14, 1981.

K. S. Krane, "Fragment Muonic X Rays Emitted Following Prompt Muon-Induced Fission," submitted to Phys. Lett. B.

E. F. Gibson, J. J. Kraushaar, T. G. Masterson, R. J. Peterson, R. S. Raymond, R. A. Ristinen, and R. L. Boudrie, "Elastic and Inelastic π^+,π^- Scattering on ^7Li," Am. Phys. Soc. Mtg., Baltimore, Maryland, April 20-23, 1981.

J. B. McClelland, J. F. Amann, T. A. Carey, W. Cornelius, B. Aas, M. Haji-Saeid, G. Igo, F. Irom, G. Pauletta, A. Rahbar, A. Wang, M. Barlett, G. Hoffmann, M. Gazzaly, and C. Glashausser, "Spin-Rotation Measurement in $^{40}Ca(p,p)^{40}Ca$ Elastic Scattering at 500 MeV," Am. Phys. Soc. Mtg., Baltimore, Maryland, April 20-23, 1981.

D. B. Holtkamp, S. J. Seestrom-Morris, S. Chakravarti, D. Dehnhard, H. W. Baer, C. L. Morris, S. J. Greene, and C. J. Harvey, "π^+,π^- Cross-Section Ratios Larger Than the Free Pion-Nucleon Value Observed in Pion Inelastic Scattering from ^{14}C," IX Int. Conf. on High-Energy Physics and Nuclear Structure, Versailles, France, July 6-10, 1981.

T. G. Masterson, J. J. Kraushaar, D. A. Lind, R. J. Peterson, R. S. Raymond, R. A. Ristinen, R. L. Boudrie, and E. F. Gibson, "A Limit on Charge Asymmetry from Elastic π-d Scattering at 143 MeV," IX Int. Conf. on High-Energy Physics and Nuclear Structure, Versailles, France, July 6-10, 1981.

A. Wriekat, G. S. Adams, M. Bleszynski, S. M. Haji-Saeid, G. Igo, J. B. McClelland, G. Pauletta, C. A. Whitten, Jr., M. Gazzaly, and N. Tanaka, "Elastic pp Scattering at 1.463 GeV/c in the Coulomb Interference Region," submitted to Phys. Lett. B.

G. W. Hoffmann, L. Ray, M. Barlett, W. R. Coker, J. McGill, G. S. Adams, G. J. Igo, F. Irom, A. T. M. Wang, C. A. Whitten, Jr., R. L. Boudrie, J. F. Amann, C. Glashausser, N. M. Hintz, G. S. Kyle, and G. S. Blanpied, "$A_y(\theta)$ for $\vec{p}$ + ^{208}Pb Elastic Scattering at 0.8 GeV and a Test of Multiple-Scattering Theory," submitted to Phys. Rev. C.

H. S. Butler, R. A. Williams, M. D. Cooper, J. R. Rolfe, S. L. Wilson, and H. D. Zeman, "An Application of Parallel Preprocessors in Data Acquistion," Topical Conf. on Computerized Data Acquisition in Particle and Nuclear Physics, Oak Ridge, Tennessee, May 28-30, 1981.

J. A. Brown, R. H. Heffner, R. L. Hutson, S. Kohn, C. E. Olsen, M. E. Schillaci, S. A. Dodds, T. L. Estle, D. A. Vanderwater, and O. D. McMasters, "Muon Depolarization by Paramagnetic Impurities in Nonmagnetic Metals," submitted to Phys. Rev. Lett.

W. F. Sommer, L. N. Kmetyk, W. V. Green, and R. P. Damjanovich, "Use of the LAMPF Accelerator as a Fusion Material — Radiation Effects Facility," 2nd Topical Mtg. on Fusion Reactor Materials, Seattle, Washington, August 9-12, 1981.

D. J. Ernst and M. B. Johnson, "Reactive Content of the Klein-Gordon Optical Potential," submitted to Phys. Rev.

M. R. Raju, J. Butler, S. Carpenter, J. Dicello, A. R. Smith, and N. Tokita, "Cell Killing by Pion Beams Used in Therapy," Radiat. Res. Soc., 29th Ann. Mtg., Minneapolis, Minnesota, May 31 - June 4, 1981.

D. J. Brenner and J. F. Dicello, "Calculations of Ionization Distributions in a Tissue-Equivalent Cloud Chamber Gas Mixture," Radiat. Res. Soc., 29th Ann. Mtg., Minneapolis, Minnesota, May 31 - June 4, 1981.

J. F. Dicello, D. J. Brenner, and R. E. Prael, "Improved Dosimetric and Microdosimetric Calculations for Clinical High-Energy Neutron Beams," Radiat. Res. Soc., 29th Ann. Mtg., Minneapolis, Minnesota, May 31 - June 4, 1981.

A. J. Jason, D. W. Hudgings, and O. B. van Dyck, "Neutralization of H^- Beams by Magnetic Stripping," Particle Accelerator Conf., Washington, DC, March 11-13, 1981.

D. G. Perry, "A Comparison of Data-Acquisition Software: Q and Multi," Topical Conf. on Computerized Data Acquisition in Particle and Nuclear Physics, Oak Ridge, Tennessee, May 28-30, 1981.

J. D. Bowman, M. B. Johnson, and J. W. Negele, "Pion Charge Exchange Reaction as a Probe of Isovector Monopole Resonances," submitted to Phys. Rev. Lett.

E. B. Shera, H. D. Wohlfahrt, and M. V. Hoehn, "On the Comparison of Optical and Muonic Isotope Shifts," IX Int. Conf. on High-Energy Physics and Nuclear Structure, Versailles, France, July 6-10, 1981.

K. M. Hanson, J. N. Bradbury, R. A. Koeppe, R. J. Macek, D. R. Machen, R. Morgado, M. A. Paciotti, and S. A. Sanford, "Proton Computed Tomography of Human Specimens," submitted to Phys. Med. Biol.

H. W. Baer, C. L. Morris, D. B. Holtkamp, S. J. Seestrom-Morris, S. Chakravarti, D. Dehnhard, S. J. Greene, and C. J. Harvey, "Strong Cancellations of Neutron and Proton Transition Amplitudes Observed in Pion Inelastic Scattering from ^{14}C," submitted to Phys. Rev. Lett.

R. Kunselman, M. V. Hoehn, E. B. Shera, H. D. Wohlfahrt, E. Bovet, and J. Gimlet, "Pionic 3d → 2p X-Ray Measurements Near Z = 24," IX Int. Conf. on High-Energy Physics and Nuclear Structure, Versailles, France, July 6-10, 1981.

A. J. Jason, D. W. Hudgings, O. B. van Dyck, W. Folkner, and D. A. Clark, "H^- Field Detachment," submitted to Phys. Rev. Lett.

D. L. Grisham, "Torus Sector Handling System," Proc. Remote Maintenance Equipment Workshop, Fusion Engineering Design Center, Oak Ridge, Tennessee, March 12, 1981.

S. J. Greene, W. J. Braithwaite, D. B. Holtkamp, W. B. Cottingame, C. F. Moore, G. R. Burleson, G. S. Blanpied, A. J. Viescas, G. H. Daw, C. L. Morris, and H. A. Thiessen, "(π^+,π^-) Double-Charge-Exchange Reactions on $^{16,18}O$ and $^{24,26}Mg$," submitted to Phys. Rev. C.

R. J. Ellis, H. J. Ziock, K. O. H. Ziock, Y. Tzeng, J. Bolger, E. Boschitz, J. Arvieux, R. Corfu, J. Piffaretti, L. C. Liu, and E. R. Siciliano, "Implications of the Reaction $^{12}C(\pi^+,\pi^+d)^{11}B$ on Deuteron Clusters and Dibaryon Resonances," submitted to Phys. Rev. Lett.

J. F. Amann, "Front-End Event Selection with an MBD Using Q," Topical Conf. on Computerized Data Acquisition in Particle and Nuclear Physics, May 28-30, 1981.

J. F. Harrison, T. Kozlowski, R. A. Floyd, J. F. Amann, G. T. Anderson, M. A. Oothoudt, and D. G. Perry, "Design of the RSX-11M Q System," Topical Conf. on Computerized Data Acquisition in Particle and Nuclear Physics, Oak Ridge, Tennessee, May 28-30, 1981.

D. Schultz, "Real-Time Interrupt Handling Using F4P Under RSX-11M," 1981 Fall DECUS U.S. Symp., Los Angeles, California, December 7-11, 1981.

D. J. Brenner, R. E. Prael, J. F. Dicello, and M. Zaider, "Improved Calculations of Energy Deposition from Fast Neutrons," 4th Symp. on Neutron Dosimetry, Neuherberg/Münich, West Germany, June 1981.

J. F. Dicello, D. J. Brenner, S. Zink, P. A. Berardo, and I. I. Rosen, "A Method for the Direct Measurement in the Treatment Volume of Neutron Dose from Pion Stars," 4th Symp. on Neutron Dosimetry, Neuherberg/Münich, West Germany, June 1981.

W. W. Kinnison, H. L. Anderson, H. S. Matis, and S. C. Wright, "A Search for $\mu^+ \rightarrow e^+\gamma$," submitted to Phys. Rev. D1.

M. W. McNaughton and E. P. Chamberlin, "pp Elastic Analyzing Power from 318 to 800 MeV," submitted to Phys. Rev. C as a "Brief Report."

S. J. Seestrom-Morris, "The Structure of ^{13}C Studied by Pion Scattering Near the [3,3] Resonance," submitted to Phys. Rev. C.

P. Wallis, "Guide to Using DRS," DRS Users Soc. Mtg., Chicago, Illinois, June 14-16, 1981.

M. Oothoudt, J. Amann, R. Floyd, J. Harrison, and T. Kozlowski, "A Memory-Resident Histogramming System" 1981 Fall DECUS U.S. Symp., Los Angeles, California, December 7-11, 1981.

G. T. Anderson, M. A. Oothoudt, J. F. Amann, and T. Kozlowski, "Dynamic Parameter-Array System (DPA)," 1981 Fall DECUS U.S. Symp., Los Angeles, California, December 7-11, 1981.

K. K. Seth, "Pionic Probes for Exotic Nuclei," invited paper, IV Int. Conf. on Nuclei Far Away from Stability," Helsingor, Denmark, June 8-13, 1981.

R. H. Heffner, "Muon Spin Depolarization in Nonmagnetic Metals Doped with Paramagnetic Impurities," 2nd Int. Topical Mtg. on Muon Spin Rotation, Vancouver, B.C., Canada, August 1980.

M. E. Schillaci, R. L. Hutson, R. H. Heffner, M. Leon, S. A. Dodds, and T. L. Estle, "Depolarization of Diffusing Spins by Paramagnetic Impurities," 2nd Int. Topical Mtg. on Muon Spin Rotation, Vancouver, B.C., Canada, August 1980.

D. B. Holtkamp, S. J. Seestrom-Morris, S. Chakravarti, D. Dehnhard, H. W. Baer, C. L. Morris, S. J. Greene, and C. J. Harvey, "Strong Cancellations of Neutron and Proton Transition Amplitudes Observed in Pion Inelastic Scattering from ^{14}C," submitted to Phys. Rev. Lett.

J. A. Brown, S. A. Dodds, T. L. Estle, R. H. Heffner, M. Leon, D. E. MacLaughlin, C. E. Olsen, and M. E. Schillaci, "Zero and Finite Field μSR in Spin Glass Ag:Mn," 2nd Int. Topical Mtg. on Muon Spin Rotation, Vancouver, B.C., Canada, August 1980.

D. E. MacLaughlin, "μSR and Other Microscopic Probes of Spin-Glass Dynamics," 2nd Int. Topical Mtg. on Muon Spin Rotation, Vancouver, B.C., Canada, August 1980.

J. A. Brown, R. H. Heffner, T. A. Kitchens, M. Leon, C. E. Olson, M. E. Schillaci, S. A. Dodds, and D. E. MacLaughlin, "Anomalous Paramagnetic-State μSR in Spin Glass Ag:Mn," 26th Ann. Conf. on Magnetism and Magnetic Materials, Dallas, Texas, November 1980.

C. L. Morris, K. G. Boyer, C. F. Moore, C. J. Harvey, K. J. Kallianpur, I. B. Moore, P. A. Seidl, S. J. Seestrom-Morris, D. B. Holtkamp, S. J. Greene, and W. B. Cottingame, "Pion Inelastic Scattering to Low-Lying States in ^{12}C and ^{40}Ca," submitted to Phys. Rev. C.

M. Leon, "Models for μ^+ Depolarization in Spin Glasses for Zero External Field," 2nd Int. Topical Mtg. on Muon Spin Rotation, Vancouver, B.C., Canada, August 1980.

W. B. Alberico, A. Molinari, R. Cenni, and M. B. Johnson, "On the Collective Modes of Infinite Nuclear Matter," submitted to Annals of Physics.

Proceedings of the Workshop on Nuclear and Particle Physics at Energies Up to 31 GeV, R. R. Silbar, J. D. Bowman, E. M. Henley, and L. S. Kisslinger, Eds., Los Alamos National Laboratory report LA-8775-C (1981).

D. E. Schultz and S. K. Brown, "On-Line Replacement of a Particle Accelerator Control Computer," submitted to IEEE Mtg. Miami, Florida, December 7-11, 1981.

LAMPF Experimental Program Reports and Publications

(Exp. 18) D. F. Geesaman, C. Olmer, B. Zeidman, R. L. Boudrie, G. S. Blanpied, M. J. Devereux, G. R. Burleson, R. E. Segel, L. W. Swenson, and H. A. Thiessen, "Elastic and Inelastic Scattering of 291-MeV Pions by ^{9}Be, Si, ^{58}Ni, and ^{208}Pb," Phys. Rev. C23, 2635-2647 (1981).

(Exp. 27) M. W. McNaughton, H. W. Baer, P. R. Bevington, F. H. Cverna, H. B. Willard, E. Winkelmann, E. P. Chamberlin, J. J. Jarmer, N. S. P. King, J. E. Simmons, M. A. Schardt, and H. Willmes, "Spin Correlation Parameter A_{nn} in pp Elastic Scattering at 796 MeV," Phys. Rev. C23, 838-844 (1981).

(Exp. 206) P. O. Egan, S. Dhawan, V. W. Hughes, D. C. Lu, F. G. Mariam, P. A. Souder, J. Vetter, G. zu Putlitz, P. A. Thompson, and A. B. Denison, "Search for Long-Lived 2S Muonic Hydrogen in H_2 Gas," Phys. Rev. A23, 1152-1163 (1981).

(Exp. 221) M. A. Schardt, J. S. Frank, C. M. Hoffman, R. E. Mischke, D. C. Moir, and P. A. Thompson, "New Measurement of the Dalitz-Decay Branching Ratio of the π^0," Phys. Rev. D23, 639-648 (1981).

(Exp. 289) F. Irom, "Small-Angle Proton-Proton and Proton-Deuteron Elastic Scattering at 800 MeV," Los Alamos National Laboratory report LA-8648-T (1981).

(Exp. 372) R. L. Hutson, J. D. Knight, M. Leon, M. E. Schillaci, H. B. Knowles, and J. J. Reidy, "Negative Muon Capture in Noble Gas Mixtures," Phys. Lett. 76A, 226-228 (1980).

(Exp. 385) M. L. Barlett, "Forward-Angle Quasi-Free Proton-Neutron Analyzing Powers at 0.8 GeV," Los Alamos National Laboratory report LA-8659-T (1981).

(Exp. 486) S. M. Haji-Saeid, "Elastic Scattering of Polarized Deuterons from Hydrogen at 2.0, 1.6, and 1.2 GeV and Search for Critical Opalescence in Inelastic Scattering of Protons from ^{12}C at 800 MeV," Los Alamos National Laboratory report LA-8662-T (1981).

(Exp. 495) C. L. Morris, R. L. Boudrie, J. Piffaretti, W. B. Cottingame, W. J. Braithwaite, S. J. Greene, C. J. Harvey, D. B. Holtkamp, C. F. Moore, and S. J. Seestrom-Morris, "Measurements of Isospin Mixing Between the 1^+ Doublet in ^{12}C Using Pion Inelastic Scattering," Phys. Lett. 99B, 387-390 (1981).

(Exp. 643) J. Kelly, W. Bertozzi, T. N. Buti, F. W. Hersman, C. Hyde, M. V. Hynes, B. Norum, F. N. Rad, A. D. Bacher, G. T. Emery, C. C. Foster, W. P. Jones, D. W. Miller, B. L. Berman, W. G. Love, and F. Petrovich, "Signatures of Density Dependence in the Two-Nucleon Effective Interaction Near 150 MeV," Phys. Rev. Lett. 45, 2012-2015 (1980).

Patents Pending

"Multipolar Corneal-Shaping Electrode," Docket #S-54,653, filed May 1981, J. D. Doss.

II. FACILITY AND EXPERIMENTAL DEVELOPMENTS

Research Support at LAMPF

The Clinton P. Anderson Meson Physics Facility (LAMPF) is available on an international basis to qualified researchers. The facility is operated by the Medium-Energy Physics (MP) Division of Los Alamos National Laboratory. Within MP Division are nine groups. Three of these have research as their main objective. Six groups provide support to the overall mission of LAMPF.

No one of these six support groups is more essential than the others; the total enterprise would founder without their contributions. This issue of *Progress at LAMPF* begins a series of brief looks at the support groups, for the dual purpose of explaining their functions to experimenters who may not be familiar with them and of providing well-deserved recognition to these important, if less visible, people who help make LAMPF function.

For the beginning of the series we select the Engineering Support Group, MP-8, because it is the group with which most experimenters first make contact. Figure 1 shows the routing of a proposal for an experiment, details its interaction with MP-8, and lists the remaining five support groups at LAMPF.

Approved and scheduled experiments have assigned to them a LAMPF Experiment Engineer who acts as the interface between MP-8 and the experiment. Almost without exception, substantial engineering support is required for every experiment. For example, the experiment may need pivoted platforms for mounting of spectrometers, mechanical support for counters, magnets of special configuration, or other special equipment. MP-8 is equipped to design, fabricate, and mount these special items. The Magnet Section, for example, can design magnets or prepare suitable units from a pool of ~100 magnets and subsequently supply field maps of the magnet. Alignment of accelerator components, beam lines, and experiments is essential to the success of research programs. The Alignment Section maintains expertise in the capability of aligning components using optical, laser, or magnetic techniques as may be required, thus providing a valuable service to the experimenter.

The Technical Support Section interfaces with the experiment, helping to install special equipment as required.

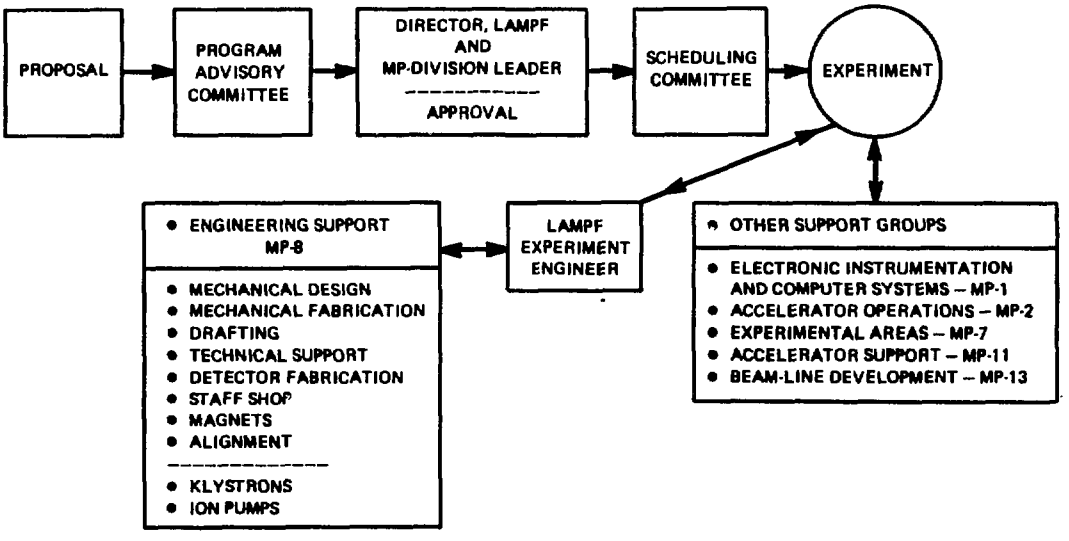

Fig. 1.

Organization of Group MP-8, showing also routing of a typical proposal and interaction with the group. Also listed are other support groups at LAMPF.

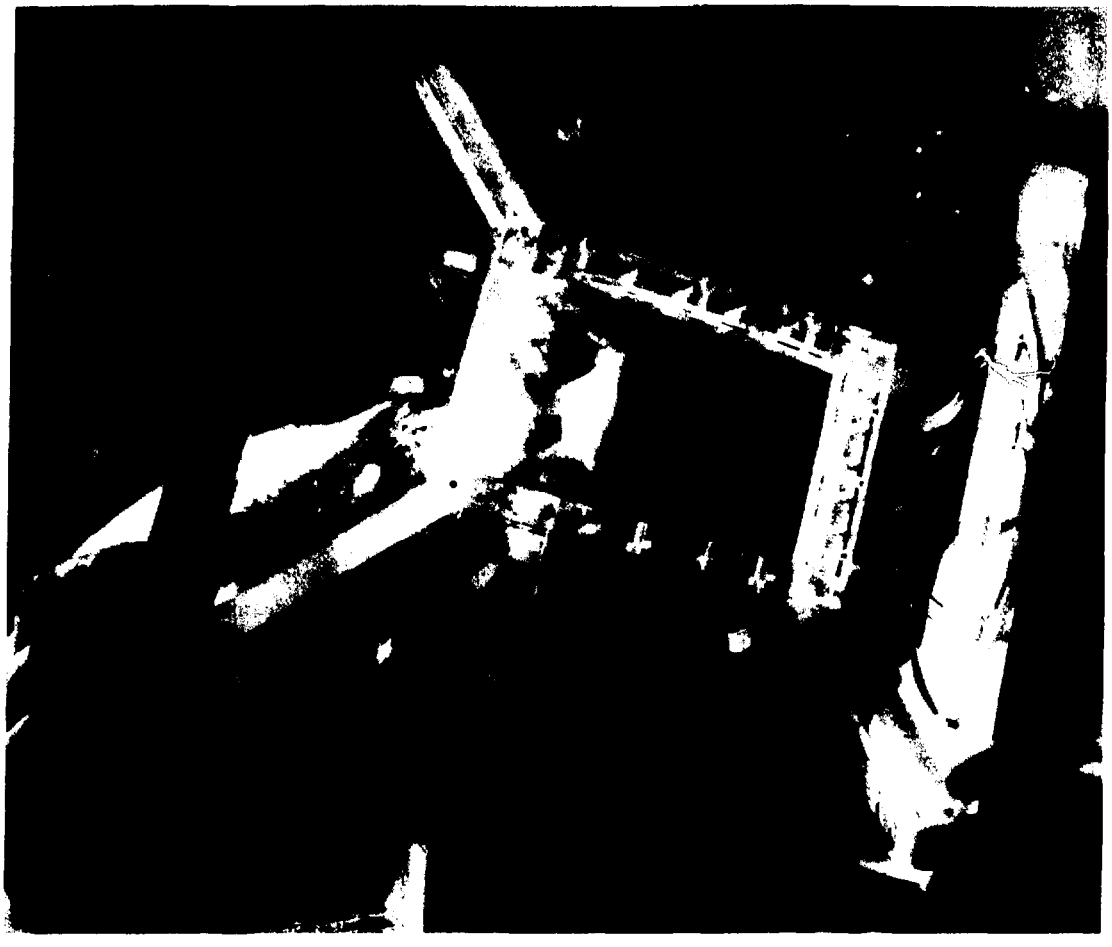

Fig. 2.
Fred Montoya, MP-8, inspects light pipes for a scintillation detector fabricated in his shop.

Less directly related to the experiment, but serving an equally important function, are the Klystron and Ion Pump Rebuild Sections, which service these important accelerator components. In addition, most major modifications to the accelerator structures are also performed by the group.

Fig. 3.
Ed Bush, MP-8 Group Leader, views a spare biomedical beam-line magnet nearing completion.

π^0 Spectrometer Program

During the winter and spring of 1981 there was a spectrometer development run at LEP. The spectrometer had been mounted with the goal of making it a general user facility. For this purpose the LEP cave area was enlarged, a steel floor was installed, the channel was extended by the addition of two quadrupole magnets and three steering magnets, a large lead shielding wall was mounted at the channel exit, an overhead boom was installed to carry electronics cables, and permanent electronics racks were mounted at the south end of the LEP counting house. Before beam was on, cosmic rays were used to set phototube high voltages, plateau all multiwire proportional counters (MWPCs), and set the timing for all scintillators and lead-glass shower detector elements.

At the beginning of the development run, 50-200-MeV pion beams were tuned through the channel extension. Then the gains of the 60 glass detectors were calibrated and the scintillators and wire chambers were plateaued and timed in. Performing this task in such a short time was made possible since gains had been set approximately with the cosmic rays. We found that the ^{207}Bi light pulsers used for calibration are quite stable and that the equivalent light values reproduced to within a few percent from the previous year. The gain stabilization is now fully incorporated and is automatic with normal data-taking. It appears that the light output from the pulsers will be constant over a period of years.

An unexpected result of the glass calibration studies with electron beams was the observed dependence of the converter light on the position of beam entry. Because of this, the highest π^0 energy resolution that can be achieved at this time is by use of only one converter in each arm. We measured a spectrum for the ^{7}Li$(\pi^+,\pi^0)^7$Be reaction at 100 MeV with one converter in each arm; the solid angle is reduced by a factor of 5 compared to running with three converters. Figure 1 shows this spectrum, taken with the channel set to $\Delta E = 0.8$-MeV beam energy spread, a 3-cm ^{7}Li target, and a target-to-converter distance of 1.92 m. The resolution is 2.0 MeV (FWHM), the best we have achieved to date.

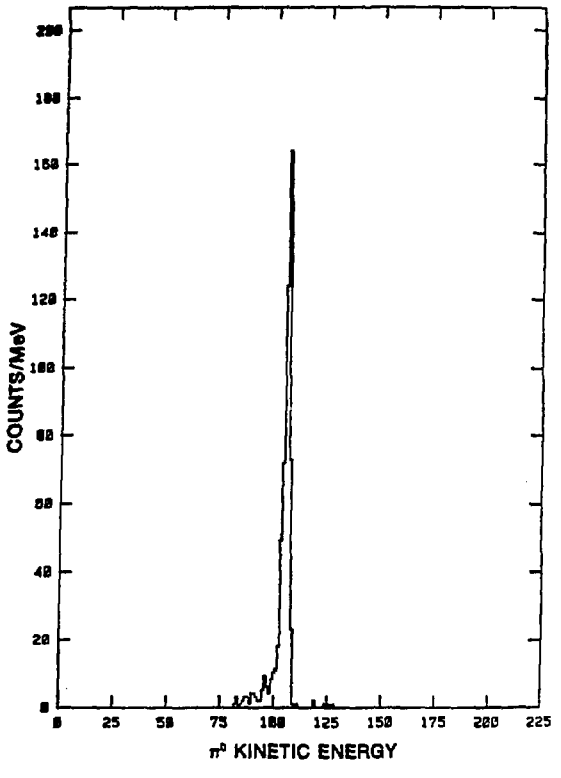

Fig. 1.
Spectrometer reconstruction of π^0 energy from $^7Li(\pi^+,\pi^0)^7Be$ charge-exchange reaction at 5° with 100-MeV incident beam.

Background shielding resulted in a major improvement in usable beam intensity. In our 1980 runs the typical π^+ flux was 2 MHz for runs at 0°, whereas the 1981 runs had a flux of 10-20 MHz under corresponding conditions.

An article describing the LAMPF π^0 spectrometer has just been published.[1] It should serve as the basic reference article for use of the π^0 spectrometer.

—H. Baer, J. D. Bowman, and M. Cooper

REFERENCE

1. H. W. Baer, R. D. Bolton, J. D. Bowman, M. D. Cooper, F. H. Cverna, R. H. Heffner, C. M. Hoffman, N. S. P. King, J. Piffaretti, J. Alster, A. Doron, S. Gilad, M. A. Moinester, P. R. Bevington, and E. Winkelmann, "Design, Construction, and Performance of a High-Resolution π^0 Spectrometer for Nuclear Physics Experiments," Nucl. Instrum. Methods 180, 445-459 (1981).

Remote Handling at LAMPF

Background

Traditionally most remote-handling operations are accomplished in hot cells using master-slave mechanical or electromechanical manipulators. Although hot cells may be satisfactory for the purposes for which they are designed, they are limited by size and geometry.

At LAMPF, most of the Area A repair work on main beam-line components must be done *in situ*. The Monitor system was developed to provide a portable remote-handling system for this job.

Remote maintenance at LAMPF began in 1976 when the prototype Monitor I was used to replace an air-cooled vacuum window with a water-cooled window in target cell A-6. The manipulators used at this time were a U. S. Navy surplus hydraulic arm (originally designed for underwater use) and a 20-year-old electromechanical manipulator. Since that time, improvements have constantly been made to keep pace with higher radiation levels and the increasing complexity of tasks.

The best single improvement to the Monitor system was the addition of bilateral force-reflecting servomanipulators, which were developed by Tele-Operator Systems Corp., under contract to LAMPF. Other major improvements include video systems with specially designed pan/tilt devices, an automatic shoulder-level drive system, and proportional controls for the crane hydraulic system.

The intial remote-handling tasks were generally very simple, for example, removal and replacement of components using very basic hand tools. The present LAMPF remote-handling capability has evolved to the point where highly complex tasks are routinely performed using specially designed equipment.

LAMPF is currently recognized as a world leader in remote-handling technology, both in capability and quantity of work successfully completed.

Description

As shown in Figs. 1 and 2, a Monitor system consists of slave manipulators mounted on a portable hydraulic crane that can be positioned in a specific work area. Work is accomplished by operating the master manipulators located in a master control station (Fig. 3), which is located a safe distance from the radioactive

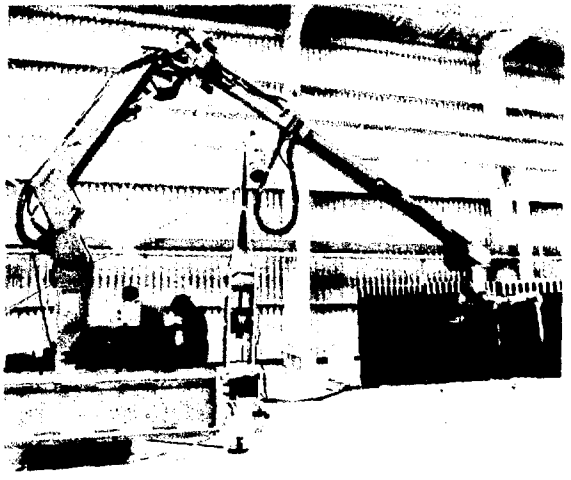

Fig. 1.
Overall view of Monitor.

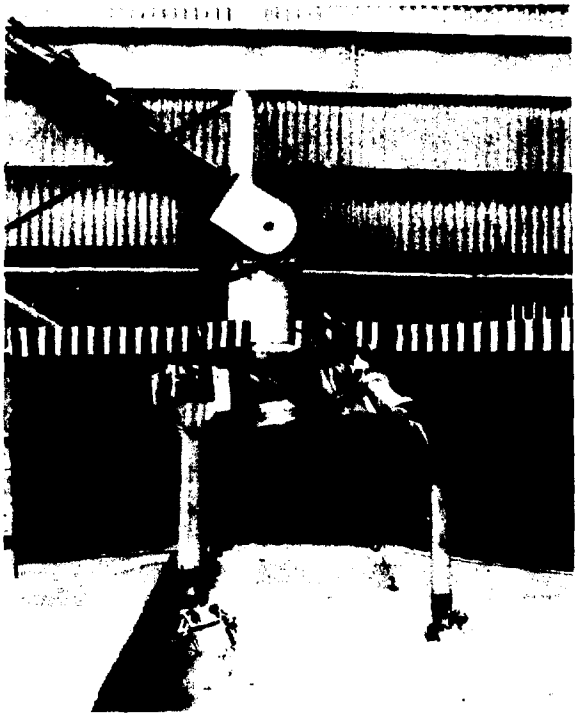

Fig. 2.
Front view of Monitor.

Fig. 3.
Overall view of master control station.

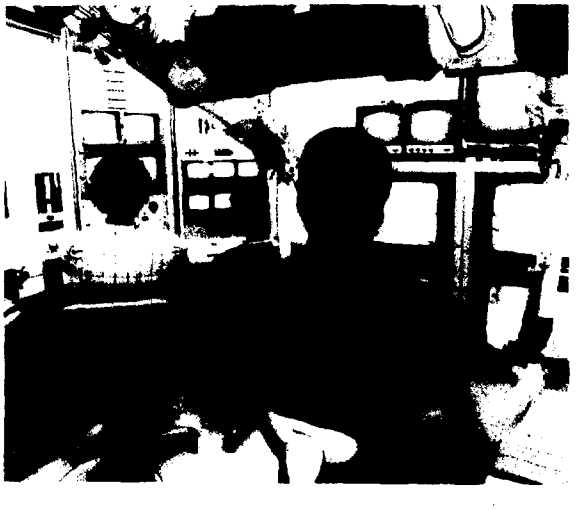

Fig. 4.
Close-up view of operating station in master control station.

work area. The work area is seen by closed-circuit television.

Operations

Figure 4 is a close-up of the three-person Monitor operating crew at work (manipulator operator at right,

crane and auxiliary equipment operator at center, and camera operator at left). Figure 5 is a close-up view showing the slave manipulators, close-in camera, shoulder rotate, and shoulder-level drive.

In normal operation the shoulder-level drive automatically maintains the shoulder and manipulator mount in a level position, regardless of crane boom angle. For work in unusual attitudes the automatic level feature is switched to the manual mode to allow discrete angular positioning.

The upper boom cameras are shown in Fig. 6. In addition to providing an overview of the work area, these cameras are necessary for initial positioning of the crane boom in the work area and withdrawal from the work areas.

The stem camera is shown in Fig. 7. This unit consists of a special camera mounted at the end of a telescoping boom. It is mounted to the Monitor crane on the side adjacent to the work area. Remotely controlled motions provide a means of positioning the camera at any desired location within a work area.

Monitor II was used for development of many new features, and was then commissioned in May 1980. Then Monitor I was retrofitted with the improvements from Monitor II.

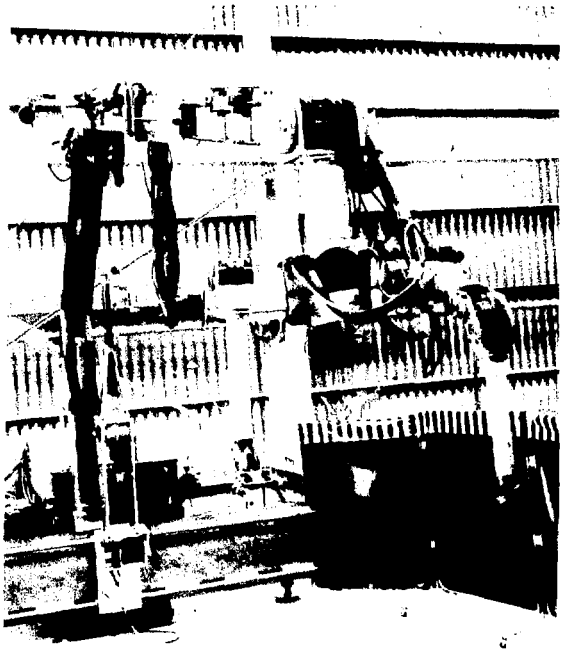

Fig. 5.
Shoulder rotate, close-in camera, and shoulder-level drive assembly.

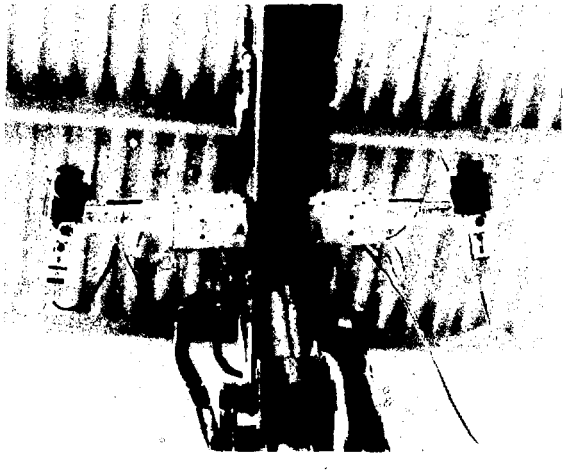

Fig. 6.
Upper boom cameras.

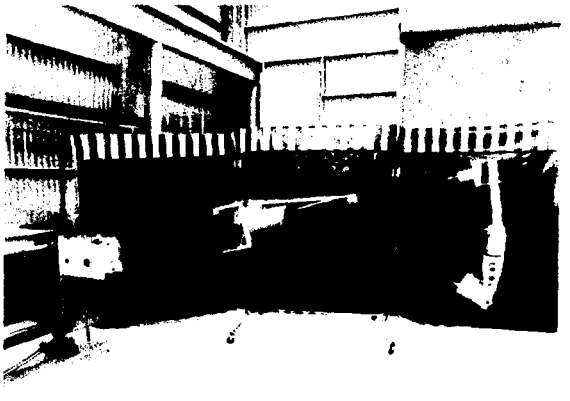

Fig. 7.
Stem camera assembly.

Capability

The following list includes some of the more difficult mechanical skills that are now performed remotely using Monitor.

- Welding [rod, metal-inert gas (MIG), oxy-acetylene]
- Soft soldering (resistance, air-acetylene, and oxy-acetylene)
- Silver soldering (air-acetylene and oxyacetylene)
- Metal cutting (sabre saw, portable band saw, and abrasive wheels)
- Stud welding (using modified Nelson stud gun)
- Drilling (air and electric portable drills)
- Grinding (air and electric).

By application of these skills it has been possible to make major repairs in highly radioactive target cells that would otherwise not be possible.

Remote MIG welding is performed using a modified Cobramatic torch, as shown in Fig. 8. MIG welding is better suited for remote application than other common methods, in that only one hand is required because the filler metal is automatically fed through the torch. Viewing is accomplished by placing a welding lens over the close-in video camera.

Silver soldering and soft soldering can easily be accomplished in many locations using a modified acetylene torch, as shown in Fig. 9. Figure 10 shows a special resistance soldering unit used for soft soldering.

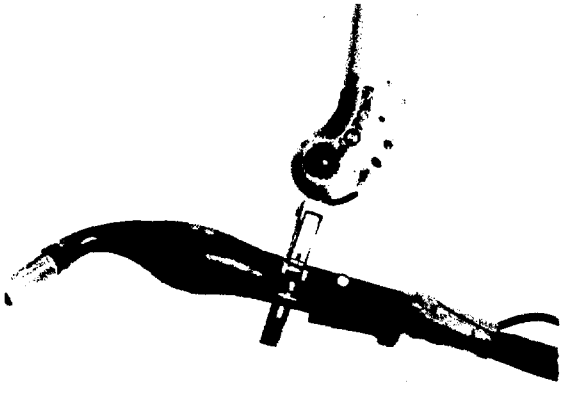

Fig. 8.
Remotely operated MIG torch.

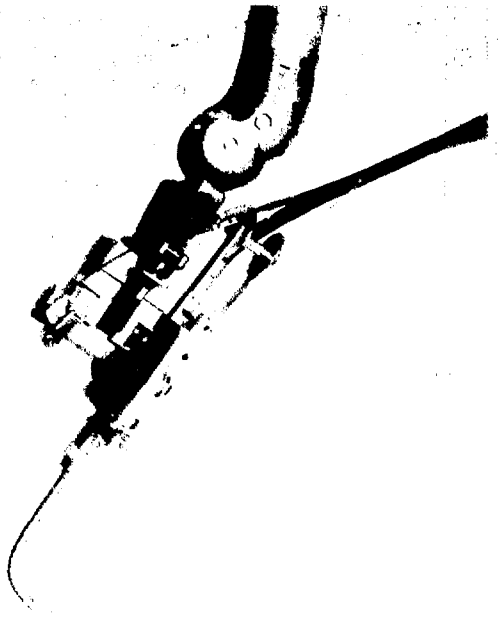

Fig. 9.
Acetylene torch for remote soldering.

Fig. 10.
Resistance soldering unit.

Figure 11 is a modified Nelson stud welder. This unit has been very useful in performing beam-line modifications that involved bolting new hardware to existing components.

Considerable time is saved by using air- and/or electric-powered wrenches where space and geometry permit. Figure 12 shows a pneumatic ratchet wrench capable of producing torque up to 11 N-m. Figure 13 shows an electric impact wrench with a maximum torque of 340 N-m.

Because of limited access to many components and water connectors, it is often necessary to fabricate special tools for each task. Figure 14 shows a special wrench that was fabricated to reach an otherwise inaccessible tube connector.

Conclusion

The remote-handling capability at LAMPF has kept pace with the needs of the experimental areas. If some of the recent equipment failures had occurred four years ago, timely repairs would not have been possible. LAMPF's remote-handling technology must continue to advance to support future experimental requirements. With the success of the Monitor system the technology is suitable for use in radioactive incidents, spills of toxic materials, and in routine handling of radioactive materials.

—D. L. Grisham and J. E. Lambert

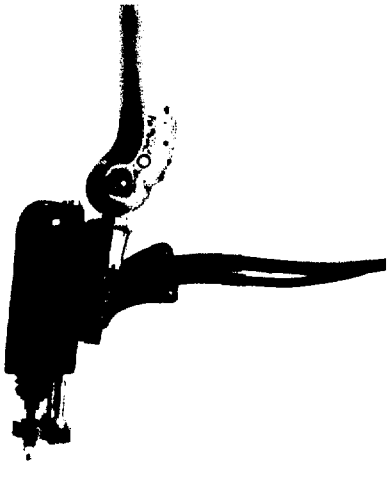

Fig. 11.
Modified Nelson stud gun.

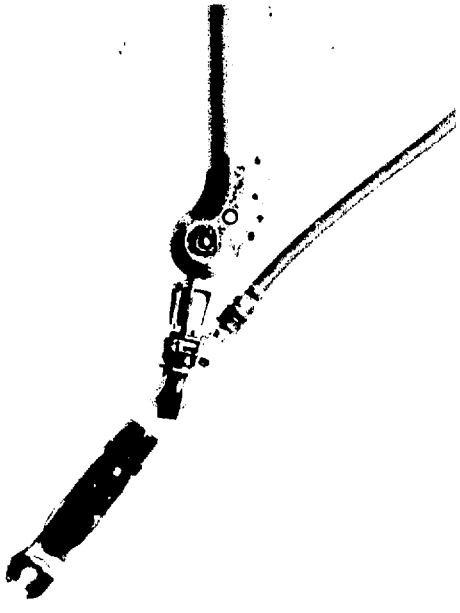

Fig. 12.
Pneumatic ratchet wrench.

Fig. 13.
Electric impact wrench.

Fig. 14.
Special tube wrench.

Special Beam-Line Instrumentation and Controls for Polarized Beams

Since polarized beam-operation began in 1977, LAMPF has been developing instrumentation to permit the usual beam diagnostic measurements on much lower intensities than previously run in primary beam lines. New requirements also developed, such as polarization measurement and beam splitting without use of ribbon or hole strippers. The additional instrumentation and controls are nearly complete, so that beam operations can proceed with reasonable efficiency.

Beam Line Polarimeter

The beam line polarimeters, EPPO and LBPO, are routinely used to measure the absolute value of the polarization to better than ±1%. The geometry of the EPB polarimeter is shown in Fig. 1. The 17° counter labeled "UP" and the 66° counter labeled "UP†" form the UP-coincidence, and so forth for DOWN, LEFT, and RIGHT. The forward-conjugate geometry is sufficiently tight to select hydrogen elastic scattering with good rejection of background events from the thin CH_2 target. The high (~0.5%) pp analyzing power from 300-800 MeV favors the 17-66° geometry. The counting rates reach the CCR computer where the program "Flex Polarimeter" (1990) calculates the transverse components P_N and P_S (from the left-right and down-up asymmetries), and the magnitude of the polarization vector (from the quench). From the combined results of both polarimeters, it is then possible, in general, to deduce the direction of the polarization vector at any point of any beam line. Precision is generally limited only by counting statistics, that is, $\pm N^{-1/2}$, where 10 pC of beam gives ~10 counts from a 0.5-mm CH_2 target.

Generally, the signals are also fed to the experiment computers where similar calculations of beam polarization and direction are performed.

Further details appear in Ref. 1.

Insertable Strip Ion Chamber Devices

The insertable strip ion chambers (IIs) are essentially wire chambers with current readout, or harps with gas

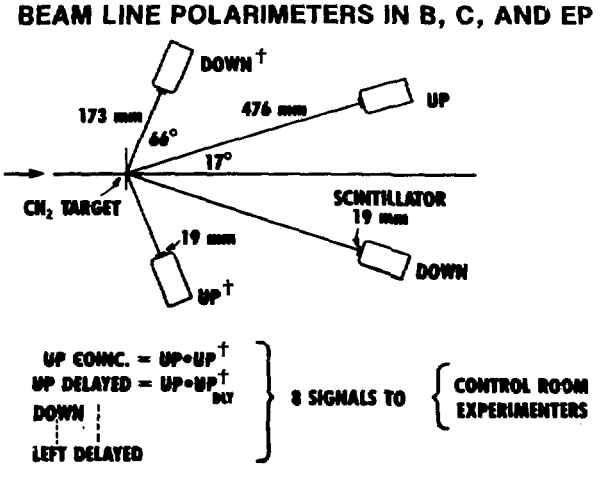

Fig. 1.
Beam-line polarimeter layout. Three similar polarimeters are installed in Lines C, B, and EPB. Each polarimeter has four counters in the vertical plane, as sketched, and four in the horizontal plane. The counters are centered near 17° (forward arm) and 66° (conjugate arm).

gain. Seven devices are presently installed in Lines B and EPB.

The IIs have either 1- or 2-mm wire spacing. With 1 mm, gain is adequate for beam intensities down to ~1 pA, whereas the increased field gradient with 2-mm pitch permits useful operation down to ~1 fA (6×10^3 particles/s). The potential may be run as high as 3 kV and is remotely controllable from CCR. The gas mix is 80:20 $Ar:CO_2$.

The devices, described in detail in Ref. 2, are multiplexed with modified harp electronics, which drives live oscilloscope readouts (in CCR and/or the experiment trailer) in addition to readout in the CCR computer. The multiplexer permits control of signal integration time; typically eight beam pulses are integrated to improve signal/noise. Beam centroids may be measured to better than ±1 mm for beam intensities of 1 fA to 100 nA. Information on beam shape is qualitative only, since the device response is generally nonlinear.

Wire Scanners

The wire-scanner system consists of the wire-scanner device, amplifier, and CAMAC-based controls. The wire scanners have 2-mm ribbon emitters for the low-intensity (H^-) beam lines, and 0.1-mm wire emitters for the high-intensity (H^+) beam line. The scanners move across the beam at 5-mm/s projected (x or y) velocity. The ribbons are mounted edgewise to the beam to improve position resolution and minimize the H^+ to H^- gain shift. High-voltage clearing field wires are used to improve the secondary-emission stability.

The amplifiers have four gain ranges presently arranged in decade steps. The highest gain range has 10-GΩ transimpedance. If a 1-nA beam 4 mm wide strikes a 2-mm ribbon with 2% secondary-emission coefficient (per side), a signal of 0.2 V is produced by the amplifier, quite adequate for CAMAC input. The amplifiers have a five-pole filter with 5-ms (per pole) time constant to suppress 60-Hz ac noise while keeping the profile slew below 0.1 mm.

The high sensitivity of the amplifier requires that the source leakage resistance be >10 MΩ. Mineral-insulated cable leakage in the wire scanner occasionally drops below this value. Otherwise, the entire system is relatively trouble free.

With 10^3 in gain range, a ±2000-count analog digital converter (ADC) in CAMAC, and a factor of 20 in wire size (H^-/H^+), a usable dynamic range of 10^6 is achieved to cover 1-mA H^+ to 1-nA H^-.

Low-Intensity Current Monitors

Beam currents ≤10 nA, typical of polarized beam operation and all beams in EPB, are below the usable range of toroid transformer beam-current monitors. The devices used instead are secondary-emission monitors [(SEMs), 4% gain], a Faraday cup (unity gain), and ion chambers (~×100 gain).

Each beam line at LAMPF, including Line A, has at least one SEM installed and read through CCR. All are essentially the same, with one emitter between two high-voltage collectors, and all are retractable. There is some small ~10% gain variation with time and beam energy, which requires some attention should accurate monitoring be necessary. One multiemitter SEM is usually available in Line C to provide higher gain for experiment use.

The ion chambers are essentially gas-filled SEMs. Typical construction details are given in Ref. 3. The active volume is typically 17-mm thick with the same gas mixture as in the IIs. The bias voltage is 500 V, low enough to prevent proportional gain. Ion gain starts to roll off at ~0.5 nA/cm² at 9% duty factor.

The Faraday cup in EPB provides a dependable absolute current standard. It is well described in Ref. 3.

The previous standard electronics on all these devices was the ORTEC 439 current integrator. To see individual beam macropulses, a high gain-bandwidth amplifier is used on some devices. This amplifier has a 20-μs time constant, a gated digitized output, and a temperature drift of 1-ppm full scale/°C (the ORTEC 439 has no specified drift). The fast time constant allows lower gain because the peak current rather than average current is seen. The gating enhances signal to noise by the reciprocal of the gate duty factor. The ability to view individual beam pulses is essential for CCR and has proved very useful to experimenters.

Stripper System

Division of the H^- beam current among Lines B, C, and EPB is controlled by H^-/H^+ stripping and magnetic separation. For polarized beam operation, particularly in the running mode where ~10 pA of protons are sent into

BR, a jaw stripper was added to the Line B/Line C split to transmit only a small fraction of beam to Line B. Previously, only a large ratio of Line B/Line C current was possible. To minimize the emittance growth of the H^+ sent to Line C, stripper materials thinner than commonly available had to be found. Thicknesses of 10^{-4} to 10^{-5} radiation lengths are required. Several materials were tried. Mylar of 1.5-μm thickness was used, but the free edge of the Mylar stripper jaw cracked after some weeks of 5-nA exposure. Beryllium jaws 8 μm thick and aluminum jaws 2 μm thick are presently in use.

The stripper jaws transmit a collimated H^- beam, as illustrated in Fig. 2. This can sometimes be undesirable, because steering on the stripper aperture becomes very critical. Furthermore, polarization selection may occur such that the outside or stripped beam has lower polarization. Therefore, we are developing a system of sieve strippers, as illustrated in the figure, to set H^+/H^- ratios without collimation. The sieve hole spacing will be 0.2 mm, and an assortment of sieves with various stripping fractions will be available.

—M. W. McNoughton and O. van Dyck

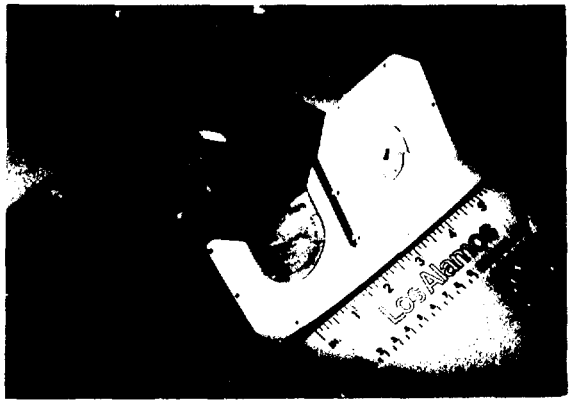

Fig. 2.
Two beam stripper foil assemblies. The hole-forming stripper jaw (right) transmits a collimated unstripped beam, as illustrated by the illuminated square area in the background. The sieve stripper provides stripped and unstripped beams sampled uniformly over the beam profile.

REFERENCES

1. M. W. McNaughton, Los Alamos National Laboratory internal reports, "EPPO and LBPO Calibrations," MP-13/MWM/A80-02; "Guide to the Beam Line Polarimeters," MP-13/MWM/I80-03; "Flex Polarimeter," MP-13/MWM/I80-09; "N-R-P-Q in Cycle 229," MP-13/MWM/I80-10; "Polarimeter HV Supply," MP-13/MWM/I81-01; and M. W. McNaughton, "LAMPF Beam Line Polarimeters," Los Alamos Scientific Laboratory report LA-8307-MS (1980).

2. M. W. McNaughton, "Guide to EP and LB II Devices," Los Alamos Scientific Laboratory internal report MP-13/MWM/I80-02.

3. R. J. Barret, B. O. Anderson, H. B. Willard, A. N. Anderson, and Nelson Jarmie, "Beam Intensity Monitoring for the External Proton Beam at LAMPF," Los Alamos Scientific Laboratory report LA-6008-MS (1975).

Polarized Targets at LAMPF

Some advanced nucleon-nucleon experiments require both polarized beam and polarized targets. Three polarized proton targets (PPT) recently used at LAMPF are listed in Table I. One target is owned by LAMPF and is further described below. It was used by Exp. 498 ($\Delta\sigma_L$) in the summer of 1980 and will be used by Exp. 512 (A_{LL}, A_{SS}, etc.) in the summer of 1981.

With present technology it is not possible to polarize pure hydrogen to a value high enough for use as a polarized target; however, it is possible to polarize the hydrogen nuclei in certain materials to high values (70-80%) by the method of dynamic nuclear polarization (DNP). The LAMPF polarized target uses this method. The basic technique consists of the following. The target material is maintained at a low temperature (<0.5 K) by a cryostat. Simultaneously, the sample is exposed to a 2.5-T magnetic field (uniform to <0.1%) and a 70-GHz rf field. This combination of low temperature, strong magnetic field, and microwave irradiation fulfills the requirements necessary for DNP. The degree of target polarization is measured by nuclear magnetic resonance (NMR) techniques.

The LAMPF polarized target consists of four basic systems:

1. a ^{3}He evaporation cryostat plus auxiliary hardware. The cryostat maintains the target sample at a temperature of <0.5 K.
2. a superconducting magnet (named Hera by the original builders at Saclay). The magnet is a split-coil solenoid in the Helmholtz configuration. For the detection of scattered particles it provides an

TABLE I

POLARIZED TARGETS AT LAMPF[a]

Magnet				Target	
Owner	Superconducting	Field (T)	Direction	Diameter (cm)	Length (cm)
P Division[b]	No	2.5	Vertical	40 cc	
Argonne/Rice	Yes	2.5	Vertical	2	5
MP Division[b]	Yes[c]	2.5	Horizontal	4	5
	→	Frozen spin		2	4

[a]Propanediol is the usual target material; free proton polarization is ~75-80%.

[b]Division of Los Alamos.

[c]From Saclay.

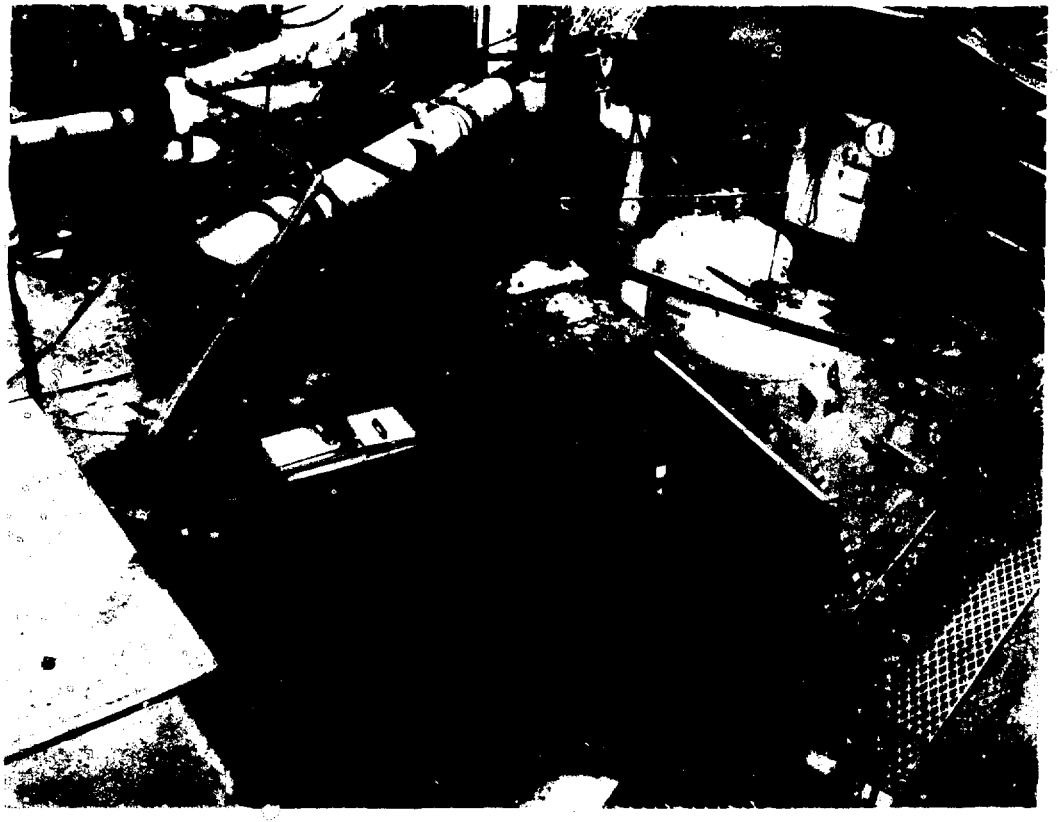

Fig. 1.
LAMPF polarized-target setup at EPB.

unobstructed cone around the field axis of 90° opening angle; the angular clearance at 90° to the field is ±7.5°.

3. a 70-GHz microwave system.
4. a 106-MHz NMR system.

The electronic controls for the target are located outside the beam area, permitting control while the beam is on.

The target was operated in the EPB area for Exp. 498 from June through October 1980. Figure 1 shows the experimental arrangement. During the course of the experiment target operation proved very stable and reproducible, and a proton polarization of 80% was typical. The system consumed about 8 ℓ/h of liquid helium (the entire system consumption including transfer line losses). The successful commissioning of the LAMPF polarized target marks another milestone in LAMPF-furnished facilities for experimental use.

—J. J. Jarmer

Cryogenics at LAMPF

The LAMPF Cryogenics Section provides cryogenic support for the LAMPF users. Services offered include engineering design, drafting, fabrication, and operation of new systems; repair of users' equipment; and loan of certain equipment.

The Section's services are basically free to approved experiments, and are scheduled by arrangement with the Section Leader (Jan Novak, 7-5510 or 7-5680). The Section Leader is also responsible for assuring the safety of apparatus used at LAMPF involving cryogenics or combustible gases (excluding detector gases), whether built at LAMPF or brought in by the user.

The section attempts to meet all requirements for cryogenic systems. The following descriptions of typical systems illustrate our capabilities.

Refrigerated Liquid Targets

Many liquid targets have been built using a closed-cycle mechanical refrigerator to liquefy hydrogen, deuterium, and neon. The section has several standard refrigerator systems that have capacities of 10 W at 20 K. To these systems we add a target liquid container (flask) and a flask vacuum chamber as appropriate to the experiment.

The simplest flask is just a thin-walled vessel, usually fabricated from 0.13-mm-thick Mylar. Common shapes are horizontal-axis cylinders with hemispherical or elliptical end caps or vertical-axis cylinders with metal end caps, as shown in Fig. 1.

Because the target liquid is under pressure and the target flask is inside an insulating vacuum, the resulting pressure differential will make thin, flat flask walls bulge outward, attempting to become hemispheres. If it is important that flat walls remain flat, the functions of containing liquid and withholding pressure must be separated, resulting in a flask within a flask. The inner flask holds the liquid and the surrounding flask is filled with gas at the same pressure as the liquid. Figure 2 shows a double flask in which the liquid container is a thin disk and the gas container is a "sphere" filled with the target element in a gaseous phase. A more complex

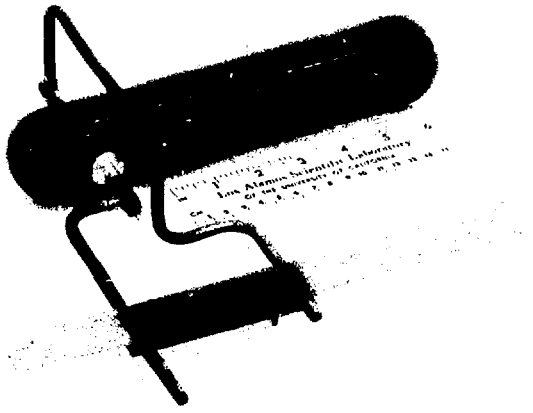

Fig. 1.
A typical basic target flask of Mylar construction.

Fig. 2.
A thin-disk liquid flask inside a spherical gas container.

gas-handling system is under development that will allow the liquid and surrounding gas to be different elements. A variation of the two-flask concept has been built using two vertical-axis, concentric Mylar cylinders with metal end caps, plumbed so that the inner cylinder is always filled with liquid but so the outer cylinder could contain either gas or liquid.

Recently, a system was built that allowed one refrigerator to condense both hydrogen and deuterium in separate flasks. The hydrogen reservoir was used as the refrigerant for the deuterium, and the 3.2 K difference in normal boiling points was accommodated with a thermal conductance resistor and an electric heater.

The heat leak to the target is far less than the refrigerator's capacity, so an electric heater makes up the difference to keep the target pressure steady. A servocontroller senses target pressure and can usually maintain it constant to within ±0.1 psi, corresponding to a liquid hydrogen density variation of ±0.04%.

Target volumes built to date range from 10 mℓ to 17 ℓ.

Refrigerated Gas Target

A thin metal target for cold gases has been built for EPICS (Fig. 3). The target section is a seamless, vertical-axis cylinder 127 mm diam by 203 mm long, with a 50-μm wall thickness, made of electroformed nickel. It is designed to hold gas at 30 psia at any temperature desired between 2 and 300 K. The target section is part of a loop. Opposite the target is a heat exchanger cooled by an open-cycle, liquid-helium-transfer refrigerator, the gas circulating in the loop by free convection. The target section is insulated by one floating radiation shield of 13-μm aluminum; the rest of the loop is heavily superinsulated. In a recent run with $^{16}O_2$ target gas, temperature at the top of the target was maintained at 125 ± 0.2 K and there was a 5 K gradient from the bottom to the top. Methane and neon were also used. A gas change could be done in ~1 h.

A second-generation target is planned to have a wall thickness of 2.5 μm. The thin-wall technology will find wide application in other targets.

Rare-Gas Targets

A sealed gas-handling system has been built that allows rare gases to be used in targets and recovered. This system will be used to operate the refrigerated gas target with $^{17}O_2$. In addition, an LN_2 bath-cooled "flat disk"-style target has been built for the π^0 spectrometer which, with the sealed gas-handling system, has been run with $^{15}N_2$.

Fig. 3.
The Cryogenics Section (as of March 1981) and the EPICS cold gas target flask. Shown from left to right are Rudy Valdez, Garlan Isom, Norm Hoffman, Jan Novak, and Robert Garcia.

The $^{15}N_2$ target flask is made of five metal plates interleaved with four layers of 0.25-mm-thick Mylar (Fig. 4). Two rectangular holes 76 by 127 mm are cut into each metal plate so that when the assembly is epoxied together two "cells" are formed. Each cell consists of a central, flat, liquid compartment 10 mm thick, flanked by two gas compartments. The cells contain either liquid $^{14}N_2$ or $^{15}N_2$, and the gas compartments contain helium at the same pressure as the liquid. The flask is cooled by LN_2 pumped to 125 torr absolute, circulating from a reservoir through tubes soldered to the central metal plate.

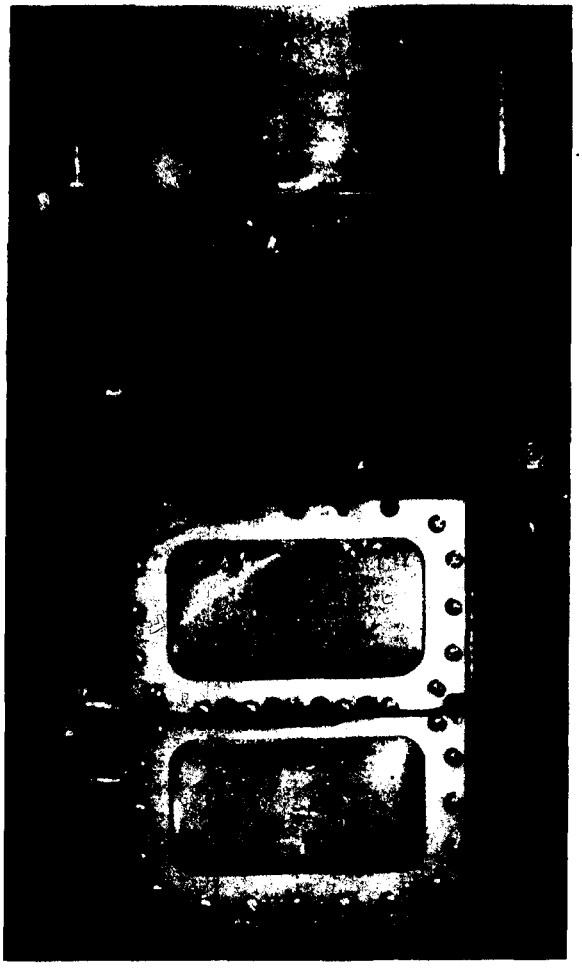

Fig. 4.
The liquid $^{15}N_2/^{14}N_2$ target flask viewed in the beam direction.

Fig. 5.
The windows and beam interaction section of the LD_2 neutron production target.

Liquid-Helium Targets

A reservoir-fed target with a flask similar to the $^{15}N_2$ flask, but containing liquid ^{3}He and ^{4}He, has been used in collaboration with the University of Virginia. Typical cells are 15- by 15- by 1-cm thick, with windows of 76-μm-thick high-strength aluminum. The body plates are high conductivity copper.

Another reservoir system has a vertical-axis cylindrical Mylar flask 76 mm diam by 0.13 mm wall thickness. The target material is ^{4}He, which is cooled below 2.1 K to eliminate boiling.

Both systems will accept a range of different geometry and size flasks.

Tritium Targets

Three experiments with cryogenic tritium have been run, two with liquid tritium and one with cold gas. All flasks were metal. The liquid flasks were cylinders 32 mm long by 25 mm diameter with hemispherical end caps, and the gas flask was a cylinder 152 mm diameter by 102 mm long with flat, thick end caps. Liquid target cooling was from an LH_2 reservoir and the gas target

was cooled with a Joule-Thompson open-cycle refrigerator.

The targets contained ~80 000 Ci of tritium; the cryogenic problems paled in comparison with the containment and safety problems.

LD_2 Neutron Production Target

Neutrons are produced for the BR channel from a closed-loop, forced-circulation, liquid-deuterium target cooled by a refrigerator. Target thickness is 254 mm, and the flask windows are 76-μm stainless steel (Fig. 5). Liquid is circulated by two axial blowers. The circulation rate is such that each beam macropulse strikes new liquid to prevent beam heating and boiling of the liquid. The refrigerator is a closed-cycle helium system with about 100 W capacity at 20 K.

Superconducting Spin-Precession Solenoid

Line B incorporates a superconducting solenoid for spin direction precession of polarized protons. The magnet has a 100-mm-diam warm bore and is 1.22 m overall. Peak field is 3.5 T and the field integral is 3.3 T-m. The coil is bath cooled with liquid helium. Consumption is ~2 ℓ/h.

—J. K. Novak

LAMPF Nuclear Chemistry Data-Acquistion System

The LAMPF Nuclear Chemistry Data-Acquistion System (DAS) is designed to provide data acquisition and data processing for a variety of users. It consists of a PDP-11/44 with peripherals on a CAMAC highway. The detectors, system operation, and development plans are described below.

The Nuclear Chemistry Laboratory instrumentation consists principally of counter systems and spectrometers, as shown in Fig. 1, for radioactive sample

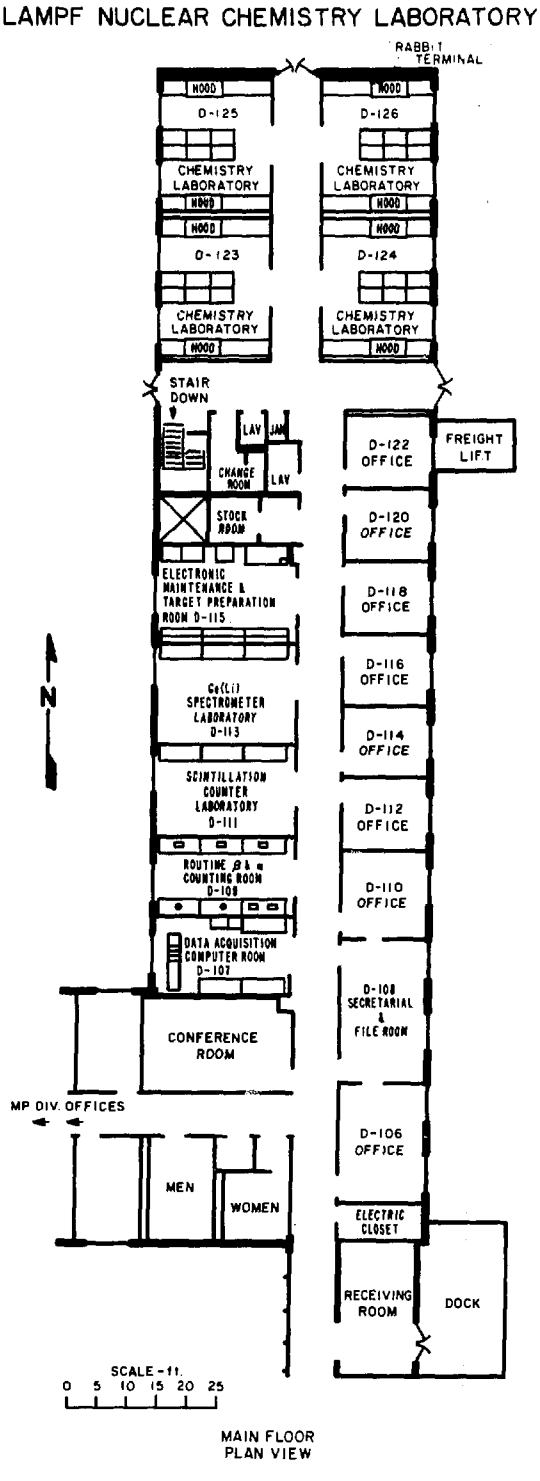

Fig. 1.
A plan view of LAMPF Nuclear Chemistry Laboratory.

Fig. 2.
Gas-flow β-proportional counters and associated electronics.

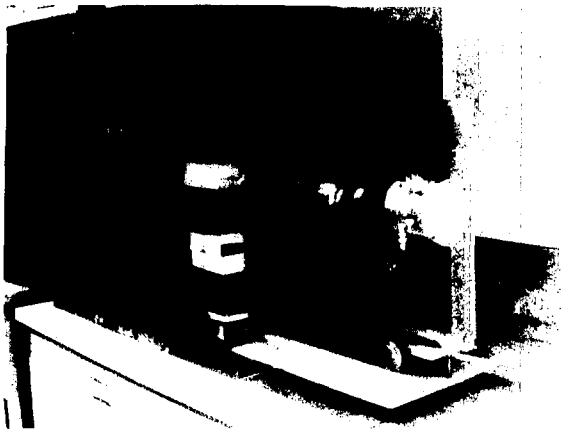

Fig. 3.
A β-γ coincidence counter.

analysis. Singles counters include α-particle and β-particle gas-flow proportional counters and gated NaI(Tℓ) γ-ray counters. Figure 2 shows the β-particle counters. A β-γ coincidence counter (Fig. 3) for absolute counting and a γ-γ coincidence/positron annihilation counter (Fig. 4) are examples of the second type. Spectrometer systems include a number of Ge(Li) γ-ray spectrometers (one is shown in Fig. 5) and solid-state α-particle (Fig. 6) and NaI(Tℓ) scintillation spectrometers; the latter two types are rarely used.

These systems can be operated in either the stand-alone mode or under computer control. They are connected to the PDP-11/44 through a four-crate CAMAC parallel branch highway, one crate in each counting lab. Data are taken from the counters by CAMAC scaler/timer modules, and from the spectrometers by multichannel analyzers (MCAs). The MCAs have dedicated tape units and CAMAC interfaces. Another CAMAC interface is used to control the automatic sample changer, shown in Fig. 7, associated with one of our Ge(Li) γ-ray spectrometers.

The PDP-11/44 computer has system peripherals comparable to a complete counting-house configuration, as shown in Fig. 8. Control and analysis programs are available, including special codes for spectral analysis. Examples of analysis programs include least-squares resolution of multicomponent radioactive decay and γ-ray stripping of complex spectra. The LAMPF-standard

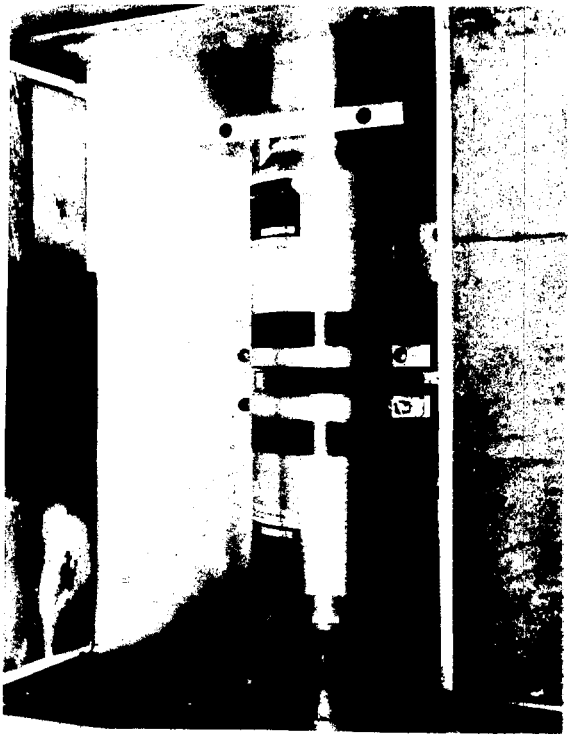

Fig. 4.
Two 7.6- by 7.6-cm NaI(Tℓ) detectors used in coincidence mode as positron annihilation counters.

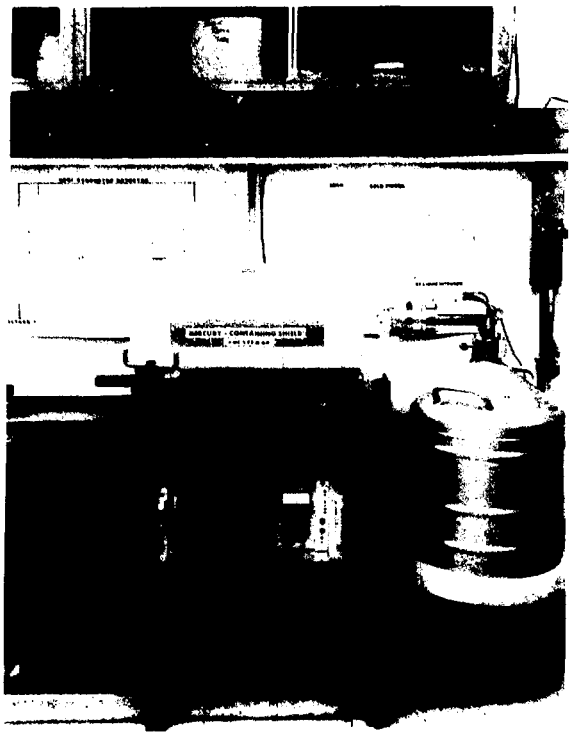

Fig. 5.
Ge(Li) spectrometer system with mercury-filled shield.

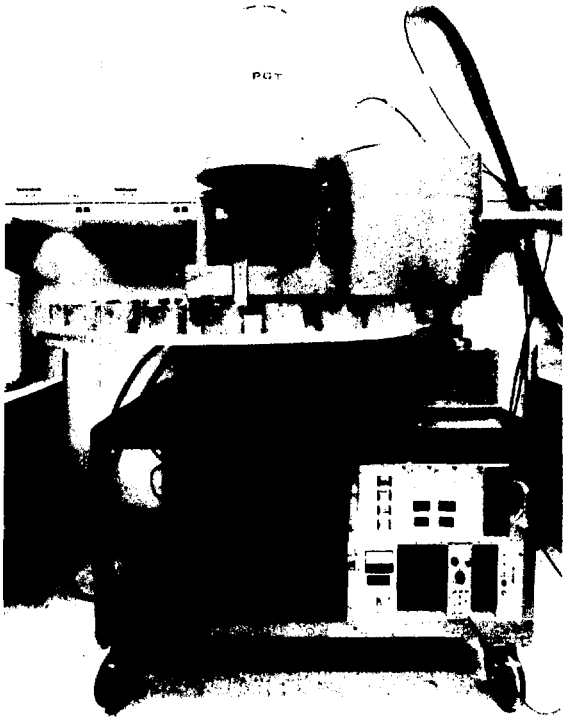

Fig. 7.
A 24-positron automatic sample changer with a Ge(Li) spectrometer.

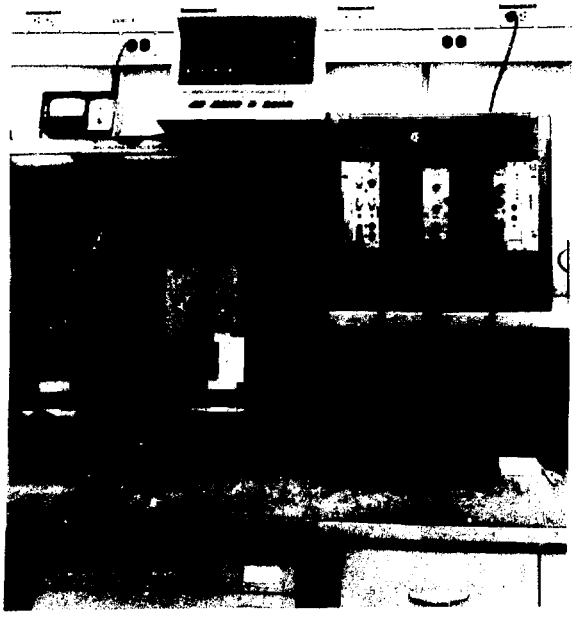

Fig. 6.
Solid-state α-particle spectrometers and their associated electronics.

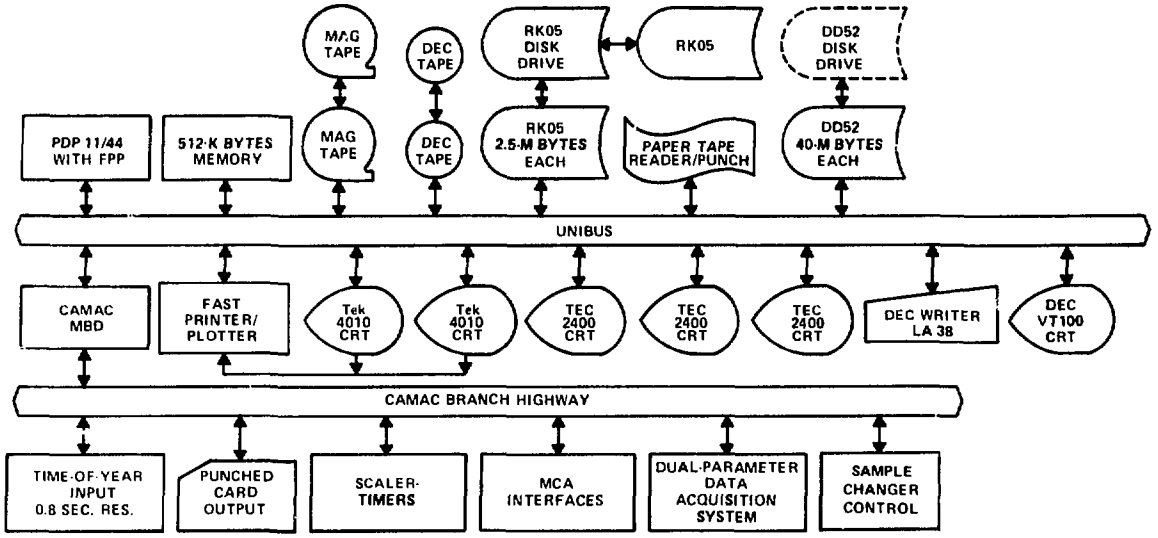

Fig. 8.
A diagram of the Nuclear Chemistry Laboratory Data-Acquistion System.

Q system is also available on this computer for data acquisition and analysis.

Future plans include restoring to operation a system with two optically separated, 38-cm-diam by 25-cm-thick NaI(Tℓ) γ-ray detectors, which can be used in anti-Compton, anticoincidence, or triple γ-ray coincidence modes. Also, a dual-parameter data-acquisition MCA will be put into operation.

For further information, see Ref. 1.

—*G. C. Giesler*

REFERENCE

1. G. Giesler, "LAMPF Nuclear Chemistry Data-Acquistion System," to be published in IEEE Trans. Nucl. Sci. NS-28 (October 1981).

Quad Unroll Experiments in the Drift-Tube Linac

The following experiments address the problem of obtaining a match of the H^+ production beam to the drift-tube linac. The last four transport quadrupoles are used to shape the beam and to obtain matched conditions at the entrance to the linac. A beam is assumed to be matched when its horizontal and vertical size does not oscillate at the end of Tank 1 when the transverse wavelength in the tank is varied by changing the quadrupole magnet strengths up and down. This procedure, called a "quad unroll," can be simulated using the computer code PARMILA. If the results of simulations agree with measurements, computer predictions can be used to shorten the tuning process.

However, with beam distributions constrained to agree with EM-3 measurements and transport quadrupoles TDQL03-04 set as they were for good unrolls, it has not been possible to make PARMILA agree with experimental results for any of four available sets of data from H^+ production beams. A typical production beam has 15-mA peak current and an emittance of 1.0-1.5 π cm·mrad at the EM-3 jaws. Disagreement between actual and simulated results can be caused by unreliable EM-3 measurements at these currents and by our inability to simulate the unknown neutralization in the transport region. Cross coupling among the transverse and longitudinal planes complicates computer simulations through the entire region under study.

To eliminate these known difficulties, we studied a low-current H^- beam with a large emittance, which removes space charge effects and insures reliable reconstruction of ellipse parameters. After the computer program TRACE was used to choose quadrupole strengths that transformed the beam from EM-3 to the matched ellipse values at the beginning of the linac, a

quad unroll was carried out. The last four transport quadrupoles then were varied in a systematic way to obtain mismatched conditions that would cause oscillations in the beam size at the end of Tank 1. PARMILA simulations agreed qualitatively with each of the experimental unrolls. Figure 1 shows the results of the matched unroll and its simulation, and Fig. 2 shows the results of one of the mismatches. The agreement is probably as good as should be expected.

We next studied low-current H^+ beams in an attempt to duplicate the H^- experiment as closely as possible. For all the H^+ measurements the source was degraded to obtain a beam with a larger emittance than is possible with the production source. For one experiment the beam was made large at the prebuncher aperture and the prebuncher was then turned on to further increase the emittance. Our objective was to have an emittance of at least 1 π cm-mrad and a peak current of a few hundred-microamperes. Although not all beams satisfied these criteria, unrolls of several matched and mismatched beams were made and compared with simulations. We conclude that the agreement is generally good. Figure 3 shows the assumed "matched" beam had an oscillation in the horizontal plane. To find the cause of this oscillation, we examined the effects of small errors in the fields of the matching quadrupoles. We found that, depending on the shape of the beam, certain quadrupoles are more important than others in causing or correcting mismatches. For this particular beam, we found that the horizontal oscillation could be easily duplicated in PARMILA by changing the second matching quadrupole by 1%. The vertical plane was insensitive to this change and remained well matched. Equipment failure and scheduled shutdown prevented experimental confirmation of beam sensitivity particular quadrupole.

In subsequent experiments the quadrupoles chosen by TRACE gave good or matched unrolls. We determined the important matching quadrupoles for these beams, and they did not include the second quadrupole. The important quadrupoles were varied to cause mismatches and the resulting experimental unrolls agreed well with PARMILA predictions.

In conducting these low-current experiments, we realized the importance of having an experimental beam that can be both accurately measured and simulated by PARMILA and TRACE. An accurate measurement at EM-3 is complicated by the time dependence of the H^+ currents and the slow rise times of the EM-3 amplifiers,

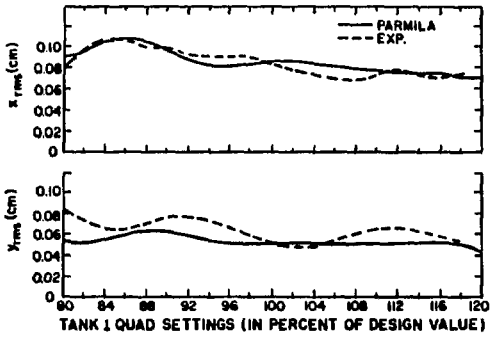

Fig. 1.
The H^- quad unroll for predicted matched conditions.

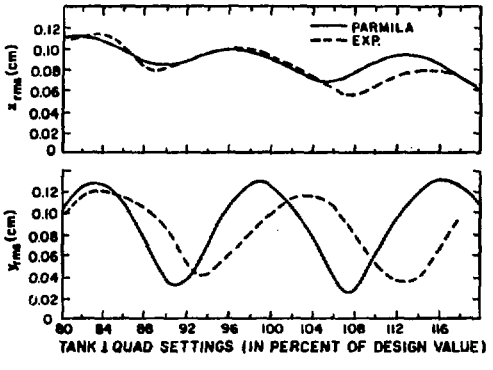

Fig. 2.
The H^- quad unroll with TDQL03-02 increased by 10%.

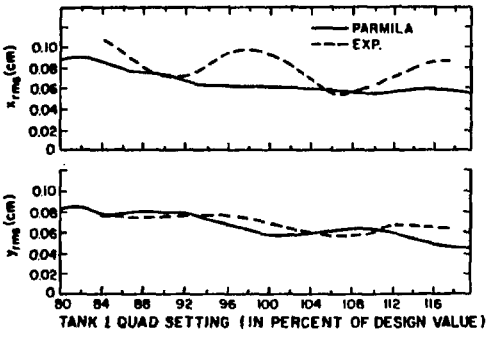

Fig. 3.
The H^+ quad unroll for predicted matched conditions.

which can and do lead to erroneous emittance measurements. Because PARMILA and TRACE assume an elliptical beam, the actual beam must have an elliptical shape that does not depend on the percentage of the beam analyzed. Furthermore, the number of samples in the emittance measurement must be sufficiently large to make meaningful the evaluation of the ellipse parameters.

Studies of 1- and 3-mA peak current beams indicate further problems. Emittance measurements depend on the EM-3 collector bias voltage, and possibly on the jaw voltage. These bias voltages have not been carefully controlled, and it is not known which voltages give the most accurate measurements. The method of calculating rms widths at the end of Tank 1 should be changed so that existing tails are not ignored, and code for PARMILA needs to be written to be more compatible with these calculations.

The conclusion drawn from these experiments is that low-current, well-shaped beams of either H^+ or H^- species can be well simulated with existing computer codes. Brighter beams still present unsolved problems.

III. ACCELERATOR OPERATIONS

This period covers operating Cycle 29. The accelerator was in operation for ~10 weeks, providing beams for research use for 52 days and for facility development for 16 days. A summary of information on beams provided for experimental use is given in Table I.

Machine operation continued to be reliable and stable. Difficulties with the initial tuning were responsible for the largest single block of unscheduled downtime. This resulted in unusually low beam availability during the brief period of H^- use at the beginning of the cycle. A summary of unscheduled facility downtime during research shifts is given in Table II. Because some of the outages were concurrent, the total is greater than the beam downtime.

During the weekend of April 18 and 19, the H^+ beam availability was 100% for a period of 43 consecutive hours. During the same period, polarized beam (P^-) availability was 90%. Availability for the 7-day period following the April 13 maintenance day was an excellent 96% for H^+ and 92% for P^-.

Accelerator development efforts continued to address various aspects of the transverse phase-space tuning problem, with emphasis shifting toward the more stringent requirements associated with future operation of the Proton Storage Ring.

—J. Bergstein

TABLE I

BEAM STATISTICS FOR CYCLE 29

	Cycle 29
No. of experiments served	52
H^+ scheduled beam hours	1264
H^- scheduled beam hours	240
P^- scheduled beam hours	1024
H^+ beam availability, %	84
H^- beam availability, %	51
P^- beam availability, %	79
H^+ average current, μA	540
H^- average current, μA	1
P^- average current, nA	~5
H^+ beam duty factor, %	6
H^-, P^- beam duty factor, %	3-6
P^- beam energy, MeV	497, 647, 800

TABLE II

UNSCHEDULED MACHINE DOWNTIME

Category	Downtime (h)	Percent of Total
201—MHz amplifiers and transmission lines	37	14
805—MHz amplifier systems	25	10
Vacuum	13	5
Magnets and magnet power supplies	9	4
Interlocks	2	1
Injectors	61	24
Cooling water systems	12	5
Computer control and data acquistion	3	1
Beam stops, plugs, targets, strippers, scrapers	6	2
Miscellaneous (utilities, etc.)	16	6
Unscheduled tuning	73	28
TOTAL	257	

IV. EXPERIMENTS RUN

Exp. No.	Experiment Title	Channel	Beam Hours
10	Search for (p,π) Reactions with HRS	HRS	55.0
123	Nuclear Structure Effects in Pion-Induced Nuclear Reactions	LEP	25.0
154	Elastic Scattering of π^+ and π^- from the Helium Isotope	P^3	316.0
194	p-p, D, R, and A Measurements	EPB	246.5
233	Search for δ-Configurations Nuclei	HRS	55.0
236	Biological Effects of Negative Pions	Biomed	34.0
267	Preparation of Radioisotopes for Medicine and the Physical Services Using the LAMPF Isotope Production Facility	ISORAD	1036.8
270	Therapy Beam Development — Biomedical Channel Tuning	Biomed	44.8
271	Therapy Beam Development — Dosimetry	Biomed	153.0
274	Pion Radiobiology	Biomed	38.0
275	Pion Clinical Trials	Biomed	574.7
294	High-Energy Nuclear Reactions	AB-Nucchem	2.4
308	An Attempt to Make Direct Atomic Mass Measurements in the Thin Target Area	TTA	983.0
334	Nuclear Charge Parameters of ^{41}Ca and Stable Cadmium and Tellurium Isotopes	SMC	45.0
349	Nuclear Reactions of ^{127}I with Pions	LEP P^3	28.0 9.0
382	μSR Investigation of the Effects of Impurities on the Trapping and Diffusion of μ^+ Particles in bcc Metals	SMC	15.0
389	Inelastic Pion Scattering from Light Nuclei ^{10}B, ^{11}B, ^{14}N, and ^{15}N	EPICS	72.0

Exp. No.	Experiment Title	Channel	Beam Hours
392	A Measurement of the Triple-Scattering Parameters D, R, A, R′, and A′ for Proton-Proton and Proton-Neutron Scattering at 800 MeV	HRS	208.6
400	Search for the Rare Decay $\mu^+ \rightarrow e^+e^+e^-$	SMC	125.0
401	Study of the Isobaric Analog Charge Exchange Reaction $^{15}N(\pi^+,\pi^0)^{15}O$	LEP	255.5
411	Measurement of Spin-Flip Probabilities in Proton Inelastic Scattering at 800 MeV and Search for Collective Spin-Flip Modes, Preliminary Survey	HRS	80.0
421	Sensitive Search for $\mu^- \rightarrow e$ Conversion	SMC	36.0
449	A Survey of Single and Double Photodetachment Cross Section of the H^- Ion from 14 to 21.8 eV	EPB	113.6
457	Measurement of the Quasi-Free pn and pp and Free pp Analyzing Powers 500-800 MeV	AB	785.0
462	Analyzing Power and Differential Cross Sections for the Reactions $p + p \rightarrow d + \pi^+$ and $p + d \rightarrow t + \pi^+$ at ~600 400 MeV	HRS	118.0
465	Radiochemical Study of Pion Single Charge Exchange	LEP P^3	29.4 46.7
473	Study of Giant Multipole Resonances with 800-MeV Protons	HRS	97.0
479	Measurement of R, A, R′, and A′ in Elastic and Inelastic Scattering of 800-MeV Protons from Light Nuclei — Revised Version of Q Proposal	HRS	72.0
491	Experimental Determination of the Strong-Interaction Shift in the 2p-1s Transition of Pionic Deuterium and Hydrogen Atoms	SMC	235.0
494	Nuclear Charge Parameters of the Stable Ruthenium and Palladium Isotopes	SMC	57.0
499	Muon Longitudinal and Transverse Relaxation Studies in Spin-Glass Systems	SMC	87.0
513	$\pi^{\pm}$ Quasi-Free Scattering from the Helium Isotopes	P^3	557.7

Exp. No.	Experiment Title	Channel	Beam Hours
523	Study of $^{14}C(\pi^+,\pi^0)^{14}N$ Reaction	LEP	78.8
524	Study of the Isovector Terms in π-Nucleus Interactions with (π^+,π^0) Reactions on $^{40,42,44,48}Ca$ and $^{112,118,124}Sn$	LEP	105.3
547	Search for Fast Muonium in Vacuum	SMC	144.0
562	Study of Pion Absorption Mechanism through the A(π,p)X Reaction at T_π = 500 MeV	P^3	428.0
570	Investigation of the Structure of ^{16}O with Pion Inelastic Scattering	EPICS	325.0
571	Muon Spin Rotation Studies of Dilute Magnetic Alloys	SMC	54.9
581	$\pi^\pm$ Elastic Scattering from Deuterium at 237 MeV	EPICS	193.0
597	The Study of Broad-Range Pion Inelastic-Scattering Spectra (with Emphasis on the Excitation of the Giant Monopole Resonance)	EPICS	55.0
603	Search for Deltas in a Complex Nucleus by a Radiochemical Technique	AB	25.0
604	An Investigation of the Near Stability of ^5H	EPICS	254.8
607	Study of Isovector Giant Resonances with Pion Charge Exchange	LEP	259.5
629	Feasibility of Helium-Jet Techniques for Studying Short-Lived Nuclei Produced at LAMPF	AB-Nucchem	23.5
634	Measurement of Parity Violation in the p-Nucleus Total Cross Sections at 800 MeV	EPB	42.0
635	Spin Measurements in pd Elastic Scattering	EPB	507.7
639	Muon Spin Rotation Study of Muon Bonding and Motion in Select Magnetic Oxides	SMC	21.0
640	Transverse and Longitudinal Field μSR Measurements in Selected Ternary Metallic Compounds	SMC	63.0

Exp. No.	Experiment Title	Channel	Beam Hours
649	$^{9}Be(p,\pi^{\pm})$ Reaction at 650 MeV	HRS	85.9
650	A Search for Neutrino Mixing via Nonexponential $\pi \rightarrow \mu\nu$ Decay	LEP	249.0

BR, a jaw stripper was added to the Line B/Line C split to transmit only a small fraction of beam to Line B. Previously, only a large ratio of Line B/Line C current was possible. To minimize the emittance growth of the H^+ sent to Line C, stripper materials thinner than commonly available had to be found. Thicknesses of 10^{-4} to 10^{-5} radiation lengths are required. Several materials were tried. Mylar of 1.5-μm thickness was used, but the free edge of the Mylar stripper jaw cracked after some weeks of 5-nA exposure. Beryllium jaws 8 μm thick and aluminum jaws 2 μm thick are presently in use.

The stripper jaws transmit a collimated H^- beam, as illustrated in Fig. 2. This can sometimes be undesirable, because steering on the stripper aperture becomes very critical. Furthermore, polarization selection may occur such that the outside or stripped beam has lower polarization. Therefore, we are developing a system of sieve strippers, as illustrated in the figure, to set H^+/H^- ratios without collimation. The sieve hole spacing will be 0.2 mm, and an assortment of sieves with various stripping fractions will be available.

—M. W. McNaughton and O. van Dyck

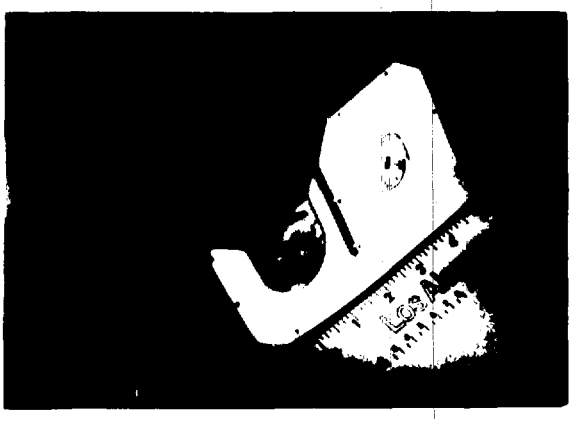

Fig. 2.
Two beam stripper foil assemblies. The hole-forming stripper jaw (right) transmits a collimated unstripped beam, as illustrated by the illuminated square area in the background. The sieve stripper provides stripped and unstripped beams sampled uniformly over the beam profile.

REFERENCES

1. M. W. McNaughton, Los Alamos National Laboratory internal reports, "EPPO and LBPO Calibrations," MP-13/MWM/A80-02; "Guide to the Beam Line Polarimeters," MP-13/MWM/180-03; "Flex Polarimeter," MP-13/MWM/180-09; "N-R-P-Q in Cycle 229," MP-13/MWM/180-10; "Polarimeter HV Supply," MP-13/MWM/181-01; and M. W. McNaughton, "LAMPF Beam Line Polarimeters," Los Alamos Scientific Laboratory report LA-8307-MS (1980).

2. M. W. McNaughton, "Guide to EP and LB II Devices," Los Alamos Scientific Laboratory internal report MP-13/MWM/180-02.

3. R. J. Barret, B. O. Anderson, H. B. Willard, A. N. Anderson, and Nelson Jarmie, "Beam Intensity Monitoring for the External Proton Beam at LAMPF," Los Alamos Scientific Laboratory report LA-6008-MS (1975).

Polarized Targets at LAMPF

Some advanced nucleon-nucleon experiments require both polarized beam and polarized targets. Three polarized proton targets (PPT) recently used at LAMPF are listed in Table I. One target is owned by LAMPF and is further described below. It was used by Exp. 498 ($\Delta\sigma_L$) in the summer of 1980 and will be used by Exp. 512 (A_{LL}, A_{ss}, etc.) in the summer of 1981.

With present technology it is not possible to polarize pure hydrogen to a value high enough for use as a polarized target; however, it is possible to polarize the hydrogen nuclei in certain materials to high values (70-80%) by the method of dynamic nuclear polarization (DNP). The LAMPF polarized target uses this method. The basic technique consists of the following. The target material is maintained at a low temperature (<0.5 K) by a cryostat. Simultaneously, the sample is exposed to a 2.5-T magnetic field (uniform to <0.1%) and a 70-GHz rf field. This combination of low temperature, strong magnetic field, and microwave irradiation fulfills the requirements necessary for DNP. The degree of target polarization is measured by nuclear magnetic resonance (NMR) techniques.

The LAMPF polarized target consists of four basic systems:

1. a ^{3}He evaporation cryostat plus auxiliary hardware. The cryostat maintains the target sample at a temperature of <0.5 K.
2. a superconducting magnet (named Hera by the original builders at Saclay). The magnet is a split-coil solenoid in the Helmholtz configuration. For the detection of scattered particles it provides an

TABLE I

POLARIZED TARGETS AT LAMPF[a]

Magnet				Target	
Owner	Superconducting	Field (T)	Direction	Diameter (cm)	Length (cm)
P Division[b]	No	2.5	Vertical	40 cc	
Argonne/Rice	Yes	2.5	Vertical	2	5
MP Division[b]	Yes[c]	2.5	Horizontal	4	5
		Frozen spin		2	4

[a]Propanediol is the usual target material; free proton polarization is ~75-80%.

[b]Division of Los Alamos.

[c]From Saclay.

Fig. 1.
LAMPF polarized-target setup at EPB.

unobstructed cone around the field axis of 90° opening angle; the angular clearance at 90° to the field is ±7.5°.

3. a 70-GHz microwave system.
4. a 106-MHz NMR system.

The electronic controls for the target are located outside the beam area, permitting control while the beam is on.

The target was operated in the EPB area for Exp. 498 from June through October 1980. Figure 1 shows the experimental arrangement. During the course of the experiment target operation proved very stable and reproducible, and a proton polarization of 80% was typical. The system consumed about 8 ℓ/h of liquid helium (the entire system consumption including transfer line losses). The successful commissioning of the LAMPF polarized target marks another milestone in LAMPF-furnished facilities for experimental use.

—J. J. Jarmer

Cryogenics at LAMPF

The LAMPF Cryogenics Section provides cryogenic support for the LAMPF users. Services offered include engineering design, drafting, fabrication and operation of new systems; repair of users' equipment; and loan of certain equipment.

The Section's services are basically free to approved experiments, and are scheduled by arrangement with the Section Leader (Jan Novak, 7-5510 or 7-5680). The Section Leader is also responsible for assuring the safety of apparatus used at LAMPF involving cryogenics or combustible gases (excluding detector gases), whether built at LAMPF or brought in by the user.

The section attempts to meet all requirements for cryogenic systems. The following descriptions of typical systems illustrate our capabilities.

Refrigerated Liquid Targets

Many liquid targets have been built using a closed-cycle mechanical refrigerator to liquefy hydrogen, deuterium, and neon. The section has several standard refrigerator systems that have capacities of 10 W at 20 K. To these systems we add a target liquid container (flask) and a flask vacuum chamber as appropriate to the experiment.

The simplest flask is just a thin-walled vessel, usually fabricated from 0.13-mm-thick Mylar. Common shapes are horizontal-axis cylinders with hemispherical or elliptical end caps or vertical-axis cylinders with metal end caps, as shown in Fig. 1.

Because the target liquid is under pressure and the target flask is inside an insulating vacuum, the resulting pressure differential will make thin, flat flask walls bulge outward, attempting to become hemispheres. If it is important that flat walls remain flat, the functions of containing liquid and withholding pressure must be separated, resulting in a flask within a flask. The inner flask holds the liquid and the surrounding flask is filled with gas at the same pressure as the liquid. Figure 2 shows a double flask in which the liquid container is a thin disk and the gas container is a "sphere" filled with the target element in a gaseous phase. A more complex

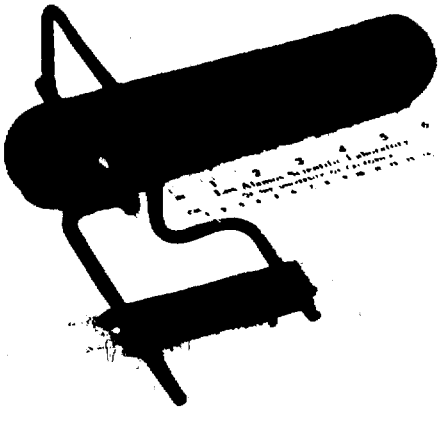

Fig. 1.
A typical basic target flask of Mylar construction.

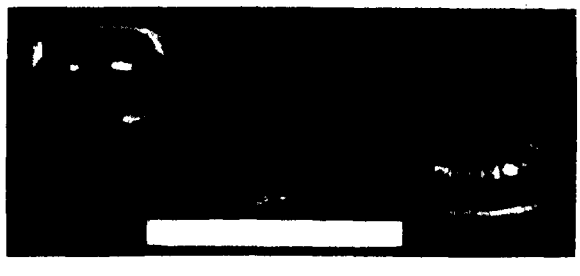

Fig. 2.
A thin-disk liquid flask inside a spherical gas container.

gas-handling system is under development that will allow the liquid and surrounding gas to be different elements. A variation of the two-flask concept has been built using two vertical-axis, concentric Mylar cylinders with metal end caps, plumbed so that the inner cylinder is always filled with liquid but so the outer cylinder could contain either gas or liquid.

Recently, a system was built that allowed one refrigerator to condense both hydrogen and deuterium in separate flasks. The hydrogen reservoir was used as the refrigerant for the deuterium, and the 3.2 K difference in normal boiling points was accommodated with a thermal conductance resistor and an electric heater.

The heat leak to the target is far less than the refrigerator's capacity, so an electric heater makes up the difference to keep the target pressure steady. A servocontroller senses target pressure and can usually maintain it constant to within ±0.1 psi, corresponding to a liquid hydrogen density variation of ±0.04%.

Target volumes built to date range from 10 mℓ to 17 ℓ.

Refrigerated Gas Target

A thin metal target for cold gases has been built for EPICS (Fig. 3). The target section is a seamless, vertical-axis cylinder 127 mm diam by 203 mm long, with a 50-μm wall thickness, made of electroformed nickel. It is designed to hold gas at 30 psia at any temperature desired between 2 and 300 K. The target section is part of a loop. Opposite the target is a heat exchanger cooled by an open-cycle, liquid-helium-transfer refrigerator, the gas circulating in the loop by free convection. The target section is insulated by one floating radiation shield of 13-μm aluminum; the rest of the loop is heavily superinsulated. In a recent run with $^{16}O_2$ target gas, temperature at the top of the target was maintained at 125 ± 0.2 K and there was a 5 K gradient from the bottom to the top. Methane and neon were also used. A gas change could be done in ~1 h.

A second-generation target is planned to have a wall thickness of 2.5 μm. The thin-wall technology will find wide application in other targets.

Rare-Gas Targets

A sealed gas-handling system has been built that allows rare gases to be used in targets and recovered. This system will be used to operate the refrigerated gas target with $^{17}O_2$. In addition, an LN_2 bath-cooled "flat disk"-style target has been built for the π^0 spectrometer which, with the sealed gas-handling system, has been run with $^{15}N_2$.

Fig. 3.
The Cryogenics Section (as of March 1981) and the EPICS cold gas target flask. Shown from left to right are Rudy Valdez, Garlan Isom, Norm Hoffman, Jan Novak, and Robert Garcia.

The $^{15}N_2$ target flask is made of five metal plates interleaved with four layers of 0.25-mm-thick Mylar (Fig. 4). Two rectangular holes 76 by 127 mm are cut into each metal plate so that when the assembly is epoxied together two "cells" are formed. Each cell consists of a central, flat, liquid compartment 10 mm thick, flanked by two gas compartments. The cells contain either liquid $^{14}N_2$ or $^{15}N_2$, and the gas compartments contain helium at the same pressure as the liquid. The flask is cooled by LN_2 pumped to 125 torr absolute, circulating from a reservoir through tubes soldered to the central metal plate.

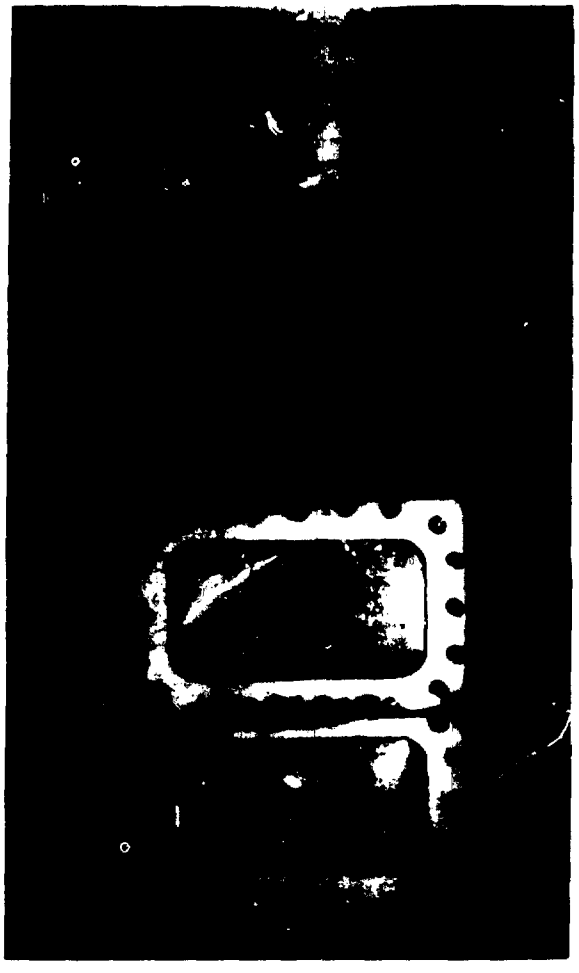

Fig. 4.
The liquid $^{15}N_2/^{14}N_2$ target flask viewed in the beam direction.

Fig. 5.
The windows and beam interaction section of the LD_2 neutron production target.

Liquid-Helium Targets

A reservoir-fed target with a flask similar to the $^{15}N_2$ flask, but containing liquid ^{3}He and ^{4}He, has been used in collaboration with the University of Virginia. Typical cells are 15- by 15- by 1-cm thick, with windows of 76-μm-thick high-strength aluminum. The body plates are high conductivity copper.

Another reservoir system has a vertical-axis cylindrical Mylar flask 76 mm diam by 0.13 mm wall thickness. The target material is ^{4}He, which is cooled below 2.1 K to eliminate boiling.

Both systems will accept a range of different geometry and size flasks.

Tritium Targets

Three experiments with cryogenic tritium have been run, two with liquid tritium and one with cold gas. All flasks were metal. The liquid flasks were cylinders 32 mm long by 25 mm diameter with hemispherical end caps, and the gas flask was a cylinder 152 mm diameter by 102 mm long with flat, thick end caps. Liquid target cooling was from an LH_2 reservoir and the gas target

was cooled with a Joule-Thompson open-cycle refrigerator.

The targets contained ~80 000 Ci of tritium; the cryogenic problems paled in comparison with the containment and safety problems.

LD_2 Neutron Production Target

Neutrons are produced for the BR channel from a closed-loop, forced-circulation, liquid-deuterium target cooled by a refrigerator. Target thickness is 254 mm, and the flask windows are 76-μm stainless steel (Fig. 5). Liquid is circulated by two axial blowers. The circulation rate is such that each beam macropulse strikes new liquid to prevent beam heating and boiling of the liquid. The refrigerator is a closed-cycle helium system with about 100 W capacity at 20 K.

Superconducting Spin-Precession Solenoid

Line B incorporates a superconducting solenoid for spin direction precession of polarized protons. The magnet has a 100-mm-diam warm bore and is 1.22 m overall. Peak field is 3.5 T and the field integral is 3.3 T-m. The coil is bath cooled with liquid helium. Consumption is ~2 ℓ/h.

—J. K. Novak

LAMPF Nuclear Chemistry Data-Acquistion System

The LAMPF Nuclear Chemistry Data-Acquistion System (DAS) is designed to provide data acquisition and data processing for a variety of users. It consists of a PDP-11/44 with peripherals on a CAMAC highway. The detectors, system operation, and development plans are described below.

The Nuclear Chemistry Laboratory instrumentation consists principally of counter systems and spectrometers, as shown in Fig. 1, for radioactive sample

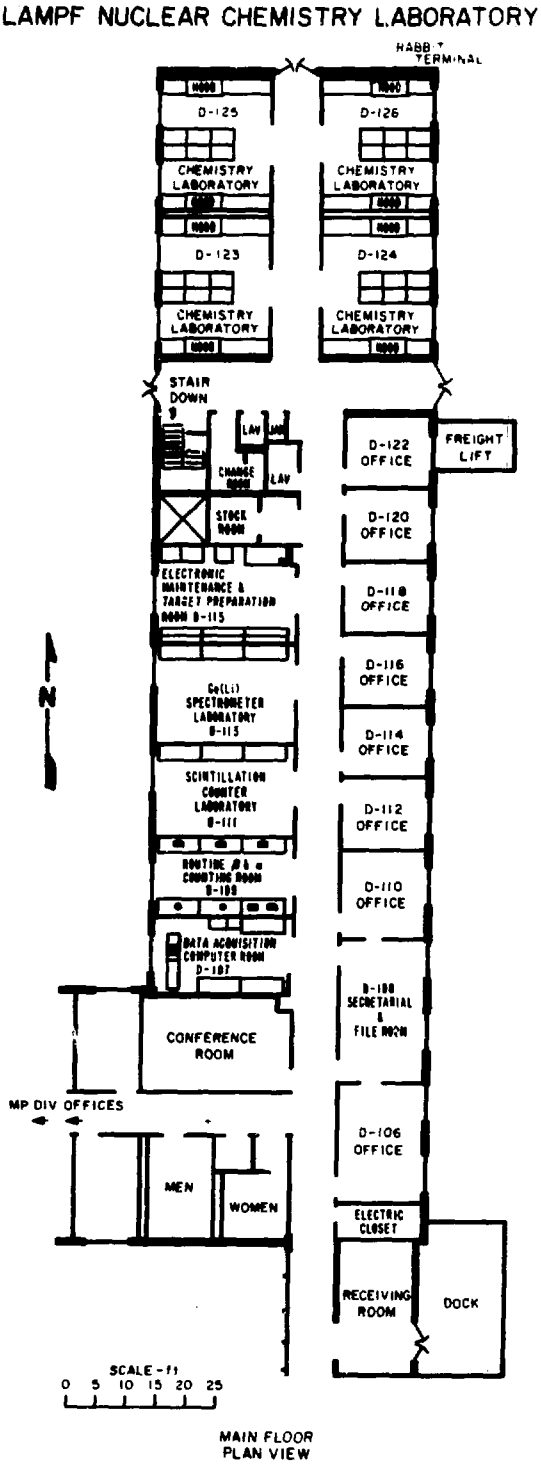

Fig. 1.
A plan view of LAMPF Nuclear Chemistry Laboratory.

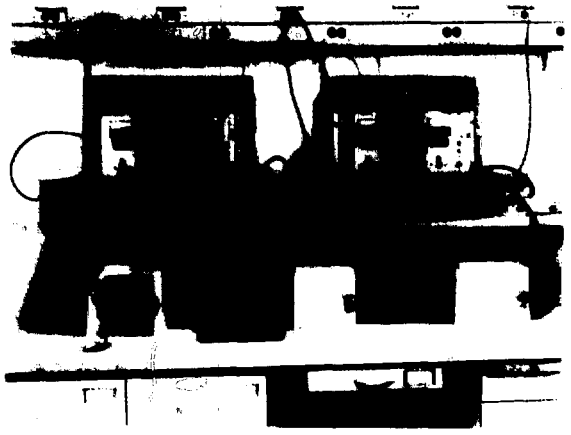

Fig. 2.
Gas-flow β-proportional counters and associated electronics.

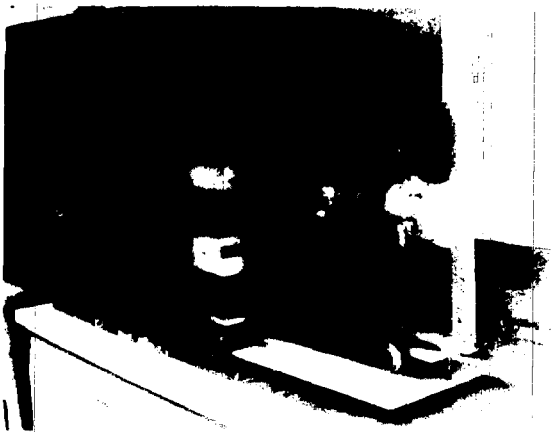

Fig. 3.
A β-γ coincidence counter.

analysis. Singles counters include α-particle and β-particle gas-flow proportional counters and gated NaI(Tℓ) γ-ray counters. Figure 2 shows the β-particle counters. A β-γ coincidence counter (Fig. 3) for absolute counting and a γ-γ coincidence/positron annihilation counter (Fig. 4) are examples of the second type. Spectrometer systems include a number of Ge(Li) γ-ray spectrometers (one is shown in Fig. 5) and solid-state α-particle (Fig. 6) and NaI(Tℓ) scintillation spectrometers; the latter two types are rarely used.

These systems can be operated in either the stand-alone mode or under computer control. They are connected to the PDP-11/44 through a four-crate CAMAC parallel branch highway, one crate in each counting lab. Data are taken from the counters by CAMAC scaler/timer modules, and from the spectrometers by multichannel analyzers (MCAs). The MCAs have dedicated tape units and CAMAC interfaces. Another CAMAC interface is used to control the automatic sample changer, shown in Fig. 7, associated with one of our Ge(Li) γ-ray spectrometers.

The PDP-11/44 computer has system peripherals comparable to a complete counting-house configuration, as shown in Fig. 8. Control and analysis programs are available, including special codes for spectral analysis. Examples of analysis programs include least-squares resolution of multicomponent radioactive decay and γ-ray stripping of complex spectra. The LAMPF-standard

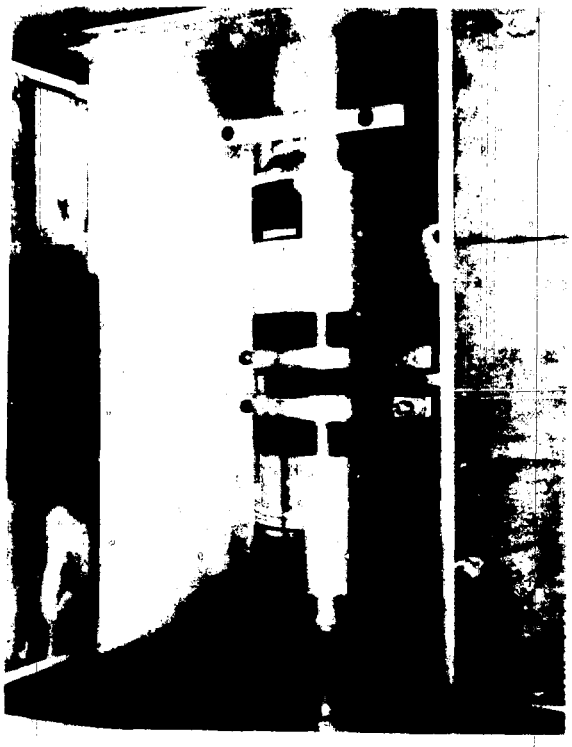

Fig. 4.
Two 7.6- by 7.6-cm NaI(Tℓ) detectors used in coincidence mode as positron annihilation counters.

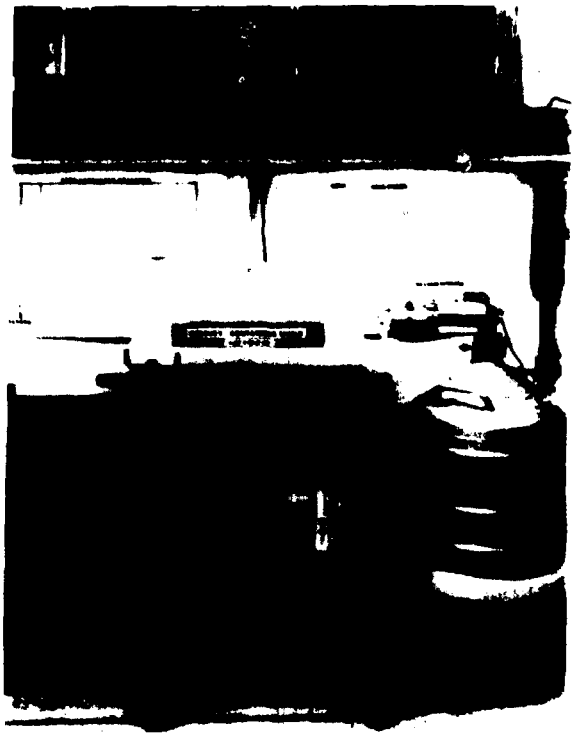

Fig. 5.
Ge(Li) spectrometer system with mercury-filled shield.

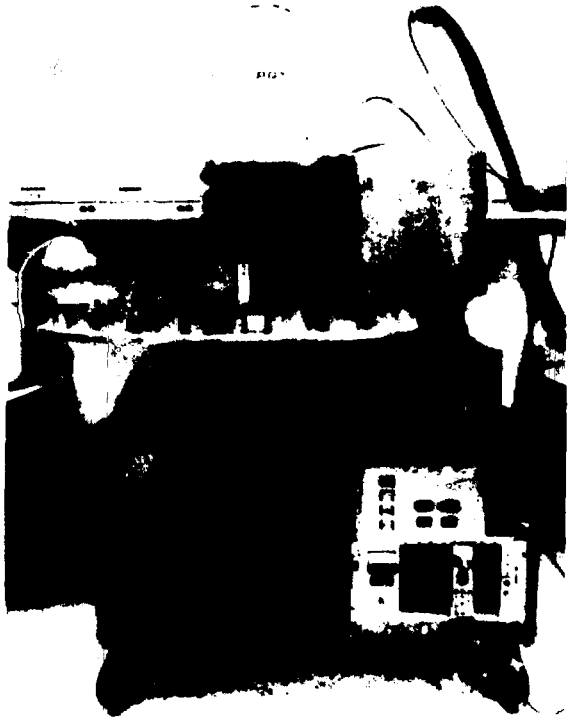

Fig. 7.
A 24-positron automatic sample changer with a Ge(Li) spectrometer.

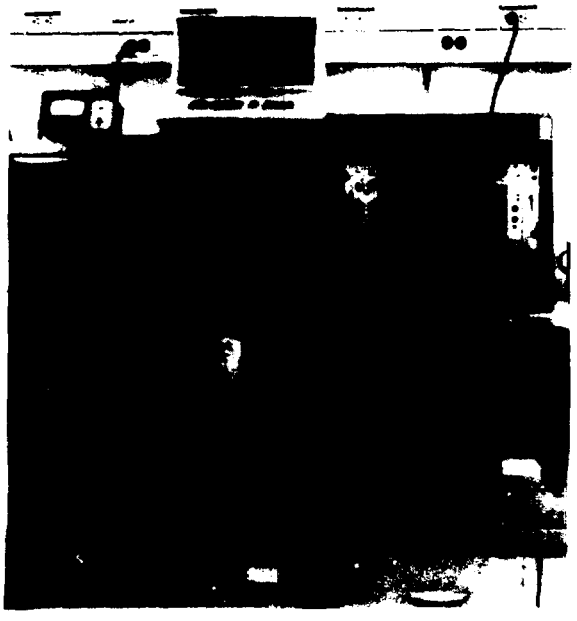

Fig. 6.
Solid-state α-particle spectrometers and their associated electronics.

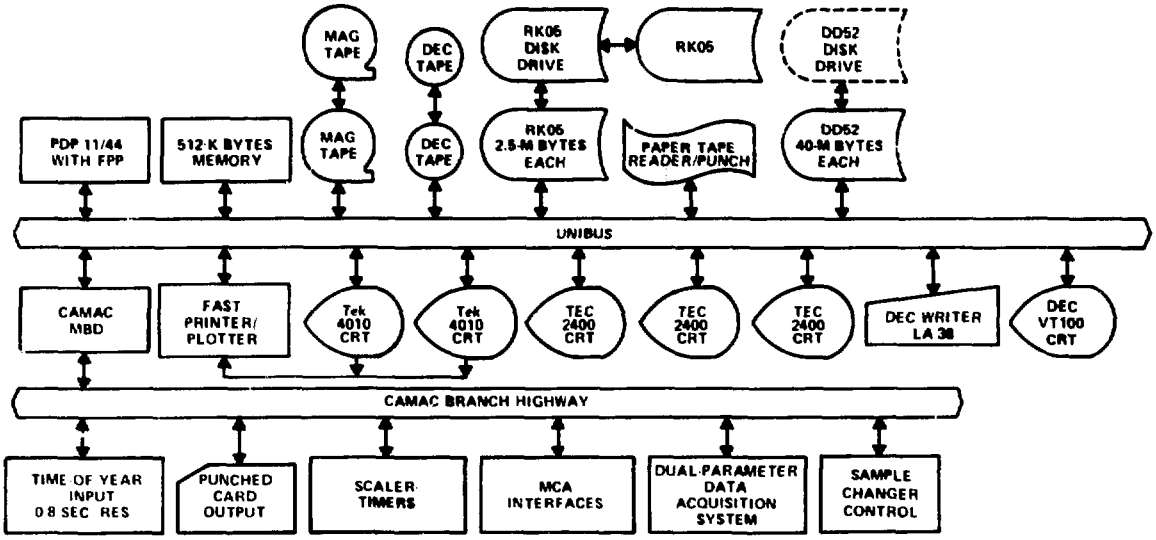

Fig. 8.
A diagram of the Nuclear Chemistry Laboratory Data-Acquistion System.

Q system is also available on this computer for data acquisition and analysis.

Future plans include restoring to operation a system with two optically separated, 38-cm-diam by 25-cm-thick NaI(Tl) γ-ray detectors, which can be used in anti-Compton, anticoincidence, or triple γ-ray coincidence modes. Also, a dual-parameter data-acquisition MCA will be put into operation.

For further information, see Ref. 1.

—*G. C. Giesler*

REFERENCE

1. G. Giesler, "LAMPF Nuclear Chemistry Data-Acquisition System," to be published in IEEE Trans. Nucl. Sci. NS-28 (October 1981).

Quad Unroll Experiments in the Drift-Tube Linac

The following experiments address the problem of obtaining a match of the H^+ production beam to the drift-tube linac. The last four transport quadrupoles are used to shape the beam and to obtain matched conditions at the entrance to the linac. A beam is assumed to be matched when its horizontal and vertical size does not oscillate at the end of Tank 1 when the transverse wavelength in the tank is varied by changing the quadrupole magnet strengths up and down. This procedure, called a "quad unroll," can be simulated using the computer code PARMILA. If the results of simulations agree with measurements, computer predictions can be used to shorten the tuning process.

However, with beam distributions constrained to agree with EM-3 measurements and transport quadrupoles TDQL03-04 set as they were for good unrolls, it has not been possible to make PARMILA agree with experimental results for any of four available sets of data from H^+ production beams. A typical production beam has 15-mA peak current and an emittance of 1.0-1.5 π cm·mrad at the EM-3 jaws. Disagreement between actual and simulated results can be caused by unreliable EM-3 measurements at these currents and by our inability to simulate the unknown neutralization in the transport region. Cross coupling among the transverse and longitudinal planes complicates computer simulations through the entire region under study.

To eliminate these known difficulties, we studied a low-current H^- beam with a large emittance, which removes space charge effects and insures reliable reconstruction of ellipse parameters. After the computer program TRACE was used to choose quadrupole strengths that transformed the beam from EM-3 to the matched ellipse values at the beginning of the linac, a

quad unroll was carried out. The last four transport quadrupoles then were varied in a systematic way to obtain mismatched conditions that would cause oscillations in the beam size at the end of Tank 1. PARMILA simulations agreed qualitatively with each of the experimental unrolls. Figure 1 shows the results of the matched unroll and its simulation, and Fig. 2 shows the results of one of the mismatches. The agreement is probably as good as should be expected.

We next studied low-current H^+ beams in an attempt to duplicate the H^- experiment as closely as possible. For all the H^+ measurements the source was degraded to obtain a beam with a larger emittance than is possible with the production source. For one experiment the beam was made large at the prebuncher aperture and the prebuncher was then turned on to further increase the emittance. Our objective was to have an emittance of at least 1 π cm·mrad and a peak current of a few hundred-microamperes. Although not all beams satisfied these criteria, unrolls of several matched and mismatched beams were made and compared with simulations. We conclude that the agreement is generally good. Figure 3 shows the assumed "matched" beam had an oscillation in the horizontal plane. To find the cause of this oscillation, we examined the effects of small errors in the fields of the matching quadrupoles. We found that, depending on the shape of the beam, certain quadrupoles are more important than others in causing or correcting mismatches. For this particular beam, we found that the horizontal oscillation could be easily duplicated in PARMILA by changing the second matching quadrupole by 1%. The vertical plane was insensitive to this change and remained well matched. Equipment failure and scheduled shutdown prevented experimental confirmation of beam sensitivity particular quadrupole.

In subsequent experiments the quadrupoles chosen by TRACE gave good or matched unrolls. We determined the important matching quadrupoles for these beams, and they did not include the second quadrupole. The important quadrupoles were varied to cause mismatches and the resulting experimental unrolls agreed well with PARMILA predictions.

In conducting these low-current experiments, we realized the importance of having an experimental beam that can be both accurately measured and simulated by PARMILA and TRACE. An accurate measurement at EM-3 is complicated by the time dependence of the H^+ currents and the slow rise times of the EM-3 amplifiers,

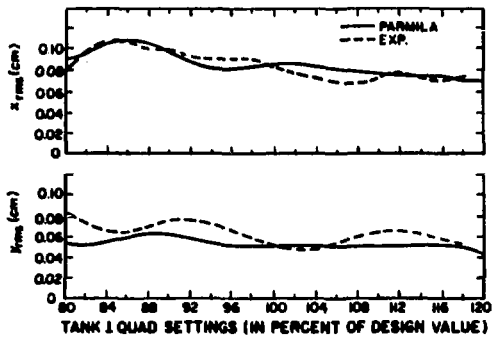

Fig. 1.
The H^- quad unroll for predicted matched conditions.

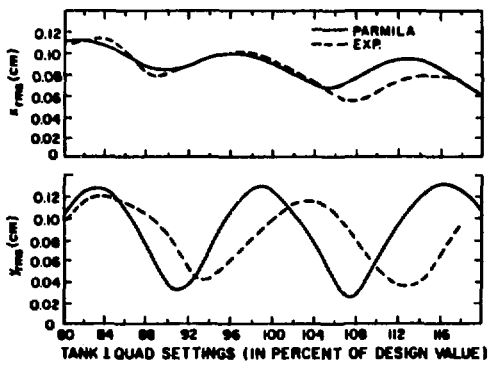

Fig. 2.
The H^- quad unroll with TDQL03-02 increased by 10%.

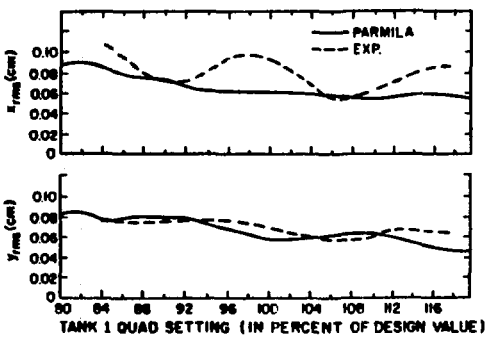

Fig. 3.
The H^+ quad unroll for predicted matched conditions.

which can and do lead to erroneous emittance measurements. Because PARMILA and TRACE assume an elliptical beam, the actual beam must have an elliptical shape that does not depend on the percentage of the beam analyzed. Furthermore, the number of samples in the emittance measurement must be sufficiently large to make meaningful the evaluation of the ellipse parameters.

Studies of 1- and 3-mA peak current beams indicate further problems. Emittance measurements depend on the EM-3 collector bias voltage, and possibly on the jaw voltage. These bias voltages have not been carefully controlled, and it is not known which voltages give the most accurate measurements. The method of calculating rms widths at the end of Tank 1 should be changed so that existing tails are not ignored, and code for PARMILA needs to be written to be more compatible with these calculations.

The conclusion drawn from these experiments is that low-current, well-shaped beams of either H^+ or H^- species can be well simulated with existing computer codes. Brighter beams still present unsolved problems.

III. ACCELERATOR OPERATIONS

This period covers operating Cycle 29. The accelerator was in operation for ~10 weeks, providing beams for research use for 52 days and for facility development for 16 days. A summary of information on beams provided for experimental use is given in Table I.

Machine operation continued to be reliable and stable. Difficulties with the initial tuning were responsible for the largest single block of unscheduled downtime. This resulted in unusually low beam availability during the brief period of H^- use at the beginning of the cycle. A summary of unscheduled facility downtime during research shifts is given in Table II. Because some of the outages were concurrent, the total is greater than the beam downtime.

During the weekend of April 18 and 19, the H^+ beam availability was 100% for a period of 43 consecutive hours. During the same period, polarized beam (P^-) availability was 90%. Availability for the 7-day period following the April 13 maintenance day was an excellent 96% for H^+ and 92% for P^-.

Accelerator development efforts continued to address various aspects of the transverse phase-space tuning problem, with emphasis shifting toward the more stringent requirements associated with future operation of the Proton Storage Ring.

—J. Bergstein

TABLE I

BEAM STATISTICS FOR CYCLE 29

	Cycle 29
No. of experiments served	52
H^+ scheduled beam hours	1264
H^- scheduled beam hours	240
P^- scheduled beam hours	1024
H^+ beam availability, %	84
H^- beam availability, %	51
P^- beam availability, %	79
H^+ average current, μA	540
H^- average current, μA	1
P^- average current, nA	~5
H^+ beam duty factor, %	6
H^-, P^- beam duty factor, %	3-6
P^- beam energy, MeV	497, 647, 800

TABLE II

UNSCHEDULED MACHINE DOWNTIME

Category	Downtime (h)	Percent of Total
201–MHz amplifiers and transmission lines	37	14
805–MHz amplifier systems	25	10
Vacuum	13	5
Magnets and magnet power supplies	9	4
Interlocks	2	1
Injectors	61	24
Cooling water systems	12	5
Computer control and data acquistion	3	1
Beam stops, plugs, targets, strippers, scrapers	6	2
Miscellaneous (utilities, etc.)	16	6
Unscheduled tuning	73	28
TOTAL	257	

IV. EXPERIMENTS RUN

Exp. No.	Experiment Title	Channel	Beam Hours
10	Search for (p,π) Reactions with HRS	HRS	55.0
123	Nuclear Structure Effects in Pion-Induced Nuclear Reactions	LEP	25.0
154	Elastic Scattering of π^+ and π^- from the Helium Isotope	P^3	316.0
194	p-p, D, R, and A Measurements	EPB	246.5
233	Search for δ-Configurations Nuclei	HRS	55.0
236	Biological Effects of Negative Pions	Biomed	34.0
267	Preparation of Radioisotopes for Medicine and the Physical Services Using the LAMPF Isotope Production Facility	ISORAD	1036.8
270	Therapy Beam Development — Biomedical Channel Tuning	Biomed	44.8
271	Therapy Beam Development — Dosimetry	Biomed	153.0
274	Pion Radiobiology	Biomed	38.0
275	Pion Clinical Trials	Biomed	574.7
294	High-Energy Nuclear Reactions	AB-Nucchem	2.4
308	An Attempt to Make Direct Atomic Mass Measurements in the Thin Target Area	TTA	983.0
334	Nuclear Charge Parameters of ^{41}Ca and Stable Cadmium and Tellurium Isotopes	SMC	45.0
349	Nuclear Reactions of ^{127}I with Pions	LEP P^3	28.0 9.0
382	μSR Investigation of the Effects of Impurities on the Trapping and Diffusion of μ^+ Particles in bcc Metals	SMC	15.0
389	Inelastic Pion Scattering from Light Nuclei ^{10}B, ^{11}B, ^{14}N, and ^{15}N	EPICS	132.0

Exp. No.	Experiment Title	Channel	Beam Hours
392	A Measurement of the Triple-Scattering Parameters D, R, A, R′, and A′ for Proton-Proton and Proton-Neutron Scattering at 800 MeV	HRS	208.6
400	Search for the Rare Decay $\mu^+ \rightarrow e^+e^+e^-$	SMC	125.0
401	Study of the Isobaric Analog Charge Exchange Reaction $^{15}N(\pi^+,\pi^0)^{15}O$	LEP	255.5
411	Measurement of Spin-Flip Probabilities in Proton Inelastic Scattering at 800 MeV and Search for Collective Spin-Flip Modes, Preliminary Survey	HRS	80.0
421	Sensitive Search for $\mu^- \rightarrow e$ Conversion	SMC	36.0
449	A Survey of Single and Double Photodetachment Cross Section of the H^- Ion from 14 to 21.8 eV	EPB	113.6
457	Measurement of the Quasi-Free pn and pp and Free pp Analyzing Powers 500-800 MeV	AB	785.0
462	Ahalyzing Power and Differential Cross Sections for the Reactions $p + p \rightarrow d + \pi^+$ and $p + d \rightarrow t + \pi^+$ at ~600 400 MeV	HRS	118.0
465	Radiochemical Study of Pion Single Charge Exchange	LEP P^3	29.4 46.7
473	Study of Giant Multipole Resonances with 800-MeV Protons	HRS	97.0
479	Measurement of R, A, R′, and A′ in Elastic and Inelastic Scattering of 800-MeV Protons from Light Nuclei — Revised Version of Q Proposal	HRS	72.0
491	Experimental Determination of the Strong-Interaction Shift in the 2p-1s Transition of Pionic Deuterium and Hydrogen Atoms	SMC	235.0
494	Nuclear Charge Parameters of the Stable Ruthenium and Palladium Isotopes	SMC	57.0
499	Muon Longitudinal and Transverse Relaxation Studies in Spin-Glass Systems	SMC	87.0
513	$\pi^\pm$ Quasi-Free Scattering from the Helium Isotopes	P^3	557.7

Exp. No.	Experiment Title	Channel	Beam Hours
523	Study of $^{14}C(\pi^+,\pi^0)^{14}N$ Reaction	LEP	78.8
524	Study of the Isovector Terms in π-Nucleus Interactions with (π^+,π^0) Reactions on $^{40,42,44,48}Ca$ and $^{112,118,124}Sn$	LEP	105.3
547	Search for Fast Muonium in Vacuum	SMC	144.0
562	Study of Pion Absorption Mechanism through the A(π,p)X Reaction at $T_\pi = 500$ MeV	P^3	428.0
570	Investigation of the Structure of ^{16}O with Pion Inelastic Scattering	EPICS	325.0
571	Muon Spin Rotation Studies of Dilute Magnetic Alloys	SMC	54.0
581	$\pi^\pm$ Elastic Scattering from Deuterium at 237 MeV	EPICS	193.0
597	The Study of Broad-Range Pion Inelastic-Scattering Spectra (with Emphasis on the Excitation of the Giant Monopole Resonance)	EPICS	55.0
603	Search for Deltas in a Complex Nucleus by a Radiochemical Technique	AB	25.0
604	An Investigation of the Near Stability of ^5H	EPICS	254.8
607	Study of Isovector Giant Resonances with Pion Charge Exchange	LEP	259.5
629	Feasibility of Helium-Jet Techniques for Studying Short-Lived Nuclei Produced at LAMPF	AB-Nucchem	23.5
634	Measurement of Parity Violation in the p-Nucleus Total Cross Sections at 800 MeV	EPB	42.0
635	Spin Measurements in pd Elastic Scattering	EPB	507.7
639	Muon Spin Rotation Study of Muon Bonding and Motion in Select Magnetic Oxides	SMC	21.0
640	Transverse and Longitudinal Field μSR Measurements in Selected Ternary Metallic Compounds	SMC	63.0

Exp. No.	Experiment Title	Channel	Beam Hours
649	$^{9}Be(p,\pi^{\pm})$ Reaction at 650 MeV	HRS	85.9
650	A Search for Neutrino Mixing via Nonexponential $\pi \rightarrow \mu\nu$ Decay	LEP	249.0

V. NEW PROPOSALS

Proposal No.	Title	Spokesmen	Institution
647	A Neutron Oscillation Experiment at LAMPF	R. J. Ellis	Los Alamos
648	Test of Equipment for the Measurement of the Σ^- for the Magnetic Moment at BNL	J. Miller	Boston Univ.
649	Asymmetry Measurements of the (p,$\pi^\pm$) Reactions on ^{6}Li and ^{9}Be at 650 MeV	B. Höistad	Univ. of Texas, Austin
650	A Search for Neutrino Mixing via Non-exponential $\pi \rightarrow \mu\nu$ Decay	J. D. Bowman	Los Alamos
651	Measurement of a Lower Limit for the Subthreshold Production of Kaons with 800-MeV Protons	C. L. Morris	Los Alamos
652	Test of Prototype Semiconductor Detectors	P. Skubic	Univ. of Oklahoma
653	Muonic X-Ray Study of ^{241}Am and ^{243}Am	E. B. Shera M. W. Johnson R. A. Naumann	Los Alamos Los Alamos Princeton Univ.
654	Measurement of the Spin-Rotation Parameter Q for 800-MeV p + ^{16}O, ^{40}Ca, and ^{208}Pb Elastic Scattering	G. W. Hoffmann	Univ. of Texas, Austin
655	$\pi^\pm$ Inelastic Scattering from ^{4}He: An Examination of Isospin Symmetry Breaking	D. B. Holtkamp W. B. Cottingame	Univ. of Minnesota New Mexico State Univ.
656	Pion Double Charge Exchange on Self-Conjugate Nuclei	S. J. Greene C. L. Morris H. T. Fortune	New Mexico State Univ. Los Alamos Univ. of Pennsylvania
657	Inelastic $\pi^\pm$ Scattering from the N = 28 Isotones	P. A. Seidl C. F. Moore	Univ. of Texas, Austin Univ. of Texas, Austin
658	Study of the Spin-Flip Probability for Elastic and Inelastic Scattering from Odd-Mass Nuclei	S. J. Seestrom-Morris T. A. Carey J. M. Moss	Los Alamos Los Alamos Los Alamos
659	Spin-Flip Giant Resonance Excitation	L. C. Bland C. F. Moore	Univ. of Pennsylvania Univ. of Texas

Proposal No.	Title	Spokesmen	Institution
660	Measurement of Polarization Parameters for M1 Transitions in the $^{90}Zr(p,p')^{90}Zr^*$ and $^{116}Sn(p,p')^{116}Sn^*$ Reactions at 500 MeV	C. Glashausser	Rutgers Univ.
661	Good Resolution Study of $^{18}O(\pi,\pi')$	C. L. Morris L. C. Bland	Los Alamos Univ. of Pennsylvania
662	Elastic and Inelastic π^- and π^+ Scattering Scattering from ^{32}S, ^{31}P and ^{90}Zr, ^{89}Y	J. J. Kraushaar R. J. Peterson	Univ. of Colorado Univ. of Colorado
663	Elastic Scattering of Polarized Protons from ^3H and ^3He at Intermediate Energies	C. J. Igo M. Bleszynski	UCLA UCLA
664	The Measurement of the Polarization Transfer Coefficients A'_t and D_t at 500, 650, and 800 MeV for the Reaction $d(\vec{p},\vec{n})2p$	G. Glass R. Stanek	Texas A&M Univ. Argonne
665	The Measurement of the Initial-State Spin-Correlation Parameters C_{LL} and C_{SL} in n-p Elastic Scattering at 500, 650, and 800 MeV	G. R. Burleson R. Wagner	New Mexico State Univ. Argonne
666	The $^{12}C(p,p'\pi)^{12}C^*$ Reaction and the Search for Coherent Isobar-Hole Resonances	C. Glashausser C. A. Whitten	Rutgers Univ. UCLA
669	Investigation of the N = 28 Neutron Shell Closure by Elastic Scattering of 800-MeV Polarized Protons	E. B. Shera H. D. Wohlfahrt	Los Alamos Los Alamos
670	Continuation of Giant Resonance Studies at HRS	J. M. Moss T. A. Carey G. S. Adams	Los Alamos Los Alamos MIT
671	Test of the Microscopic IBA Model via Pion Nucleus Scattering on the Palladium Isotopes	A. Saha K. K. Seth	Northwestern Univ. Northwestern Univ.
672	Study of Giant Resonances in ^{90}Zr, ^{116}Sn, and ^{208}Pb with π^+ and π^- Inelastic Scattering	T. A. Carey J. M. Moss S. J. Seestrom-Morris	Los Alamos Los Alamos Los Alamos

Proposal No.	Title	Spokesmen	Institution
673	Measurement of the Angular Dependence of Tensor Polarization in the $^{2}H(\pi^{+},\pi^{+})^{2}\vec{H}$ Reaction at T_{π} = 180 and 256 MeV	R. J. Holt	Argonne
674	Measurements of Pion-Nucleus Elastic and Double-Charge-Exchange Scattering at Energies above 300 MeV	G. R. Burleson C. L. Morris	New Mexico State Univ. Los Alamos
675	Nuclear Distributions from the Study of the 2p States of Pionic Atoms	A. R. Kunselman	Univ. of Wyoming
676	Study of Pion Absorption on ^{58}Ni at T_{π} = 160 MeV	N. S. Chant P. G. Roos R. P. Redwine	Univ. of Maryland Univ. of Maryland MIT
677	A Determination of $\Delta S = 1$ Contributions in Inelastic Pion Scattering from Odd-A Nuclei	D. B. Holtkamp H. O. Funsten	Univ. of Minnesota College of William & Mary
678	Study of the M1 Transition in ^{48}Ca by Inelastic Scattering of π^{+} and π^{-}	D. Dehnhard C. L. Morris	Univ. of Minnesota Los Alamos
679	A Radiochemical Study of the $^{209}Bi(p,\pi^{0})^{210}Po$, $^{209}Bi(p,\pi^{-}xn)^{210-x}At$, and $^{209}Bi(p,p2\pi^{-}xn)^{209-x}At$ Pion Production Reactions at 500-800 MeV	J. L. Clark	Los Alamos
680	Angular Distributions for $^{24,26}Mg(\pi^{+},\pi^{-})^{24,26}Si$	S. J. Greene	New Mexico State Univ.
681	Measurements of Large-Angle Pion-Nucleus Scattering with EPICS	G. R. Burleson	New Mexico State Univ.
682	Search for Dibaryon Resonances in the Reaction $\pi D \rightarrow p\pi n$ at P_{L}^{π} = 200-600 MeV/c	K. Imai S. J. Greene	Argonne New Mexico State Univ.
683	Measurement of $\Delta\sigma_{L}$ in Free Neutron-Proton Scattering at 500, 650, and 800 MeV	W. R. Ditzler J. E. Simmons	Argonne Los Alamos
684	Polarization Effects in the Deuteron Production by Proton-Nucleus Collisions	J. Källne B. Höistad	Univ. of Virginia Univ. of Texas, Austin

Proposal No.	Title	Spokesmen	Institution
685	Spin Correlations in the Reaction $\vec{p}(\vec{d},d)\vec{p}$ at 500 MeV	G. J. Igo M. Bleszynski	UCLA UCLA
686	Determination of Neutron Transition Densities in ^{16}O and ^{208}Pb by Inelastic Scattering of ~400-MeV Protons	N. M. Hintz	Univ. of Minnesota
687	Measurement of the Spin-Rotation Parameters in ^{208}Pb and in ^{40}Ca at 400 MeV	G. J. Igo	UCLA
688	Study of the Mass and Energy Dependence of Low-Energy Pion and Single Charge Exchange	M. J. Leitch M. D. Cooper	Los Alamos Los Alamos
689	A. Neutron Counter Calibration Using Tagged Neutrons from the Reaction $\pi^-d \rightarrow nn$ B. Feasibility Study: Measurements of the Differential Cross Section for $\pi^-d \rightarrow nn$ to Test Charge Symmetry and Isospin Invariance	B. M. K. Nefkens D. H. Fitzgerald	UCLA UCLA
690	Simulations of Cosmic-Ray-Produced Gamma Rays from Thick Targets	R. C. Reedy	Los Alamos
691	Simulation of Cosmic-Ray Production of Nuclides by Spallation-Produced Neutrons	R. C. Reedy	Los Alamos
692	Germanium Detector Low-Level Radiation-Damage Equilibration Experiment	R. C. Reedy	Los Alamos
693	Investigation of the Two-Photon Decay Rate from the $(\mu^4He)^+_{2s}$ State as a Function of Pressure	J. J. Reidy	Univ. of Mississippi
694	Isospin Mixing in ^4He	K. K. Seth	Northwestern Univ.
695	Study of Transfer Effects in Muon Capture in Gas Targets	J. J. Reidy R. L. Hutson	Univ. of Mississippi Los Alamos
696	The Angular Distribution Anomaly in Pion Double Charge Exchange	K. K. Seth	Northwestern Univ.

(For a complete list of active and complete experiments by channel, see Appendix A. Appendix B lists active spokesmen, institutions, and experiments.)

VI. MEETINGS

Technical Advisory Panel

The Technical Advisory Panel (TAP) met February 23-24, 1981.

The LEP spectrometer report, given by Robert Burman (Los Alamos) and Klaus Ziock (University of Virginia), described the new ideas on the "Enge" orange peel spectrometer. The TAP recommended that highest priority be given the support of this LEP spectrometer with achromatic beam.

The time-of-flight spectrometer report by Arthur Poskanzer (Lawrence Berkeley Laboratory) and David Vieira (Los Alamos) described a facility ideally suited for LAMPF. Nuclear chemistry has given priority to the funding of this work, and TAP also recommended that this project be given high priority.

The Stopped-Muon Channel report was given by Gary Sanders (Los Alamos), after which the TAP recommended that beam splitting be studied further. A subcommittee will examine the users' needs and determine whether compatible beam-splitting arrangements are feasible.

Wayne Cornelius and Robbie York (Los Alamos) reported on the optically pumped polarized ion source. The TAP felt that this project should have additional time and manpower and that the present team should have a reduction of other programmatic responsibilities so they can concentrate on this work.

Another recommendation was the construction of a neutrino facility, conceived as a general-purpose neutrino beam area at the Proton Storage Ring (PSR). The TAP encouraged the draft of a facility proposal so it can be acted upon by the Nuclear Science Advisory Committee (NSAC) as soon as possible.

Neutrino oscillations is a field of great visibility. Richard Slansky (Los Alamos) reviewed the current physics importance and the need for research in this area.

A special LUGI *ad hoc* committee was proposed by the TAP to review the neutrino proposals recommended by the Program Advisory Committee. With emphasis on budgetary considerations and feasibility, the *ad hoc* committee will also consider cross sections, background assumptions, signal rates, sensitivity to δm^2 for full mixing as well as for $\sin^2(2\theta) = 0.2$, and time scales.

Experiment 225 has had a cost overrun. TAP recommended help to resolve the financial crisis so that work on Exp. 225 can continue.

After the discussion of the LAMPF Electronics Equipment Pool (LEEP), the TAP expressed concern about the diminishing funds in this area and proposed that the LEEP budget be classified as a "line item," with funding considerably above the present level.

Board of Directors

The Board of Directors of the LAMPF Users Group, Inc., (LUGI) met Tuesday, February 24, 1981.

The following were named to the Nominating Committee for 1981 under the chairmanship of Isaac Halpern (University of Washington): Andrew Bacher (Indiana University), Helmut Baer (Los Alamos), Frank Tabakin (University of Pittsburgh), and Arthur Poskanzer (Lawrence Berkeley Laboratory). This committee will nominate candidates for Chairman-Elect (3-year term) and two Board of Directors' positions (2-year terms) to begin in 1982.

Donald R. F. Cochran (Los Alamos) was reappointed as the Liaison Officer of LUGI for 1981.

The 1980 Financial Statement for LUGI was reviewed and accepted. Other reports gave statistical data of LUGI membership and housing requirements for LAMPF users during 1980.

The TAP report and recommendations were accepted.

The chairman recommended that the Board of Directors play a more active role, within the bylaws of LUGI, to help guide scientific policy and long-range planning at LAMPF. Also discussed were specific tasks of the Board

- to represent the interests of the user community at DOE and elsewhere and actively support the Director's efforts to obtain adequate funding, and
- to initiate in-depth studies for long-range projects, such as neutrino research at LAMPF, physics possibilities at the PSR, and the kaon factory.

LAMPF Visitors Center

Research guests who visited LAMPF during this report period totaled 330; of this number 68 were foreign visitors. A total of 308 visitors checked in and 272 checked out of the Visitors Center. A complete list of visitors during this report period is given in Appendix C.

A breakdown of user statistics follows.

•MEMBERSHIP

Non-Los Alamos National Laboratory	732
Los Alamos National Laboratory	188
TOTAL	920

•FIELDS OF INTEREST

Nuclear and Particle Physics	717
Nuclear Chemistry	135
Solid-State Physics and Materials Science	176
Theory	177
Biomedical and Biological Applications	237
Weapons Neutron Research	91
Data Acquisition	159
Administration, Coordination, Facilities, Operations, Practical Applications, etc.	148
Isotope Production	85

(Note: These numbers do not add to total membership because of duplicate interests.)

•INSTITUTIONAL DISTRIBUTION

Membership by Institutes

Los Alamos National Laboratory	188
National or Government Laboratories	89
U.S. Universities	364
Industry	44
Foreign	170
Hospitals	51
Non-Affiliated	14
TOTAL	920

Number of Institutes

National or Government Laboratories	21
U.S. Universities	108
Industry	35
Foreign	83
Hospitals	40
Non-Affiliated	6
TOTAL	293

•REGIONAL BREAKDOWN

East (Pennsylvania, New Jersey, Delaware, Washington, DC, Massachusetts, New York, Connecticut, Vermont, Rhode Island, New Hampshire, Maine)	124
Midwest (Ohio, Missouri, Kansas, Indiana, Wisconsin, Michigan, Illinois, North Dakota, South Dakota, Nebraska, Iowa, Minnesota)	99
South (Maryland, Virginia, Tennessee, Arkansas, West Virginia, Kentucky, North Carolina, South Carolina, Alabama, Mississippi, Louisiana, Georgia, Florida)	77
Southwest, Mountain (Montana, Idaho, Utah, Wyoming, Arizona, Colorado, New Mexico, Oklahoma, Texas) (excluding Los Alamos)	144
West (Alaska, Hawaii, Nevada, Washington, Oregon, California)	118
Foreign	170
Los Alamos National Laboratory	188
TOTAL	920

VII. LAMPF NEWS

A Workshop on new and future aspects of nuclear and particle physics at energies up to 31 GeV was held in Los Alamos from January 5-8. About 200 participants gathered to discuss recent developments in the weak and unified interactions (including neutrino oscillations), hadronic and quark descriptions of the strong interactions, hypernuclei, and new and future experimental facilities. The Workshop was organized by J. David Bowman, Ernest M. Henley, Leonard S. Kisslinger, and Richard R. Silbar.

One of the motivations for organizing this Workshop was to explore physics justifications for a future high-intensity proton accelerator that would use the present LAMPF accelerator as an injector. Such an accelerator could provide intense beams of protons, kaons, pions, and neutrinos in an energy region where there will soon be no machine available in the U.S. for experimentation. A general conclusion of many, if not most, of the participants in the Workshop is that there are many interesting questions in physics that can be profitably addressed by such a new facility.

Conference proceedings are available at cost from the LAMPF Users Group Liaison Office, Mail Stop 830, Los Alamos National Laboratory, Los Alamos, NM 87545.

Jere D. Knight, Group CNC-11, received the John Dustin Clark Award of the Central New Mexico Section of the American Chemical Society for 1980. The award was presented on January 16, 1981. It consists of a medal and a stipend, and recognizes outstanding chemists for meritorious service in the field of chemistry in New Mexico.

Knight received his bachelor of science degree in chemistry from St. John's University (Minnesota) and his doctorate from the University of Minnesota. He joined the Laboratory in 1949 and has been here since, except for a sabbatical at Brookhaven National Laboratory in 1954. His research fields include nuclear and radiochemistry, photonuclear reactions, nuclear fission, short-lived isotopes and isomers, heavy elements, and nuclear structure and reactions. Most recently, at LAMPF, he has worked in the new field of chemical effects in the capture of negative muons in matter.

Darragh E. Nagle was appointed a Senior Fellow and J. David Bowman, Robert L. Burman, Jere D. Knight, and Donald A. Swenson were appointed Laboratory Fellows on February 11, 1981.

To be eligible for this appointment, full-time employees must have demonstrated outstanding contributions in some field of scientific or technical endeavor and

Jere D. Knight, CNC-11

Louis Rosen, Director of LAMPF.

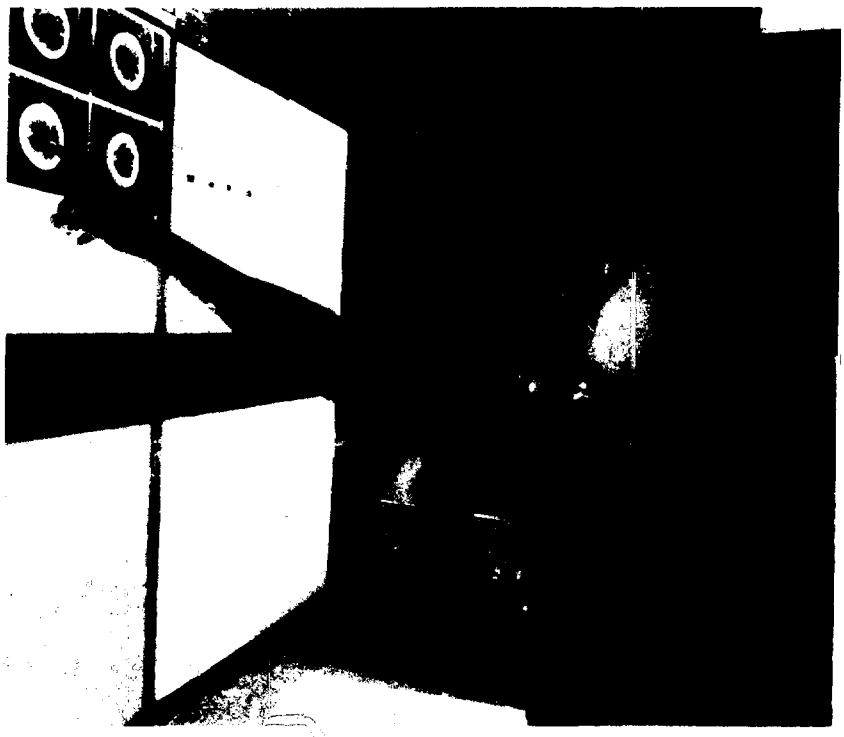

Steven Bush, M.D., foreground.

have shown exceptional promise for continued professional achievement.

Fellows will devote most of their time to research on topics of their own choosing within their area of competence. It will be their responsibility to produce fresh ideas and research initiatives to further the Laboratory's contributions to national defense, arms control commitments, and a secure energy supply for the future.

Louis Rosen, leader of the Medium-Energy Physics Division and Director of LAMPF, has been named Sesquicentennial Honorary Professor by his alma mater, the University of Alabama. This recognition symmetrizes a previous designation of Alumni Fellow by his other alma mater, Pennsylvania State.

The University's honorary professor program identifies and recognizes outstanding alumni for their pursuits of excellence and intellectual accomplishments since graduation. Rosen will have the rights and responsibilities of adjunct professor and will be invited to lecture when visiting the campus.

A sesquicentennial medallion and an honorary professor plaque bearing Rosen's name will be mounted in the Student Alumni Hall of Fame.

As of March 1981, Steven E. Bush, M.D., was named both principal investigator at the pion cancer treatment project at LAMPF and Chief of Radiation Oncology at the University of New Mexico Cancer Research and Treatment Center.

Bush came to Los Alamos two years ago after completing his residency at Stanford University in 1979. He replaces M. M. Kligerman, M.D., who resigned in September 1980.

Chairman Felix Boehm (California Institute of Technology) of the LAMPF Users' Group, Inc., convened the LAMPF Users Group *Ad Hoc* Board of Directors Committee, shown below, to review neutrino oscillation proposals at LAMPF on March 23, 1981. Presentations to the committee were made by Tom Dombeck (University of Maryland), T. Y. Ling and Tom Romanowski (Ohio State), Lloyd Hyman (Argonne National Laboratory), H. H. Chen (University of California at Irvine), and J. B. Roberts and G. C. Phillips (Rice University).

Members of the Committee are seated at the table: on the left, P. Rosen, D. R. F. Cochran (LUGI Liaison Officer), B. Barish, and F. Boehm; on the right, A. Mann, G. J. Stephenson, R. Redwine, and P. Nemethy.

At the Baltimore meeting of the American Physical Society, April 20-23, 1981, 7 invited and 38 contributed papers related to LAMPF were presented, a record number. Staff members from Los Alamos who presented invited papers included T. S. Bhatia, J. N. Ginocchio, and

Meeting of Ad Hoc *Committee on Neutrino Oscillations of the LAMPF Users Group, Inc.*

J. M. Moss. Other LAMPF Users who presented invited papers were F. Boehm (Users Chairman, California Institute of Technology), H. H. Chen (University of California at Irvine), R. D. McKeown (California Institute of Technology), and E. Moniz (Massachusetts Institute of Technology).

Effective June 1, 1981, Earl Hoffman was appointed Group Leader of MP-1. Earl has formerly served as Staff Member in MP-13.

CLINTON P. ANDERSON MESON PHYSICS FACILITY

MILESTONES

Official Ground Breaking	February 15, 1968
Spinoff: Adoption of LAMPF Accelerating Structure for X-Ray Therapy and Radiography Machines	*ca* 1968
5-MeV Beam Achieved	June 10, 1970
Adoption of a LAMPF Standard Data-Acquisition System	August 1970
100-MeV Beam Achieved	June 21, 1971
211-MeV Beam Achieved	August 27, 1971
800-MeV Beam Achieved	June 9, 1972
Spinoff: First Use of Electrosurgical Forceps in Open-Heart Surgery (University of New Mexico)	September 13, 1972
Discovery of ^{236}Th (Experiment Zero)	September 25, 1972
Dedication to Senator Clinton P. Anderson	September 29, 1972
Spinoff: First Hyperthermic Treatment of Animal Tumors	October 1972
First H^- Injector Beam	March 28, 1973
First Simultaneous H^+ and H^- Beams	May 4, 1973
Beam to Area B	July 15, 1973
First Experiment (#56) Received Beam	August 24, 1973
First Meson Production, Beam to Area A	August 26, 1973
Beam to Area A-East	February 6, 1974
First Medical Radioisotope Shipment	July 30, 1974
Usable 100-μA Beam to Switchyard	September 5, 1974
Pi-Mesic Atoms with "Ticklish" Nuclei	October 13, 1974
First Experimental Pion Radiotherapy	October 21, 1974
First Tritium Experiment (80 000 Ci)	November 1974
Start of Great Shutdown	December 24, 1974
New Precise Measurements of Muonium Hyperfine Structure Interval and μ^+ Magnetic Moment	1975-77-80
Q Data-Acquisition Software Operational	June 1975
Spinoff: First Use of ^{82}Rb for Myocardial Imaging in Humans (Donner Laboratory, Lawrence Berkeley Laboratory)	June 1975
Spinoff: First Hyperthermic Treatment of Human Cancer (University of New Mexico)	July 11, 1975
Accelerator Turn On Starts	August 1, 1975
Acceptable Simultaneous 100-μA H^+ and 3-μA H^- Beams to Switchyard	September 14, 1975
Production Beam to Area B	October 7, 1975
First Pions Through EPICS Channel	March 18, 1976
Production Beam in Area A and Area A-East: End of Great Shutdown	April 5, 1976
Muon Spin Rotation Program	June 1976
Spinoff: First Hyperthermic Treatment of "Cancer Eye" in Cattle (Jicarilla Reservation)	June 3, 1976
100-μA Production Beam in Area A	August 1976

MILESTONES

(Continued)

Experiment in Atomic Physics (H^- + laser beam): Observation of Feshbach and Shape Resonances in H^-	October 1976
Double Charge Exchange in ^{16}O: LEP Channel	October 5, 1976
Startup of Isotope Production Facility	October 15, 1976
HRS Operation Begins	November 1976
Maintenance by "Monitor" System of Remote Handling	Fall 1976
Proton Beam to WNR	March 12, 1977
Polarized Proton Beam Available	April 1977
Spinoff: First Practical Applications Patent Licensed to Private Industry	April 12, 1977
Pion Radiotherapy with Curative Intent	May 1977
Proton Computed Tomography Program	June 1977
Experimental Results at Neutrino Facility	July 1977
Cloud and Surface Muon Beams: SMC Channel	July 1977
EPICS Operation Begins	August 1977
300-μA Production Beam in Area A	Fall 1977
AT Division Established	January 1, 1978
π^0 Spectrometer Begins Operation	February 1978
Operation of Polarized Proton Target	Spring 1978
Successful Water-Cooled Graphite Production Target	November 1978
Spinoff: First Thermal Modification of Human Cornea (University of Oklahoma)	July 11, 1979
600-μA Production Beam in Area A	November 1979
New Limit on $\mu \rightarrow e\gamma$	December 1979
Commercial Production of Radioisotopes	January 1980
Spin Precessor Begins Operation	February 1980
Data-Analysis Center Operational	April 1980
Variable-Energy Operation	June 1980
Single Isobaric Analog States in Heavy Nuclei	June 1980
Spinoff: First Use of ^{82}Rb for Brain Tumor Imaging in Humans (Donner Laboratory, Lawrence Berkeley Laboratory)	September 1980
Double Isobaric Analog States in Heavy Nuclei	October 1980
Focal Plane Polarimeter Operational at HRS	October 1980
Safety Award to LAMPF Users Group, Inc., for Working One Million Man-Hours Since 1975 Without a Disabling Injury	October 27, 1980
New Measurement of Pion Beta Decay — Improved Test of Conserved Vector Current	November 1980

APPENDIX A

ACTIVE AND COMPLETE EXPERIMENTS BY CHANNEL

AREA B NEUTRONS AND PROTONS (AB)

Exp. No.	Title	Spokesman	Phase No. *=Complete	Beam Hours
56	STUDY OF NEUTRON SPECTRUM FROM PROTON BOMBARDMENT OF DEUTERIUM IN THE 300-600-MeV REGION	NORTHCLIFFE SIMMONS	1 * 2 *	0.0 0.0
65	NEUTRON-PROTON POLARIZATION MEASUREMENTS USING A POLARIZED TARGET — PHASE I: THE *n-p* POLARIZATION OBSERVABLE $P(\theta)$	SIMMONS	1 *	996.8
66	NEUTRON-PROTON POLARIZATION MEASUREMENTS WITH A POLARIZED TARGET — PHASE II: THE n-p SPIN-CORRELATION OBSERVABLE	SIMMONS	1 * 2 *	343.4 472.0
125	ELASTIC NEUTRON-PROTON BACK-ANGLE DIFFERENTIAL CROSS-SECTION MEASUREMENTS 300-800 MeV	DIETERLE	1 *	0.0
129	PION PRODUCTION IN NEUTRON-PROTON COLLISIONS	WOLFE	1 *	319.0
189	SEARCH FOR CONDENSED NUCLEAR STATES AND STUDY OF HIGH-q^2 LOW-ν NUCLEAR INTERACTIONS	VAN DYCK	1 *	0.0
193	MEASUREMENT OF SMALL-ANGLE NEUTRONS ELASTIC SCATTERING FROM PROTONS	DIETERLE McFARLANE	1 * 2 *	1091.1 0.0
205	(n,p) CHARGE-EXCHANGE AND NEUTRON-INDUCED QUASI-FREE SCATTERING	KENEFICK RILEY	1 *	38.5
255	MEASUREMENT OF $[\sigma(\theta)]$ FOR n-p SCATTERING AT 460 MeV	NORTHCLIFFE	1 *	5.0
262	TEST OF ISOSPIN INVARIANCE IN THE REACTION $np \rightarrow d\pi^0$	BONNER	1 *	304.8
263	MEASUREMENT OF THE ENERGY AND ANGULAR VARIATION OF THE np CHARGE-EXCHANGE CROSS SECTIONS	BONNER	1 *	237.1
264	MEASUREMENT OF THE ENERGY VARIATIONS OF THE nd ELASTIC DIFFERENTIAL CROSS SECTIONS NEAR 180°	BONNER	1 *	473.1
279	TEST OF CHARGE SYMMETRY IN nd AND pd SCATTERING	DIETERLE McFARLANE	F S*[a]	101.0
360	THE MEASUREMENT OF THE POLARIZATION TRANSFER COEFFICIENT D_t AND A_t AT 800 MeV FOR THE REACTIONS d(p,n)2p, ^{6}Li(p,n)^{6}Be, AND ^{9}Be(p,n)^{9}B	RILEY SIMMONS	1 *	493.5
366	NONRESONANT PION PRODUCTION IN THE REACTION $np \rightarrow \pi^- pp$	MAYES MUTCHLER	1 *	427.7

[a] FEASIBILITY STUDY.

402	A MEASUREMENT OF THE POLARIZATION TRANSFER COEFFICIENTS $D_t(0°)$ AND $A_t'(0°)$ IN THE REACTION POLARIZED $\vec{p}p \rightarrow \vec{n}X$ AT 800 MeV	GLASS SIMMONS	1 * 2 *	166.1 83.8
403	A MEASUREMENT OF THE TRIPLE-SCATTERING PARAMETER D_t FOR THE CHARGE-EXCHANGE REGION IN np SCATTERING	BONNER	1 * 2 *	0.0 223.8
457	MEASUREMENT OF THE QUASI-FREE pn AND pp AND FREE pp ANALYZING POWERS 500-800 MeV	BHATIA SIMMONS	1 *	785.0
492	POLARIMETER CALIBRATIONS AND SEARCH FOR ENERGY-DEPENDENT STRUCTURE IN pp ELASTIC SCATTERING VIA CROSS SECTION, ANALYZING POWER, AND WOLFENSTEIN PARAMETER MEASUREMENTS	McNAUGHTON WILLARD	1	860.2
498	MEASUREMENTS OF LONGITUDINAL CROSS-SECTION DIFFERENCE FOR LONGITUDINAL POLARIZED BEAM AND TARGETS (pp, pd, np)	WAGNER BURLESON	3	0.0
504	MEASUREMENT OF THE TOTAL CROSS-SECTION DIFFERENCE FOR PROTON-PROTON AND PROTON-NEUTRON SCATTERING IN PURE TRANSVERSE INITIAL SPIN STATES IN THE 400-800-MeV REGION	PHILLIPS	1 *	1568.0
505	MEASUREMENT OF THE TRANSVERSE SPIN-SPIN ASYMMETRY IN THE REACTION $pp \rightarrow d\pi^+$ IN THE 500-800-MeV REGION	PHILLIPS	1 2	860.2 0.0
528	EXPLORATORY MEASUREMENT OF $\Delta\sigma_L$ IN FREE NEUTRON-PROTON SCATTERING AT 800 MeV	SIMMONS NORTHCLIFFE	1	0.0
603	SEARCH FOR DELTAS IN A COMPLEX NUCLEUS BY A RADIOCHEMICAL TECHNIQUE	TURKEVICH	1 2	25.0 0.0
664	THE MEASUREMENT OF THE POLARIZATION TRANSFER COEFFICIENTS A_t' AND D_t AT 500, 650, AND 800 MeV FOR THE REACTION $D(\vec{p},\vec{n})2p$	GLASS STANEK	1	0.0
665	THE MEASUREMENT OF THE INITIAL-STATE SPIN-CORRELATION PARAMETERS C_{LL} AND C_{SL} IN n-p ELASTIC SCATTERING AT 500, 650, AND 800 MeV	BURLESON WAGNER	1	0.0
683	MEASUREMENT OF $\Delta\sigma_L$ IN FREE NEUTRON-PROTON SCATTERING AT 500, 650, AND 800 MeV	DITZLER SIMMONS	1	0.0

AREA B NUCLEAR CHEMISTRY (AB-Nucchem)

Exp. No.	Title	Spokesman	Phase No. *=Complete	Beam Hours
103	SPALLATION YIELD DISTRIBUTIONS FOR PION INTERACTIONS WITH COMPLEX NUCLEI	HUDIS	2 *	0.4
104	PROPOSAL FOR LAMPF EXPERIMENT: STUDIES OF THE PROTON- AND PION-INDUCED FISSION OF MEDIUM-MASS NUCLIDES	PATE	1 * 2 *	0.0 5.0
105	NUCLEAR SPECTROSCOPY STUDIES OF PROTON-INDUCED SPALLATION PRODUCTS	BUNKER	1 * 2 *	10.0 58.6
106	PROTON-INDUCED SPALLATION REACTIONS RELATED TO THE ISOTOPE PRODUCTION PROGRAM AT LAMPF	O'BRIEN	1 * 2	0.7 37.6

118	FRAGMENT EMISSION FROM PION INTERACTIONS WITH COMPLEX NUCLEI	PORILE	1 * 2	0.0 0.0
119	CROSS SECTIONS OF SIMPLE NUCLEAR REACTIONS INDUCED BY π^- MESONS	KAUFMAN	2 *	15.2
123	NUCLEAR STRUCTURE EFFECTS IN PION-INDUCED NUCLEAR REACTIONS	KAROL	1 * 2 *	0.0 1.0
150	SEARCH FOR POLYNEUTRON SYSTEMS	TURKEVICH	1 * 2 *	0.0 14.2
169	PROTON IRRADIATIONS FOR PROJECT JUMPER	ORTH SATTIZAHN	1 *	0.0
243	RECOIL STUDIES OF DEEP SPALLATION AND FRAGMENTATION PRODUCTS FROM THE INTERACTION OF 800-MeV PROTONS WITH HEAVY ELEMENTS	PORILE	1 *	55.8
282	MEASUREMENT OF CROSS SECTIONS FOR PROTON-INDUCED FORMATION OF SPALLATION PRODUCTS IN COPPER BY ACTIVATION ANALYSIS	DONNERT	1 * 2 * 3 *	0.6 1.5 0.1
294	HIGH-ENERGY NUCLEAR REACTIONS	KAROL	1	9.7
301	IMPAIRMENT OF SUPERCONDUCTING CHARACTERISTICS BY PROTON IRRADIATION	WILSON	1 *	185.0
326	ELECTRICAL COMPONENT RADIATION EFFECTS STUDY	HARVEY	1	179.9
407	THE EFFECT OF DISLOCATION VIBRATION ON VOID GROWTH IN METALS DURING IRRADIATION	SOMMER	1 * 2	516.2 0.0
410	RADIATION EFFECTS IN AMORPHOUS METALS DUE TO 800-MeV PROTONS	COST	1 *	583.0
416	STUDY OF FAST PION-INDUCED FISSION OF URANIUM	DROPESKY	4	0.0
424	PRELIMINARY EXPERIMENTS FOR DOUBLE CHARGE EXCHANGE AND (μ^-,e^+) SEARCHES	TURKEVICH WARREN	1 *	8.0
465	RADIOCHEMICAL STUDY OF PION SINGLE CHARGE EXCHANGE	RUNDBERG	1 *	0.5
554	IRRADIATION OF TECHNOLOGICALLY IMPORTANT METALS WITH 800-MeV PROTONS USING THE ISOTOPE PRODUCTION FACILITY AT LAMPF	BROWN COST	1	75.2
557	EXPOSURE, IN A PARASITIC MODE, OF A 3-cm BY 3-cm BY 1-cm STACK OF SOLID TRACK DETECTORS TO A π^- BEAM	COWSIK	1	0.0
579	A RADIOCHEMICAL STUDY OF NEUTRON-DEFICIENT PRODUCTS FROM 500 MeV AND ^{238}U	FAUBEL	1	0.8
610	USE OF LAMPF BEAM STOP TO OBTAIN ^{60}Fe	HENNING KUTSCHERA	1	0.0
629	FEASIBILITY OF HELIUM-JET TECHNIQUES FOR STUDYING SHORT-LIVED NUCLEI PRODUCED AT LAMPF	GREENWOOD BUNKER TALBERT, J.	1	23.5

679	A RADIOCHEMICAL STUDY OF THE $^{209}Bi(p,\pi^0)^{210}Po$, $^{209}Bi(p,\pi^-xn)^{210-x}At$, AND $^{209}Bi(p,p2\pi^-xn)^{209-x}At$ PION PRODUCTION REACTIONS AT 500-800 MeV	CLARK	1	0.0
690	SIMULATIONS OF COSMIC-RAY-PRODUCED GAMMA RAYS FROM THICK TARGETS	REEDY	1	0.0
691	SIMULATION OF COSMIC-RAY PRODUCTION OF NUCLIDES BY SPALLATION-PRODUCED NEUTRONS	REEDY	1	0.0
692	GERMANIUM DETECTOR LOW-LEVEL RADIATION-DAMAGE EQUILIBRATION EXPERIMENT	REEDY	1	0.0

BIOMEDICAL PION CHANNEL (Biomed)

Exp. No.	Title	Spokesman	Phase No. *=Complete	Beam Hours
44	RADIOBIOLOGY OF π^- MESONS, A PRELIMINARY STUDY	CARLSON	1 *	75.0
84	QUALITY OF MESON RADIATION FIELDS	PHILLIPS	1 *	0.0
143	STUDY OF THE RADIOBIOLOGICAL PROPERTIES OF NEGATIVE PIONS	KLIGERMAN KNAPP	1 * 2 * 3 *	0.0 0.0 0.0
151	AN INVESTIGATION OF PION DOSIMETRY BY PASSIVE PARTICLE DETECTORS	KNOWLES	1 *	8.0
167	HEAVY FRAGMENT FORMATION FOLLOWING THE ABSORPTION OF π^- IN ^{12}C	ZIOCK	1 *	0.0
171	STUDY OF NEGATIVE PION BEAMS BY MEANS OF PLASTIC NUCLEAR TRACK DETECTORS	BENTON	1	0.0
187	NUCLEAR GAMMA RAYS PRODUCED BY NEGATIVE PIONS STOPPING IN CARBON, NITROGEN, OXYGEN, AND TISSUE	REIDY	1	21.6
195	NUCLEAR RESONANCE EFFECT IN PIONIC ATOMS	LEON REIDY	1 * 2 *	0.0 155.2
196	A VISUALIZATION EXPERIMENT WITH CHARGED PARTICLES	DANIEL REIDY	1 *	0.0
198	EFFECTS OF PIONS ON DNA OF NONDIVIDING CELL SYSTEMS	POWERS	1 *	0.0
207	MEASUREMENT OF NEUTRON SPECTRUM AND INTENSITY RESULTING FROM π^- CAPTURE IN WATER PHANTOM AND HUMAN TISSUE	BRADBURY ALLRED	1 *	0.0
209	PION INTERACTIONS IN NUCLEAR EMULSIONS	BRADBURY ALLRED	1 *	0.0
212	COMPARATIVE EFFECTIVENESS OF NEGATIVE PIONS vs ^{252}Cf IN A TUMOR ANIMAL SYSTEM	MEWISSEN	1 *	0.0
215	VISUALIZATION OF STOPPING PION DISTRIBUTION	PEREZ-MENDEZ BRADBURY	1	172.1

217	π^- PRODUCTION CROSS SECTIONS	PACIOTTI	1	5.9
218	PION DOSIMETRY WITH NUCLEAR EMULSIONS AND ALANINE	KATZ	1	0.0
235	RADIATION REPAIR OF NORMAL MAMMALIAN TISSUES	GILLETTE	1	68.4
236	BIOLOGICAL EFFECTS OF NEGATIVE PIONS	RAJU	1	556.0
239	STUDY OF ^{11}C AND ^{13}N PRODUCTION BY π^- IRRADIATION OF CARBON, NITROGEN, OXYGEN, AND TISSUE FOR RADIOTHERAPY MONITORING	FRIEDLAND MAUSNER	1 * 2 *	55.0 8.0
242	SURVIVAL OF SYNCHRONIZED CULTURED HUMAN KIDNEY T-1 CELLS EXPOSED TO STOPPING PIONS AND X RAYS AT VARIOUS TIMES AFTER MITOSIS	TODD	1 *	105.5
244	SYSTEMS DEVELOPMENT FOR EFFICIENT UTILIZATION OF HIGH-PURITY GERMANIUM MOSAIC DETECTORS FOR TUMOR UTILIZATION	BRILL	1	0.0
270	THERAPY BEAM DEVELOPMENT — BIOMEDICAL CHANNEL TUNING	PACIOTTI	1	854.8
271	THERAPY BEAM DEVELOPMENT — DOSIMETRY	SMITH	1	2917.4
272	THERAPY BEAM DEVELOPMENT — MICRODOSIMETRY	DICELLO	1	551.2
273	THERAPY BEAM DEVELOPMENT — LET MEASUREMENTS	RICHMAN	1	783.7
274	PION RADIOBIOLOGY	BUSH	1	2520.0
275	PION CLINICAL TRIALS	BUSH	1	6302.7
285	MIGRATION OF ^{11}C AND ^{13}N RADIOACTIVITY PRODUCED *IN VIVO* BY π^-	MAUSNER	1 *	13.0
300	NEGATIVE PIONS COULOMB CAPTURE AND NEGATIVE PIONS TRANSFER IN TISSUE, TISSUE-EQUIVALENT LIQUID, AND SIMPLE COMPONENTS	DANIEL LEON	1 *	37.0
.304	STUDY OF THE AUGER PROCESS IN PIONIC ATOMS	LEON MAUSNER	1 *	9.2
380	RBE AND OER FOR NORMAL AND TUMOR TISSUE	PHILLIPS GOLDSTEIN	1	52.1
384	PF USING MOUSE TESTES AS A BIOLOGICAL TEST SYSTEM	GERACI	1	23.7

BEAM STOP A RADIATION (BSA-RAD)

Exp. No.	Title	Spokesman	Phase No. *=Complete	Beam Hours
45	RADIATION-DAMAGE STUDIES — HIGH-TEMPERATURE REACTOR MATERIALS AND TYPE II SUPERCONDUCTORS	DUDZIAK GREEN GIORGI	1 * 2 *	0.0 1833.0
111	SEARCH FOR NEW NEUTRON-RICH NUCLIDES PRODUCED BY FAST NEUTRONS	HILL	1 * 2 *	0.0 10.8

113	RADIATION DAMAGE AND HELIUM EMBRITTLEMENT IN ELEVATED TEMPERATURE REACTOR STRUCTURAL ALLOYS	MICHEL	1	0.0
161	THE MICRODISTRIBUTION OF THORIUM IN METEORITES	BURNETT	1	11.7
174	INVESTIGATION OF THE CHEMICAL REACTIONS OF ATOMIC ^{18}F AS A MEANS FOR DIRECT SYNTHESIS OF ^{18}F-LABELED COMPOUNDS	ROWLAND MILLER	1 * 2 *	0.0 7.0
326	ELECTRICAL COMPONENT RADIATION EFFECTS STUDY	HARVEY	1	294.5
406	NEUTRON FLUX CHARACTERIZATION AT A-6 RADIATION EFFECTS FACILITY	HARVEY	1	1306.3
415	TWO-NUCLEON-OUT PRODUCTS FROM STOPPED π^- INTERACTIONS	ORTH	1 *	0.0
467	IRRADIATION IN SUPPORT OF FERFICON STUDIES	GILMORE	1	0.4
542	FEASIBILITY STUDY — USING AN EXISTING NEUTRON BEAM PIPE AT LAMPF BEAM STOP FOR CRYSTAL DIFFRACTION SPECTROMETER EXPERIMENTS	LU	1 * 2	699.7 0.0
545	FUSION MATERIALS NEUTRON IRRADIATIONS — A PARASITE EXPERIMENT	BROWN	1	0.0
560	STUDY OF NEUTRON-IRRADIATION-INDUCED GROWTH OF METALS AT RADIATION EFFECTS FACILITY	HARVEY	1	63.4

EXTERNAL PROTON BEAM (EPB)

Exp. No.	Title	Spokesman	Phase No. *=Complete	Beam Hours
26	NEUTRON TIME-OF-FLIGHT EXPERIMENT AT BEAM STOP	VEESER	1 *	0.0
27	p-p SPIN-CORRELATION EXPERIMENTS	WILLARD	1 * 2 *	0.0 1141.8
42	BREAKUP OF FEW-NUCLEON SYSTEMS AND NUCLEI	COLE	1 *	530.8
81	STUDY OF NEUTRON-PROTON AND PROTON-PROTON COINCIDENCE SPECTRA FROM $p + d \rightarrow n + p + p$ REACTION	PHILLIPS	1 * 2 *	0.0 600.5
128	WNR STORAGE RING STRIPPER EXPERIMENT	HAYWARD	1 *	0.0
137	SEARCH FOR PARITY VIOLATING CONTRIBUTION TO SCATTERING OF HADRONS	NAGLE MISCHKE FRAUENFELDER	1 * 2 * 3 *	316.6 363.4 346.5
153	INVESTIGATION OF NUCLEAR GAMMA RAYS RESULTING FROM IN-FLIGHT PION AND PROTON REACTIONS	EISENSTEIN	1 *	0.0
159	CHARGED-PARTICLE EMISSION IN PROTON-INDUCED REACTIONS AS A FEASIBILITY STUDY IN THE USE OF INTRINISIC GERMANIUM DETECTORS WITH THE PRIMARY LAMPF BEAM	EISENSTEIN	1 *	0.0
176	p-NUCLEUS TOTAL AND TOTAL REACTION CROSS-SECTION MEASUREMENTS	ANDERSON	1 * 2 *	0.0 296.6

192	MEASUREMENT OF THE EMITTANCE GROWTH IN H^- STRIPPING	HAYWARD	1 *	70.0
194	p-p, D, R, AND A MEASUREMENTS	McNAUGHTON	1 *	185.2
			2 *	496.5
197	INVESTIGATION REACTION $p + d \rightarrow {}^3He + \pi^0$ AT LAMPF ENERGIES	HUNGERFORD	1 *	383.0
200	STUDY OF THE PHOTODETACHMENT SPECTRUM OF H^- IN THE VICINITY OF 11 eV	BRYANT	1 *	128.8
219	DOUBLE PION PRODUCTION IN PROTON-PROTON SCATTERING	BEVINGTON	1 *	422.0
223	STUDIES OF THE (p,np) CHARGE-EXCHANGE REACTION	HOFFMANN	F S*	66.3
241	DIRECT LEPTON PRODUCTION AT LAMPF ENERGIES	HOFFMAN MISCHKE	1 *	531.2
278	STUDY OF REACTION MECHANISMS USING INTERNAL CONVERSION TECHNIQUES	HOFFMANN MOORE	1 *	53.0
279	TEST OF CHARGE SYMMETRY IN nd AND pd SCATTERING	DIETERLE McFARLANE	F S* 1 *	67.0 0.0
289	MEASUREMENT OF THE PHASE OF THE FORWARD NUCLEON-NUCLEON SPIN-INDEPENDENT ELASTIC-SCATTERING AMPLITUDE AT 800 MeV	WHITTEN	1 *	354.6
323	STARK EFFECT QUENCHING OF RESONANCES IN THE PHOTODISINTEGRATION OF THE H^- ION	BRYANT GRAM	1 *	350.6
336	STUDY OF THE SPIN DEPENDENCE OF PROTON-PROTON PION PRODUCTION REACTIONS	MUTCHLER PINSKY	1 *	419.4
			2	0.0
			3	0.0
			4	0.0
339	SURVEY OF PHOTODETACHMENT CROSS SECTION OF H^- FROM THRESHOLD TO 15 eV AND ITS DEPENDENCE UPON ELECTRIC FIELD	BRYANT GRAM	1 *	1363.1
341	STUDY OF $pd \rightarrow d\pi^+n$ REACTION MECHANISMS	PHILLIPS	1 *	229.0
449	SURVEY OF SINGLE AND DOUBLE PHOTODETACHMENT CROSS SECTION OF THE H^- ION FROM 14 TO 21.8 eV	BRYANT DONAHUE	1 *	570.7
			2	113.6
468	MECHANISMS OF LUMINESCENCE INDUCED BY PROTONS INCIDENT OF ULTRAVIOLET GRADE OPTICAL MATERIALS	BECHER	1 *	70.8
492	POLARIMETER CALIBRATIONS AND SEARCH FOR ENERGY-DEPENDENT STRUCTURE IN pp ELASTIC SCATTERING VIA CROSS SECTION, ANALYZING POWER, AND WOLFENSTEIN PARAMETER MEASUREMENTS	McNAUGHTON WILLARD	1	0.0
498	MEASUREMENTS OF LONGITUDINAL CROSS-SECTION DIFFERENCE FOR LONGITUDINAL POLARIZED BEAM AND TARGETS (pp, pd, np)	WAGNER BURLESON	1 *	1664.5
			2	0.0
512	PROTON-PROTON ELASTIC-SCATTERING MEASUREMENTS OF THE $A_{ss}(\theta)$, $A_{LL}(\theta)$, AND $A_{sL}(\theta)$ SPIN-CORRELATION PARAMETERS AT 500, 650, and 800 MeV	GREENE IMAI	1	0.0
			2	0.0
			3	0.0
			4	0.0

517	POLARIZED BEAM AND TARGET EXPERIMENTS IN THE p-p SYSTEM: PHASE 1. A_y AND A_{yy} FOR THE $d\pi^+$ CHANNEL AND A_{yy} FOR THE ELASTIC CHANNEL FROM 500-800 MeV	SIMMONS JARMER NORTHCLIFFE	1	0.0
518	POLARIZED BEAM AND TARGET EXPERIMENTS IN THE p-p SYSTEM: PHASE 2. MEASUREMENTS OF A_{zz} AND A_{xz} FOR THE $d\pi^+$ CHANNEL AND FOR THE ELASTIC CHANNEL FROM 500-800 MeV	SIMMONS JARMER NORTHCLIFFE	1	0.0
530	H^- MAGNETIC STRIPPING RATES	JASON	1 *	237.2
586	A STUDY OF THE EFFECTS OF VERY STRONG ELECTRIC FIELDS ON THE STRUCTURE OF THE H^- ION	BRYANT GRAM	1	0.0
587	FUNDAMENTAL EXPERIMENTS WITH RELATIVISTIC HYDROGEN ATOMS — EXPLORATORY WORK	SMITH DONAHUE	1	0.0
588	A SEARCH FOR LONG-LIVED STATES OF THE H^- ION	CLARK BRYANT	1	0.0
589	FREE FORWARD np ELASTIC-SCATTERING ANALYZING POWER MEASUREMENTS AT 800 MeV	GLASS NORTHCLIFFE	1	0.0
590	MEASUREMENT OF D(θ) IN p-n AND n-p SCATTERING AT 800, 650 MeV, AND OTHER ENERGIES WITH ASSOCIATED p-p MEASUREMENTS	SIMMONS NORTHCLIFFE	1A 1B 2	0.0 0.0 0.0
591	AN INVESTIGATION OF INCLUSIVE ONE-PION PRODUCTION IN PROTON-NUCLEUS COLLISIONS	DEVRIES DIGIACOMO	1	0.0
592	AN INVESTIGATION OF TWO-PION PRODUCTION AND CORRELATIONS IN PROTON-NUCLEUS COLLISIONS AT 800 MeV	DEVRIES DIGIACOMO	1	0.0
633	MEASUREMENT OF p-p ELASTIC SCATTERING IN THE COULOMB INTERFERENCE REGION BETWEEN 300 AND 800 MeV	PAULETTA IROM	1	0.0
634	MEASUREMENT OF PARITY VIOLATION IN THE p-NUCLEUS TOTAL CROSS SECTIONS AT 800 MeV	CARLINI TALAGA YUAN	1	42.0
635	SPIN MEASUREMENTS IN pd ELASTIC SCATTERING	BONNER IGO BLESZYNSKI	1	507.7
636	A MEASUREMENT OF THE WOLFENSTEIN POLARIZATION PARAMETERS D_{LL}, D_{SL}, K_{LL}, AND K_{SL} FOR p-p ELASTIC SCATTERING	HOLLAS	1	0.0
637	A MEASUREMENT OF THE VECTOR POLARIZATION OF THE DEUTERON IN THE REACTION $pp \rightarrow d\pi^+$	BONNER	1	0.0

ENERGETIC PION CHANNEL SPECTROMETER (EPICS)

Exp. No.	Title	Spokesman	Phase No. *=Complete	Beam Hours
9	ELASTIC AND INELASTIC PION SCATTERING FROM CALCIUM ISOTOPES	MCCARTHY MORRIS	1 *	646.7

13	STUDY OF π^+-INDUCED DOUBLE-CHARGE-EXCHANGE REACTIONS	SETH	1 *	334.5
14	π^+ AND π^- ELASTIC AND INELASTIC SCATTERING FROM ^{16}O	THIESSEN	1 * 2 *	798.8 216.0
18	SURVEY OF π SCATTERING BY COMPLEX NUCLEI	ZEIDMAN	1 * 2 * 3 *	289.8 196.4 64.3
23	A SURVEY OF PION-NUCLEUS ELASTIC AND INELASTIC SCATTERING AT 180 MeV	WHARTON	1 *	300.5
39	SEARCH FOR (π,p) REACTIONS WITH EPICS	MACEK THIESSEN	1 *	295.5
74	STUDY OF PION-INDUCED DOUBLE-CHARGE-EXCHANGE REACTIONS ON LOW-Z ELEMENTS	PEREZ-MENDEZ STETZ	1 *	346.0
87	π^+ AND π^- SCATTERING FROM ^3He AND ^4He	McCARTHY	1 *	358.1
130	EPICS TUNEUP PROPOSAL: PION CARBON SCATTERING	THIESSEN	1 * 2 *	221.0 674.4
133	PRELIMINARY PION CHANNELING EXPERIMENTS	GEMMELL	1 *	200.9
156	SURVEY OF QUASI-ELASTIC PION SCATTERING	SWENSON	1 *	190.0
229	π^+ vs π^- INELASTIC EXCITATION OF LOW-LYING COLLECTIVE STATES IN ^{28}N NUCLEI	BRAITHWAITE MOORE	1 *	281.8
245	STUDY OF THE (π^-,π) AND (π,πp) REACTIONS IN $^{3,4}He$ AND HEAVIER NUCLEI BY DETECTING RECOILING TRITONS OR DEUTERONS	KALLNE THIESSEN	1 *	943.9
246	STUDIES OF π^+ SCATTERING AT 50 MeV FROM LIGHT NUCLEI	EISENSTEIN	1 *	564.0
265	STUDY OF PROMPT NUCLEAR DEEXCITATION GAMMA RAYS FROM PION INTERACTIONS WITH $^{6,7}Li$ AND ^{12}C	MORRIS BRAITHWAITE	1 *	319.0
310	(π^+,π^-) DOUBLE-CHARGE-EXCHANGE REACTIONS USING CORE 2n TARGETS	BRAITHWAITE MORRIS	1 *	265.2
317	INELASTIC PION SCATTERING TO THE 1^+ STATES OF ^{12}C	PETERSON	1 *	246.5
325	PION AND MUON MULTIPLE COULOMB-SCATTERING EXPERIMENT ON THE EPICS BEAM LINE	HANSON	1 *	69.7
342	STUDY OF THE (π^+,p) REACTION IN ^{12}C	McCARTHY KALLNE	1 *	151.2
368	ELASTIC PION SCATTERING TO THE 19.2 ± 0.3 MeV STATE IN ^{12}C	MOORE	1 *	246.5
369	INELASTIC PION SCATTERING BY ^{17}O, ^{18}O, AND ^{19}F	DEHNHARD	1	44.1
389	INELASTIC PION SCATTERING FROM LIGHT NUCLEI ^{10}B, ^{11}B, ^{14}N, AND ^{15}N	MORRISON ZEIDMAN	1 * 2 * 3 *	685.0 0.0 132.0
391	INELASTIC $\pi^\pm$ SCATTERING ON ^7Li	PETERSON	1 *	201.7

413	MASS MEASUREMENT OF ^{20}Ne AND ^{40}Ar BY THE (π^-,π^+) REACTION	SETH NANN	1 *	0.0
419	π^+ vs π^- INELASTIC EXCITATION OF SINGLE-PARTICLE AND CORE-COUPLED STATES IN ^{207}Pb AND ^{209}Bi	BRAITHWAITE MORRIS MOORE	1 *	25.3
442	STUDY OF THE INCLUSIVE PION DOUBLE-CHARGE-EXCHANGE REACTION	KALLNE	1 *	124.7
446	STUDY OF E0 GIANT RESONANCES	HALPERN EISENSTEIN THIESSEN	1	0.0
448	STUDY OF π^+ DOUBLE-CHARGE-EXCHANGE SCATTERING AT SMALL ANGLES ON VARIOUS NUCLEI	BURLESON	1 *	399.7
452	ELASTIC AND INELASTIC SCATTERING OF $\pi^\pm$ BY ^{13}C	DEHNHARD	1 *	219.5
456	THE (π,d) REACTION ON ^{12}C AT 60 MeV	HOISTAD	1	0.0
460	AN INVESTIGATION OF THE STABILITY OF ^{6}H, ^{7}H, AND ^{9}He BY (π^-,π^+) REACTIONS	SETH	1 *	444.7
463	COMPARATIVE STUDY OF THE (π^+,π^-) AND (π^-,π^+) REACTIONS ON ^{12}C	NANN SETH	1 *	444.7
478	$\pi^\pm$ ELASTIC SCATTERING FROM DEUTERIUM	MASTERSON	1 *	148.3
481	EXCITATION OF HIGH-SPIN STATES IN $T_z = 0$ s-d SHELL NUCLEI BY PION ELASTIC SCATTERING	GEESAMAN	1 *	134.7
484	INELASTIC PION SCATTERING FROM ^{148}Sm AND ^{152}Sm	MORRIS	1	0.0
495	ISOSPIN MIXING IN ^{12}C	MORRIS BRAITHWAITE	1 *	424.1
506	INELASTIC PION SCATTERING TO THE UNNATURAL PARITY LEVELS IN ^{12}C AND ^{6}Li	COTTINGAME BRAITHWAITE	1 *	0.0
510	ENERGY DEPENDENCE OF ELASTIC AND INELASTIC SCATTERING OF $\pi^\pm$ BY ^{13}C BETWEEN 116 AND 280 MeV	DEHNHARD	1 * 2	61.1 0.0
516	THE (π^+,p) REACTION OF ^{16,18}O	ANDERSON HOISTAD	1 *	36.0
522	EXCITATION OF GIANT RESONANCE STATES IN ^{90}Zr AND ^{208}Pb WITH 150-MeV PIONS	KING ANDERSON PETERSON	1 *	198.6
539	SEARCH FOR PURE NEUTRON/PROTON TRANSITIONS IN ^{14}C	BAER HOLTKAMP	1 *	345.7
546	INVESTIGATION OF THE SPIN FORM FACTOR OF TRITIUM AND ^{3}He	BRISCOE NEFKENS	F S* 1	60.9 0.0
549	A STUDY OF THE DCX REACTION MECHANISM — THE ^{42}Ca(π^+,π^-)^{42}Ti REACTION	SETH	1 *	349.3
550	EXCITED-STATE SPECTRA OF THE EXOTIC NUCLEI ^{15}C AND ^{20}Ne BY (π^-,π^+) DCX REACTIONS	SETH	1	0.0

558	MEASUREMENT OF (π^+,π^-) REACTIONS ON $^{13,14}C$ AND ^{26}Mg	BAER BURLESON	1	0.0
565	EXCITATION OF HIGH-SPIN PARTICLE-HOLE STATES IN ^{54}Fe AND ^{58}Ni	ZEIDMAN GEESAMAN	1	0.0
570	INVESTIGATION OF THE STRUCTURE OF ^{16}O WITH PION INELASTIC SCATTERING	HOLTKAMP FORTUNE	1 *	325.0
572	A-DEPENDENCE OF THE (π^+,π^-) REACTION AND THE WIDTH OF A DOUBLE ISOBARIC ANALOG STATE IN HEAVY NUCLEI	GREENE MOORE	1	0.0
573	PION SCATTERING FROM ^{24}Mg AND ^{26}Mg	BLANPIED	1	0.0
577	MEASUREMENT OF ANGULAR DISTRIBUTIONS FOR $^{16}O(\pi^+,\pi^-)^{16}Ne$	GREENE FORTUNE	1	0.0
581	$\pi^\pm$ ELASTIC SCATTERING FROM DEUTERIUM AT 237 MeV	MASTERSON BOUDRIE	1 *	193.0
597	THE STUDY OF BROAD-RANGE PION INELASTIC SCATTERING SPECTRA (WITH EMPHASIS ON THE EXCITATION OF THE GIANT MONOPOLE RESONANCE)	HALPERN EISENSTEIN	1	55.0
598	INELASTIC PION SCATTERING TO THE UNNATURAL PARITY LEVELS IN ^{6}Li	COTTINGAME	1	0.0
601	DETERMINATION OF ISOSCALAR AND ISOVECTOR TRANSITION RATES FOR LOW-LYING COLLECTIVE STATES IN ^{90}Zr AND ^{208}Pb BY π^+ AND π^- INELASTIC SCATTERING	HINTZ	1	0.0
602	NEUTRON-PROTON COMPONENTS OF INELASTIC TRANSITIONS IN PION SCATTERING ON ^{23}Na AND ^{25}Mg	HARVEY DEHNHARD	1	0.0
604	AN INVESTIGATION OF THE NEAR STABILITY OF ^{5}H	SETH	1 *	254.8
605	A DIBARYON SEARCH AT EPICS	SETH	1	0.0
606	TESTS OF THE (N − Z) DEPENDENCE OF PION DOUBLE CHARGE EXCHANGE	SETH	1	0.0
617	A STUDY OF THE (3/2,3/2) RESONANCE IN LIGHT NUCLEI	ZIOCK	1	0.0
619	INELASTIC PION SCATTERING TO 0^+ AND 2^+ STATES IN ^{40}Ca AND ^{42}Ca	MOORE FORTUNE MORRIS	1	0.0
622	INVESTIGATION OF THE STRONG CANCELLATIONS OF NEUTRON-PROTON TRANSITION AMPLITUDES IN ^{14}C	HOLTKAMP BAER	1	0.0
625	INELASTIC SCATTERING OF PIONS TO GIANT RESONANCES	KING ANDERSON PETERSON	1	0.0
651	MEASUREMENT OF A LOWER LIMIT FOR THE SUBTHRESHOLD PRODUCTION OF KAONS WITH 800-MeV PROTONS	MORRIS	1	0.0
655	$\pi^\pm$ INELASTIC SCATTERING FROM ^{4}He — AN EXAMINATION OF ISOSPIN SYMMETRY BREAKING	HOLTKAMP COTTINGAME	1	0.0

656	PION DOUBLE CHARGE EXCHANGE ON SELF-CONJUGATE NUCLEI	GREENE MORRIS FORTUNE	1	0.0
657	INELASTIC $\pi^{\pm}$ SCATTERING FROM THE N = 26 ISOTONES	SEIDL MOORE	1	0.0
659	SPIN-FLIP GIANT RESONANCE EXCITATION	BLAND MOORE	1	0.0
661	GOOD-RESOLUTION STUDY OF $^{16}O(\pi,\pi')$	MORRIS BLAND	1	0.0
662	ELASTIC AND INELASTIC π^- AND π^+ SCATTERING FROM ^{32}S, ^{31}P AND ^{90}Zr, ^{89}Y	KRAUSHAAR PETERSON	1	0.0
671	TEST OF THE MICROSCOPIC IBA MODEL VIA PION-NUCLEUS SCATTERING ON THE PALLADIUM ISOTOPES	SAHA SETH	1	0.0
672	STUDY OF GIANT RESONANCES IN ^{90}Zr, ^{116}Sn, AND ^{208}Pb WITH π^+ AND π^- INELASTIC SCATTERING	CAREY MOSS	1	0.0
677	A DETERMINATION OF $\Delta S = 1$ CONTRIBUTIONS IN INELASTIC PION SCATTERING FROM ODD-A NUCLEI	HOLTKAMP FUNSTEN	1	0.0
678	STUDY OF THE M1 TRANSITION IN ^{40}Ca BY INELASTIC SCATTERING OF π^+ AND π^-	DEHNHARD MORRIS	1	0.0
680	ANGULAR DISTRIBUTIONS FOR $^{24,26}Mg(\pi^+,\pi^-)^{24,26}Si$	GREENE	1	0.0
681	MEASUREMENTS OF LARGE-ANGLE PION-NUCLEUS SCATTERING WITH EPICS	BURLESON	1	0.0
694	ISOSPIN MIXING IN ^4He	SETH	1	0.0
696	THE ANGULAR DISTRIBUTION IN PION DOUBLE CHARGE EXCHANGE	SETH	1	0.0

HIGH-RESOLUTION SPECTROMETER (HRS)

Exp. No.	Title	Spokesman	Phase No. *=Complete	Beam Hours
4	LARGE-ANGLE ELASTIC SCATTERING OF PROTONS FROM HELIUM AND QUASI-ELASTIC KNOCKOUT OF ALPHA PARTICLES BY 800-MeV PROTONS	IGO	1 *	458.0
5	INELASTIC SCATTERING OF 800-MeV PROTONS FROM NUCLEI TO STUDY QUASI-FREE MODES	CHRIEN PALEVSKY	1 *	532.7
10	SEARCH FOR (p,π) REACTIONS WITH HRS	SPENCER	1 *	167.9
15	ELASTIC SCATTERING AND TOTAL CROSS-SECTION MEASUREMENTS OF PROTON ON HYDROGEN, DEUTERIUM, AND HELIUM	IGO TANAKA	1 * 2 * 3 *	0.0 75.0 249.0
49	ELASTIC AND INELASTIC PROTON SCATTERING FROM THE NICKEL ISOTOPES AND FROM ^{89}Y	PETERSON	1 *	68.3

117	HIGH-RESOLUTION STUDY OF THE NEUTRON PICK-UP REACTION	IGO	1 *	273.2
138	INELASTIC PROTON SCATTERING AND EXCITATION OF STATES OF INTERMEDIATE COLLECTIVITY IN OPEN-SHELL NUCLEI	McDANIELS SWENSON	1 *	184.2
139	PRELIMINARY PROTON SCATTERING SURVEY WITH HRS	SPENCER TANAKA	1 *	695.1
178	PROTON SCATTERING SURVEY ON s-d SHELL NUCLEI	SPENCER HINTZ	1 *	209.3
183	PROTON SCATTERING SURVEY ON HEAVY DEFORMED NUCLEI	HINTZ SPENCER	1 *	382.1
202	(p,t) REACTION ON SPHERICAL NUCLEI	IGO	1 *	0.0
204	EXCITATION AND ASYMMETRY MEASUREMENT OF $T \simeq 1$, HIGH-SPIN, NONNORMAL PARITY PARTICLE-HOLE STATE BY (p,p') SCATTERING IN THE INTERMEDIATE-ENERGY RANGE	IGO	1 *	127.0
223	STUDIES OF THE (p,np) CHARGE-EXCHANGE REACTION	HOFFMANN	F S*	0.0
233	SEARCH FOR DELTA-CONFIGURATIONS NUCLEI	SETH SPENCER	1 *	167.9
249	THE (p,π^+) REACTION ON ^{4}He WITH 800-MeV PROTONS	WHITTEN	1	199.7
256	p-NUCLEUS ELASTIC SCATTERING AT $q^2 = 8$ GeV^2 IN Be, C, AND THE STUDY OF p-NUCLEUS INTERACTIONS IN Co AND Au UP TO $m^* = q^2/\nu \gtrsim 20$	FRANKEL	1 *	107.6
258	STUDY OF MECHANISMS FOR THE EJECTION OF HIGH-MOMENTUM PARTICLES FROM NUCLEI BY STUDY OF THE COINCIDENCE SPECTRUM IN $p + a \rightarrow (p,d,t) + (p,d,t) + X$	FRANKEL FRATI	1 * 2	178.7 0.0
261	INTERMEDIATE-ENERGY (p,d) REACTION MECHANISM STUDIES	RICKEY SHEPARD PETERSON	1 *	0.0
311	ELASTIC-SCATTERING SURVEY USING POLARIZED PROTONS	HOFFMANN	1 * 2 *	715.3 245.6
346	STUDY OF HIGH-MOMENTUM COMPONENTS IN NUCLEI USING A POLARIZED PROTON BEAM	FRANKEL	1 *	209.8
347	SEARCH FOR ORBIT-FLIP STATES BY INELASTIC PROTON SCATTERING	HINTZ	1 *	209.3
352	DETERMINATION OF NEUTRON-MASS DISTRIBUTION FROM ELASTIC PROTON MEASUREMENTS [P(t) AND $d\sigma/dt$] ON ISOTOPES IN THE CALCIUM REGION	WHITTEN	1 *	204.6
354	SCATTERING OF 800-MeV PROTONS FROM ^{12}C AND ^{13}C AT MOMENTUM TRANSFER >4 F^{-1}	BLANPIED	1 *	324.1
355	FURTHER ELASTIC SCATTERING CROSS SECTION AND ANALYZING POWER MEASUREMENTS ON ^{208}Pb AND ^{116,124}Sn	HOFFMANN	1 * 2 *	130.0 55.0

366	ANALYZING POWER AND CROSS-SECTION MEASUREMENTS FOR INELASTIC PROTON EXCITATION OF SIMPLE STATES	GLASHAUSSER BAKER SCOTT	1 * 2	199.9 0.0
385	MEASUREMENT OF THE POLARIZED PROTONS + NEUTRONS ANALYZING POWER, $A_y(\theta)$ FROM $\theta_{c.m.}$ 10-70°	HOFFMANN	1 * 2 *	140.6 108.8
386	TOTAL REACTION CROSS SECTIONS FOR p^+ NUCLEI AT 800 MeV	HOFFMANN BURLESON YOKOSAWA	1 * 2	256.1 0.0
392	A MEASUREMENT OF THE TRIPLE-SCATTERING PARAMETERS D, R, A, R', AND A' FOR PROTON-PROTON AND PROTON-NEUTRON SCATTERING AT 800 MeV	HOFFMANN	1 2	208.6 0.0
395	THE (p,π^+) REACTION ON ^{16}O AND ^{48}Ca	BAUER HOISTAD NANN	1 *	195.8
399	EXCITATION OF GIANT MULTIPOLE RESONANCES BY 200-400-MeV PROTONS	BERTRAND	1	0.0
405	THE (p,π^-) REACTION ON ^{12}C AND ^{13}C	HOISTAD BAUER SETH	1	162.7
411	MEASUREMENT OF SPIN-FLIP PROBABILITIES IN PROTON INELASTIC SCATTERING AT 800 MeV AND SEARCH FOR COLLECTIVE SPIN-FLIP MODES, PRELIMINARY SURVEY	HINTZ MOSS	1	200.0
425	PROTON ELASTIC SCATTERING AT ~600 MeV BY $^{40,48}Ca$, ^{90}Zr, AND ^{208}Pb	SETH HOFFMANN	1 *	283.2
431	CROSS SECTION AND ANALYZING POWER FOR INELASTIC PROTON EXCITATION OF UNNATURAL PARITY STATES IN ^{6}Li, ^{12}C, ^{14}N, AND ^{16}O	GLASHAUSSER MOSS	1 *	181.0
432	CROSS SECTION FOR EXCITATION OF UNNATURAL PARITY STATES IN ^{12}C AT E_p < 800 MeV	GLASHAUSSER MOSS	1	148.9
433	ELASTIC SCATTERING DIFFERENTIAL CROSS SECTIONS AND ANALYZING POWERS FOR POLARIZED p + $^{40,48}Ca$, ^{90}Zr, AND ^{208}Pb AT ~400 MeV	HOFFMANN SETH	1 *	0.0
438	THE (p,d) REACTIONS ON $^{12,13}C$, ^{7}Li, ^{16}O, ^{25}Mg, ^{28}Si, AND ^{40}Cu BETWEEN 650 AND 800 MeV	IGO	1	162.5
451	INELASTIC PROTON SCATTERING IN THE RANGE 300 TO 500 MeV	HINTZ	1 2	221.3 0.0
462	ANALYZING POWER AND DIFFERENTIAL CROSS SECTIONS FOR THE REACTIONS p + p → d + π^+ AND p + d → t + π^+ AT ~600 AND 400 MeV	SETH NANN	1 *	118.0
470	REACTIVE CONTENT OF THE OPTICAL POTENTIAL	BARLETT HOFFMANN	1 *	247.5
472	STUDY OF THE (p,d) REACTION ON ^{90}Zr, ^{140}Ce, AND ^{208}Pb AT 800 MeV	WHITTEN	1 *	79.5

473	STUDY OF GIANT MULTIPOLE RESONANCES WITH 800-MeV PROTONS	MOSS ADAMS CAREY	1 * 2 *	110.8 197.7
474	A MEASUREMENT OF SPIN-DEPENDENT EFFECTS IN p + d ELASTIC AND INELASTIC SCATTERING	CORNELIUS	1	0.0
475	SCATTERING OF 0.8-GeV PROTONS FROM ^{20}Ne AND ^{22}Ne	BLANPIED	1 * 2	154.9 0.0
476	THE ANALYZING POWER FOR POLARIZED PROTONS + ^{24,26}Mg AT 500 AND 800 MeV	BLANPIED	1	82.9
479	MEASUREMENT OF R, A, R', AND A' IN ELASTIC AND INELASTIC SCATTERING OF 800-MeV PROTONS FROM LIGHT NUCLEI — REVISED VERSION OF Q PROPOSAL	IGO	1 *	178.3
485	THE ENERGY DEPENDENCE IN THE (p,$\pi^{\pm}$) REACTION	HOISTAD	1	0.0
486	INELASTIC SCATTERING OF PROTONS POPULATING THE 4^- (3.44-MeV) LEVEL OF ^{208}Pb — A SEARCH FOR CRITICAL OPALESCENCE	IGO GLASHAUSSER MOSS	1 *	65.6
489	SEARCH FOR M1 GIANT RESONANCES IN THE (p,p') REACTION AT E_p = 800 MeV	MOSS	1 *	63.9
508	DIBARYON RESONANCES IN PION PRODUCTION	SETH	1 * 2	178.0 0.0
519	STUDY OF THE REACTION p(pol) + d → (p,π) + X TO MEASURE THE ANALYZING POWER AND STRUCTURE FUNCTION FOR BACKWARD PARTICLES	FRANKEL	1 *	130.3
520	STUDY OF THE REACTION p(POLARIZED) + ^{3,4}He → (p,d,π..) + X TO MEASURE THE ANALYZING POWER STRUCTURE FUNCTIONS FOR BACKWARDS PARTICLES	FRANKEL	1	0.0
531	EXCITATION OF UNNATURAL PARITY STATES IN ^{12}C AT 500 MeV	GLASHAUSSER MOSS	1	101.3
532	MEASUREMENTS OF CROSS SECTIONS AND ANALYZING POWER IN THE (p,2p) REACTION ON DEUTERIUM	FRANKEL	1	0.0
533	THE ASYMMETRY IN THE (p,π) REACTION ON ^{6}Li AT 800 MeV	HOISTAD SETH	1	0.0
535	A STUDY OF THE RELATION BETWEEN THE (p,d) AND (π,p) REACTION IN A PION EXCHANGE MODEL	ANDERSON HOISTAD	1	0.0
538	ANALYZING POWER AND CROSS-SECTION MEASUREMENTS OF THE ^{4}He(p,d)^{3}He REACTION	SHEPARD KING	1 2	0.0 0.0
540	ELASTIC SCATTERING FROM LIGHT NUCLEI	IGO BLESZYNSKI	1	0.0
556	A PROPOSAL TO STUDY THE (p,p') PROCESS LEADING TO π ATOMIC STATES	BERTOZZI	1	52.6
563	p + p ELASTIC SCATTERING AT 800 AND 500 MeV	HOFFMANN	1	0.0
580	CROSS SECTIONS AND ANALYZING POWERS FOR ELASTIC AND INELASTIC SCATTERING OF 515-MeV PROTONS FROM ^{12}C	SEESTROM-MORRIS DEHNHARD	1	43.6

583	MEASUREMENT OF C_{LL} IN THE COULOMB INTERFERENCE REGION	PAULETTA GAZZALY	1	0.0
585	MEASUREMENT OF p-p AND p-d ELASTIC SCATTERING IN THE COULOMB INTERFERENCE REGION BETWEEN 500 AND 800 MeV	PAULETTA	1	0.0
616	NUCLEAR INFORMATION FROM THE SPIN ROTATION AND DEPOLARIZATION PARAMETERS IN THE $^{12}C(p,p')$ REACTION TO THE 1^+, 12.72-MeV T = 0 AND TO THE 1^+, 15.11-MeV T = 1 LEVELS	BLESZYNSKI McCLELLAND HINTZ MOSS	1	0.0
623	MEASUREMENT OF CROSS SECTION, ANALYZING POWER, AND DEPOLARIZATION PARAMETERS IN THE $^{28}Si(p,p')^{28}Si$ (6^-, T = 0 AND T = 1) REACTION AT 400 MeV	GLASHAUSSER	1	0.0
627	MEASUREMENT OF THE RELATIVE SIGN OF NEUTRON AND PROTON TRANSITION MATRIX ELEMENTS IN (p,p') REACTIONS	HYNES BERNSTEIN	1	0.0
630	A STUDY OF PROTON INELASTIC SCATTERING AT 0° AND A SEARCH FOR GIANT MONOPOLE AND GIANT MAGNETIC DIPOLE EXCITATIONS	CAREY HINTZ McCLELLAND MOSS	1 * 2	0.0 0.0
642	REACTIVE CONTENT OF THE OPTICAL POTENTIAL — PHASE 2	McGILL HOFFMANN	1	0.0
643	STRUCTURE OF STATES IN THE OXYGEN ISOTOPES VIA MEASUREMENTS OF THE SPIN DEPOLARIZATION AND SPIN-ROTATION OBSERVABLES	AAS HYNES	1 2	0.0 0.0
649	$^9Be(p,\pi^\pm)$ REACTION AT 650 MeV	HOISTAD	1 * 2	85.9 0.0
654	MEASUREMENT OF THE SPIN-ROTATION PARAMETER Q FOR 800-MeV p + ^{16}O, ^{40}Ca, AND ^{208}Pb ELASTIC SCATTERING	HOFFMANN	1	0.0
658	STUDY OF THE SPIN-FLIP PROBABILITY FOR ELASTIC AND INELASTIC SCATTERING FROM ODD-MASS NUCLEI	SEESTROM-MORRIS CAREY MOSS DEHNHARD	1	0.0
660	MEASUREMENT OF POLARIZATION PARAMETERS FOR M1 TRANSITIONS IN THE $^{90}Zr(p,p')^{90}Zr^*$ AND $^{116}Sn(p,p')^{116}Sn^*$ REACTIONS AT 500 MeV	GLASHAUSSER	1	0.0
663	ELASTIC SCATTERING OF POLARIZED PROTONS FROM ^3H AND ^3He AT INTERMEDIATE ENERGIES	IGO BLESZYNSKI	1	0.0
666	THE $^{12}C(p,p'\pi)^{12}C$ REACTION AND THE SEARCH FOR COHERENT ISOBAR-HOLE RESONANCES	GLASHAUSSER WHITTEN	1	0.0
669	INVESTIGATION OF THE N = 28 NEUTRON SHELL CLOSURE BY ELASTIC SCATTERING OF 800-MeV POLARIZED PROTONS	SHERA WOHLFAHRT	1	0.0
670	CONTINUATION OF GIANT RESONANCE STUDIES AT THE HRS	MOSS CAREY ADAMS	1	0.0

684	POLARIZATION EFFECTS IN THE DEUTERON PRODUCTION BY PHOTON-NUCLEUS COLLISIONS	KALLNE HOISTAD	1	0.0
685	SPIN CORRELATIONS IN THE REACTION $\vec{p}(\vec{d},d)\vec{p}$ AT 500 MeV	BLESZYNSKI IGO	1	0.0
686	DETERMINATION OF NEUTRON TRANSITION DENSITIES IN ^{16}O AND ^{208}Pb BY INELASTIC SCATTERING OF ~400-MeV PROTONS	HINTZ	1	0.0
687	MEASUREMENT OF THE SPIN-ROTATION PARAMETERS IN ^{208}Pb AND IN ^{40}Ca AT 400 MeV	AAS	1	0.0

ISOTOPE PRODUCTION AND RADIATION-EFFECTS FACILITY (ISORAD)

Exp. No.	Title	Spokesman	Phase No. *=Complete	Beam Hours
184	PRODUCTION OF ^{82}Sr	O'BRIEN	1 *	0.0
210	ISOTOPE PRODUCTION FACILITY IRRADIATION VANADIUM, MOLYBDENUM, AND LANTHANUM TARGETS	O'BRIEN	1 *	0.0
211	NEUTRON IRRADIATION OF COPPER SINGLE CRYSTALS	GREEN	1 *	0.0
267	PREPARATION OF RADIOISOTOPES FOR MEDICINE AND THE PHYSICAL SERVICES USING THE LAMPF ISOTOPE PRODUCTION FACILITY	O'BRIEN	1	13615.7
554	IRRADIATION OF TECHNOLOGICALLY IMPORTANT METALS WITH 800-MeV PROTONS USING THE ISOTOPE PRODUCTION FACILITY AT LAMPF	BROWN COST	1	0.0

LOW-ENERGY PION (LEP)

Exp. No.	Title	Spokesman	Phase No. *=Complete	Beam Hours
2	TOTAL PION CROSS SECTIONS	JAKOBSON	1 *	0.0
			2 *	663.4
25	PION DOUBLE-CHARGE-EXCHANGE REACTION	BURMAN	1 *	0.0
			2 *	681.2
			3 *	268.2
28	STUDIES OF THE π^+,π^0 REACTION	YAVIN	1 *	195.0
29	ELASTIC SCATTERING OF π^+ AND π^- AT 10-30 MeV	PREEDOM	1 *	0.0
			2 *	0.0
35	CLUSTER EFFECTS IN NUCLEAR PION CAPTURE	ZIOCK	1 *	297.5
50	RADIATIVE PION CAPTURE IN LIGHT NUCLEI	CROWE	1 *	0.0
		ROWE	2 *	460.3
54	ELASTIC SCATTERING OF MESONS IN THE ENERGY RANGE 20-60 MeV	PREEDOM	1 *	264.6
			2 *	707.4

67	DEVELOPMENT OF PION BEAM-MONITORING TECHNIQUES	DROPESKY	1 * 2 *	0.0 87.5
79	CALIBRATION OF THE PION BEAM TRANSPORT SYSTEMS AND A PION BEAM MONITOR	PHILLIPS	1 *	0.0
96	SCATTERING OF 20-50-MeV $\pi^{\pm}$ BY HYDROGEN AND DEUTERIUM	NAGLE	1 * 2 *	0.0 728.0
102	EXCITATION FUNCTIONS AND ANGULAR DISTRIBUTION RECOIL STUDIES OF SIMPLE PION-INDUCED NUCLEAR REACTIONS	MARKOWITZ	1 *	0.0
121	PION-INDUCED NUCLEAR REACTIONS	SEGEL	1 * 2 *	0.0 150.0
122	PIONIC ATOM X RAYS AND NUCLEAR DISTRIBUTIONS	KUNSELMAN	1 *	0.0
123	NUCLEAR STRUCTURE EFFECTS IN PION-INDUCED NUCLEAR REACTIONS	KAROL	5	25.0
131	A STUDY OF THE $\pi^+ + d \rightarrow p + p$ REACTION AT PION ENERGIES 10-60 MeV	PREEDOM	1 * 2 *	0.0 260.0
140	STUDY OF THE ($\pi^{\pm}$,d) REACTION WITH AN INTRINSIC GERMANIUM DETECTOR	BARNES	1 * 2 * 3 *	0.0 385.0 0.0
144	SEARCH FOR THE C-VIOLATING DECAY $\pi^0 + 3\gamma$	HIGHLAND MACEK	1 *	333.0
162	STUDIES OF THE (π^+,π^0) REACTION ON LIGHT ELEMENTS	YAVIN ALSTER	1 *	0.0
164	PION TOTAL CROSS-SECTION MEASUREMENTS WITH AN ORIENTED ^{166}Ho TARGET	FISHER MARSHAK	1 *	88.0
170	STUDY OF REACTION $^{13}C(\pi^+,\pi^0)^{13}N$ (GROUND STATE)	ALSTER	1 *	0.0
180	ELASTIC AND INELASTIC π^+-NUCLEUS SCATTERING AT 25, 50, AND 75 MeV	EISENSTEIN	1 * 2 *	0.0 191.3
181	MEASUREMENTS OF THE $\pi^-p \rightarrow \pi^0n$ ANGULAR DISTRIBUTION AT LOW ENERGIES AND CALIBRATION OF THE π^0 SPECTROMETER	ALSTER BOWMAN	1 * 2 *	346.0 859.2
190	A PRECISION MEASUREMENT OF THE $\pi^- - \pi^0$ MASS DIFFERENCE	ZIOCK	1 2	0.0 0.0
191	π^+ NUCLEUS INELASTIC SCATTERING TO GIANT RESONANCES	HALPERN	1 * 2 * 3 * 4 *	0.0 292.7 484.4 284.4
209	PION INTERACTIONS IN NUCLEAR EMULSIONS	BRADBURY ALLRED	1 *	0.0
234	A STUDY OF THE INELASTIC PION SCATTERING REACTION AT PION ENERGIES 10-100 MeV	GOTOW	1 *	436.3
247	DISTRIBUTION OF PRODUCTS FROM INTERACTIONS OF STOPPED π^- WITH SEVERAL MEDIUM- AND HEAVY-MASS NUCLEI	ORTH	1 * 2 *	35.6 59.5

284	MEASUREMENT OF THE $^{3}He(\pi^{-},\pi^{0})^{3}He$ ANGULAR DISTRIBUTION	COOPER WHITNEY	1	209.0
293	STUDY OF THE DOMINANT REACTION MODES FOR PIONS INTERFACING WITH COMPLEX NUCLEI	SEGEL	1 *	151.0
295	STUDY OF THE PION-DEUTERON SINGLE-CHARGE-EXCHANGE REACTION $d(\pi^{-},\pi^{0})2n$	BOWMAN MOINESTER	1	0.0
299	AN INVESTIGATION OF THE REACTION $(\pi^{+},\pi^{+} + p)$	ZIOCK	1 * 2 * 3 *	0.0 960.1 0.0
303	A SURVEY OF PION SINGLE-CHARGE-EXCHANGE SCATTERING USING BACK-ANGLE GAMMA SPECTROSCOPY	JACKSON	1 * 2 * 3	152.8 290.9 0.0
315	HIGH-RESOLUTION STUDY OF THE $(\pi^{+},2p)$ REACTION	WHARTON	1 * 2 * 3	0.0 338.1 233.4
316	π^{-}-NUCLEUS ELASTIC SCATTERING BETWEEN 20 AND 50 MeV	SETH BURLESON	1 * 2 *	699.6 0.0
320	A COMPARISON OF $(\pi^{+},x\pi)$ AND $(\pi^{-},x\pi)$ REACTIONS	CHURCH	3 * 4	33.0 0.0
322	SYSTEMATIC STUDY OF PION-INELASTIC SCATTERING AT ENERGIES BELOW 100 MeV	BERTRAND GOTOW	1 *	877.1
324	PRECISION MEASUREMENT OF RATIOS OF CERTAIN LIGHT ELEMENT PION EXCITATION FUNCTIONS	HALPERN	1 *	118.6
333	$\pi^{\pm}$-NUCLEAR ELASTIC SCATTERING AT ENERGIES BETWEEN 50 AND 100 MeV	GOTOW	1 *	512.2
348	STUDY OF GIANT RESONANCES WITH RADIATIVE PION CAPTURE ON MEDIUM-Z NUCLEI AT LEP	CROWE	1 *	761.7
349	NUCLEAR REACTIONS OF ^{127}I WITH PIONS	PORILE	2 * 3	25.0 28.0
350	STUDY OF PION-ABSORPTION MECHANISMS IN NUCLEI	SEGEL SCHIFFER	1 *	225.8
388	LOW-ENERGY PION ELASTIC SCATTERING FROM THE PROTON AND DEUTERON AT 180°	HOLT	1 *	392.2
393	ANGULAR DISTRIBUTION MEASUREMENTS OF THE PION SINGLE-CHARGE-EXCHANGE REACTION ON ^{13}C	ALSTER MOINESTER	1	279.8
401	STUDY OF THE ISOBARIC ANALOG CHARGE-EXCHANGE REACTION $^{15}N(\pi^{+},\pi^{0})^{15}O$	BOWMAN COOPER	1 * 2	357.1 0.0
412	SEARCH FOR ANALOG STATE TRANSITIONS IN (π^{+},π^{0}) REACTIONS ON ^{7}Li, ^{27}Al, ^{93}Zr, ^{120}Sn, AND ^{208}Pb AND FOR COLLECTIVE ISOVECTOR STATES IN THE (π^{-},π^{0}) REACTION ON ^{93}Zr	BAER BOWMAN CVERNA	1 * 2	270.6 0.0
415	TWO-NUCLEON-OUT PRODUCTS FROM STOPPED π^{-} INTERACTIONS	ORTH	1 *	121.6
416	STUDY OF FAST PION-INDUCED FISSION OF URANIUM	DROPESKY	3 *	15.0

465	RADIOCHEMICAL STUDY OF PION SINGLE CHARGE EXCHANGE	RUNDBERG	1 * 2	13.0 29.4
483	MEASUREMENT OF THE ANGULAR DEPENDENCE OF TENSOR POLARIZATION IN THE $^{3}H(\pi^{+},\pi^{+})^{3}H$ REACTION	HOLT	1 *	478.3
487	MEASUREMENT OF THE NUCLEAR RESONANCE EFFECT IN SOME PIONIC ATOMS	REIDY LEON	1 *	202.8
523	STUDY OF $^{14}C(\pi^{+},\pi^{0})^{14}N$ REACTION	GOODMAN BAER	1	103.4
524	STUDY OF THE ISOVECTOR TERMS IN π-NUCLEUS INTERACTIONS WITH (π^{+},π^{0}) REACTIONS ON $^{40,42,44,48}Ca$ AND $^{112,118,124}Sn$	BAER BOWMAN CVERNA	1	243.9
525	EXCITATION OF ISOVECTOR TRANSITIONS WITH PION SINGLE CHARGE EXCHANGE ON ^{12}C	KING MOINESTER	1	9.2
527	STUDY OF THE $^{10}B(\pi^{-},\pi^{0})^{10}B$ REACTION	BAER BOWMAN	1	0.0
536	*EFFICIENCY MEASUREMENTS FOR π^{+} IDENTIFICATION* IN THE PLASTIC BALL DETECTOR	GUTBROD	1 *	106.7
541	A SEARCH FOR NUCLEAR CRITICAL OPALESCENCE USING THE REACTION $^{40}Ca(\pi^{+},2\gamma)$	COOPER	1	0.0
543	A PRODUCT RECOIL STUDY OF THE $(\pi^{\pm},\pi^{\pm}n)$ REACTION	CARETTO	1 *	7.8
544	SEARCH FOR A FAST FISSION PROCESS	WILHELMY	1 * 2	48.0 0.0
553	STUDY OF TARGET THICKNESS EFFECTS IN THE CROSS-SECTION MEASUREMENT OF THE PION SINGLE-CHARGE-EXCHANGE REACTION $^{13}C(\pi^{+},\pi^{0})^{13}N$ (g.s.) FROM 50 TO 350 MeV	RUNDBERG	2	69.0
561	$\pi^{\pm}$-NUCLEAR ELASTIC SCATTERING AT ENERGIES BETWEEN 30 AND 80 MeV	BLECHER OBENSHAIN HYNES	1	0.0
567	A STUDY OF THE $\pi^{+} + d \rightarrow p + p$ REACTION AT PION ENERGIES 5-200 MeV	GOTOW MINEHART RITCHIE	1	0.0
576	STUDY OF THE $(\pi^{+},2p)$ AND $(\pi^{\pm},2p)$ REACTIONS ON THE ISOTOPIC PAIRS ^{16}O-^{18}O AND ^{40}Ca-^{48}Ca	ROOS PREEDOM CHANT	1	0.0
607	STUDY OF ISOVECTOR GIANT RESONANCES WITH PION CHARGE EXCHANGE	ALSTER BAER BOWMAN	1 * 2	259.5 0.0
611	EXCITATION FUNCTIONS OF THE FOUR $^{130}Te(\pi^{\pm},\pi^{\pm}n)$ REACTIONS	HOGAN	1	0.0
650	A SEARCH FOR NEUTRINO MIXING VIA NONEXPONENTIAL $\pi \rightarrow \mu\nu$ DECAY	BOWMAN MOINESTER	1	249.0
675	NUCLEAR DISTRIBUTIONS FROM THE STUDY OF THE 2p STATES OF PIONIC ATOMS	KUNSELMAN	1	0.0

676	STUDY OF PION ABSORPTION ON ^{58}NI AT T_π = 160 MeV	CHANT REDWINE ROOS	1	0.0
688	STUDY OF THE MASS AND ENERGY DEPENDENCE OF LOW-ENERGY PION SINGLE CHARGE EXCHANGE	LEITCH COOPER	1	0.0

LINE B (Line-B)

Exp. No.	Title	Spokesman	Phase No. *=Complete	Beam Hours
179	DIFFERENTIAL PRODUCTION CROSS SECTIONS OF MULTIPLY CHARGED FRAGMENTS IN PROTON AND PION-INDUCED SPALLATION OF LIGHT NUCLEI	BOWMAN	1 *	1341.4

LINE X BEAM STOP (Line-X-BS)

Exp. No.	Title	Spokesman	Phase No. *=Complete	Beam Hours
184	PRODUCTION OF ^{82}Sr	O'BRIEN	1 *	0.0

NEUTRINO AREA (Neutrino A)

Exp. No.	Title	Spokesman	Phase No. *=Complete	Beam Hours
31	A NEUTRINO EXPERIMENT TO TEST MUON CONSERVATION	NEMETHY	1 * 2 *	6713.2 1097.4
148	NEUTRINO ELECTRON ELASTIC SCATTERING AT LAMPF (A FEASIBILITY STUDY)	CHEN REINES	1 * 2 *	0.0 1132.0
225	A STUDY OF NEUTRINO ELECTRON ELASTIC SCATTERING	CHEN	1	0.0
254	FEASIBILITY STUDY FOR THE MEASUREMENT OF THE INELASTIC NEUTRINO SCATTERING CROSS SECTIONS IN ^{39}K	FIREMAN	1 *	1026.0
559	SEARCH FOR NEUTRINO OSCILLATIONS AND VIOLATION OF LEPTON-NUMBER CONSERVATION	DUONG-VAN PHILLIPS	1	0.0
609	ANTINEUTRINO OSCILLATION EXPERIMENTS AT LAMPF	KRUSE	1	0.0
638	A SEARCH FOR OSCILLATIONS USING MUON-NEUTRINOS	DOMBECK	1	0.0
645	A SEARCH FOR NEUTRINO OSCILLATIONS AT LAMPF	LING ROMANOWSKI	1 2	0.0 0.0
647	A NEUTRON OSCILLATION EXPERIMENT AT LAMPF	ELLIS	1	0.0

PROTON IRRADIATION PORT (PIP)

Exp. No.	Title	Spokesman	Phase No. *=Complete	Beam Hours
302	800-MeV PROTON IRRADIATION OF AN ALUMINUM SAMPLE	GREEN	1 *	326.6
327	PIP, PROTON IRRADIATION PORT	WILSON	1 *	16.9

PION PARTICLE PHYSICS (P^3)

Exp. No.	Title	Spokesman	Phase No. *=Complete	Beam Hours
32	PRECISION MEASUREMENT OF THE PROCESSES $\pi^{\pm} \rightarrow \pi^0 + E^{\pm} + \nu$	McFARLANE MACEK	1 * 2 *	0.0 1092.2
34	ELASTIC SCATTERING OF $\pi^{\pm}$ ON DEUTERONS	MINEHART	1 *	0.0
58	MEASUREMENT OF $\pi^- + p \rightarrow \gamma + n$	NEFKENS FITZGERALD	1 *	0.0
67	DEVELOPMENT OF PION BEAM MONITORING TECHNIQUES	DROPESKY	1 * 2 *	0.0 220.2
79	CALIBRATION OF THE PION BEAM TRANSPORT SYSTEMS AND A PION BEAM MONITOR	PHILLIPS	1 *	0.0
80	FORWARD ELASTIC SCATTERING OF π^+ AND π^- FROM ^{12}C, ^{13}C, ^{16}O, ^{40}Ca, ^{208}Pb	PHILLIPS	1 * 2 *	0.0 528.8
82	INVESTIGATION OF PION-INDUCED REACTIONS ON LIGHT ELEMENTS WITH THREE PARTICLES IN THE FINAL STATE	PHILLIPS	1 *	425.3
90	A TEST OF THE REVERSAL INVARIANCE IN SINGLE-PION PHOTOPRODUCTION THROUGH A STUDY OF RECIPROCITY IN THE REACTIONS π^--$^3He \leftrightarrows \gamma t$ (AND ITS INVERSE) AND $\pi + t \leftrightarrows {}^3He\gamma$ (AND ITS INVERSE)	SHERMAN SHIVELY GLODIS SPENCER WADLINGER NEFKENS	1 * 2 *	0.0 806.9
99	MEASUREMENT OF THE CROSS SECTION FOR $\pi^- + p \rightarrow \pi^- + \pi^+ + n$ WITH A MAGNETIC SPECTROMETER	REBKA GRAM	1 * 2 *	0.0 646.0
102	EXCITATION FUNCTIONS AND ANGULAR DISTRIBUTION RECOIL STUDIES OF SIMPLE PION-INDUCED NUCLEAR REACTIONS	MARKOWITZ	1 *	0.0
103	SPALLATION YIELD DISTRIBUTIONS FOR PION INTERACTIONS WITH COMPLEX NUCLEI	HUDIS	1 * 2 *	0.0 295.7
104	PROPOSAL FOR LAMPF EXPERIMENT: STUDIES OF THE PROTON- AND PION-INDUCED FISSION OF MEDIUM-MASS NUCLIDES	PATE	1 * 2 *	0.0 118.7
118	FRAGMENT EMISSION FROM PION INTERACTIONS WITH COMPLEX NUCLEI	PORILE	1 * 2 *	0.0 97.0

119	CROSS SECTIONS OF SIMPLE NUCLEAR REACTIONS INDUCED BY π-MESONS	KAUFMAN	1 * 2 *	27.8 186.8
120	MEASUREMENT OF THE POLARIZATION ASYMMETRY AND THE DIFFERENTIAL CROSS SECTION OF PION-NUCLEON CHARGE EXCHANGE FROM 160-500 MeV	NEFKENS FITZGERALD	1 * 2	870.2 90.3
121	PION-INDUCED NUCLEAR REACTIONS	SEGEL	1 * 2 *	0.0 0.0
123	NUCLEAR STRUCTURE EFFECTS IN PION-INDUCED NUCLEAR REACTIONS	KAROL	1 * 2 * 3 * 4 *	0.0 75.0 135.1 0.0
144	SEARCH FOR THE C-VIOLATION DECAY $\pi^0 + 3\gamma$	HIGHLAND MACEK	2 *	602.1
153	INVESTIGATION OF NUCLEAR GAMMA-RAYS RESULTING FROM IN-FLIGHT PION AND PROTON REACTIONS	EISENSTEIN	1 *	0.0
154	ELASTIC SCATTERING OF π^+ AND π^- FROM THE HELIUM ISOTOPE	MINEHART McCARTHY	1 * 2	7.2 316.0
181	MEASUREMENTS OF THE $\pi p \rightarrow \pi^0 n$ ANGULAR DISTRIBUTION AT LOW ENERGIES AND CALIBRATION OF THE π^0 SPECTROMETER	ALSTER BOWMAN	2 *	204.3
195	NUCLEAR RESONANCE EFFECT IN PIONIC ATOMS	LEON REIDY	2 * 3 *	0.0 163.1
201	$\pi^+ d \rightarrow 2d$ REACTION AT 100-500 MeV	MINEHART	1 *	338.0
214	PIONIC X-RAY ABSOLUTE YIELDS AS A FUNCTION OF Z	HARGROVE LEON	1 *	199.1
221	PRECISION MEASUREMENT OF THE DECAY RATE FOR THE DALITZ DECAY MODE OF THE π^0 MESON	HOFFMAN	1 *	351.5
222	MEASUREMENT OF THE DECAY RATE FOR $\pi^0 \rightarrow e^+e^-$	MISCHKE	1 *	945.8
247	DISTRIBUTION OF PRODUCTS FROM INTERACTIONS OF STOPPED π^- WITH SEVERAL MEDIUM- AND HEAVY-MASS NUCLEI	ORTH	2 *	28.0
248	STUDY OF THE $(\pi,\pi n)$, (π,Δ), (π,B_Δ), AND (π,n) REACTIONS IN ^{3,4}He AND ^{6}Li BY MEASURING RECOIL SPECTRA	KALLNE McCARTHY GUGELOT	1 *	674.4
283	CHARGED-PARTICLE EMISSION FOLLOWING μ^- CAPTURE	KRANE SHARMA	1 *	31.0
286	PROTON AXIAL TOMOGRAPHY	HANSON	1 *	345.5
304	STUDY OF THE AUGER PROCESS IN PIONIC ATOMS	LEON MAUSNER	1 *	78.6
309	INCLUSIVE π^+ AND π^- DOUBLE CHARGE EXCHANGE ON ^{16}O AND ^{40}Ca	REBKA	1	0.0
319	DETERMINING THE MECHANISM FOR MULTINUCLEON AND CLUSTER REMOVAL IN 200-MeV π-NUCLEAR INTERACTIONS	LIND	1 *	283.0

320	A COMPARISON OF (π^+,xn) AND (π^-,xn) REACTIONS	CHURCH	1 * 2 *	57.8 170.1
337	MEASUREMENT OF THE CROSS SECTION FOR $\pi^-p \rightarrow \pi^-\pi^+n$ AT 200 AND 229 MeV	REBKA GRAM	1 *	999.8
349	NUCLEAR REACTIONS OF ^{127}I WITH PIONS	PORILE	1 * 2 * 3	74.5 55.2 9.0
358	ELASTIC SCATTERING OF PION FROM DEUTERIUM	MINEHART	1 *	514.0
363	MEASUREMENT OF $\pi^{\pm}$ + p ELASTIC SCATTERING	SADLER NEFKENS	1 * 2 *	700.5 844.5
373	A COMPARISON OF RESIDUAL NUCLEI YIELDS FROM π^- ABSORPTION IN ^{112}Cd (GROUND STATE) AND ^{112}D (FIRST EXCITED STATE)	REIDY LEON	1 *	94.1
390	A STUDY OF INCLUSIVE INELASTIC PION SCATTERING NEAR THE $\Delta(3/2,3/2)$ RESONANCE	JACKSON	1 *	453.0
394	APPLICATION OF PROTON COMPUTED TOMOGRAPHY	HANSON	1 *	195.3
396	COMPARISON OF MEASURED PIONIC ATOM CASCADE INTENSITIES WITH THEORETICAL INTENSITIES OBTAINED USING PARAMETERS FROM MUONIC ATOM STUDIES	REIDY	1 *	110.9
400	SEARCH FOR THE RARE DECAY $\mu^+ \rightarrow e^+e^+e^-$	DUONG-VAN HOFFMAN	1	156.8
404	A KINEMATICALLY COMPLETE STUDY OF THE $(\pi,\pi'p)$ REACTION ON ^{16}O ABOVE THE RESONANCE BY DETECTING PIONS AND PROTONS IN COINCIDENCE	HAMM SWENSON	1 *	401.5
416	STUDY OF FAST PION-INDUCED FISSION OF URANIUM	DROPESKY	1 * 2 * 3 *	141.0 17.0 11.0
420	DEVELOPMENT OF A HIGH-RESOLUTION LIQUID-ARGON CHARGED-PARTICLE DETECTOR OF MEDIUM-ENERGY PARTICLES	GRUHN FLYNN	1	0.0
439	PARTICLE GAMMA-RAY COINCIDENCE STUDIES FROM π-NUCLEAR REACTIONS	LIND	1 * 2	239.0 0.0
455	HIGH-PRECISION STUDY OF THE μ^+ DECAY SPECTRUM	ANDERSON	1	0.0
458	THE EXCITATION FUNCTION FOR THE SINGLE-CHARGE-EXCHANGE REACTION $^{65}Cu(\pi^-,\pi^0)^{65}Ni$	KAUFMAN	1 *	80.4
459	CROSS-SECTION MEASUREMENTS OF THE $^{14}N(\pi^+,\pi^0)^{14}O$ (GROUND STATE) REACTION	VIEIRA	1 *	96.0
465	RADIOCHEMICAL STUDY OF PION SINGLE CHARGE EXCHANGE	RUNDBERG	1 * 2	99.1 46.7
466	NUCLEAR CONFIGURATION OF INDIVIDUAL CORE-COUPLED STATES IN ^{209}Bi FROM INELASTIC $\pi^{\pm}$ SCATTERING	FUNSTEN PLENDL	1 *	219.6
469	STUDY OF THE $^{91}Zr(\pi^+,\pi^0p)^{90}Zr$ CHARGE-EXCHANGE REACTION	McGILL HOFFMANN	1	0.0

480	DISCRETE STATES FROM PION DOUBLE CHARGE EXCHANGE ON HEAVY NUCLEI	ZEIDMAN	1	0.0
500	FISSION FRAGMENT DISTRIBUTIONS IN FAST PION-INDUCED FISSION OF ^{238}U	RUNDBERG	1	72.2
513	$\pi^{\pm}$ QUASI-FREE SCATTERING FROM THE HELIUM ISOTOPES	McCARTHY MINEHART	1 * 2	0.0 557.7
543	A PRODUCT RECOIL STUDY OF THE $(\pi^{\pm},\pi^{\pm}n)$ REACTION	CARETTO	1 *	25.0
553	STUDY OF TARGET THICKNESS EFFECTS IN THE CROSS-SECTION MEASUREMENT OF THE PION SINGLE-CHARGE-EXCHANGE REACTION $^{13}C(\pi^{+},\pi^{0})^{13}N$ (g.s.) FROM 50 TO 350 MeV	RUNDBERG	1	61.3
555	TOTAL CROSS-SECTION MEASUREMENTS OF THE SINGLE-CHARGE-EXCHANGE REACTION $^{12}C(\pi^{+},\pi^{0})^{12}N$ (g.s.)	IMANISHI VIEIRA	1 *	139.0
562	STUDY OF THE PION ABSORPTION MECHANISM THROUGH THE A(π,p)X REACTION AT T_{π} = 500 MeV	JACKSON SCHIFFER	1	428.0
564	STUDY OF SMALL-ANGLE $^{4}He(\pi^{-},\pi^{+})$ REACTION	McKEOWN	1	0.0
595	AN ON-LINE γ-RAY STUDY OF PION-INDUCED SINGLE-NUCLEON REMOVAL REACTIONS ON ^{13}C AND ^{48}Ca	ORTH VIEIRA	1	0.0
611	EXCITATION FUNCTIONS OF THE FOUR $^{130}Te(\pi^{\pm},\pi^{\pm}n)$ REACTIONS	HOGAN	1	0.0
614	STUDIES OF SCALAR AND VECTOR PARTS OF THE π-n INTERACTION BY MEASURING NUCLEAR DEEXCITATION γ-RAY CORRELATION FOLLOWING INELASTIC PION SCATTERING	FUNSTEN	1	0.0
617	A STUDY OF THE (3/2,3/2) RESONANCE IN LIGHT NUCLEI	ZIOCK	1	0.0
628	STUDY OF THE (π,πp) REACTION AND QUASI-FREE SCATTERING IN ^{4}He	ASHERY	1	0.0
673	MEASUREMENTS OF THE ANGULAR DEPENDENCE OF TENSOR POLARIZATION IN THE $^{2}H(\pi^{+},\pi^{-})^{2}\overrightarrow{H}$ REACTION AT T_{π} = 180 AND 256 MeV	HOLT	1	0.0
674	MEASUREMENTS OF PION-NUCLEUS ELASTIC AND DOUBLE-CHARGE EXCHANGE SCATTERING AT ENERGIES ABOVE 300 MeV	BURLESON MORRIS	1	0.0
682	SEARCH FOR DIBARYON RESONANCES IN THE REACTION $\pi d \rightarrow p\pi n$ AT P_{L}^{π} = 200 TO 600 MeV/c	IMAI GREENE	1	0.0
689	A. NEUTRON COUNTER CALIBRATION USING TAGGED NEUTRONS FROM THE REACTION $\pi^{-}d \rightarrow nn$. B. FEASIBILITY STUDY: MEASUREMENT OF THE DIFFERENTIAL CROSS SECTION FOR $\pi^{-}d \rightarrow nn$ TO TEST CHARGE SYMMETRY AND ISOSPIN INVARIANCE	NEFKENS FITZGERALD	1	0.0

RADIATION DAMAGE A-1 (RADAMAGE-1)

Exp. No.	Title	Spokesman	Phase No. *=Complete	Beam Hours
302	800-MeV PROTON IRRADIATION OF AN ALUMINUM SAMPLE	GREEN	1 *	0.0

STOPPED MUON CHANNEL (SMC)

Exp. No.	Title	Spokesman	Phase No. *=Complete	Beam Hours
7	NUCLEAR STRUCTURE PHYSICS USING STOPPED MUONS	SHERA	1 * 2 *	0.0 617.3
12	MUONIC X RAYS AND NUCLEAR CHARGE DISTRIBUTIONS	POWERS KUNSELMAN	1 * 2 *	173.0 141.9
37	ULTRAHIGH-PRECISION MEASUREMENTS OF MUONIUM GROUND-STATE ENERGY LEVELS, HYPERFINE STRUCTURE INTERVAL AND MUON MAGNETIC MOMENT	HUGHES CRANE	1 * 2 *	0.0 940.4
51	TECHNIQUES FOR MATERIALS IDENTIFICATION AND ANALYSIS	MALANIFY	1 *	119.3
60	CHEMICAL EFFECTS IN THE CAPTURE OF NEGATIVE MESONS IN MATTER	KNIGHT SCHILLACI	1 * 2 *	0.0 451.5
76	SEARCH FOR MUONIUM-ANTIMUONIUM TRANSITION	CHANG KANE	1 *	0.0
85	GAMMA-NEUTRINO CORRELATION AFTER NEGATIVE MUON CAPTURE	WELSH	1 *	193.6
100	TISSUE CHEMICAL ANALYSIS WITH MU-MESIC X RAYS	HUTSON	1 * 2 *	0.0 167.0
101	FEASIBILITY STUDIES. MEASUREMENT OF MUONIC X RAYS AND NUCLEAR GAMMA RAYS WITH CRYSTAL DIFFRACTION SPECTROMETERS AT LAMPF	BOEHM LU	F S*	103.0
122	PIONIC ATOM X RAYS AND NUCLEAR DISTRIBUTIONS	KUNSELMAN	2 *	64.8
142	NEGATIVE MUON-INDUCED FISSION IN THE ACTINIDE ELEMENTS	HUIZENGA	1 * 2 *	0.0 520.3
163	INVESTIGATION OF CHANGES IN CHARGE DISTRIBUTIONS FOR NUCLEI NEAR Z = 28 BY ELECTRON SCATTERING AND MUONIC X RAYS	PERKINS SHERA	1 *	0.0
165	MUONIUM FORMATION IN HELIUM AND OTHER RARE GASES	HUGHES	1 *	0.0
166	MUONIC X RAYS AND NUCLEAR CHARGE DISTRIBUTIONS ELECTRIC QUADRUPOLE MOMENTS OF $_{67}Ho^{165}$ AND $_{73}Ta^{181}$	POWERS	1 *	0.0
173	PHYSICS OF THE PION AND THE PIONIC ATOM	BOEHM VOGEL	1 * 2 *	600.9 309.6

175	SEARCH FOR THE FORMATION OF MUONIC HELIUM ($\alpha\mu^-e$)	HUGHES	1 *	0.0
206	SEARCH FOR THE 2S METASTABLE STATE OF MUONIC HYDROGEN	HUGHES EGAN	1 *	497.0
213	MUON TRANSFER STUDY	SHERA STEFFEN	1 *	50.9
240	ISOTOPE AND ISOTONE SHIFTS IN THE $1f_{7/2}$ SHELL	SHERA WOHLFAHRT	1 *	294.1
266	TRAPPING OF POSITIVE MUONS AT DEFECTS IN METALS	GAUSTER HEFFNER	1 * 2 * 3 *	223.0 106.1 9.0
268	MEASUREMENT OF THE GROUND-STATE HYPERFINE STRUCTURE INTERVAL OF THE MUONIC HELIUM ATOM ($\alpha\mu^-e^-$)	SOUDER HUGHES	1 *	518.6
276	PERTURBED CIRCULAR POLARIZATION OF MUONIC X RAYS	YAMAZAKI	1 * 2 * 3 *	0.0 183.8 235.1
277	MUONIC X-RAY ANALYSIS OF CORE SAMPLES FROM OIL-BEARING FORMATIONS	ALLRED	1 *	33.0
283	CHARGED-PARTICLE EMISSION FOLLOWING μ^- CAPTURE	KRANE SHARMA	1 * 2 *	138.3 88.6
288	STUDIES OF μ^- CAPTURE PROBABILITIES FOR SOLID-STATE SOLUTIONS	NAUMANN	1 *	180.1
292	NEUTRON EMISSION FROM MUON-INDUCED REACTIONS ON ACTINIDE ELEMENTS	HUIZENGA	1 * 2 *	196.2 138.3
297	A BICENTENNIAL PROPOSAL TO STUDY THE BEHAVIOR OF POSITIVE MUONS IN SOLIDS	BROWN	1 * 2 * 3 *	144.1 137.1 47.1
328	MEASUREMENT OF THE DECAY RATE AND PARITY VIOLATING ASYMMETRY FOR $\mu^+ \rightarrow e^+\gamma$	BOWMAN COOPER	1 *	1666.3
330	FUNDAMENTAL MUONIC X-RAY MEASUREMENTS OF INTEREST TO MATERIALS ANALYSIS	HUTSON YATES-WILLIAMS	1 * 2 *	90.4 67.8
331	FAST MUON REACTIONS WITH ^{12}C, ^{46}Ti, AND ^{58}Ni	ORTH	1 * 2 *	97.2 78.0
334	NUCLEAR CHARGE PARAMETERS OF ^{41}Ca AND STABLE CADMIUM AND TELLURIUM ISOTOPES	SHERA WOHLFAHRT	1 * 2 *	162.4 170.3
335	MONOPOLE AND QUADRUPOLE CHARGE DISTRIBUTIONS IN THE SAMARIUM AND GADOLINUM ISOTOPES	SHERA YAMAZAKI	1 * 2	298.7 0.0
344	HIGHER PRECISION MEASUREMENT OF MUON MAGNETIC MOMENT AND OF MUONIUM hfs INTERVAL	HUGHES	1 *	425.6
357	MUONIC X-RAY SPECTRA OF GASES: 1. DENSITY AND ADMIXTURE EFFECTS	KNIGHT	1 *	145.1
364	SEARCH FOR THE EXCITED 2S STATE OF MUONIUM	EGAN DENISON HUGHES	1 * 2 *	535.8 167.7

371	MUONIC X-RAY SPECTRA OF GASES: 2. CAPTURE PROBABILITIES IN MIXTURES	HUTSON	1 *	122.7
374	μ^- CAPTURE PROBABILITIES FOR SELECTED SOLID BINARY COMPOUNDS	SCHILLACI	1 *	161.7
375	μSR STUDY OF DIFFUSION IN METALS IN THE PRESENCE OF PARAMAGNETIC IONS	SCHILLACI	1 * 2 * 3 *	194.6 287.0 45.0
377	INVESTIGATION ON THE EFFECT OF GRAIN SIZE IN MUON CAPTURE IN INHOMOGENEOUS SYSTEMS	REIDY	1 *	28.0
382	μSR INVESTIGATION OF THE EFFECTS OF IMPURITIES ON THE TRAPPING AND DIFFUSION OF μ^+ PARTICLES IN bcc METALS	KOSSLER	1	111.4
400	SEARCH FOR THE RARE-DECAY $\mu^+ \rightarrow e^+e^+e^-$	DUONG-VAN HOFFMAN	1 2 *	54.4 125.0
408	MACROSCOPIC DIFFUSION STUDIES IN METALS	HEFFNER LEON	1 *	81.0
414	BONE CALCIUM ASSAY WITH MUONIC X RAYS — SIGNAL/NOISE AND REPRODUCIBILITY STUDIES	HUTSON REIDY	1 *	118.6
417	STUDY OF THE NUCLEAR AUGER PROCESS IN HEAVY MUONIC ATOMS	HUIZENGA	1 *	120.0
421	SENSITIVE SEARCH FOR $\mu^- \rightarrow e$ CONVERSION	SOUDER FRANKEL HUGHES	1	42.0
427	MAGNET RESONANCE STUDIES OF μ^+-ELECTRON DEFECT COMPLEXES IN NONMETALS	ESTLE	1 * 2 3	253.3 140.4 24.0
436	NEGATIVE MUON SPIN ROTATION AND RELAXATION IN MAGNETIC MATERIALS	YAMAZAKI HAYANO	1 *	196.2
444	SEARCH FOR THE DECAY $\mu \rightarrow e\gamma$	BOWMAN HOFSTADTER	1	0.0
445	SEARCH FOR THE LEPTON-FLAVOR-VIOLATING DECAY $\mu^+ \rightarrow e^+\gamma\gamma$	MATIS BOWMAN	1 *	54.4
454	MEASUREMENT OF THE ETA PARAMETER IN MUON DECAY	CROWE	1 * 2 *	73.5 0.0
464	RADIATIVE MUON CAPTURE IN GASEOUS ^{3}He	WU DUGAN HUGHES LU EGAN	1	0.0
491	EXPERIMENTAL DETERMINATION OF THE STRONG INTERACTION SHIFT IN THE 2p-1s TRANSITION OF PIONIC DEUTERIUM AND HYDROGEN ATOMS	BOVET	1 2	646.6 235.0
494	NUCLEAR CHARGE PARAMETERS OF THE STABLE RUTHENIUM AND PALLADIUM ISOTOPES	HOEHN	1	108.0

499	MUON LONGITUDINAL AND TRANSVERSE RELAXATION STUDIES IN SPIN-GLASS SYSTEMS	DODDS MACLAUGHLIN HEFFNER	1 * 2	329.6 87.0
529	PART 1: MEASUREMENT OF THE RESIDUAL MUON POLARIZATION IN ^{3}He MUONIC ATOM (A FEASIBILITY TEST FOR PART 2), AND PART 2: ANGULAR CORRELATIONS IN THE CAPTURE OF POLARIZED MUONS IN GASEOUS ^{3}He	WU DUGAN HUGHES	1 * 2 3	136.0 0.0 0.0
547	SEARCH FOR FAST MUONIUM IN VACUUM	EGAN HUGHES KANE	1 * 2 * 3	231.4 144.0 0.0
552	ULTRAHIGH-PRECISION MEASUREMENTS ON MUONIUM	HUGHES EGAN	1	0.0
571	MUON SPIN-ROTATION STUDIES OF DILUTE MAGNETIC ALLOYS	DODDS HEFFNER SCHILLACI	1	263.4
594	PRECISION DETERMINATIONS OF SOME RELATIVE MUONIC COULOMB CAPTURE RATIOS IN OXIDES OF DIFFERENT VALENCES	REIDY	1	0.0
639	MUON SPIN-ROTATION STUDY OF MUON BONDING AND MOTION IN SELECT MAGNETIC OXIDES	BOEKEMA DENISON	1	21.0
640	TRANSVERSE AND LONGITUDINAL FIELD μSR MEASUREMENTS IN SELECTED TERNARY METALLIC COMPOUNDS	DODDS HEFFNER MACLAUGHLIN	1	63.0
646	HYPERFINE STRUCTURE OF MUONIC ^{3}He AND MUONIC ^{4}He ATOMS	HUGHES EGAN	1	0.0
653	THE ^{241}Am AND ^{243}Am MUONIC ATOM STUDIES	SHERA JOHNSON NAUMANN	1	0.0
693	INVESTIGATION OF THE TWO-PHOTON DECAY RATE FROM THE $(\mu^4He)^+_{2s}$ STATE AS A FUNCTION OF PRESSURE	REIDY	1	0.0
695	STUDY OF TRANSFER EFFECTS IN MUON CAPTURE IN GAS TARGET	REIDY HUTSON	1	0.0

SWITCHYARD LINE A BEAM STOP (SWY-LABS)

Exp. No.	Title	Spokesman	Phase No. *=Complete	Beam Hours
105	NUCLEAR SPECTROSCOPY STUDIES OF PROTON-INDUCED SPALLATION PRODUCTS	BUNKER	1 *	0.0
118	FRAGMENT EMISSION FROM PION INTERACTIONS WITH COMPLEX NUCLEI	PORILE	1 *	0.0
269	800-MEV PROTON IRRADIATION OF METAL SAMPLES	GREEN	1 *	4.5

381	ALUMINA CERAMIC RADIATION EFFECTS STUDY	HARVEY	1 *	0.0
648	TEST OF EQUIPMENT FOR THE MEASUREMENT OF THE Σ^- FOR THE MAGNETIC MOMENT AT BNL	MILLER	1	0.0
652	TESTS OF PROTOTYPE SEMICONDUCTOR DETECTORS	SKUBIC	1	0.0

THIN TARGET AREA (TTA)

Exp. No.	Title	Spokesman	Phase No. *=Complete	Beam Hours
86	COUNTER EXPERIMENTS IN THE THIN TARGET AREA	POSKANZER	1 *	0.0
			2 *	743.0
			3 *	1128.0
308	AN ATTEMPT TO MAKE DIRECT ATOMIC MASS MEASUREMENTS IN THE THIN TARGET AREA	BUTLER POSKANZER	1	5299.5

APPENDIX B

ACTIVE SPOKESMEN, INSTITUTIONS, AND EXPERIMENTS

SPOKESMEN	INSTITUTIONS	EXPERIMENTS
AAS, B.	UCLA	643
ALSTER, J.	TEL AVIV UNIV.	393, 607
ANDERSON, H. L.	LOS ALAMOS	455
ANDERSON, R. E.	UNIV. OF NORTH CAROLINA	535, 625
ASHERY, D.	TEL AVIV UNIV.	628
BAER, H. W.	LOS ALAMOS	412, 523, 524, 527, 558, 607, 622
BAKER, F. T.	UNIV. OF GEORGIA	356
BAUER, T. S.	SACLAY	405
BENTON, E. V.	UNIV. OF SAN FRANCISCO	171
BERNSTEIN, A. M.	MIT	627
BERTOZZI, W.	MIT	556
BERTRAND, F. E.	OAK RIDGE	399
BLANPIED, G. S.	UNIV. OF SOUTH CAROLINA	475, 476, 573
BLECHER, M.	VPI/STATE UNIV.	561
BLESZYNSKI, M.	UCLA	540, 616, 635
BOEKEMA, C.	LOS ALAMOS	639
BONNER, B. E.	LOS ALAMOS	635, 637
BOVET, E.	CALTECH	491
BOWMAN, J. D.	LOS ALAMOS	295, 401, 412, 444, 445, 524, 527, 607, 650
BRADBURY, J. N.	LOS ALAMOS	215
BRILL, A. B.	VANDERBILT UNIV.	244
BRISCOE, W. J.	UCLA	546
BROWN, R. D.	LOS ALAMOS	545, 554
BRYANT, H. C.	UNIV. OF NEW MEXICO	449, 586, 588
BUNKER, M. E.	LOS ALAMOS	629
BURLESON, G. R.	NEW MEXICO STATE UNIV.	386, 498, 558
BURNETT, D. S.	CALTECH	161
BUSH, S.	UNIV. OF NEW MEXICO	274, 275
BUTLER, G. W.	LOS ALAMOS	308
CAREY, T. A.	LOS ALAMOS	630
CARLINI, R.	LOS ALAMOS	634
CHANT, N. S.	UNIV. OF MARYLAND	576
CHEN, H. H.	UNIV. OF CALIFORNIA, IRVINE	225
CHURCH, L. B.	REED COLLEGE, OREGON	320
CLARK, D. A.	UNIV. OF NEW MEXICO	588
COOPER, M. D.	LOS ALAMOS	284, 401, 541
CORNELIUS, W. D.	LOS ALAMOS	474
COST, J. R.	LOS ALAMOS	554
COTTINGAME, W. B.	NEW MEXICO STATE UNIV.	598
COWSIK, R.	WASHINGTON UNIV.	557
CVERNA, F. H.	LOS ALAMOS	412, 524
DEHNHARD, D.	UNIV. OF MINNESOTA	369, 510, 580, 602
DENISON, A. B.	UNIV. OF WYOMING	639
DEVRIES, R. M.	LOS ALAMOS	591, 592
DICELLO, J. F.	LOS ALAMOS	272
DIGIACOMO, N.	LOS ALAMOS	591, 592
DODDS, S. A.	RICE UNIV.	499, 571, 640
DOMBECK, T. W.	UNIV. OF MARYLAND	638
DONAHUE, J. B.	LOS ALAMOS	449, 587
DROPESKY, B. J.	LOS ALAMOS	416
DUGAN, G.	COLUMBIA UNIV.	464, 529
DUONG-VAN, M.	LOS ALAMOS	400, 559
EGAN, P. D.	YALE UNIV.	464, 547, 552, 646
EISENSTEIN, R. A.	CARNEGIE-MELLON UNIV.	446, 597
ELLIS, R. J.	LOS ALAMOS	647
ESTLE, T. L.	RICE UNIV.	427

APPENDIX C

VISITORS TO LAMPF DURING THE PERIOD
JANUARY 1 — JUNE 30, 1981

Bjarne Aas ..... UC, Los Angeles
Gary S. Adams ..... Massachusetts Inst. of Tech.
Yasuyuki Akine ..... UNM Cancer Center
Wanda Alberico ..... Univ. of Torino
Richard C. Allen ..... UC, Irvine
John C. Allred ..... Consultant
Jonas Alster ..... Tel Aviv Univ.
Howard I. Amols ..... Rhode Island Hospital
Barbara L. Anstey ..... UNM Cancer Center
Richard A. Arndt ..... VPI/State Univ.
Mary Jean Arntzen ..... UNM Cancer Center
Daniel Ashery ..... Tel Aviv Univ.
Andrew D. Bacher ..... Indiana Univ.
Andreas Badertscher ..... Univ. of Berne
Toni A. Balch ..... UNM Cancer Center
Barry Barish ..... California Inst. of Tech.
Martin L. Barlett ..... Univ. of Texas
Charles A. Barnes ..... California Inst. of Tech.
William Bertozzi ..... Massachusetts Inst. of Tech.
Tarlochan S. Bhatia ..... Texas A&M Univ.
Ewart W. Blackmore ..... TRIUMF
Leslie C. Bland ..... Univ. of Pennsylvania
Gary S. Blanpied ..... Univ. of South Carolina
Elizabeth H. Bleszynski ..... UC, Los Angeles
Thomas H. Blewitt ..... Argonne
Carolyn A. Blies ..... UNM Cancer Center
Charles L. Blilie ..... Univ. of Minnesota
Edwin M. Blume ..... Univ. of Chicago
Felix H. Boehm ..... California Inst. of Tech.
Paul R. Bolton ..... Yale Univ.
Fred O. Borcherding ..... UC, Los Angeles
Jonathan S. Boswell ..... Univ. of Virginia
Eric Bovet ..... Univ. de Neuchâtel
Dale E. Boyce ..... Univ. of Chicago
Kenneth Boyer ..... Univ. of Texas
James A. Bridge ..... Consultant
William J. Briscoe ..... UC, Los Angeles
Howard C. Bryant ..... Univ. of New Mexico
Douglas Bryman ..... TRIUMF
George R. Burleson ..... New Mexico State Univ.
Steven E. Bush ..... UNM Cancer Center
Jeanne L. Butler ..... UNM Cancer Center
Kenneth B. Butterfield ..... Univ. of New Mexico
David C. Carey .... Fermi National Accelerator Lab.
Jim B. Carroll ..... Lawrence Berkeley Lab.
Herbert H. Chen ..... UC, Irvine
David A. Clark ..... Univ. of New Mexico
W. Rory Coker ..... Univ. of Texas
Nance L. Colbert ..... UC, Irvine
John M. Collier ..... UNM Cancer Center
David C. Cook ..... Univ. of Minnesota
William Cottingame ..... New Mexico State Univ.
Mary L. Courtright ..... UNM Cancer Center
Donna J. Cremans ..... Univ. of Texas
Kincaid Davidson ..... UNM Cancer Center
Glen H. Daw ..... UNM/New Mexico State Univ.
W. Kenneth Dawson ..... Univ. of Alberta
James M. DeNiro ..... UNM Cancer Center
Dietrich Dehnhard ..... Univ. of Minnesota
Peter P. Denes ..... Univ. of New Mexico
Arthur B. Denison ..... Univ. of Wyoming
Kailash C. Dhingra ..... Univ. of New Mexico
Byron D. Dieterle ..... Univ. of New Mexico
W. Rodney Ditzler ..... Argonne
Stanley A. Dodds ..... Rice Univ.
George W. Dodson ..... Boston Univ.
Peter J. Doe ..... UC, Irvine
Thomas W. Donnelly ... Massachusetts Inst. of Tech.
Alexander Doron ..... Tel Aviv Univ.
Mohan Doss ..... Univ. of Washington
Robert W. Dunn ..... Univ. of New Mexico
M. V. Duong-Van Stanford Linear Accelerator Center
Thanasis E. Economou ..... Univ. of Chicago
David A. Edrich ..... UC, Irvine
Patrick O. Egan ..... Yale Univ.
Robert A. Eisenstein ..... Carnegie-Mellon Univ.
Mortimer M. Elkind ..... Argonne
Richard J. Ellis ..... Consultant
Stephen F. Elston ..... Univ. of Texas
Adoram Erell ..... Tel Aviv Univ.
David J. Ernst ..... Texas A&M Univ.
Thomas Estle ..... Rice Univ.
John A. Faucett ..... Univ. of Oregon
Raymond W. Fergerson ..... Univ. of Texas
Daniel Fitzgerald ..... UC, Los Angeles
Donald G. Fleming ..... TRIUMF
Orris B. Fletcher ..... Argonne
Will M. Foreman ..... UNM Cancer Center

H. Terry Fortune ..... Univ. of Pennsylvania
Michael Franey ..... Univ. of Minnesota
Charles A. Frost ..... Sandia Labs.
Chris J. Gardner ..... Yale Univ.
David A. Garelick ..... Northeastern Univ.
Carol A. Gauthier ..... UNM Cancer Center
David H. Gay ..... Univ. of Minnesota
M. Magdy Gazzaly ..... Univ. of Minnesota
Jorge V. Geaga ..... UC, Los Angeles
Donald F. Geesaman ..... Argonne
Robert J. Gehrke ..... EG&G, Idaho
Joseph P. Geraci ..... Univ. of Washington
Edward F. Gibson ..... Univ. of Colorado
David R. Gill ..... TRIUMF
Christopher Gilman ..... UNM Cancer Center
James L. Gimlett ..... California Inst. of Tech.
Michael Gladisch ..... Univ. Heidelberg
George Glass ..... Texas A&M Univ.
Timothy W. Glover ..... New Mexico State Univ.
Charles D. Goodman ..... Indiana Univ.
Peter W. Gorham ..... UC, Irvine
Abigail R. Gould ..... UNM Cancer Center
C. A. Goulding .. EG&G, Los Alamos/Univ. of Texas
Michael G. Greene ..... Yale Univ.
Steven J. Greene ..... New Mexico State Univ.
Ghislain S. Gregoire ..... Univ. of Louvain
Chilton B. Gregory ..... Univ. of New Mexico
Ana M. Guevara ..... UNM Cancer Center
Ricardo L. Guevara ..... UNM Cancer Center
P. C. Gugelot ..... Univ. of Virginia
William Haberichter ..... Argonne
Mohammad Haji-Saeid ..... UC, Los Angeles
Isaac Halpern ..... Univ. of Washington
A. Dayle Hancock ..... Univ. of Houston
Ronnie W. Harper ..... Univ. of Illinois
Carol J. Harvey ..... Univ. of Texas
David W. Hertzog ..... College of William & Mary
John C. Hiebert ..... Texas A&M Univ.
Virgil L. Highland ..... Temple Univ.
Robert A. Hilko ..... UNM Cancer Center
Daniel A. Hill ..... Argonne
Edward A. Hinds ..... Yale Univ.
Norton M. Hintz ..... Univ. of Minnesota
Gerald W. Hoffmann ..... Univ. of Texas
Bo Höistad ..... Univ. of Texas
Charles L. Hollas ..... Univ. of Texas
James A. Holt ..... UC, Los Angeles
Randy Holt ..... Consultant
Roy J. Holt ..... Argonne
David B. Holtkamp ..... Univ. of Minnesota
Irma S. Holtkamp ..... Univ. of Texas
Minoru Hosoba ..... Shimadzu Corp.
E. Barrie Hughes ..... Stanford Univ.
Vernon W. Hughes ..... Yale Univ.
David Hussey ..... M. D. Anderson Hospital
George J. Igo ..... UC, Los Angeles
Kenichi Imai ..... Argonne
Farokh Irom ..... UC, Los Angeles
Steven G. Iversen ..... Northwestern Univ.
Vincent Jaccarino ..... UC, Santa Barbara
Harold E. Jackson ..... Argonne
Linwood E. Jackson ..... UNM Cancer Center
Mark J. Jakobson ..... Univ. of Montana
Randolph H. Jeppesen ..... Univ. of Montana
Ronald G. Jeppesen ..... Univ. of Montana
Wayne A. Johnson ..... UC, Irvine
Garth Jones ..... TRIUMF
Kevin W. Jones ..... Rutgers Univ.
Laurie D. Kain ..... UNM Cancer Center
Mark O. Kaletka ..... Northwestern Univ.
Jan Källne ..... Univ. of Virginia
John R. Kane ..... College of William & Mary
Paul J. Karol ..... Carnegie-Mellon Univ.
Thomas E. Kasprzyk ..... Argonne
Sheldon Kaufman ..... Argonne
Charles A. Kelsey ..... UNM Cancer Center
Robert A. Kenefick ..... Texas A&M Univ.
Charles R. Key ..... UNM Cancer Center
Mirkutub M. Khan ..... UNM Cancer Center
Mahbubul A. Khandaker ..... Univ. of Washington
Danuta Kielczewska ..... Northwestern Univ.
Donald K. Kohl ..... Consultant
William J. Kossler ..... College of William & Mary
Kenneth S. Krane ..... Oregon State Univ.
Jack J. Kraushaar ..... Univ. of Colorado
Raymond Kunselman ..... Univ. of Wyoming
Dieter Kurath ..... Argonne
Deborah A. Landt ..... UNM Cancer Center
Richard G. Lane ..... UNM Cancer Center
Daniel B. Laubacher ..... Purdue Univ.
Paul L. Lee ..... California Inst. of Tech.
E. Scott Leherissey ..... Temple Univ.
Samuel M. Levenson ..... Argonne
David A. Lind ..... Univ. of Colorado
Earle L. Lomon ..... Massachusetts Inst. of Tech.
Daniel C. Lu ..... Yale Univ.
J. T. Lyman ..... Lawrence Berkeley Lab.
Douglas MacLaughlin ..... UC, Riverside
Christopher J. Maher ..... Carnegie-Mellon Univ.
Hansjuerg Mahler ..... UC, Irvine

Charles E. Manger ..... Consultant
D. Mark Manley ..... Univ. of Wyoming
John Manley ..... Consultant
Robert T. Marchini ..... Univ. of New Mexico
Fesseha Mariam ..... Yale Univ.
Jill Ann Marshall ..... Univ. of Texas
Myrna P. Marsteller ..... UNM Cancer Center
Jo Ann Martinez ..... UNM Cancer Center
Thomas G. Masterson ..... Univ. of Colorado
Howard S. Matis ..... Consultant
Bill W. Mayes ..... Univ. of Houston
James S. McCarthy ..... Univ. of Virginia
Egan D. McCormick ..... UNM Cancer Center
David K. McDaniels ..... Univ. of Oregon
John A. McGill ..... Rutgers Univ./Univ. of Texas
Robert D. McKeown ..... California Inst. of Tech.
Kok-Heong McNaughton Case Western Reserve Univ.
Fred A. Mettler ..... UNM Cancer Center
Gerald A. Miller ..... Univ. of Washington
James P. Miller ..... Boston Univ.
Daniel F. Milligan ..... UNM Cancer Center
Cas Milner ..... Univ. of Texas
Ralph C. Minehart ..... Univ. of Virginia
Murray Moinester ..... Tel Aviv Univ.
Alireza Mokhtari ..... UC, Los Angeles
Alfredo Molinari ..... Univ. of Torino
C. Fred Moore ..... Univ. of Texas
Ingrid B. Moore ..... Univ. of Texas
Donald W. Mueller ..... Consultant
Sirish K. Nanda ..... Rutgers Univ.
Subrata Nath ..... Texas A&M Univ.
Robert A. Naumann ..... Princeton Univ.
B. M. K. Nefkens ..... UC, Los Angeles
Barry J. Nelson ..... Univ. of Texas
Patricia M. Nichols ..... UNM Cancer Center
Lee C. Northcliffe ..... Texas A&M Univ.
Vincent J. Novick ..... EG&G, Idaho
Muhammad Numan ..... College of William & Mary
Francis E. O'Brien ..... Boston Univ.
Deborah C. O. Dean ..... UNM Cancer Center
Yoshitaka Ohkubo ..... Purdue Univ.
M. Margaret Onstott ..... UNM Cancer Center
Jean M. Oöstens ..... Univ. of Oklahoma
Lewis J. Orphanos ..... Univ. of Virginia
Joanne D. Ortega ..... UNM Cancer Center
Alison M. Pannell ..... UNM Cancer Center
Jorge Paradelo ..... UNM Cancer Center
Gianni Pauletta ..... UC, Los Angeles
Roy J. Peterson ..... Univ. of Colorado
David J. Pierotti ..... UNM Cancer Center
Chandra Pillai ..... Oregon State Univ.
Barry M. Preedom ..... Univ. of South Carolina
Ali Rahbar ..... UC, Los Angeles
Mark T. Rakowski ..... Yale Univ.
Brenda S. Ramsey ..... UNM Cancer Center
Ronald D. Ransome ..... Consultant/Univ. of Texas
Arthur M. Rask ..... Argonne
Richard S. Raymond ..... Univ. of Colorado
Robert P. Redwine ..... Massachusetts Inst. of Tech.
James J. Reidy ..... Univ. of Mississippi
Louis P. Remsberg ..... Brookhaven
James H. Richardson ..... Consultant
Peter J. Riley ..... Univ. of Texas
Robert A. Ristinen ..... Univ. of Colorado
Barry G. Ritchie ..... Univ. of South Carolina
Michael W. Ritter ..... Yale Univ.
Raymond F. Rodebaugh ..... Univ. of Texas
Joseph Rolfe ..... Stanford Univ.
Isaac I. Rosen ..... UNM Cancer Center
Mike A. Rumore ..... Univ. of Colorado
A. Minick Rushton ..... UC, Irvine
Michael E. Sadler ..... Abilene Christian Univ.
Arunava Saha ..... Northwestern Univ.
Jose M. Sala ..... UNM Cancer Center
John P. Schiffer ..... Argonne
Stefan J. A. Schmitz ..... UC, Los Angeles
Walter W. Schultz ..... UNM Cancer Center
S. Seestrom-Morris .. Los Alamos/Univ. of Minnesota
Ralph E. Segel ..... Northwestern Univ.
Peter A. Seidl ..... Univ. of Texas
Robert Serber ..... Columbia Univ.
Kamal K. Seth ..... Northwestern Univ.
Seiichi Shibata ..... Carnegie-Mellon Univ.
Frank T. Shively ..... Lawrence Berkeley Lab.
Edward R. Siciliano ..... Univ. of Colorado
Robert T. Siegel ..... College of William & Mary
Roy T. Slice ..... UNM Cancer Center
Alfred R. Smith ..... UNM Cancer Center
Chester R. Smith ..... Consultant
David E. Smith ..... Northwestern Univ.
Nancy J. Smith ..... UNM Cancer Center
Winthrop W. Smith ..... Univ. of Connecticut
John W. Somers ..... UNM Cancer Center
Paul Souder ..... Yale Univ.
James R. Specht ..... Argonne
Harold M. Spinka ..... Argonne
Patrick M. Stafford ..... UNM Cancer Center
Richard H. Stark ..... UNM Cancer Center
Rolf M. Steffen ..... Purdue Univ.
Robert T. Stein ..... Rice Univ.

Kenneth E. Stephenson ..... Argonne
Derek W. Storm ..... Univ. of Washington
Sidney J. Stuart ..... New Mexico State Univ.
John W. Sweet ..... Univ. of Pennsylvania
L. Wayne Swenson ..... Oregon State Univ.
Frank Tabakin ..... Univ. of Pittsburgh
Henry H. Tamura ..... UNM Cancer Center
Yasutoshi Tanaka ..... Purdue Univ.
Robert L. Tanner ..... Consultant
Mark W. Tate ..... Abilene Christian Univ.
W. Bradford Tippens ..... Texas A&M Univ.
Michael J. Tobin ..... Carnegie-Mellon Univ.
Kouichi Toshioka ..... Argonne
Anthony L. Turkevich ..... Univ. of Chicago
Stephen E. Turpin ..... Rice Univ.
Yiharn Tzeng ..... Univ. of Virginia
Shuzo Uehara ..... Kyushu Univ.
Jeffrey E. Ungar ..... California Inst. of Tech.
Jeannie C. Van Cleve ..... UNM Cancer Center
Jurgen Vetter ..... Univ. Heidelberg
Clara G. Villareal ..... UNM Cancer Center
Erich Vogt ..... TRIUMF
Robert G. Wagner ..... Argonne
Gloria S. Walker ..... UNM Cancer Center
Stephen J. Wallace ..... Univ. of Maryland
Angel T. M. Wang ..... UC, Los Angeles
Keh-Chung Wang ..... UC, Irvine
John E. Warren ..... Lakehead Univ.
Mial E. Warren ..... Rice Univ.
Johannes Weertman ..... Northwestern Univ.
William R. Wharton ..... Carnegie-Mellon Univ.
R. Roy Whitney ..... Univ. of Virginia
Jeffrey D. Wicks ..... UNM Cancer Center
Stephany Wilson ..... UNM Cancer Center
Steven L. Wilson ..... Stanford Univ.
David Wolfe ..... Univ. of New Mexico
Ming-Jen Yang ..... Univ. of Chicago
Vincent Yuan ..... Univ. of Illinois
Benjamin Zeidman ..... Argonne
Herbert D. Zeman ..... Stanford Univ.
J. Floyd Zimmerman ..... Consultant
Klaus O. H. Ziock ..... Univ. of Virginia
Paul Zupranski ..... Northwestern Univ.

INFORMATION FOR CONTRIBUTORS

Progress at LAMPF is the progress report of MP Division of Los Alamos National Laboratory. In addition it includes brief reports on *research done at LAMPF* by researchers from other institutions and Los Alamos National Laboratory divisions.

Progress at LAMPF is published semiannually on April 1 and October 1. This schedule requires that manuscripts be received by December 1 and June 1, respectively.

Published material is edited to the standards of the *Style Manual* of the American Institute of Physics. Papers are not refereed, hence presentation in this report does not constitute professional publication of the material nor does it preempt publication in other journals.

Contributors can expedite the publication process by giving special care to the following specifics:

1. Drawings and figures submitted should be of quality suitable for direct reproduction after reduction to single-column width, 83 cm (3-1/4 in.).

2. Figure captions and table headings should be furnished.

3. References should be complete and accurate.

4. Abbreviations and acronyms should be avoided if possible (in figures and tables as well as text), and when used must be defined.

5. All numerical data should be given in SI units.

6. Authors are reminded that it helps the reader to have an introduction, which states the purpose(s) of the experiment, before presentation of the data.

Research reports should be brief, one printed page or less, including figures (approximately three double-spaced typed pages). A list of recent publications relating to the experiment, for separate tabulation in this report, is much appreciated.

Contributors are encouraged to include as authors all participants in experiments so that they may receive credit for authorship and participation.

Questions and suggestions should be directed to: John C. Allred, Los Alamos National Laboratory, MS 850, Los Alamos, NM 87545.

ERRATA

In the Los Alamos National Laboratory report LA-8768-PR, *Progress at LAMPF*, July-December 1980, on p. 14, the spokesmen for Exps. 400/445 were listed incorrectly. The correct spokesmen are: Minh Duong-Van and C. Hoffman (Exp. 400) and J. D. Bowman and H. Matis (Exp. 445), (Los Alamos National Laboratory).

January - June 1981
☆U.S. GOVERNMENT PRINTING OFFICE: 1981-0-777-022/132